



GEORGIA INSTITUTE OF TECHNOLOGY  
OFFICE OF CONTRACT ADMINISTRATION

NOTICE OF PROJECT CLOSEOUT

Closeout Notice Date 03/19/93

Project No. E-20-X19 \_\_\_\_\_ Center No. 10/24-6-R7551-0A0\_  
Project Director MAYNE P W \_\_\_\_\_ School/Lab CIVIL ENGR \_\_\_\_\_  
Sponsor US DEPT OF TRANSPORTATION/FED HIGHWAY ADMIN \_\_\_\_\_  
Contract/Grant No. DTFH61-92-P-01468 \_\_\_\_\_ Contract Entity GTRC  
Prime Contract No. \_\_\_\_\_  
Title LOAD TESTS ON DRILLED SHAFT FOUNDATIONS IN THE PIEDMONT PROVINCE \_\_\_\_\_  
Effective Completion Date 930104 (Performance) 930104 (Reports)

Closeout Actions Required:	Y/N	Date Submitted
Final Invoice or Copy of Final Invoice	Y	_____
Final Report of Inventions and/or Subcontracts	N	_____
Government Property Inventory & Related Certificate	N	_____
Classified Material Certificate	N	_____
Release and Assignment	Y	_____
Other _____	N	_____

Comments EFFECTIVE DATE 7-1-91. CONTRACT VALUE \$9,870. \_\_\_\_\_

Subproject Under Main Project No. \_\_\_\_\_

Continues Project No. \_\_\_\_\_

Distribution Required:

Project Director	Y
Administrative Network Representative	Y
GTRI Accounting/Grants and Contracts	Y
Procurement/Supply Services	Y
Research Property Management	Y
Research Security Services	N
Reports Coordinator (OCA)	Y
GTRC	Y
Project File	Y
Other HARRY VANN-FMD _____	Y
FRED CAIN-OOD _____	Y

**ADSC/ASCE Research Study**

**AXIAL LOAD-DISPLACEMENT BEHAVIOR OF  
DRILLED SHAFT FOUNDATIONS IN PIEDMONT  
RESIDUUM**

**Technical Report Submitted To**

**Federal Highway Administration  
Turner-Fairbanks Highway Research Center  
McLean, Virginia**

**FHWA Reference No. 41-30-2175  
Order No. DTFH61-92-P-01468**

**Prepared by**

**Georgia Tech Research Corporation  
Geotechnical Engineering Division  
Georgia Institute of Technology  
School of Civil Engineering  
Atlanta, GA 30332-0355**

**February 2, 1993**

ADSC/ASCE Research Study

**AXIAL LOAD-DISPLACEMENT BEHAVIOR  
OF DRILLED SHAFT FOUNDATIONS  
IN PIEDMONT RESIDUUM**

Technical Report Submitted To

Federal Highway Administration  
Turner-Fairbanks Highway Research Center  
McLean, Virginia

FHWA Reference No. 41-30-2175  
Order No. DTFH61-92-P-01468

Prepared By

Georgia Tech Research Corporation  
Geotechnical Engineering Division  
Georgia Institute of Technology  
School of Civil Engineering  
Atlanta, GA 30332-0355

February 2, 1993

## ABSTRACT

A series of instrumented load tests on two drilled shaft foundations situated in residual soil and partially-weathered rock of the Piedmont geology were conducted to evaluate load-displacement and load-transfer response. Both shafts were 0.76 meters (30 inches) in diameter and subjected to axial compression loading. One shaft was essentially end-bearing with a constructed length of 21.4 m (70.2 feet) in weathered rock and the other foundation considered a floating shaft in residual silty sands with an embedded length of 16.9 m (55.5 feet). Both load tests confirmed that most of the applied axial loads are transferred in side resistance. At working stress levels, only 22 and 8 percent of the loads were transmitted to the tip for the end-bearing and floating shafts, respectively. At the interpreted failure loads, shaft resistance accounted for approximately 65 percent of the measured axial capacity for the end-bearing shaft and 85 percent for the floating shaft. Clearly, design and construction practices should acknowledge this phenomenon.

The Piedmont residuum is a difficult soil material to characterize properly due to the relict saprolite features, effects of partial saturation, strain rate, and sampling disturbance. An extensive array of in-situ tests (SPT, CPT, PMT, DMT, SASW) and laboratory tests on soils (index, mineralogy, triaxial, one-dimensional consolidation) were therefore carried out for determination of relevant soil properties. A methodology is developed where the axial capacities of drilled shafts in the Piedmont are determined as the sum of side and base components using a hybrid  $\alpha$ - $\beta$  approach. Elastic continuum analyses are shown to be useful for approximating the load-displacement-transfer behavior of drilled shafts under axial compression loading.

## ACKNOWLEDGMENTS

The load test program was conceived by a committee comprised of local affiliate members of the International Association of Foundation Drilling (ADSC) and the American Society of Civil Engineers (ASCE) from the Atlanta area. The actual work was implemented by a number of volunteers from local foundation contractors, consultants, and industry, as well as a plethora of civil engineering students. Supplies and equipment were donated to the project through the generosity of local industries, contractors, and businesses. The participating group included:

Allied Fence Company	ATEC Consultants
Atlanta Testing & Engineering	Brainard-Kilman
Chatham Brothers Grading	CH <sub>2</sub> M-Hill
Coastal Caisson	Dames and Moore
Georgia Dept. of Transportation	Georgia Power
Georgia Institute of Technology	GeoSyntec, Inc.
Golder Associates	Johnson Drilling Company
Law Engineering	Long Foundation Drilling Co.
McLean-Behm	McKinney Drilling Company
R.H. Harris, Inc.	Russo Corporation
Stan Agee Company	Tensar Corporation
Thomas Concrete, Inc.	Turner Engineering
Vulcan Materials	W.T. Mayfield & Sons Trucking

Financial contributions were provided by the FHWA and ADSC and their assistance is greatly appreciated. A number of key individuals who participated in the program included: Bob Bachus, Warren Bailey, Dick Barksdale, Rudy Bonaparte, George Cloud, Rich Curtis, Greg Dewberry, Jeff Endres, John Erigha, Scott Fletcher, Dean Harris, Ron Harris, Ron Hicks, Hubert Johnson, Bruce Long, Paul Mayne, Hal McKewen, Karl Myers, Jim Niehoff, Michael

Pagano, Nader Rad, Glenn Rix, Bud Stebbins, Mike Turner, Paul Wilson, and Buddy Yokely. Several outsiders assisted in the success of the test program and these included: Barry Berkovitz, Al DiMillio, Carl Ealy, Scot Litke, and Mike O'Neill.

The test site for the program was loaned to the ADSC/ASCE group by the Office of Facilities, Georgia Institute of Technology, and the help and assistance of Bill Ray, Brad Satterfield, and Paul vander Horst are duly acknowledged. Appreciation is also due Don Berghaus, Vicki Clopton, Jerry Conner, Jack Fenwick, Faith Gleason, Janis Goddard, Jim Priest, Seph Scott, Ken Thomas, and Larry Westbrook of Georgia Tech. Thanks are offered to all the graduate students at Georgia Tech who helped in-between class periods, weekends, and evenings, including: Jorge Alba, Alberto Bechara, Doug Brown, Barry Shi-Yo Chen, Jon Indridason, Kevin Lee, Fred Meyer, Sung-Yoon Rah, Shabana Rashid, David Scott, Haroon Shami, Jaime Sierra, Alan Still, and Amin Tomeh. Finally, appreciation is extended to all others who participated and assisted in the successful completion of these efforts.

February 2, 1993

ADSC/ASCE Research Study: **AXIAL LOAD-DISPLACEMENT BEHAVIOR  
OF DRILLED SHAFT FOUNDATIONS  
IN PIEDMONT RESIDIUM**

Report submitted to: **Federal Highway Administration  
Turner-Fairbanks Highway Research Center  
6300 Georgetown Pike  
McLean, Virginia 22101-2296**

Technical Officer: Carl Ealy, HNR-30  
FHWA Reference No. 41-30-2175  
Order No. DTFH61-92-P-01468  
Purchase Request No. 41-30-2175

Prepared by: **Geotechnical Engineering Division  
Georgia Institute of Technology  
School of Civil Engineering  
Atlanta, GA 30332-0355**

Project Director: Paul W. Mayne  
Research Engineer: Dean E. Harris  
GTRC Project No. E-20-X19  
Center No. 10/24-6-R7551-0A0



## TABLE OF CONTENTS

<u>SECTION</u>	<u>Page</u>
ABSTRACT	i
ACKNOWLEDGMENTS	ii
COVER SHEET	iv
TABLE OF CONTENTS	v
1. CHAPTER 1	
1.0 Introduction	1
1.1 Purpose of Study	1
1.2 Scope of Research	4
2. CHAPTER 2	
2.0 Current Practice for Drilled Shaft Foundations	5
2.1 Construction Procedures	5
2.2 Calculation of Ultimate Axial Capacity	6
2.2.1 Direct Correlative Methods	7
2.2.2 Total Stress Methods	7
2.2.3 Effective Stress Method	8
2.3 Modelling Axial Load-Displacement Behavior	11
2.3.1 Subgrade Reaction Analysis	11
2.3.2 Continuum Theory	11
2.4 Drilled Shafts in the Piedmont	12
2.5 Summary	13
3. CHAPTER 3	
3.0 Site Characterization	15
3.1 Site Location and Description	16
3.2 Field Testing	17
3.2.1 Drilling and Standard Penetration Testing	18
3.2.2 Dilatometer Testing	23
3.2.3 Pressuremeter Testing	26
3.2.4. Cone Penetrometer Soundings	28
3.2.5 Spectral Analysis of Surface Waves	29
3.2.6 Summary of In-Situ Tests	30
3.3 Laboratory Testing	31
3.3.1 Soil Classification Tests	31
3.3.2 Triaxial Shear Tests	33
3.3.3 Consolidation Tests	36
3.3.4 Mineralogy	39
3.4 Summary of In-Situ and Lab Testing	40

## TABLE OF CONTENTS (Continued)

<u>SECTION</u>	<u>Page</u>
4. CHAPTER 4	
4.0 Foundation Load Testing	41
4.1 Synopsis	41
4.2 Load Test Program	41
4.3 Construction Operations	43
4.4 Load Testing Equipment	45
4.5 Instrumentation	46
4.5.1 Strain Gauge Measurements	47
4.5.2 Butt Displacements	49
4.5.3 Tip Displacements	49
4.6 Load Application Procedures	49
4.7 Summary of Load Testing	50
5. CHAPTER 5	
5.0 Load Test Results	51
5.1 Load-Displacement Response	51
5.1.1 End-Bearing Shaft C1	51
5.1.2 Floating Shaft C2	52
5.1.3 Deep Plate Load Test C3	54
5.1.4 Interpretation of Axial Capacity	54
5.2 Load Transfer Distributions	56
5.2.1 Load-Distribution Curves	57
5.2.2 Shaft and Base Components	57
5.2.3 Tell-Tale Measurements	60
5.2.4 Unit Side and Base Resistances	62
5.3 Summary of Load Test Results	63
6. CHAPTER 6	
6.0 Ultimate Capacity in Axial Compression	64
6.1 Soil Property Characterization	64
6.1.1 Soil Strength	65
6.1.2 Effective Horizontal Effective Stress	66
6.1.3 Apparent Preconsolidation Stress	67
6.2 Routine Calculations of Ultimate Capacity	72
6.3 Analysis of Drilled Shaft Capacity in the Piedmont	72
6.3.1 Proposed Methodology	73
6.4 Summary of Ultimate Capacity Determinations	76

## TABLE OF CONTENTS (Continued)

<u>SECTION</u>	<u>Page</u>
7. CHAPTER 7	
7.0 Load-Displacement Behavior for Axial Compression	77
7.1 Axial-Displacement Predictions	78
7.2 Load Transfer	79
7.3 Application to Load Tests	80
7.4 Summary	85
8. CHAPTER 8	
8.0 Conclusions and Recommendations	86
8.1 Summary of Results	86
8.2 Directions for Future Research	86
9. REFERENCES	88
APPENDIX A - Results of Field Tests and In-Situ Test Data	95
Load Test Results for End-Bearing Shaft C1	96
Load Test Results for Floating Shaft C2	97
Load Test Results for Deep Plate Load Test C3	98
Cone Penetration Tests CPT-1 and CPT-2	99
Dilatometer Tests	100
Soil Boring Logs and SPT Data	103
Spectral Analysis of Surface Waves Survey	124
Pressuremeter Tests	125
APPENDIX B - Results of Laboratory Soil Testing	126
Index Properties and Grain Size Analyses	127
Consolidation Tests	130
Triaxial Shear Tests	136
APPENDIX C - Concrete Testing Results	139
APPENDIX D - Calculations of Axial Capacity and Load-Displacement Response	155

## CHAPTER 1

### 1.0 INTRODUCTION

#### 1.1 PURPOSE OF STUDY

Residual soils of the Piedmont Geologic Province underlie an important urban growth area of the southeastern to central-eastern United States, extending from Georgia to Pennsylvania. Major cities located within the Piedmont include: Atlanta-GA, Charlotte-NC, Raleigh-NC, Richmond-VA, Washington-DC, Baltimore-MD, Wilmington-DE, and Philadelphia-PA, as shown by Figure 1-1. In the Piedmont, drilled shafts are a common foundation type used for heavily loaded structures (Gardner, 1987). Despite their relative popularity, the approach to drilled shaft design varies considerably throughout the Piedmont, and in some instances local precedence has limited use of more cost effective design procedures (Schwartz, 1987). The side resistance, or "skin friction" developed in these residual soils has been a particularly controversial issue, as well as the relative proportions of load transferred to the shaft and base.

Because of these issues, members of the Geotechnical Committee of the Georgia Section of the American Society of Civil Engineers (ASCE) formed a joint committee with the Southeastern Chapter of the International Association of Foundation Drilling (ADSC) to implement a load test program. The load test program was conducted at the Georgia Institute of Technology campus with the goal of evaluating load transfer and load displacement characteristics of drilled shafts in the Piedmont residual soils. The scope of the load test program included site characterization by field and laboratory testing, and full-scale axial compression load tests of two drilled shaft foundations. The purpose of this research report is to present the results of the load test program, including site characterization, and to evaluate the load test results within a such a framework that the results may be extended to predictions of drilled shaft behavior elsewhere in the Piedmont.

Residual soils of the U.S. Piedmont are often difficult to characterize by in-situ and laboratory tests because they are "gray" materials, exhibiting behavioral aspects of both clay and sand. Special sampling procedures have not been developed, probably because the

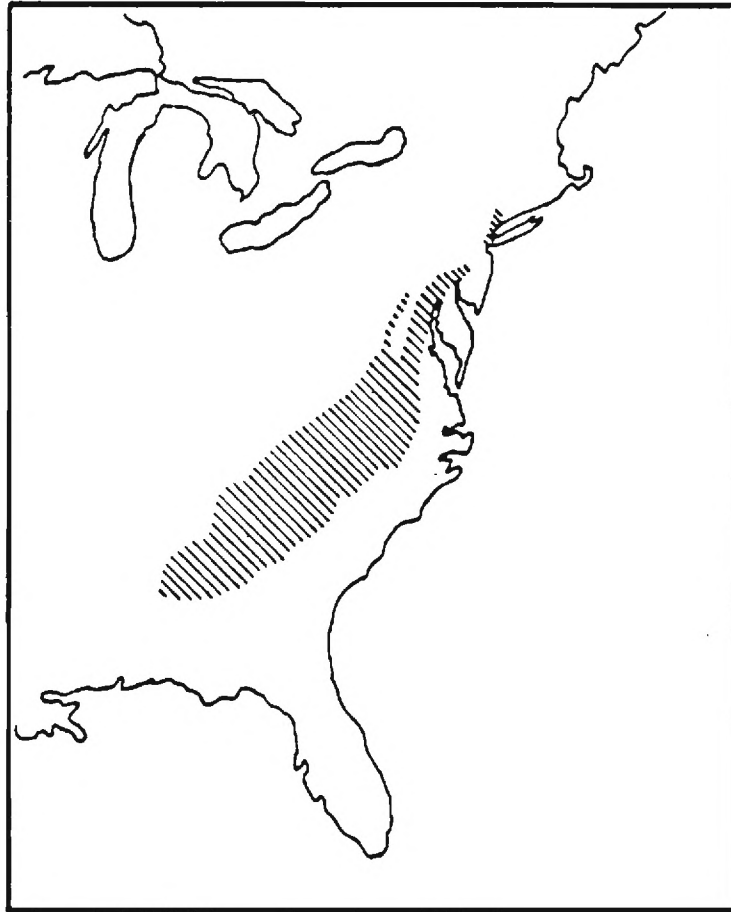


Figure 1-1. Region of the Atlantic Piedmont Province in the Eastern U.S. (Gardner, 1987).

materials are cohesive enough to permit recovery. However, sampling disturbance effects are severe, likely caused by swelling of the micaceous mineral components and destructurization of fabric incurred by standard sampling methods. In-situ test interpretation is hindered by poorly-understood rate effects, partial drainage, and the high silt-sand content associated with these materials.

A variety of in-situ tests have been used in the Piedmont Province. A major difficulty with most of these tests is that the profile undergoes a transition from weathered residual soil at shallow depths to partially-weathered rock and rock-like material with increasing depth. A typical soil to rock profile in the Piedmont is shown in Figure 1-2.

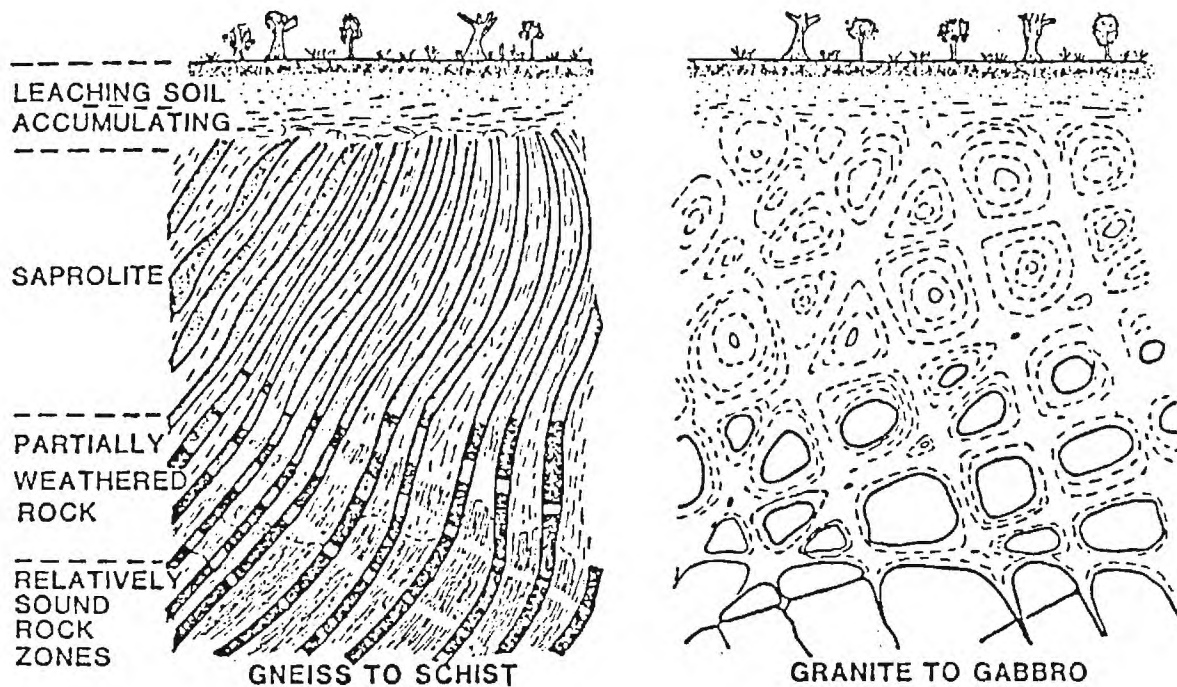


Figure 1-2. Typical Weathering Profiles in Metamorphic and Igneous Rocks of the Piedmont  
(From Sowers and Richardson, 1983)

Few in-situ tests can accommodate the difficult and vast transition from soil to rock. Consequently, extensive use of the standard penetration test (SPT) has prevailed because of its robustness (Martin, 1977). The pressuremeter test (PMT) has also been used, although primarily with the conventional Menard-type probe in pre-bored holes (Martin, 1987). Full-depth penetration by cone penetration tests (CPT) may be hindered by the presence of small rock fragments of gravel size and corestones within the soil matrix and the inability to probe into partially-weathered rock (PWR). In this regard, dilatometer tests (DMT) have proven somewhat more amenable to practice since the blade can be driven with a hammer if premature "refusal" is encountered during the hydraulic push (Mayne and Frost, 1988). In each of these tests, it is observed that the in-situ resistance increases with depth, reflecting the lesser degree of weathering at depth and the gradual transition from soil to rock-like

material. Consequently, due to the lack of a clear interface between soil and rock, seismic refraction methods have not generally proven to be useful as an exploratory tool in the residual soil profiles of the Piedmont. However, research work presented herein indicates promise with recent surface wave techniques as a means of site characterization.

## 1.2 SCOPE OF RESEARCH PROGRAM

This report presents the results of load tests on two drilled shafts situated in residual soil and partially-weathered rock of the Piedmont in Atlanta, Georgia. For this purpose, an extensive array of field and laboratory tests were performed to fully characterize the load test site discussed herein. Both load tests were instrumented to measure load-displacement response at the butt (top) and tip (base), as well as load transfer distribution with depth using embedded strain gauges within the reinforced concrete. These measurements permitted a determination of the relative magnitude of the components of side and base resistance, confirming that most of the applied axial loads in compression are transferred in side friction.

A review of common drilled shaft construction techniques and design methods are discussed in Chapter 2. The site characterization procedures used for the load test program are given in Chapter 3. Chapter 4 provides a discussion of the procedures and equipment used to perform the load tests included in this program and the results of the instrumented load test program are presented in Chapter 5. A discussion of the axial capacities is given in Chapter 6 and models for representing load-displacement response under axial compression loading are included in Chapter 7. Conclusions and recommendations from the load test program are summarized in Chapter 8. Finally, the appendices contain summaries of the measured field, in-situ, and laboratory test data for the load test program.

## CHAPTER 2

### 2.0 CURRENT PRACTICE FOR DRILLED SHAFT FOUNDATIONS

Drilled shaft foundations are constructed by excavating a cylindrical hole, placing reinforcing steel, and filling the excavation with fresh concrete. Also known as drilled piers, bored piles and caissons, these foundations have been used in the United States dating back to 1894 (Greer and Gardner, 1986). Since that time, methods of constructing them have evolved from hand excavations to modern truck and crane-mounted drill rigs. Major advances have also been made in understanding the behavior of drilled shafts, particularly during the past 10 years. With the accompanying development of a specialized drilled shaft contracting industry, the popularity of drilled shaft foundations has grown steadily. Drilled shafts are now seen by some as the foundation of choice for many design applications and have become the dominant foundation type in many geologic settings (Kulhawy, 1991).

With proper construction techniques, drilled shafts can be constructed in almost any soil condition available to other pile types. They are capable of supporting loads of almost any configuration: compression, uplift, lateral, moment, and torsion. Another advantage is their ability to carry very heavy loads with a single shaft, precluding the need for a pile cap. Vibration and noise from construction is negligible, and therefore, less disturbing to existing nearby structures and neighboring communities.

One uncertainty associated with drilled shafts stems from their sensitivity to soil conditions; i.e., construction and performance can vary depending on the soils present, requiring experience and judgment throughout design and construction. A series of properly controlled and instrumented load tests are therefore useful to substantiate the expected design factors, as well as quantify the importance of each variable affecting their response.

#### 2.1 CONSTRUCTION PROCEDURES

For modern drilled shaft construction, truck-mounted drill rigs are used to excavate the shaft. Short auger sections are rotated into the ground, until the flights are completely buried. The auger is then removed from the excavation, and the soil is removed by rapidly



spinning the auger in the reverse direction. In cohesive materials, the drilled hole may be self-supporting. In some non-cohesive soils, the sides of the excavation must be prevented from collapsing by using either temporary steel casing, slurry, or a combination of both (Reese, 1978). Temporary casing is required if personnel are needed to inspect the exposed bearing strata. After the excavation is completed, the reinforcing cage is placed in the excavated hole and positioned. The shaft is then filled with fresh concrete. Concrete is usually placed using tremie methods, but has been allowed to free-fall in many instances, as long as it is prevented from directly striking the reinforcing cage, or the sides of the excavation. Concrete must be allowed to cure for a sufficient period of time before any subsequent construction can occur.

Typical diameters of drilled shafts range from 1 to 3 m (3 to 10 ft), though diameters up to 6 m (20 ft) are possible (Greer and Gardner, 1986). Typical lengths are in the range of 3 to 30 m (10 to 100 feet), although lengths of up to 80 m (260 ft) are possible with special equipment. In the past, some shafts were constructed with enlarged bottoms, or bells, but more commonly today they consist of straight shafts.

## 2.2 ULTIMATE AXIAL CAPACITY

A number of procedures have been proposed for predicting the axial compression capacity of piles and drilled shafts. Only a brief description of some of the more conventional methods is included herein. Reference is made to Poulos (1989) for detailed discussions regarding the calculation of axial capacities of deep foundations.

In common consulting practice, drilled shaft capacity predictions are made based on consideration of limit equilibrium and shear strength of the supporting soil medium. The ultimate capacity of a drilled shaft can be estimated based on either: (1) methods which use direct correlations with results from in-situ tests, or (2) a more rational approach that relies on the characterization of soil engineering properties. The latter may be subdivided into either total stress approaches (e.g., the alpha method) or effective stress approaches (e.g. beta method). Despite their differences, each of these methods separate the calculation of total axial load capacity of the foundation into a base component (end bearing) and a side or shaft component (skin friction) in the following manner:

$$\text{Total:} \quad Q_t = Q_s + Q_b \quad (2-1)$$

$$\text{Shaft:} \quad Q_s = \sum f_{si} A_{si} \quad (2-2)$$

$$\text{Base:} \quad Q_b = q_{ult} A_{tip} \quad (2-3)$$

in which:

- $Q_t$  = total compression capacity of the drilled shaft
- $Q_s$  = shaft or side capacity in compression
- $Q_b$  = base or tip capacity in compression
- $f_{si}$  = unit side resistance for a layer or sublayer
- $A_{si}$  = shaft surface area within a layer or sublayer
- $q_{ult}$  = ultimate bearing capacity at tip on base
- $A_{tip}$  = shaft tip area

### 2.2.1 Direct Correlative Methods

Direct methods, such as those proposed by Meyerhof (1976) and Bustamante and Gianeselli (1982), rely on empirical correlations between field measurements from in-situ (or lab) tests and the unit side resistance, as well as separate relationships for estimating the magnitude of tip resistance. These methods are empirical, not based on theoretical or fundamental soil mechanics, and are only applicable for the specific types of soils, geologic settings, and ground conditions from which they were developed.

### 2.2.2 Total Stress Methods

From an engineering viewpoint, a more rational approach interprets the axial capacity of the foundation in terms of soil strength and state of stress associated with a limit equilibrium analysis. The total stress method (or  $\alpha$  method) evaluates the strength of the pile within such a framework, however it is based on empirical correlations between the undrained shear strength  $s_u$  of the soil, and the unit side resistance ( $f_s$ ). For assumed conditions of undrained loading, the unit side resistance is termed the adhesion ( $f_s = c_a$ ), such that:

$$c_a = \alpha s_u \quad (2-4)$$

The factor  $\alpha$  is determined from backanalysis of previous load test results and primarily has been correlated to  $s_u$ . The total stress method has been used since the 1950's. Many studies have shown the variation of  $\alpha$  to be dependent upon pile type, pile length, soil type, construction methods, overburden depth, and site stratigraphy (Tomlinson, 1986). However, the inherent assumption of the relationship between the unit side resistance and  $s_u$  is based simply on empirical correlation. Because of this, it is difficult to accurately predict or explain rationally the observed variability of the factor  $\alpha$ . Some recent attempts at this have related the  $\alpha$  coefficient to the in-situ state of stress and frictional behavior of the soil (Kulhawy and Jackson, 1989; Sladen, 1992).

In total stress analyses, the base resistance is calculated using limit plasticity solutions for bearing capacity, assuming undrained loading and accounting for foundation shape. An estimate of the base resistance is given by the simple expression:

$$q_{ult} = N_c s_u \quad (2-5)$$

where  $N_c = 9.33$  is from the Prandtl-Meyerhof solution and  $s_u$  is the undrained shear strength below the foundation base. In a more rigorous setting, soil rigidity should be considered in bearing capacity calculations (Kulhawy 1991).

### 2.2.3 Effective stress methods

The effective stress method represents an effort to relate the unit side resistance to fundamental parameters, using principles of soil mechanics, rather than empirical relationships. Ideally, by using a fundamental basis, the variability of the unit side resistance can be explained more rationally. The effective stress approach requires more design input, however, and as in the total stress method, it is difficult to fully quantify the effects of construction.

The effective stress method determines the side resistance using the effective angle of friction between the shaft concrete and the soil ( $\delta$ ), and the effective horizontal stress ( $\sigma_h'$ ) acting along the shaft. The value of  $\sigma_h'$  is usually related to the effective vertical stress by a lateral stress coefficient,  $K = \sigma_h'/\sigma_v'$ , and includes considerations of geostatic states of

stress as well as changes incurred by construction. At a particular depth, the unit side resistance,  $f_s$ , is calculated from:

$$f_s = (K \tan \delta) \sigma_{vo}' \quad (2-6)$$

The value of  $\delta$  depends on the soil type, mineralogy, roughness, and quality of construction, and can be expressed as a function of the soil angle of internal friction ( $\phi'$ ). Construction techniques in drilling shafts can affect the value of  $K$ , causing it to be less than the original in-situ coefficient of lateral earth pressure ( $K_o$ ). In contrast, driven pile foundations may increase  $K_o$ . Kulhawy et al. (1983) discusses the probable ranges in variation of both  $\delta$  and  $K$ . As a first approximation,  $K$  can be assumed to equal  $K_o$ , and  $\delta$  can be assumed equal to  $\phi'$  of the soil. Often the  $K \tan \delta$  term is termed the  $\beta$  factor such that:

$$f_s = \beta \sigma_{vo}' \quad (2-7)$$

The shaft tip resistance is calculated using bearing capacity factors based on limit plasticity or cavity expansion theories, assuming drained conditions. In a simple form, neglecting soil rigidity and foundation shape and depth factors, the base resistance is calculated from:

$$q_{ult} = N_q \sigma_{vo}' \quad (2-8)$$

$$N_q = K_p \exp(\pi \tan \phi') \quad (2-9)$$

$$K_p = (1 + \sin \phi') / (1 - \sin \phi') \quad (2-10)$$

where  $\phi'$  is the effective stress friction angle,  $N_q$  = Prandtl-Meyerhof bearing capacity factor from limit plasticity theory, and  $K_p$  = Rankine passive earth pressure coefficient. Total axial capacity for compression loading is calculated as the sum of shaft plus base capacity. Figure 2-1 summarizes the basic approaches for calculating side and base resistances for total and effective stress methods.

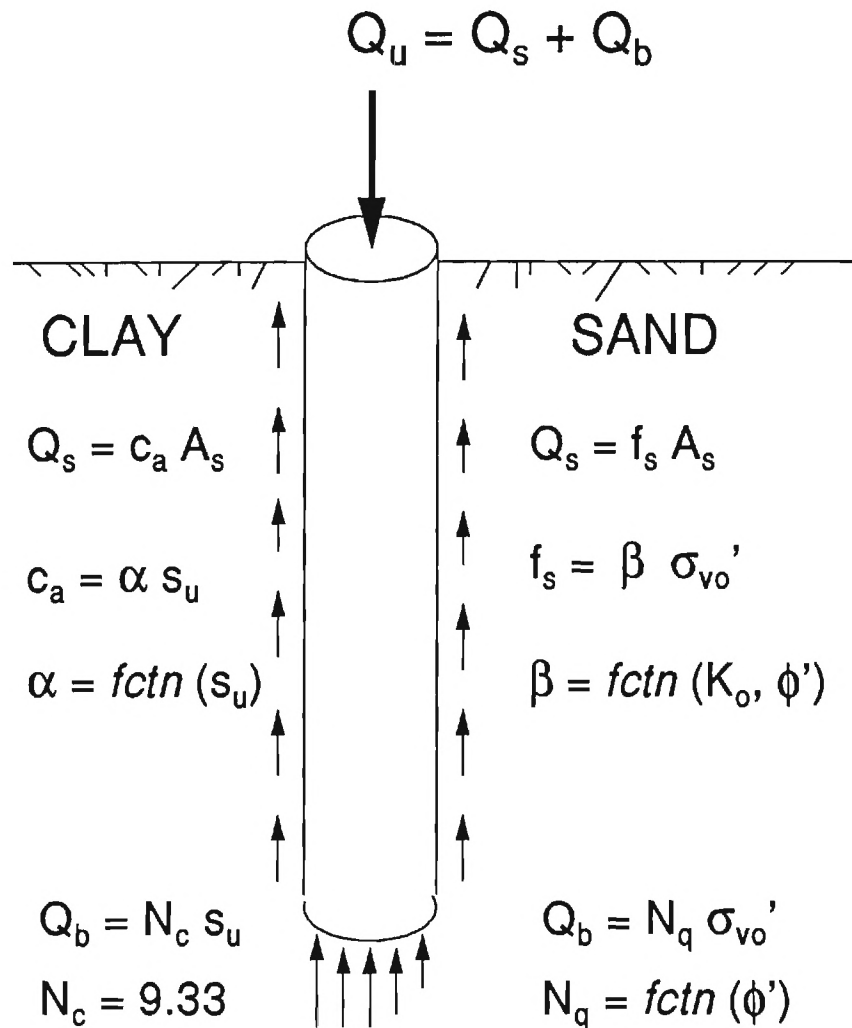


Figure 2-1. Total and Effective Stress Methods for Calculating Axial Compression Capacity.

Both the total stress and the effective stress methods require judgment in practice, since many parameters are subject to interpretation. In addition, the parameters must be adjusted to account for construction effects. However, the advantages of the effective stress method are that it is more fundamentally rational and appears applicable to all soil types (sand, silt, clay), whereas total stress analysis can be applied only to clays and cohesive silts.

## 2.3 MODELLING AXIAL LOAD-DISPLACEMENT BEHAVIOR

Often the permanent settlement of a foundation element under service load is a more stringent design criterion than ultimate load considerations. Two common methods of predicting the load settlement behavior of drilled shafts include: (1) subgrade reaction analysis, and (2) elastic continuum theory.

### 2.3.1 Subgrade Reaction Analysis

In the subgrade reaction analysis, the shaft is divided into segments joined together by elastic springs which simulate the deformability of the individual segments. The side and base resistances are represented by either linear or nonlinear springs, and load transfer is based on either empirical or theoretical curves. The method uses an iterative procedure that is initiated by assuming a small deformation at the base of the shaft, and solving for the mid-segment deformation and side resistance. The same procedure is followed for each segment in a successive manner. This solution is not exact because it does not consider interaction between adjacent segments. Specific details are given in Reese and O'Neill (1977).

### 2.3.2 Continuum Theory

Continuum analyses are based on elastic theory and have been developed by Poulos and Davis (1980) and by Randolph and Wroth (1978, 1979). The approach suggested by Poulos and Davis is an integral equation analysis based on the Mindlin solution for a point load acting in the interior of an elastic half space. The solution by Randolph and Wroth is an approximate closed-form solution which idealizes the deformation of the soil around the shaft as the shearing of concentric cylinders. Both of these methods have been shown to provide consistent results.

For a more detailed discussion of these design methods, the reader is encouraged to consult the work of Poulos (1989), Kulhawy (1991), Poulos and Davis (1980), and Reese and O'Neill (1977).

## 2.4 DRILLED SHAFTS IN THE PIEDMONT

The installation techniques used in constructing drilled shafts can have a significant effect on their capacity. Most importantly, since the shaft is constructed by open excavation, the soil expands or relaxes, and consequently may lose strength, especially if there is a significant delay between excavation and concreting. The installation and removal of casing, as well as the time delay between excavation and concreting, can reduce the interface friction between the shaft and surrounding soil, thus limiting the side resistance capacity. In addition, water from the concrete can cause softening of the soil near the shaft.

In the Atlanta area, the local practice is to completely ignore the contribution of side resistance to the capacity of drilled shafts, due to concerns regarding the effects of construction. In addition, the Piedmont materials are comprised of residual silty sands, sandy silts, and decomposed rocks that are difficult to characterize in terms of traditional soil mechanics. Instrumented load tests can resolve the disputes regarding the load-carrying capacity of drilled shafts in the Piedmont residuum, but they are expensive. Much of the knowledge about the load response of drilled shafts has been gained by performing field load tests, as well as scale-model tests, and from numerical simulations. In particular, the results of field load tests on shafts have been invaluable in developing many design methods and serve as the most reliable means of verifying design procedures (Kulhawy and Hirany, 1988). When performed with the proper instrumentation, a load test can reveal valuable information regarding the total load capacity of the shaft, the relationship between load and settlement, as well as the load transfer aspects and relative proportions of side resistance and base resistance.

Even though there is a substantial database of information regarding load tests in various geologic settings, there has been little published research regarding load testing of drilled shaft foundations in the Piedmont. Watson (1970) conducted axial compression and uplift tests on small drilled shafts with 0.46 m (18 in) diameters and lengths varying from 4.6 to 6.7 m (15 to 22 ft). These tests were located on the Georgia Tech Campus, near the current location of the student center. Load-displacement results for these series of tests are presented in Figure 2-2. Values of uncorrected SPT-N resistances were quite varied on

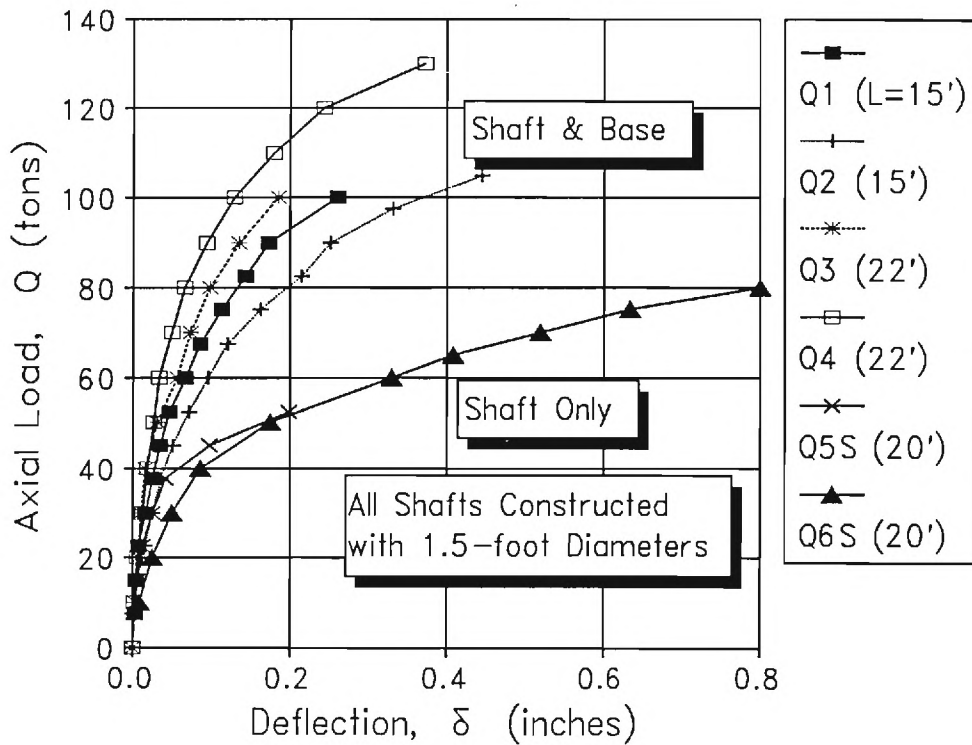


Figure 2-2. Measured Load Test Response on Small Drilled Shafts in the Piedmont.  
(Data from Watson, 1970, PhD Thesis, Georgia Institute of Technology).

the small site, but averaged 24 bpf. Several zones of partially-weathered rock were also noted on the boring logs, with corresponding N-values > 100 bpf. Other load test data on drilled shafts in the Piedmont are reported by Mayne and Frost (1987) and O'Neill (1992).

## 2.5 SUMMARY

During the past two decades, advances in drilled shaft technology have made this foundation one of the dominant types throughout the world. These advances have included better means of constructing the foundations, and increases in understanding of their behavior



under loading. There exists a variety of methods for estimating the load carrying capacity of drilled shafts. Rational methods may be generally categorized as either total stress or effective stress approaches. In both, the total axial compression capacity is calculated as the sum of two components: (1) frictional resistance or adhesion along the sides of the shaft, and (2) the point bearing resistance of the base.

In certain areas of the Piedmont Physiographic Province, current practice does not utilize the component of side resistance available to drilled shafts because of concerns regarding the effects of construction and uncertainties associated with the characterization of soil properties. Full scale load tests have been the source of much of the increased knowledge concerning the behavior of these foundation types, and offer an excellent means of investigating their behavior in the Piedmont residuum. To date, few shaft load tests have been performed in the Piedmont soils, and therefore, the methodology for characterizing the relevant parameters is not well-defined.

## CHAPTER 3

### 3.0 SITE CHARACTERIZATION

An extensive site characterization program was conducted for the ASCE/ADSC drilled shaft load test program. The purpose of the site characterization was to develop a representative profile of the residual soil to rock transition and to estimate applicable engineering properties. To achieve this goal, a program of field exploration, in-situ testing, and laboratory testing was developed by a committee comprised of members of the local ASCE Geotechnical section. The field and laboratory testing procedures are outlined in this section, and measured values of engineering parameters needed for interpretation of the load test results are presented.

The soils of the Piedmont are primarily the product of the in-place weathering of schists, gneisses, and granites. In a typical soil profile, the degree of soil weathering decreases with depth, and the soils retain the mineral segregation, mineral alignment, and structural defects of the parent rock. These factors cause the soil to exhibit nonhomogeneity and anisotropy. In particular, the banded nature of gneiss results in a weathered profile that often contains wide variations in penetration resistance over short distances in both the horizontal and vertical direction. Similar features occur due to foliation patterns associated with schist, and orthogonal jointing in granites. Often, the soil may retain internal stresses which are the result of tectonic stresses on the parent rock and have no relationship to the overburden stress. For additional discussion, Sowers and Richardson (1983) give a detailed description of the engineering properties of the Piedmont soils.

The factors above make it difficult to characterize residual soils since many traditional concepts of soil mechanics are based on investigations of sedimentary soils and may or may not be applicable (Vaughan, 1985). For instance, it is difficult to define the preconsolidation pressure of these soils, given their transformation from rock to soil. Considering the mineral segregation and other structural characteristics retained from the parent rock, many traditional concepts (especially classification systems) may even be irrelevant. In addition to the aforementioned, the soils of the Piedmont typically consist of very silty sands, and very sandy silts, further complicating the issue of modelling their engineering characteristics.

Most models of soil behavior are developed based on consideration of sand or clay alone, with little or no consideration of silts, or mixtures of more than one soil type.

Because of these difficulties, site characterization can be an uncertain task for geotechnical projects in the Piedmont. Nevertheless, it is very important to understand the engineering behavior of the soils at a load test site. Without a thorough site characterization, the load test results are only useful for the particular location, geometry, and loading conditions present at the load test (Kulhawy and Hirany, 1988). Quantifications of the engineering parameters of the soil allow an interpretation of the load test within the framework of engineering theory, and thus make it possible to compare the results to other case histories.

### 3.1 SITE LOCATION AND DESCRIPTION

The load test program was performed on the west side of the Georgia Institute of Technology campus, in Atlanta, Georgia. The test site is located on the southern side of Sixth Street, at the curve where Sixth Street turns north and becomes Curran Street. The western edge of the site is bounded by Northside Drive, and the WREK radio tower is located just north of the parcel. A site location map is shown in Figure 3-1. Use of this site was made available by the Georgia Tech Office of Campus Planning and Architecture. After the load test, construction of a new 6-story dormitory commenced just northeast of the ADSC/ASCE load test site. Future access to the site is therefore restricted.

The site was located at the top of a small hill, and before construction of the test shafts began, the ground surface sloped down to the north with elevations ranging from about +304 m (+997 ft) msl, to about +305 m (+1003 ft) msl. This area had apparently been previously used to discard construction and landscaping debris, and the ground was covered with mulch, concrete, and stone rubble. To provide access to the proposed test shaft locations, the surface debris was cleared, and the ground surface was levelled using a front-end loader. The final ground surface elevation at this time was approximately +304 m (+997 ft) msl. Survey elevations and ground control was established using an engineering level and datum referenced to an existing benchmark shown on the site plans for the new dormitory now nearing completion.

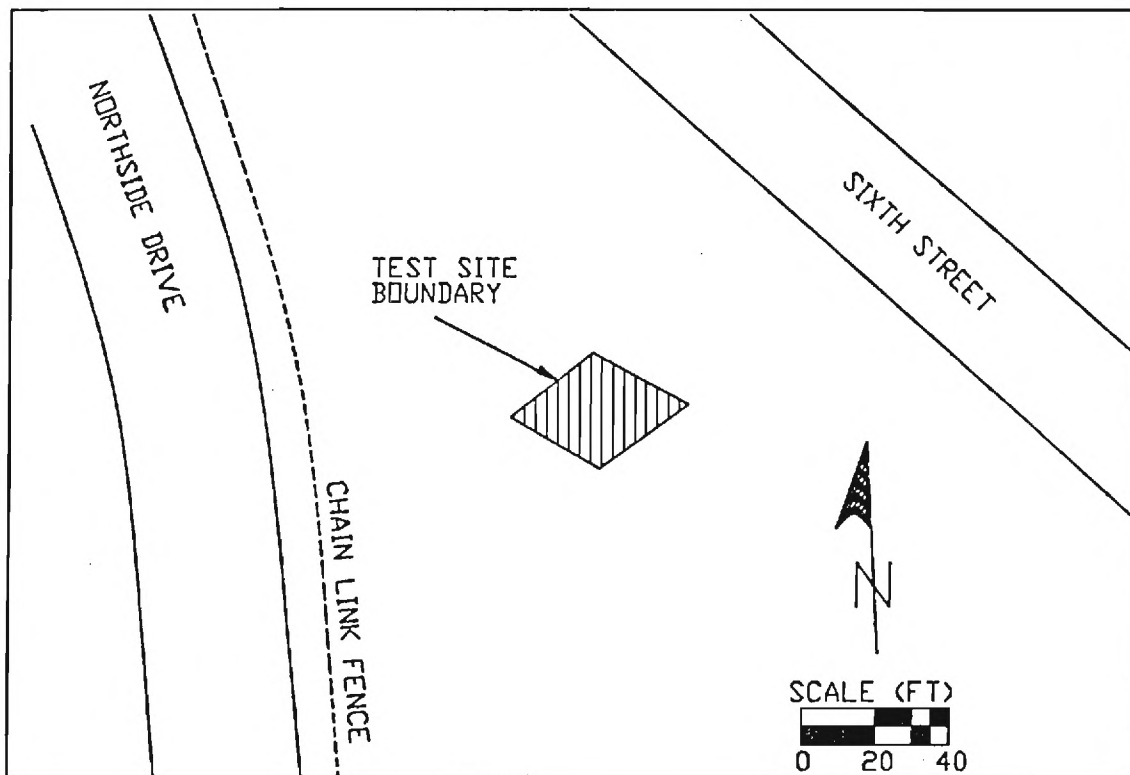


Figure 3-1. Site Location Plan for Drilled Shaft Load Tests on Georgia Tech Campus.

### 3.2 FIELD TESTING

A field testing program was planned to obtain soil samples for laboratory testing and to perform in-situ tests. Field tests performed at the site included Standard Penetration Tests (SPT), Flat Blade Dilatometer Tests (DMT), Pressuremeter Tests (PMT), Cone Penetrometer Tests (CPT), and Spectral Analysis of Surface Waves (SASW). Rock coring was also performed after refusal in several of the borings.

Locations of the field tests performed at the site are shown in Figure 3-2. Testing at the site was performed by local offices of several engineering consulting and testing companies, the Georgia Department of Transportation, and by faculty and students of Georgia Tech. Test locations were chosen to coincide with the locations of the test and

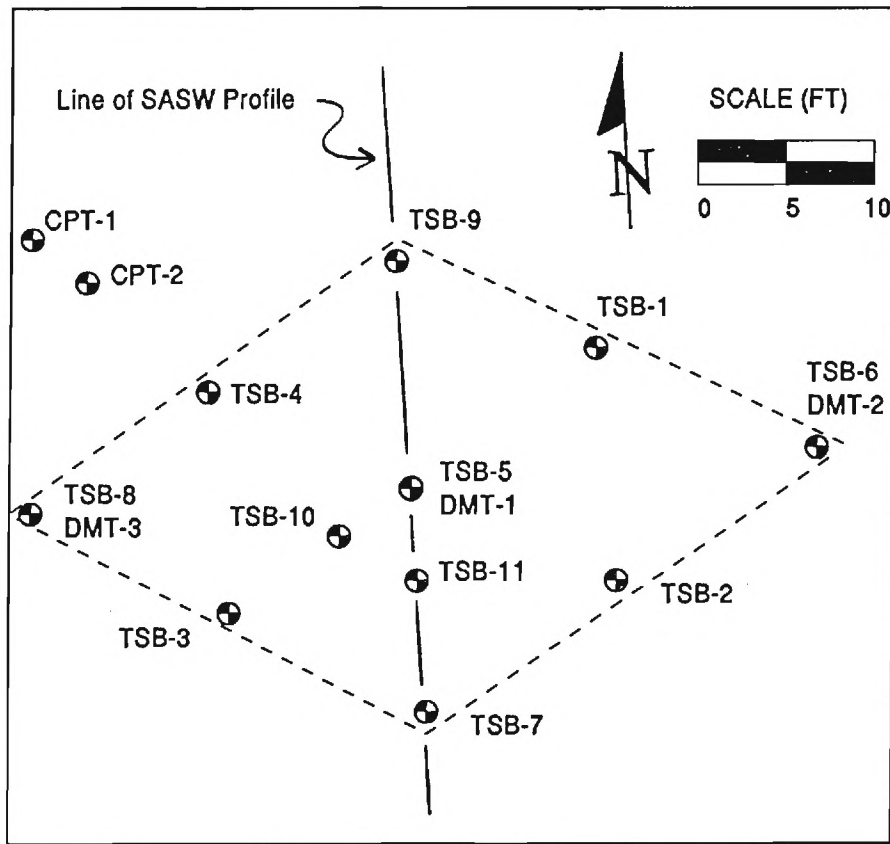


Figure 3-2. Locations of In-Situ Field Tests at Experimental Test Site.

reaction shafts. Originally, the load test program had been planned to include five test shafts, and four reaction shafts, and the test locations were chosen based on these plans.

### 3.2.1 Drilling and Standard Penetration Testing

Eleven borings were made at the site for soil sampling and testing. Of these, 7 were advanced using continuous hollow stem augers and 4 using rotary drilling and wash-boring techniques. Nine of the borings were advanced to perform split-spoon sampling and standard penetration testing. One boring was performed to obtain relatively undisturbed "Shelby" tube samples, and another was advanced to permit pressuremeter testing (PMT). Rock coring was performed in 5 of the borings, beginning at depths ranging from 20 to 25 m (66

to 82 feet), with typical core lengths of 3 m (10.0 feet). Total depths of the borings, including depths of coring, ranged from 20 to 28 m (66 to 92 feet) below the ground surface.

Standard Penetration Tests (SPTs) were performed in nine of the borings (TSB-1 through TSB-9) at regular intervals of approximately 1.5 m (5 ft.). SPTs are performed by driving a hollow 5.1 cm (2 in.) O.D., 3.5 cm (1.375 in.) I.D. standard split spoon sample tube into the soil at the bottom of the borehole, using a 63.5 kg (140 lb) hammer. The driller, using mechanical equipment, repeatedly raises and drops the hammer from a height of 76 cm (30 in.) and records the number of blows required to drive the sample tube a total of 45.7 cm (1.5 ft.) into the ground in three successive 15.2 cm (6 in.) increments. The number of blows recorded for the last two increments are added together to give the Standard Penetration Resistance or N-Value. The sample tube is removed from the ground, split apart, and a sample cleaned from the tube for storage in a glass jar. Procedures of the Standard Penetration Test are discussed in detail in ASTM D-1586.

At boring TSB-10, nine thin-walled, 1.2 cm (3.0 in) O.D. "Shelby" tube samples were obtained at 1.5 m (5.0 ft.) intervals, starting at a depth of 3.1 m (10.0 ft.) and ending at 15.2 m (50 ft.). These tubes were then transported to several different laboratories for further testing.

At one test location, pressuremeter testing was performed in a prebored hole advanced using wash boring techniques (boring TSB-11). These tests were carried out using a conventional Menard-type probe.

Boring logs were prepared using the results of the SPTs and engineering examination of the recovered field samples. These logs were developed using the gINT software program and are presented in Appendix A. The logs show a profile of residual soils typical of the Atlanta area, except that old fill and debris were encountered at the surface of many of the borings, with depths of fill ranging from 0.6 to 3.7 m (2 to 12 ft.). Primarily, the fill was comprised of silts and sands which are native materials to this area. Beneath this fill, residual silty sands were encountered to depths ranging from 15.8 to 19.5 m (52 to 64 ft.). Underlying this silty sand, the borings encountered what is commonly termed partially weathered rock (PWR). This less weathered soil retains much more of the structure and hardness of the parent rock, though it was typically sampled as a silty sand due to the hammering action of the sample tube. The thickness of the partially weathered rock layer

varied from 0.6 to 7.3 m (2 to 24 ft.). Bedrock refusal was encountered in the borings at depths ranging from 20.0 to 24.8 m (65.5 to 81.5 ft.) and consisted of schistose to granitic gneiss. Recovery from the coring ranged from 49 to 100 percent, with rock quality designations (RQDs) ranging from 29 to 47 percent. Coring was performed in general accordance with ASTM D 2113.

Groundwater levels were recorded at the time of drilling in all but one of the borings and typically ranged from 16.7 to 19.1 m (54.8 to 62.7 ft.) below the ground surface. In one boring (TSB-1), the water level after drilling was measured at 7.0 m (23.0 ft.), but this was a wash boring, and the water level measured at the time of drilling is not representative of ambient water levels. Water levels were measured after 24 hours of stabilization in 4 borings, with depths ranging from 15.8 to 16.8 m (52.0 to 55.2 ft.).

Standard Penetration Test resistances (N values) measured in the residual silty sand typically varied from about 8 to 31 blows per foot. True N values were not recorded in the partially weathered rock, since typically more than 50 blows of the hammer were required to drive the samples only a fraction of its total length. These values were converted to equivalent N values by dividing the number of blows by the actual penetration of the sample. Figure 3-3 shows a summary profile of N values measured at the site by three different crews. The profile illustrates a trend of increasing N values with depth. Though there is usually no well-defined boundary between residual soil and partially weathered rock (Sowers and Richardson, 1983), this figure shows a marked increase in standard penetration resistance at the interface, which occurs at a depth ranging from about 16.8 to 19.8 m (55 to 65 ft.).

The N values are shown again in Figure 3-4, but the scale has been expanded in order to show detail in the more shallow soils. Inspection of Figure 3-4 reveals that the N values from the three different crews show the same trend, yet plot in almost distinctly different portions of the graph. The differences between the N values measured by the three crews are better illustrated in Figure 3-5 where average profiles of Standard Penetration Resistance are shown for each crew. Though some variability in N values should be expected due to the nature of the soil being tested, consistent differences between the values measured by the three crews are evident, indicating that the variations are most likely due to different efficiencies of the individual drill crews and equipments. The susceptibility of the Standard

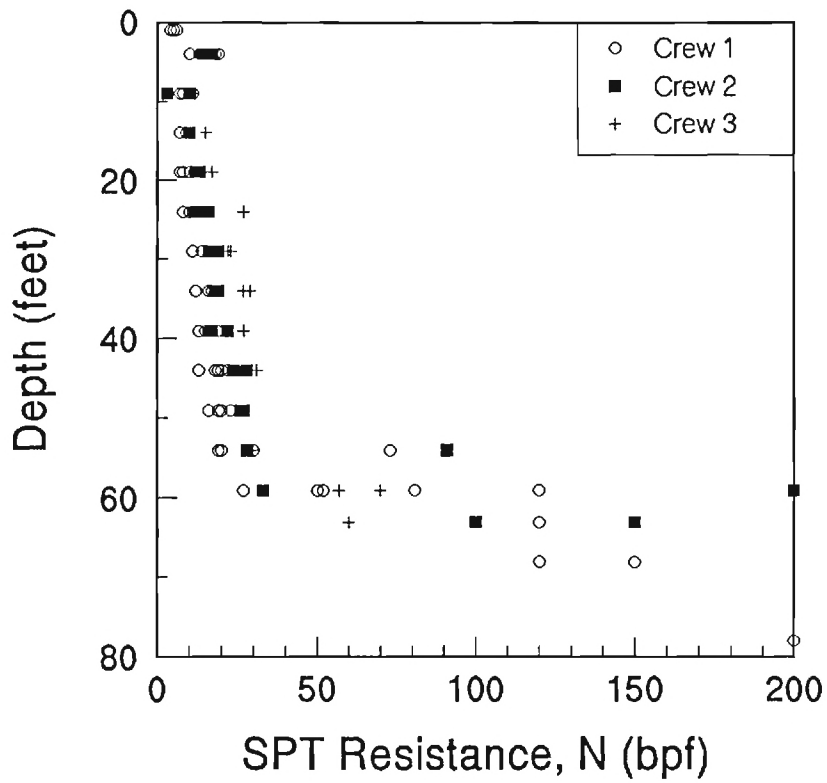


Figure 3-3. Summary of SPT-N Values Over the Full Depth at the Test Site.

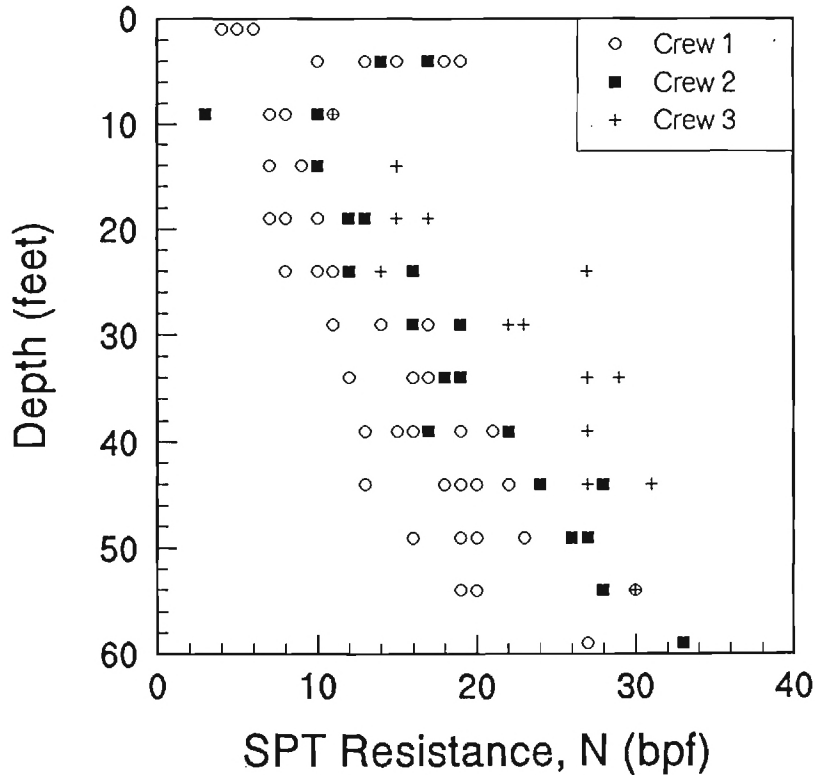


Figure 3-4. Summary of SPT-N Values Within the Residual Soil Matrix.



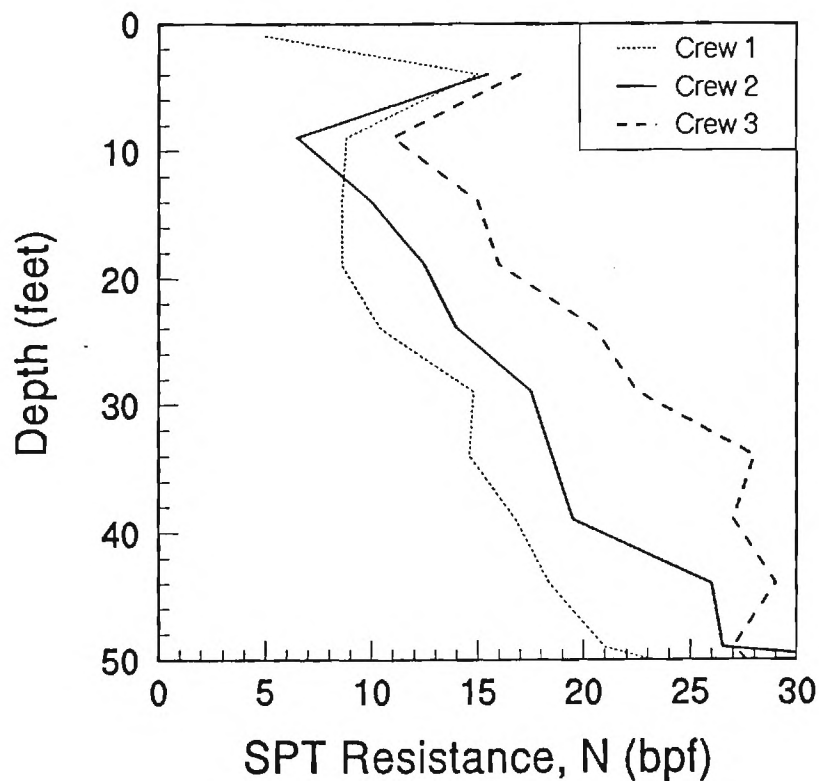


Figure 3-5. Average Trends of SPT Resistances For Three Crews.

Penetration Test to errors resulting from inefficient equipment and operator technique has been well-documented (Kovacs, et al. 1983).

Since the true N values are not known without proper calibration of the equipment, all values at each depth were averaged. A profile of the average N value, plus and minus one standard deviation is shown in Figure 3-6. It is assumed henceforth that the mean profile of SPT resistances are representative of common drilling practice in the U.S. and, therefore are approximately equal to  $N_{60}$ , designating that 60 percent efficiency has been achieved, since this is considered the norm for U.S. practice (Skempton, 1986). A more accurate approach would be to measure the ENTHRU energy of each crew and rig using procedures given in ASTM D-4633. It is therefore recommended that this calibration be performed before use of SPT results.

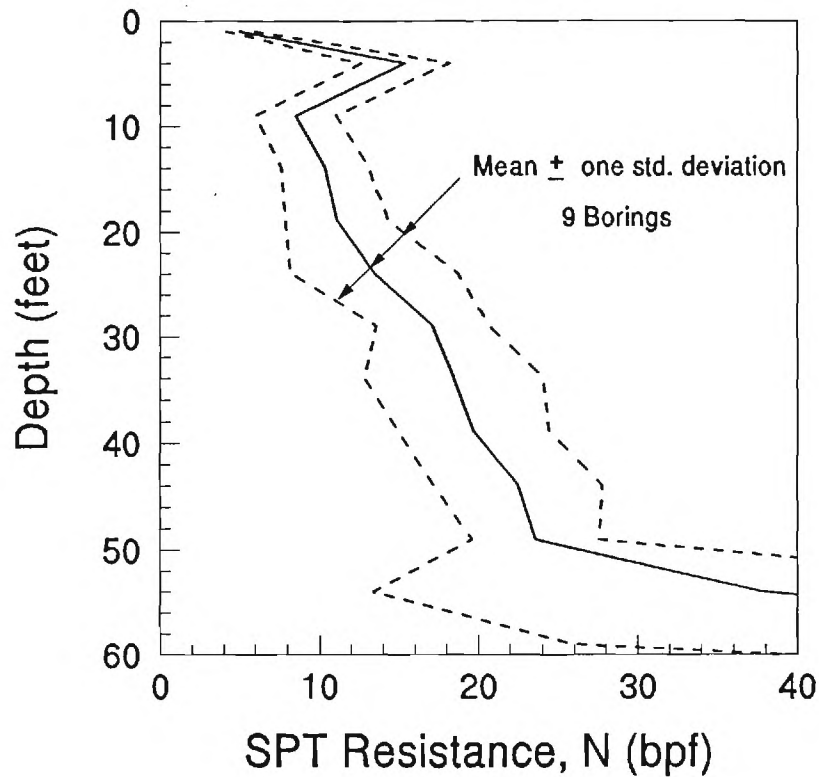


Figure 3-6. Average Profile of SPT Resistance (Assumed Henceforth to be  $N_{60}$ ).

The average N-value in the silty sands increases linearly from an average of about 9 bpf at a depth of 3.0 m (10 ft.) to about 25 bpf at 15.2 m (50 ft.). Below a depth of approximately 18 m (60 ft.), the SPT resistances increase typically over 50 bpf, indicative of the transitional PWR material. The borings were subsequently terminated at either auger refusal or SPT refusal, defined as N-values exceeding 50 blows per 1 inch of penetration ( $> 50$  blow/25 mm). The logs in Appendix A indicate the specific depths to refusal and the average refusal depth for nine borings was 22 m (72 ft.). Upon refusal in borings TSB-1 through 5, rock coring techniques were used to sample the parent bedrock material.

### 3.2.2 Dilatometer Tests

Three dilatometer test (DMT) soundings were made at the site to depths ranging from 10.4 m to 13.0 m (34.1 to 42.5 ft.). The DMT test uses a sharp edged blade which has a flexible, stainless steel membrane located near the center (Marchetti 1980). The blade is

pushed into the ground to the desired depth, and high pressure nitrogen gas is used to inflate the membrane. When pushed into the ground, the force required to push the blade (termed the thrust or blade resistance,  $q_D$ ) can be monitored. During expansion of the membrane two readings are recorded: (1) the pressure required to lift the membrane from its seating (A reading); (2) and the pressure on the membrane after 1.1 mm (0.04 in.) of deflection has occurred (B reading). Both of these readings must be corrected for the membrane stiffness in air to determine the parameters  $p_0$  and  $p_1$  (Schmertmann, 1986).

In the three soundings made at this site, the DMT blade was pushed using the drill rig hydraulics, and blade resistance ( $q_D$ ) measurements were made by recording the hydraulic pressure at the top of the drill rods. Figure 3-7 shows the profiles of  $q_D$ ,  $p_0$ , and  $p_1$ .

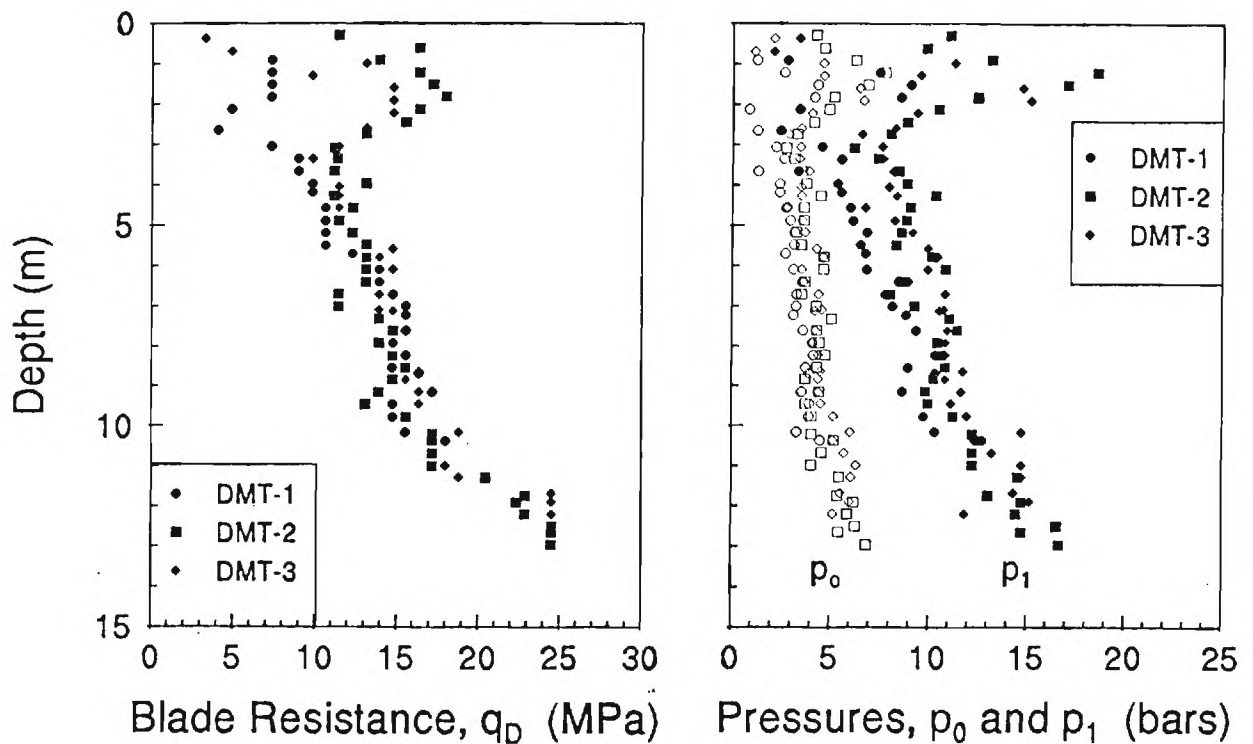


Figure 3-7. Summary of Flat Dilatometer Measurements at Test Site.

The two DMT parameters are used to calculate several dilatometer parameters, including the horizontal stress index ( $K_D$ ), the material index ( $I_D$ ), and the dilatometer modulus ( $E_D$ ). These values are in the DILLY5 software program to classify the soil and estimate parameters including coefficient of lateral stress ( $K_0$ ), unit weight ( $\gamma$ ), undrained shear strength ( $s_u$ ), overconsolidation ratio (OCR), and elastic soil modulus ( $E$ ). The results of the dilatometer tests performed at the load test site are presented in this format in Appendix A of this report. The  $q_D$  values are used to determine the effective  $\phi'$  in granular soil materials.

Profiles of  $I_D$ ,  $K_D$ , and  $E_D$  are shown together in Figure 3-8. As with the  $N$  values from the SPTs, the DMT strength and deformability parameters ( $q_D$ ,  $p_0$ ,  $p_1$ , and  $E_D$ ) each show a trend of increasing value with depth.

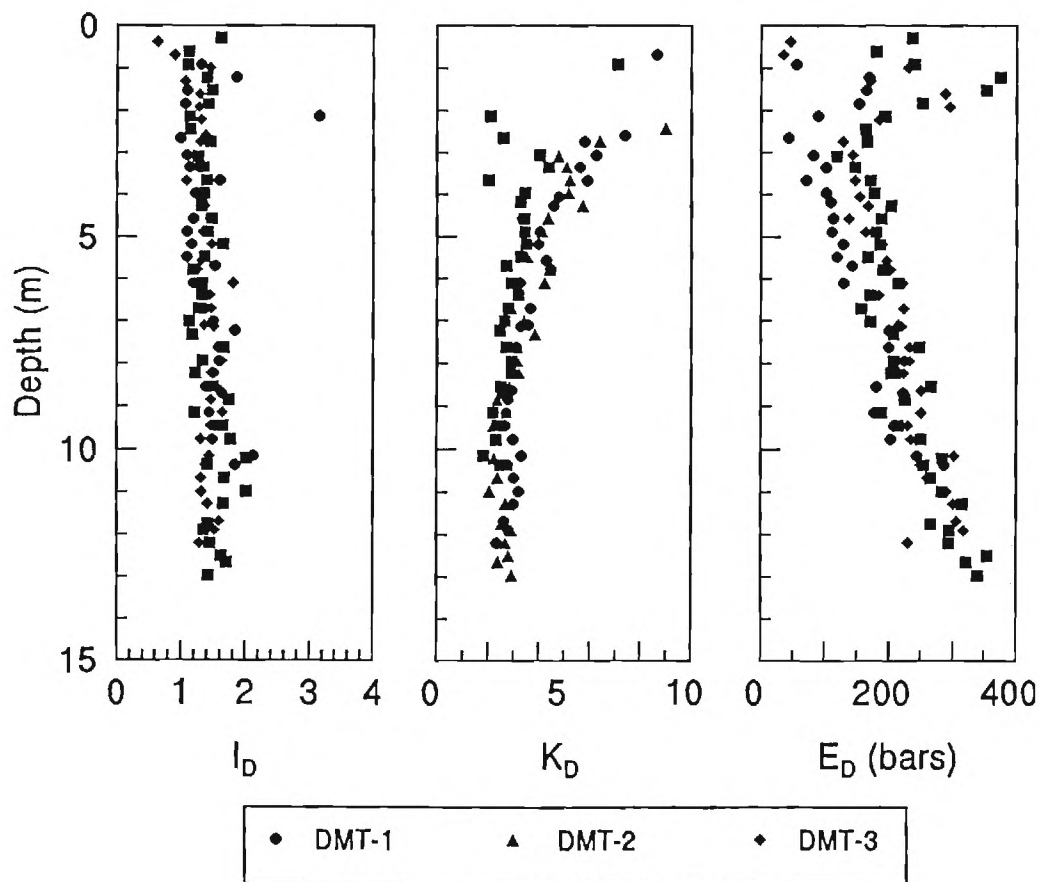


Figure 3-8. Profiles of Derived Index Parameters from DMT Soundings.

### 3.2.3 Pressuremeter Testing

The pressuremeter tests (PMT) consisted of a double-cell cylindrical probe placed in a prebored hole and expanded using air and water pressure. During the expansion of the probe, volume measurements were made via a burette on the control panel. A detailed description of the procedures for the test are contained in ASTM D-4719. A Menard-type GAM pressuremeter, with a probe diameter of 70 mm (2.76 in.) and initial volume of 790 cc (48.2 in.<sup>3</sup>) was used here. Five PMTs were made in a single boring (TSB-11) that was advanced using rotary drilling methods and slurry to limit borehole caving. Plots showing the measured pressure-volume curves from the five tests are shown in Figure 3-9.

Procedures for reduction of pressuremeter data are described by Baguelin, Jezequel, and Shields (1978). Under ideal conditions, the pressuremeter can be used to make measurements of the in-situ lateral stress, limiting stress, deformability, and strength. The total horizontal earth pressure is usually determined by inspection of the pressure-volume

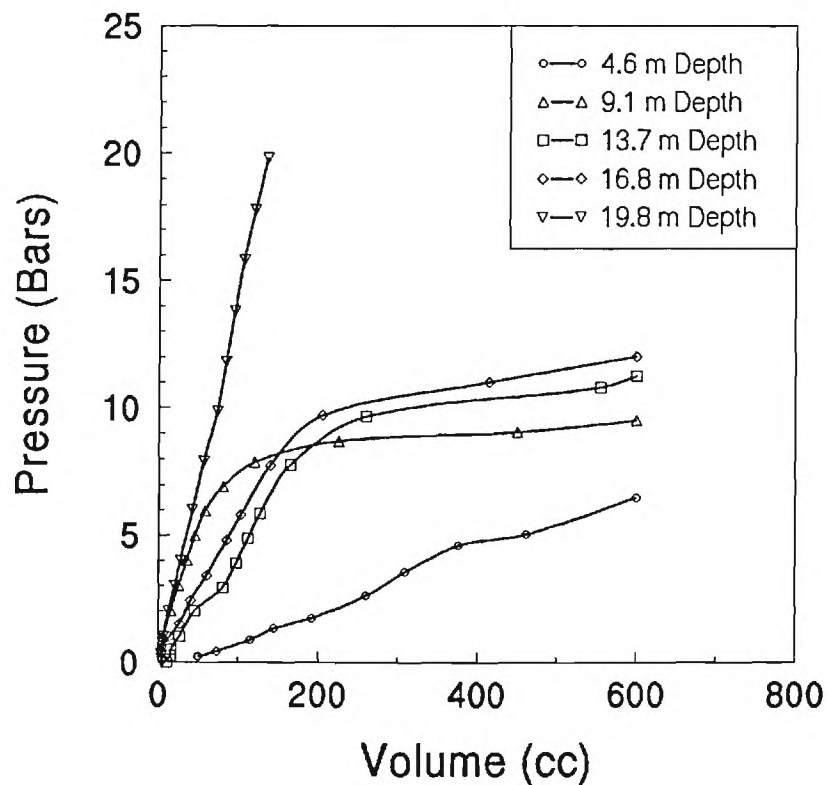


Figure 3-9. Measured Pressure-Volume Change Data From Pressuremeter Tests.

curves and choosing a "lift-off" stress, or point where the pressure begins increasing. The limit pressure  $P_L$  is used to calculate strength and bearing capacity parameters. The conventional definition for  $P_L$  is an extrapolated value of pressure at which the probe volume doubles relative to its initial volume. Using such a definition, the limit pressure can be determined by extrapolation from a plot of volume versus the logarithm of volumetric strain. The pressuremeter modulus is obtained from the pressure-volume curves. The undrained shear strength ( $s_u$ ) of the soil can also be calculated from the PMT results by plotting the pressure versus the natural log of the volumetric strain, and determining  $s_u$  as the slope during the latter portion of the test (Wroth, 1984).

With pressuremeters that rely on prebored holes, borehole disturbance effects often make it difficult to decipher soil parameters with accuracy. Estimation of the horizontal stress is particularly affected by disturbance, and inspection of the pressure-volume curves showed uncertainties in clearly choosing a lift-off pressure. Values of  $p_L$ ,  $\sigma_{ho}$ ,  $s_u$ , and  $E_{PMT}$  have been interpreted from the PMT data and these are presented in Figure 3-10.

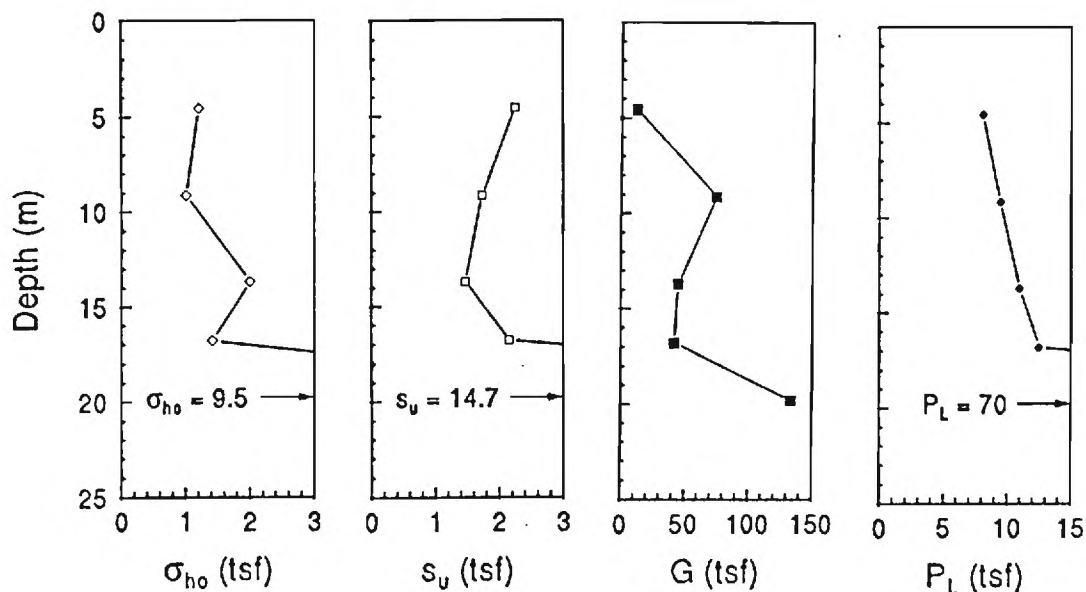


Figure 3-10. Derived Parameters From Pressuremeter Test Data.

### 3.2.4 Cone Penetrometer Soundings

Two cone penetration tests (CPT) were performed using an electric friction cone penetrometer with a 60° apex, 10 cm<sup>2</sup> (1.55 in<sup>2</sup>) projected cone tip area, and 150 cm<sup>2</sup> (23.25 in<sup>2</sup>) friction sleeve. The CPT is performed by advancing a conical penetrometer at 2 cm/second (0.78 in/sec), while measuring the resistances against the tip ( $q_c$ ) and friction sleeve ( $f_s$ ). With continuous readings, the cone penetrometer provides very detailed information about the soil profile.

The CPTs were performed to depths of 19.2 m (63.0 ft.) and 9.7 m (31.8 ft.) below ground surface. The deeper sounding (CPT-1) was performed in approximately 1.25 hours including extraction, and was terminated only because the total available length of E-rods had been used. The results are presented in Figure 3-11.

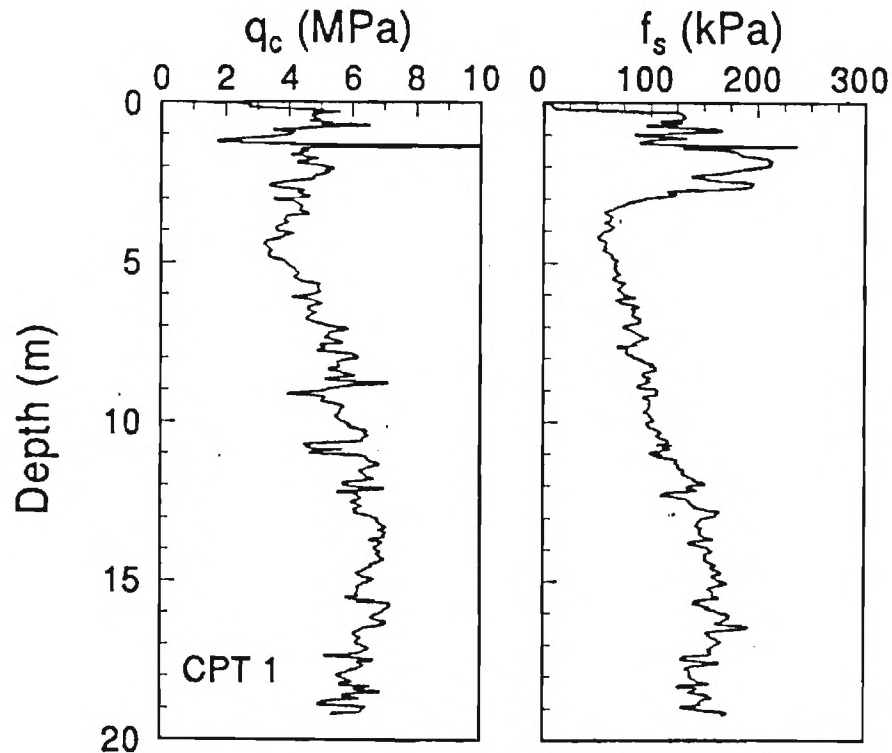


Figure 3-11. Profiles of Cone Tip and Sleeve Resistance from CPT-1.

Sounding CPT-2 was encountered an obstruction at 9.7 m (probable rock fragment). Because of this, and also due to the initiation of rainy weather, the sounding was terminated at this depth. Detailed logs from both of the soundings are presented in Appendix A. As with the previous in-situ tests,  $q_c$  and  $f_s$  both increase with depth within the residual soil matrix. In addition, in the upper 3-meter (10-foot) regions of the soundings, the evidence of heterogeneous fill may be seen.

### 3.2.5 Spectral Analysis of Surface Waves

The spectral analysis of surface waves (SASW) method (Stokoe et al. 1989) is an in-situ geophysical method in which surface stress waves (Rayleigh waves) of varying wavelengths are generated at a point. The procedure is based on the principle that the longer the wavelength, the deeper the wave penetrates into a soil profile. By measuring the velocities of several waves of different wavelengths, a profile of material properties can be developed. The shear modulus obtained from the SASW method is a low strain modulus, designated ( $G_{max}$ ). Data from the SASW survey at the load test site is given in Table 3-1. The profile of the shear wave velocity ( $V_s$ ) obtained from the SASW testing is shown in Figure 3-12. The data reduction assume a total soil unit weight  $\gamma = 19.2 \text{ kN/m}^3$  (122 pcf) and Poisson's ratio of  $\nu = 0.3$ .

Table 3-1. Summary of Spectral Analysis of Surface Wave Data.

Depth		Velocity, $V_s$		Shear Modulus, G		Elastic Mod., E	
(ft)	(m)	(fps)	(m/s)	(tsf)	(MPa)	(tsf)	(MPa)
10	3.0	551	168	575	55	1495	143
20	6.1	788	240	1176	112	3058	292
30	9.1	932	284	1645	157	4278	409
40	12.2	1058	322	2120	202	5513	527
50	15.2	1168	356	2584	247	6719	643
70	21.3	1268	386	3046	291	7919	757
Half space		1599	487	4843	463	12593	1205



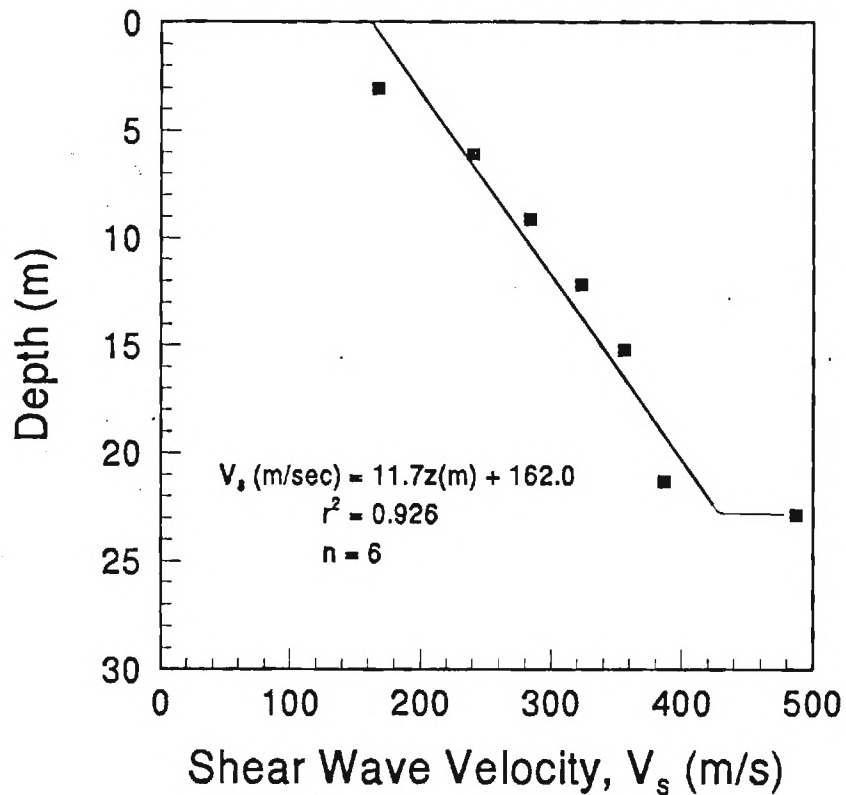


Figure 3-12. Shear Wave Velocity Profile from SASW Survey.

### 3.2.6 Summary of In-Situ Tests

The data from the various in-situ test methods generally show profiles of increasing penetration resistance or test measurement value with depth within the profile of the residual soil matrix. Consequently, regression analyses were conducted on the available data from each test are summarized and given in Table 3-2. The statistical table includes the least squares relationship, number of data points ( $n$ ), and coefficient of determination ( $r^2$ ). The results strictly apply to the natural residual soils and do not include values from the heterogeneous upper fill or the lower stratum of partially-weathered rock material. Also note that the relationships are unit-dependent.

Table 3-2. Summary of Statistical Analyses on In-Situ Test Data.

<u>Test</u>	<u>Least Squares Relationship</u>	<u>No. Data</u>	<u>Coefficient</u>
SPT	$N(\text{bpf}) = 4.6 + 1.30z(\text{m})$	$n = 80$	$r^2 = 0.58$
CPT	$q_c(\text{MPa}) = 3.1 + 0.25z(\text{m})$	$n = 831$	$r^2 = 0.75$
	$f_s(\text{kPa}) = 18.2 + 9.33z(\text{m})$	$n = 831$	$r^2 = 0.93$
DMT	$q_o(\text{MPa}) = 5.12 + 1.29z(\text{m})$	$n = 90$	$r^2 = 0.82$
	$p_o(\text{bars}) = 1.87 + 0.30z(\text{m})$	$n = 90$	$r^2 = 0.63$
	$p_i(\text{bars}) = 3.60 + 0.86z(\text{m})$	$n = 90$	$r^2 = 0.76$
PMT	$p_L(\text{bars}) = 9.37 + 0.353z(\text{m})$	$n = 4$	$r^2 = 0.99$
SASW	$V_s(\text{m/s}) = 162.0 + 11.7z(\text{m})$	$n = 6$	$r^2 = 0.93$
	$E_d(\text{MPa}) = 82.5 + 11.7z(\text{m})$	$n = 6$	$r^2 = 0.97$

### 3.3 LABORATORY TESTING

Samples obtained during the field exploration phase were subjected to a series of laboratory tests including grain size analyses (mechanical and hydrometer), Atterberg limits, triaxial shear tests, and one-dimensional consolidation tests. The scope of the laboratory testing program was determined by the ASCE load test committee and performed by the geotechnical laboratory of the Georgia Department of Transportation, Georgia Tech, Golder Associates, and Geosyntec Services.

#### 3.3.1 Soil Classification Tests

Grain size distributions were determined using mechanical sieves and hydrometer tests. These tests are described in detail in ASTM D-422. A total of 113 tests were performed on samples obtained from standard penetration testing at the site. Due to space limitations, individual plots of the grain size distributions are not provided, though the data are provided in tabular form in Appendix B. The results from the tests were used to make a summary plot of the average grain size distribution, shown in Figure 3-13. Average

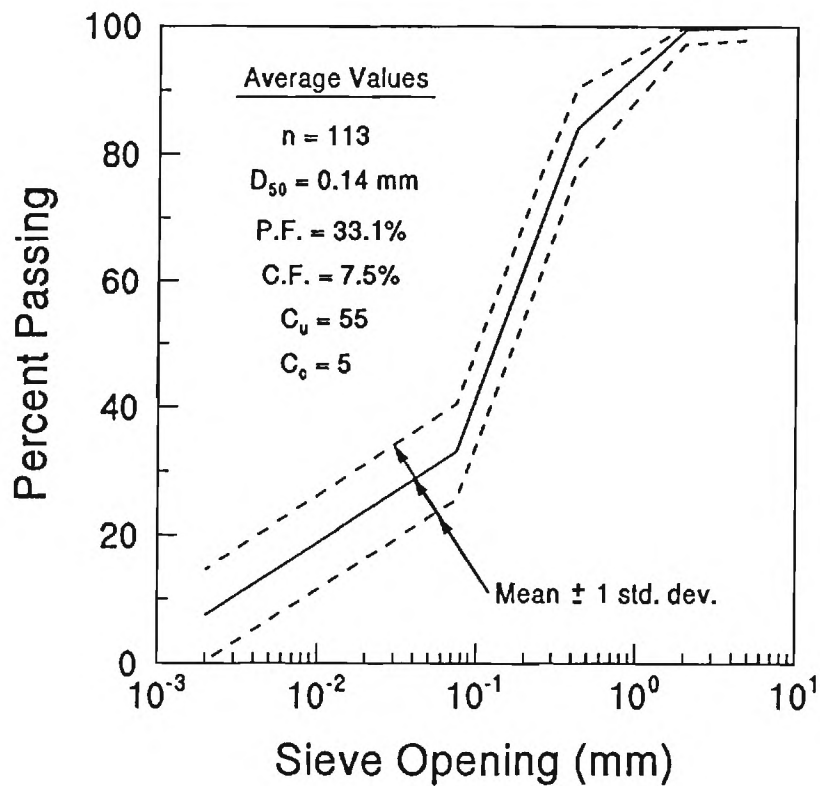


Figure 3-13. Summary Grain Size Distribution For Piedmont Residuum.

statistical values for several classification parameters are shown in the figure. The median grain size is  $D_{50} = 0.14 \text{ mm}$  (5.5 mils) and the material technically classifies as a silty fine sand (SM). The plot shows that the soils have an average fines content (percent passing #200 sieve) of 33% and a clay content (percent finer than 0.002 mm) averaging 8%.

The Atterberg limits testing was performed in accordance with the procedures recommended by ASTM D 4318, and revealed that almost all of the soils are non-plastic, except for some of the fill and near-surface residual soils. Results of the tests are shown in tabular form with the results of the grain size analyses in Appendix B. The boring logs from the standard penetration tests, shown in Appendix A, include classifications according to the Unified Soil Classification System (USCS), based on the results of the grain size distributions and the Atterberg limits testing.

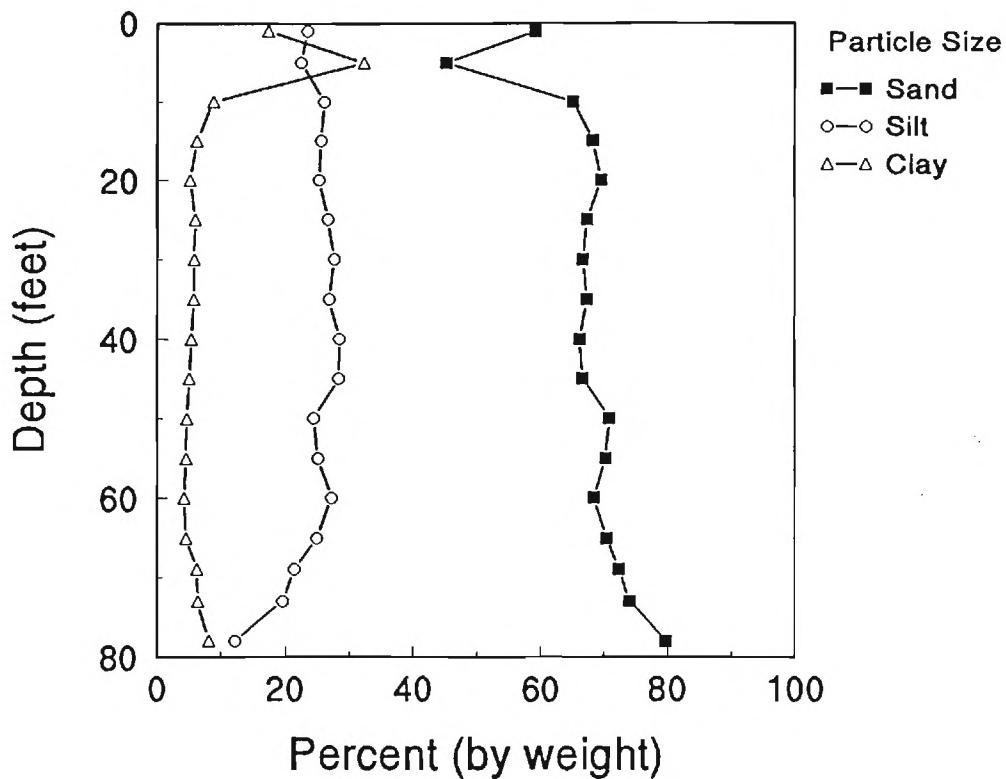


Figure 3-14. Profile of Soil Classification Distribution.

A profile of the soil classifications based on the grain size distributions is given in Figure 3-14, indicating extreme uniformity of particle sizes within the natural residual soils. Surprisingly, this holds true beyond the transition from soil into partially-weathered rock below depths of 18 m (60 ft.).

### 3.3.2 Triaxial Shear Tests

Thirteen isotropically-consolidated undrained triaxial compression (CIUC) tests were performed on specimens retrieved from the tube samples obtained at boring TSB-10. The triaxial tests are listed individually in Table 3-3. Specimens from the tubes were extruded and then trimmed to 7.1 cm (2.8 in.) diameter. The CIUC tests were performed by saturating and consolidating each specimen under an isotropic confining stress, and then shearing the specimen by application of vertical stress under a constant rate of strain.

Table 3-3. Results of Consolidated Undrained Triaxial Compression Tests

Approximate Sample Depth		Initial Data		Isotropic	Parameters at Failure		Mod.	
(ft.)	(m)	$w_n$ (%)	$\gamma_{tot}$ (pcf)	$\sigma_c'$ (psi)	$p_f'$ (psi)	$q_f = s_u$ (psi)	$\phi'$ (deg.)	$E_{50}$ (psi)
15	4.57	16.6	104.9	7.0	9.9	5.6	34.4°	2430
16	4.88	17.0	118.2	11.8	6.6	4.3	40.6°	2118
17	5.18	17.3	103.1	23.8	22.7	13.3	35.9°	2660
30	9.14	19.4	99.2	11.6	10.9	5.6	30.9°	2715
31	9.45	22.7	99.2	81.6	79.4	44.4	34.0°	5431
35	10.67	32.6	118.3	6.9	9.4	4.7	30.0°	1111
36	10.97	31.5	111.8	13.9	14.7	7.8	32.0°	1861
37	11.27	33.0	110.7	27.8	22.3	12.6	34.4°	2778
45	13.72	28.3	103.9	36.0	44.7	25.9	35.4°	2549
46	14.02	26.9	103.4	71.2	64.8	38.6	36.6°	5819
50	15.24	26.2	107.3	19.6	35.0	21.9	38.7°	1410
51	15.54	25.3	107.3	38.9	61.8	37.9	37.8°	5924
52	15.85	23.9	107.3	77.8	125.8	74.0	36.0°	847

Notes:  $s_u = q_f' =$  peak value of  $(\sigma_1' - \sigma_3')/2$ ; failure defined at max. deviator stress.  
 $p_f' = (\sigma_1' + \sigma_3')/2 =$  average effective stress at failure.  
 $\sigma_c' =$  initial effective confining stress =  $p_o'$ .  
 $\phi' =$  secant angle of internal friction ( $\sin \phi' = q_f/p_f'$ ).  
 $E_{50} = (\sigma_1 - \sigma_3)/\epsilon =$  secant elastic modulus defined at 50% ultimate strength.  
 Units conversion: 1 psi = 6.89 kN/m<sup>2</sup>; 1 pcf = 6.36 kN/m<sup>3</sup>.

Skempton's pore pressure parameter (B), was measured to check saturation, prior to shearing the specimen. A minimum B value of 0.96 was used as a criteria for determining saturation. Tests were generally performed at an axial strain rate of 1 percent/hour. Pore pressure measurements were made during the tests to enable the determination of effective stress strength parameters. ASTM D-4767 provides the recommended procedures for performing the CIUC test. Strain-rate controlled tests were conducted.

The original scope of the triaxial series included testing of three specimens from each tube sample at three different confining stresses selected by the load test committee. Generally, the effective confining stresses ( $\sigma_c'$ ) were chosen to equal: (1) one-half of the in-situ effective vertical overburden stress ( $0.5\sigma_{vo}'$ ), (2) the effective overburden stress ( $\sigma_{vo}'$ ),

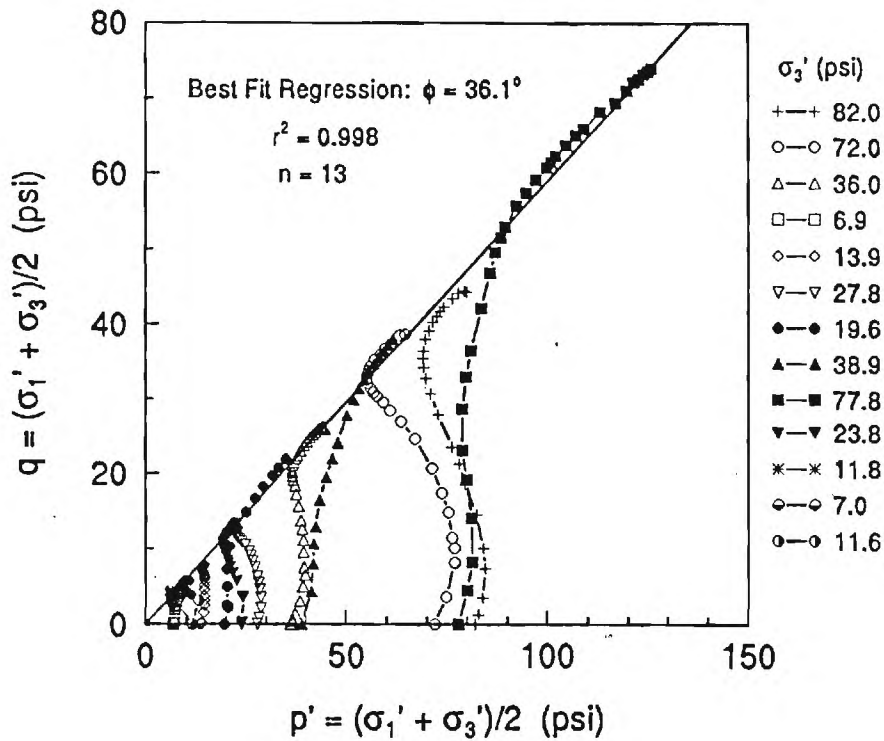


Figure 3-15. Effective Stress Paths for CIUC Triaxial Tests.

and (3) twice the effective overburden stress ( $2\sigma_{v_0}'$ ). However, many of the samples were damaged or highly disturbed during the extruding process, limiting the total number of tests performed. In some instances, only one or two specimens were available from a sample, and multi-stage tests were performed on these specimens. In the multi-stage test, the specimen is consolidated to an initial effective confining stress, and then sheared to a point near failure. The sample is then consolidated to a higher effective confining stress, where it is again loaded to a point near failure. This process can be repeated a third time to define a failure envelope. The multi-stage test is not a particularly desirable approach, however.

Stress paths from the tests are shown together in Figure 3-15 in MIT  $q$ - $p$  space. It is apparent from inspection of the data that the failure envelope passes through the origin, with no cohesion intercept ( $c'$ ). A least squares regression between  $q$  and  $p'$  confirmed that  $c' = 0$ . Therefore, a best fit regression (with a forced intercept of zero) was made and has been shown along with the data. The failure envelope indicates an average effective angle of internal friction ( $\phi'$ ) of 36.1 degrees. The trend of the effective stress paths is indicative

of materials that are somewhat contractive, i.e., positive pore water generation and decrease in volume during shear. This is characteristic of low OCR soils.

Table 3-3 lists the individual triaxial specimens tested and measured parameters derived from the test data. The undrained shear strengths ( $s_{ult}$ ) were defined at peak deviatoric stress levels. Effective stress friction angles ( $\phi'$ ) were calculated as secant values for each specimen assuming  $c' = 0$ . Finally, secant moduli ( $E_{50}$ ) were calculated at one-half the maximum deviator stress. Individual deviator stress versus axial strain curves from the CIUC tests are included in Appendix B.

### 3.3.3 Consolidation Tests

A total of 14 one-dimensional consolidation tests were performed on specimens trimmed from the Shelby tube samples obtained from boring TSB-10. Procedures for performing the consolidation test are given in ASTM D-2435. The tests were conducted in dead-weight oedometers (Wykeham-Farrance type) and pneumatic consolidometer devices. Results from the individual consolidation tests are presented as plots of void ratio ( $e_v$ ) versus log effective vertical stress ( $\sigma_v'$ ) in Appendix B. A summary of the tests is given in Table 3-4. Procedures used in trimming the consolidation specimens were found to have a significant effect on the results of the tests, as discussed below.

Consolidation testing of silty sandy soils such as those encountered at this site is made difficult by disturbance of the soil. Unlike many clays that "remember" much of their stress history, even though they have been disturbed, sand does not typically reflect a clear delineation of stress history in consolidation tests. In addition, the results of consolidation tests on sand are easily obscured by the effects of sample disturbance. Sample disturbance arises from the field drilling operations, sampling techniques, vibrations and jolts during transportation to the lab, cutting of the sample tube, and trimming during specimen preparation for laboratory testing. In addition, during extrusion of the sample, the horizontal stresses retained within the soil are released. In an attempt to minimize the effects of disturbance the specimen trimming techniques were modified, after review of the first series of tests indicated significant disturbance.

Table 3-4. Summary of Consolidation Test Results

Specimen Number	Depth (ft)	Depth (m)	$w_n$ (%)	$e_o$	$C_c$	$C_r$
1-1	10	3.05	19.1	0.70	0.25	0.04
2-1	15	4.57	20.0	0.73	0.26	0.03
2-2	16	4.88	20.0	0.73	0.26	0.03
3-1	20	6.09	19.5	0.72	0.31	0.02
4-1	25	7.61	18.0	0.74	0.24	0.05
4-2	26	7.92	17.8	0.73	0.30	--
4-3	27	8.22	19.0	0.71	0.35	--
5-1	30	9.14	18.6	0.71	0.20	0.04
6-1	35	10.66	18.4	0.83	0.19	0.02
7-1	40	12.19	14.2	0.63	0.15	0.03
7-2	41	12.50	17.3	0.74	0.28	--
7-3	42	12.80	18.0	0.71	0.27	0.06
8-1	45	13.72	18.2	0.68	0.41	0.04
9-1	50	15.24	14.7	0.67	0.26	0.01

Notes: Depths are only approximate.  
Individual  $e_o$ - $\log \sigma_{vo}$ ' curves given in Appendix B.

Each of the specimens were sawed from the end of the Shelby tube samples, with the tube section remaining intact around the specimen. The specimens were designated by a sample number, indicating which of the Shelby tube samples they were cut from, and a specimen number, to distinguish between specimens cut from the same tube. After cutting, specimens were sealed until they could be tested.

Method 1. In the first series of testing, nine of the specimens were trimmed by extruding them from the tube section. These were carefully pushed into a consolidometer ring with a cutting edge, while trimming excess away from the edges. After completing these tests, and reviewing the results, it was apparent that the samples had been disturbed, and that interpretation of the results would be difficult.

Method 2. One specimen (Sample 4, Specimen 2) was then prepared by sawing the end from the Shelby tube, allowing the specimen to remain inside the tube section. The specimen was then placed in a cell to allow it to be saturated, while loading using a Conbel



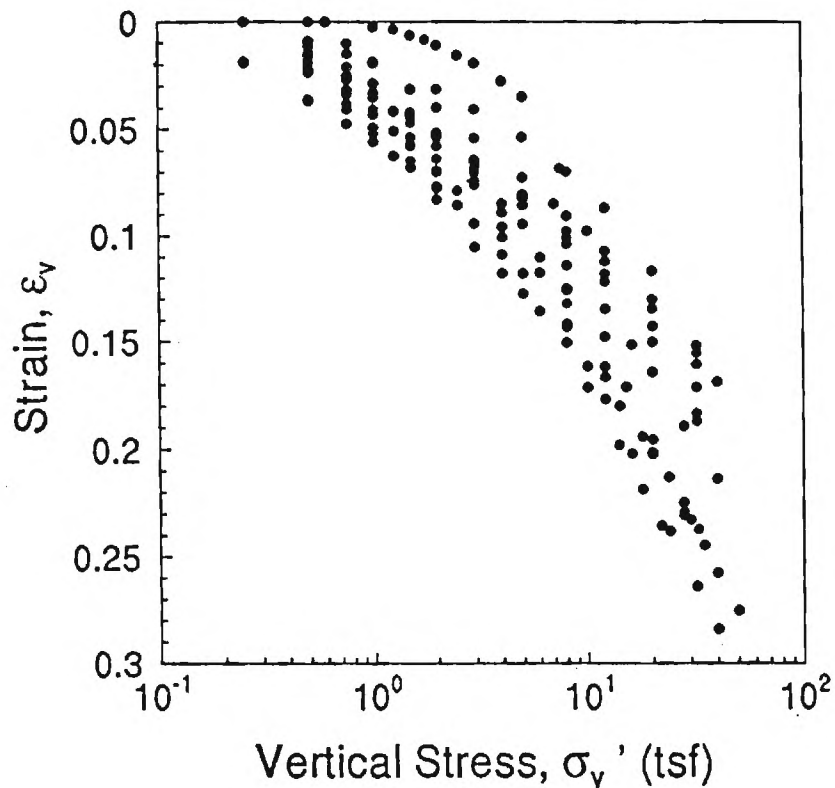


Figure 3-16. Summary Graph of Consolidation Test Results.

pneumatic consolidometer. The results of this test appeared promising, however, the stiffness of the tube section was not considered adequate. ASTM D-2435 requires that lateral strain of the sample remain less than 3 percent. Without measuring lateral strains, or adding a stiffener to the tube, the results should be considered questionable.

Method 3. An additional four specimens (1-1, 4-3, 7-2, 7-3) were trimmed by slowly extruding the specimen, and gently pressing the consolidometer ring into the soil as it exited the tube, preventing much of the expansion that occurred in the previous tests. Specimens trimmed in this manner in general appeared to show less disturbance, except in one case.

Figure 3-16 presents a summary graph for all fourteen tests in terms of vertical strain ( $\epsilon_v$ ) vs.  $\log \sigma_{v0}'$ , indicating the relative uniformity of compressibility characteristics of the Piedmont silty sands. A listing of the individual consolidation tests and derived parameters measured in the tests is given in Table 3-4. The mean value of natural water content ( $w_n$ )

was determined to be 18.1 percent and initial void ratio ( $e_0$ ) averaged 0.716. The virgin compression index ( $C_c$ ) averaged 0.267 and mean value of swelling index ( $C_s$ ) from an unload-reload cycle was 0.034.

Most of the void ratio curves were so highly affected by sample disturbance that a clear determination of a preconsolidation stress ( $\sigma_p'$ ) was very difficult. Eight different methods were used to interpret a yield stress from the test data (Table 3-5).

Table 3-5. Different Procedures for Defining Yield Stress from Consolidation Data

Reference	Graphical Construction
1. Casagrande (1936)	$e$ vs. $\log \sigma_v'$
2. Schmertmann (1955)	reconstructed $e$ vs. $\log \sigma_v'$
3. Sowers (1979)	$e$ vs. $\log \sigma_v'$
4. Janbu (1963); Crawford (1986)	constrained modulus vs. $\sigma_v'$
5. Jamiolkowski & Marchetti (1969)	$\log(M)$ vs. $\log \sigma_v'$
6. Butterfield (1979)	$\log$ specific volume vs. $\log \sigma_v'$
7. Holtz & Kovacs (1981)	reconstructed $\epsilon_v$ vs. $\log \sigma_v'$
8. Becker, et al. (1987)	work energy method

The results of these interpretations varied widely, and in many instances, a clear delineation of  $\sigma_p'$  was not possible. The values estimated using the methods of Becker, et al. (1987) and Holtz and Kovacs (1981) appeared to be the most credible and consistent. Further discussion of yield stresses is given in Section 6.13 of this report.

### 3.3.4 Mineralogy

X-ray mineralogy testing was performed on nine specimens of silty sand taken from the site. An analysis of the results indicate that the predominant mineral is quartz (40 to 55 percent), with varying amounts of feldspar (10 to 20 percent), mica (25 to 30 percent), and kaolinite (5 to 20 percent). Piedmont residual soils are also known to have trace amounts of iron-oxides which give the material a red-orange color.

### 3.4 SUMMARY

A proper evaluation of the results of the load tests required a complete characterization of the engineering properties of the soils that influence drilled shaft behavior. Such characterization of the Piedmont soils is difficult because of the poor understanding of residual soils and their relationship to traditional soil mechanics principles. An ambitious site characterization phase was therefore included in the ADSC/ASCE load test program.

The site characterization included sampling and in-situ tests such as the standard penetration test (SPT), dilatometer test (DMT), pressuremeter test (PMT), cone penetrometer test (CPT), and the spectral analysis of surface waves (SASW). Laboratory testing was performed on recovered samples and included: grain size distributions, index properties, mineralogy, triaxial shear tests, and one-dimensional consolidation tests. The test procedures, equipment, and summary of results have been discussed in this section of the report. Specific data from individual tests are given in the appendices.

## CHAPTER 4

### 4.0 FOUNDATION LOAD TEST PROGRAM

#### 4.1 SYNOPSIS

The load test program consisted of axial compression tests of two 76.2 cm (30 in.) diameter drilled shafts: one a 16.8 m (55.5 ft.) long "floating" shaft, and the other, an end-bearing shaft with a length of 21.4 m (70.2 ft.). In addition, a deep plate load test was performed at a depth of 19.6 m (64.4 ft.) on a 76 mm (3 in.) thick, 610 mm (24 in.) diameter steel plate. Excavation and construction required for the load tests were performed by members of the Southeastern Chapter of the International Association of Foundation Drillers (ADSC). The load testing was performed using a calibrated 9 MN (1000 ton) hydraulic jack, and a reaction system composed of a steel beam and three 122 cm (48 in.) diameter reaction shafts. In the plate load test, a steel column was placed in the shaft excavation to transfer load from the jack at the surface, to the plate at the bottom of the excavation. A description of the procedures used in this program follows.

#### 4.2 LOAD TEST PROGRAM

The scope and layout of the foundation load tests was developed by the ADSC/ASCE load test committee with the goal of quantifying the magnitudes and proportions of side and base resistance. Originally, the program was to consist of five load tests on shafts constructed in various configurations. However, the scope of the load test had to be reduced due to time constraints associated with use of the project site, as well as budget limitations.

Use of the load test site was made possible by the Georgia Tech Office of Campus Planning and Landscape Architecture. The site was made available with an agreement that the load test program would be completed in time for the scheduled start of construction of a new residence hall on the site. In addition, the site was to be regraded after the load test, and the upper portion of the shafts were to be removed, so as not to interfere with the proposed new construction. Consequently, a deadline of June 1, 1992 was established for completion of all field work.

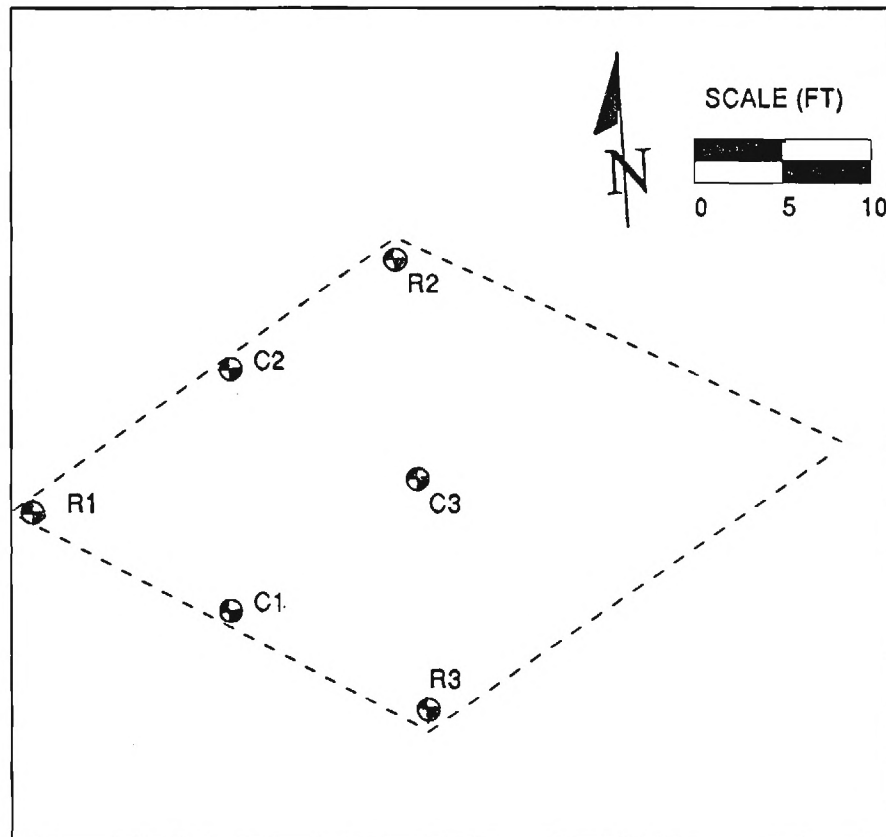


Figure 4-1. Layout of Foundation Load Test Program.

In order to perform the program within the allocated time and budget, the original scope was shortened to include only two drilled shaft load tests and the deep plate load test. According to the revised scope, one of the drilled shafts was constructed to bear on rock and was designated test shaft C1. The depth to rock was defined as the refusal depth encountered by the CME 550 drill rig used for standard penetration testing at that particular location. The second shaft was constructed entirely within the residual soil profile and designated as test shaft C2. The deep plate load test was conducted on partially weathered rock and designated test C3. Locations of the test shafts (C1 and C2), plate load test (C3), and reaction shafts (R1, R2 and R3) are shown on Figure 4-1.

### 4.3 CONSTRUCTION OPERATIONS

A Hughes LDH auger rig was used to excavate each shaft, and construction began on May 11, 1992. Both test shafts (C1 and C2) were excavated using earth augers only. The reaction shafts (R1, R2, and R3) were constructed using earth augers until partially weathered rock was encountered, whereupon rock augers were then used for further advancement. Table 4-1 provides the details concerning the construction of each shaft. At some locations, excavation through the surface fill and debris was difficult, with large boulders and concrete falling from the sides of the hole to the bottom of the hole. Temporary steel casing was installed in the top 5 to 6 m (17 to 20 ft.) of the reaction shafts, and within 15.8 m (52 ft.) of the ground surface in the plate load test excavation, to prevent sloughing of the sides of the holes. Temporary casing was not used during construction of shafts C1 and C2.

Table 4.1 Summary of Shaft Construction Operations

No.	Date of Construction & Completion	Temp. Casing		Fdn. Dimensions		Auger Type	Final Rate (in/min)	Concrete Slump (in)
		Diam. (in)	Length (feet)	Diam. (in)	Length (feet)			
R-2	5/11/92	60	17.0	48	68.0	RA	1.7	6.0
R-1	5/11,12/92	54	20.5	48	65.5	RA	0.0	6.5
C-1	5/12/92	--	----	30	70.2	EA	6.0	5.0
R-3	5/12,13/92	54	17.7	48	72.9	RA	5.0	5.0
C-2	5/13/92	--	----	30	55.5	EA	0.8	6.5
C-3	5/13/92	36*	24*	24	64.4**	EA	2.0	N.A.
		30*	52*					

Notes: RA denotes rock auger.  
 EA denotes earth auger.  
 C-3 is 76 mm (3 in) thick steel plate for deep plate load test.  
 \* Two lengths and sizes of temporary casing used for test C-3.  
 \*\*Depth of deep plate load test.  
 Units conversions: 1 in = 25.4 mm; 1 ft = 0.305 m.

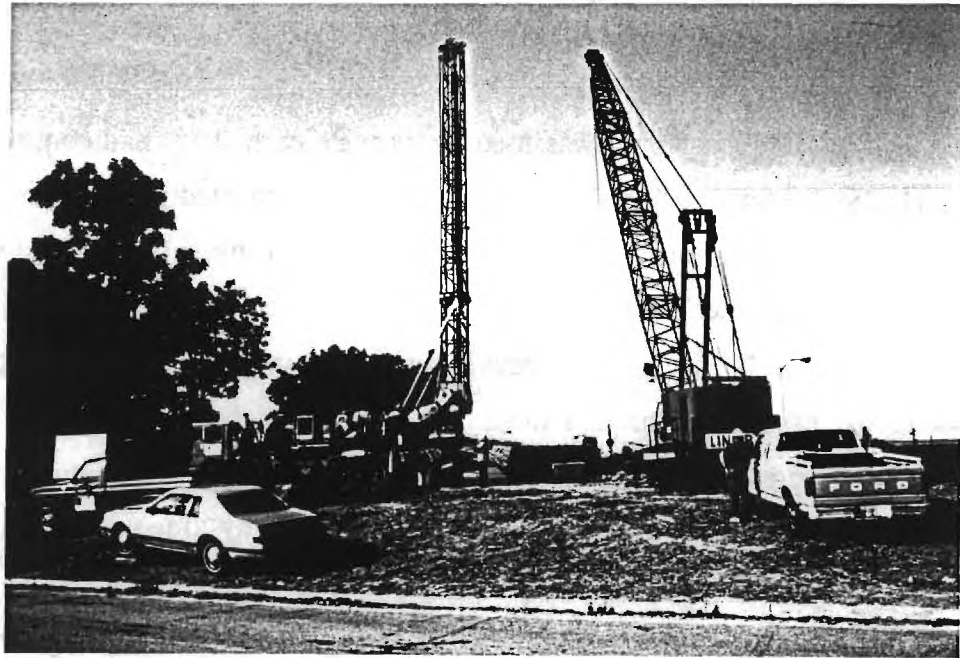


Figure 4-2. Hughes LDH Drill Rig During Shaft Construction at the Site.

When the excavation neared the groundwater level, the advance of the auger was temporarily halted, until concrete arrived at the site. With the arrival of concrete, the excavation proceeded until reaching the pre-selected depth or refusal criteria. The bottom of each of the test shafts was machine cleaned, before lowering the reinforcing steel cage. Figure 4-2 shows a photograph of the drilling rig in operation at the test site.

When the steel cages had been properly positioned, concrete was allowed to free fall into the shaft excavations, though hand shovels were used to guide the flow, and to minimize the amount of concrete striking the reinforcing steel or the sides of the excavation. Slump tests were made from each concrete truck arriving at the site and concrete cylinders cast. Compression tests were performed on the cylinders to monitor the strength of the concrete

and to determine when load testing could begin. Concrete testing is described in more detail in Appendix C.

After excavating for the plate load test, and setting the steel plate and column, progress was interrupted due to operational problems, and the load test could not be resumed until 6 days later. The problems centered around non-matching threads between dywidag bars and the reaction frame. The plate and column remained in the open excavation during this time, whereby exposure to air and water resulted in extensive deterioration of the partially weathered rock.

The upper 5 to 6 m (17 to 20 ft.) of the reaction shafts were not concreted since the concrete would have to be removed after completion of the load test due to the regrading requirement. The casing inserted during excavation was left in place, until load testing was completed. A reinforcing cage of dywidag bars was embedded in the concrete, and extended above the ground surface, for connection to the load test beam.

Reinforcing steel used in construction of the drilled shafts consisted of 15 No. 11 bars in the 122 cm (48 in.) diameter reaction shafts and 8 No. 9 bars in the 76.2 cm (30 in.) diameter test shafts.

#### 4.4 LOAD TEST EQUIPMENT

The load tests were performed by using a hydraulic jack which was placed on top of the test shafts and jacked against a steel beam. The beam was fixed at the ends by using high grade steel dywidag bars to attach it to the reaction shafts. The load test beam and the hydraulic jack were loaned to the project by the Long Foundation Company of Nashville, Tennessee.

The load test beam was a composite beam specially fabricated for use in load testing of drilled shaft foundations. The beam measured 10.4 m (34.0 ft) in length, with a width of 1.7 m (5.6 ft) and a height of 1.9 m (5.6 ft). The hydraulic jack had a maximum rated capacity of 17.8 MN (2000 tons) and had been calibrated approximately 8 months prior to the load test. Figure 4-3 shows a photograph of the assembled load test system in operation at the Georgia Tech site.



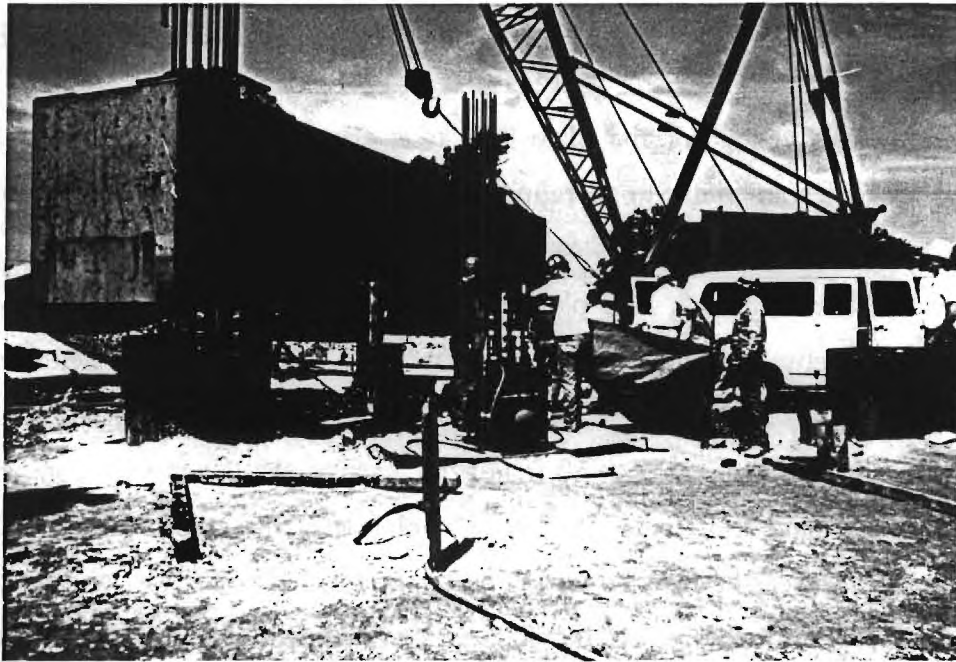


Figure 4-3. Load Test Frame Set-up and Reaction System.

#### 4.5 INSTRUMENTATION

Instrumentation devices included in the load test program were used to measure axial loads at various depths in the shafts and to measure deflections of the test shafts. These included dial gauges, engineer scales, and tell-tales for measuring deflection, and vibrating wire strain gauges for measuring axial load distribution in the shafts. Strain gauge measurements were made in the two test shafts (C1 and C2) and in two of the reaction shafts (R1 and R3). Each of the three reaction shafts were used in two of the load tests. For reaction shaft R3, the strain gauge measurements were obtained in two tests. Tip and butt deflections were measured during load testing of both of the test shafts. Butt deflections of the reaction shafts were also measured.

#### 4.5.1 Strain Gauge Measurements

The strain gauges used for measuring axial load transfer in the shafts were vibrating wire strain gauges manufactured by the Slope Indicator Co. The strain gauges utilize a vibrating wire enclosed in a steel tube, attached to a thin, flat piece of steel which is welded to a specially prepared section of the reinforcing steel. The period of vibration varies with the square root of the length of wire. Thus, any change in length of the reinforcing steel is reflected in a change in period. Strain measurements can be converted to axial load, if the moduli of elasticity of the concrete and steel are known. Procedures for calculating strain and axial load are discussed in more detail in Chapter 5.

A pickup sensor, placed on the strain gauge, induces oscillation, and measures the period of the vibrating wire. The sensor is connected to an indicator box at the surface with an LCD display. The indicator box allows the user to select output consisting of either direct strain readings, or period measurements. Instructions provided by the Slope Indicator Co. indicate that period readings should be used for higher accuracy. Temperature readings can also be made with the indicator box to correct for thermal strain effects.

To install the gauges on the reinforcing steel, the gauge locations were prepared by using a power grinder to prepare a flat surface, and then hand filing and sanding the area until it was smooth. After cleaning the surface with alcohol, the strain gauges were then spot welded to the reinforcing steel. Welding was accomplished using a battery operated portable strain gauge welding/soldering unit manufactured by Measurements Group. Welding of the gauges requires an energy of approximately 40 joules (29 ft-lbs). After each gauge was spot welded on the reinforcing steel, the pickup sensor was positioned over it, and then strapped in place using plastic ties. The Slope Indicator Company recommends that the pickup sensors be strapped to the steel using thin metal straps which are welded to the steel. However to weld these, all contact points must be prepared by grinding and sanding. Instead, the plastic ties were used to save time and these performed well with the modified installation.

After securing the pickup sensor with the plastic ties, epoxy was used to seal the gaps between the edge of the sensor and the reinforcing steel, and to prevent water from entering

and corroding the strain gauge. After the epoxy was allowed to cure, the unit was then wrapped several times with friction tape and duct tape.

Vibrating wire gauges were placed at the butt and base of each test shaft, at mid-depth of shaft C2, and two intermediate depths in shaft C1. Gauges were placed at the top to allow correlation with the pressures on the hydraulic jack, since the axial load and the jack load should be approximately equal at this point. In shaft C1, the remaining gauges were placed at 9.1, 16.8, and 21.3 m (30, 55, and 70 ft) below ground. In shaft C2, the gauges were placed at 9.1 and 16.8 m (30 and 55 ft) below ground. These depths were chosen in order to separate the side resistance from regions with different N-value ranges, and to separate the effects of partially weathered rock from those of the soil. Four gauges were placed at each depth for redundancy. Figure 4-4 shows a generalized residual soil profile and representation of the test shafts and strain gauge configuration.

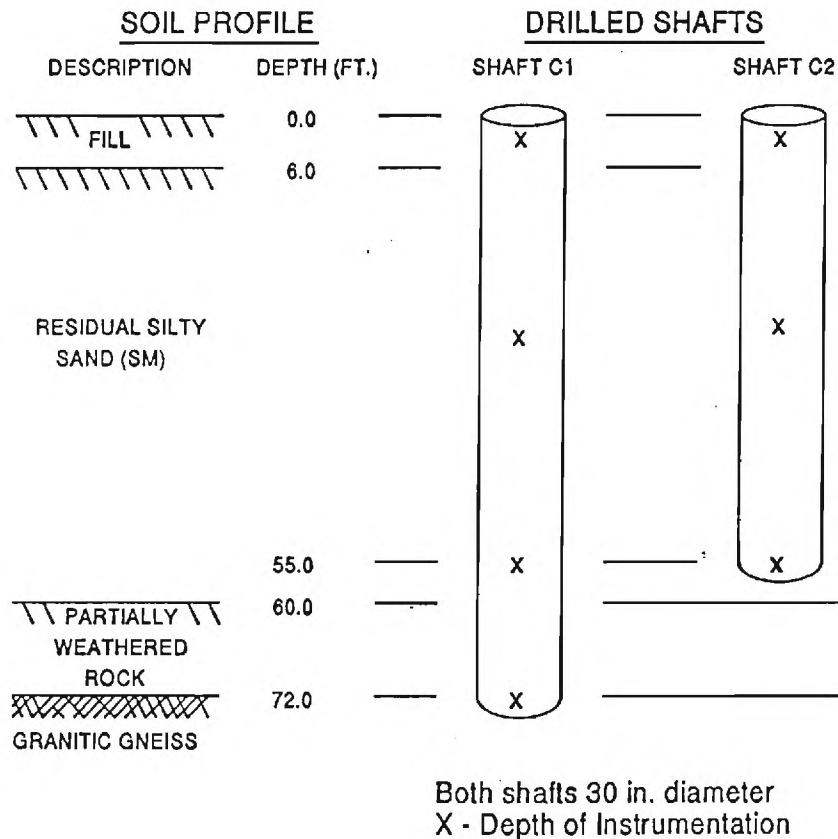


Figure 4.4 Profile of Residual Soil Conditions and Test Shafts.

#### 4.5.2 Butt Displacements

Displacements at the tops of the test shafts, reaction shafts, and steel column (plate load test) were measured using dial gauges fixed to the top of the shaft and marked scales fixed to the hydraulic jack. For the test shafts, four separate measurements of the butt deflection were made: two dial gauges and two scales, each read by separate methods.

The two dial gauges were clamped to immobile reference beams mounted adjacent to the test shafts, and were used to measure deflection at the top of the shaft. The reference beams were shielded from sunlight using tarps stretched from the load test beam. This was done to limit warping of the beams from temperature changes. The resolution of the dial gauges permitted them to be read within 0.03 mm (0.001 in). Scales were mounted on the hydraulic jack by first taping a small mirror to the jack, and then mounting the scale on the mirror. A taut wire was stretched in front of the scale to read the displacement. The mirror was used to help ensure that the scale was read directly, without peering down or up the scale, and making inconsistent readings. Scales were also attached to the dywidag bars extending from one of the reaction shafts during each load test. These scales and an additional scale on the jack were read using an engineer's level.

#### 4.5.3 Tip Displacements

Tip displacements of the test shafts (C1 and C2) were measured using a tell-tale system made by casting a 2.5 cm (1 in.) diameter PVC pipe to the shaft base within the concrete during construction. In the deep plate load test (C3), the pipe was placed in the open excavation, and fixed to the steel column to prevent swaying. A metal rod, equal to the length of the shaft was placed in the pipe, and the dial gage was used to measure the movement of this rod, which was assumed to be equal to the tip displacement.

### 4.6 LOAD APPLICATION PROCEDURES

The loading of the drilled shafts followed a quick loading procedure, similar to the guidelines recommended by ASTM D-1143. Using this procedure, the shaft is loaded in

equal increments, usually equal to 10 to 15 percent of the proposed design load, or anticipated failure load, and each load is maintained for a minimal period of time, generally about 2.5 minutes. In this program, shaft displacement readings were made immediately upon reaching each load level, and again after a period of stabilization, during which time, readings from the vibrating wire gauges were taken. The time required to read all of the vibrating wire gauges varied from about 3 to 5 minutes. After completion of all readings and the second reading of the shaft displacement, the load on the shaft was then increased to the next load level.

For this load test program, an initial load increment of 220 kN (25 tons) was used to apply a seating load to each of the two drilled shafts. After removing this seating load, increments of 890 kN (100 tons) were applied to shaft C1 during testing and increments of 445 kN (50 tons) were applied to shaft C2. Two unload-reload loops were included in each of the load tests. An initial seating load of 668 kN (75 tons) was used for the plate.

#### 4.7 SUMMARY

The scope of the load test was developed by a joint committee of local ADSC/ASCE members to evaluate the performance of drilled shafts in the Piedmont. The load test program included axial compression tests of two drilled shafts: (1) an end-bearing shaft constructed so as to bear on rock; and (2) a floating shaft constructed entirely within the residual soil profile. The program also included a deep plate load test performed on partially weathered rock. The test shafts and plate were loaded using a calibrated 8.9 MN (1000 ton) capacity hydraulic jack and a steel reaction beam. The reaction system also included a set of three embedded drilled shafts to anchor the load test beam.

The drilled shafts were instrumented to measure tip and butt displacements, as well as axial load at several depths within the shaft. This instrumentation included dial gauges, marked scales, telltales, and vibrating wire strain gauges which were embedded within the concrete. Load testing was performed using a quick loading procedure as recommended in ASTM D-1143.

## CHAPTER 5

### 5.0 LOAD TEST RESULTS

The results of the ADSC/ASCE field load test program on axially-loaded drilled shafts are presented in this chapter and include the following: (1) load-displacement measurements at the butt, (2) discussion of the axial capacity of the shafts under compression loading, and (3) load-transfer distributions obtained using the measurements from vibrating wire strain gauges and tell-tales.

#### 5.1 LOAD-DISPLACEMENT RESPONSE

The load-displacement response was obtained at the butt (top) of each shaft during incremental axial compression loading. The axial loads were measured from pressure gauge readings taken on the calibrated hydraulic jack. Deflections were obtained from four independent displacement readings using dial gauges and marked scales fixed to the butt of the shaft and hydraulic jack. The equipment and instrumentation were discussed in detail in Chapter 4.

Displacement readings were taken twice at each load level: one reading was made immediately after application of the load increments and a second reading taken after a stabilization period, during which time readings from the vibrating wire strain gauges were also obtained. Since the time period between the two sets of readings was variable, the first set of readings were used for load-displacement responses of the two drilled shafts. Appendix A contains the tabulated load and dial gauge readings from each of the load tests.

##### 5.1.1 End-Bearing Shaft C1

The load-displacement response for the 21.4 m (70.2 ft) long end bearing shaft (C1) is shown in Figure 5-1. The figure shows four load-displacement curves: two from the separate dial gauges attached to the top of the shaft but on opposite sides; one from a scale attached to the jack, which was read using a taut wire stretched across the face of the scale;

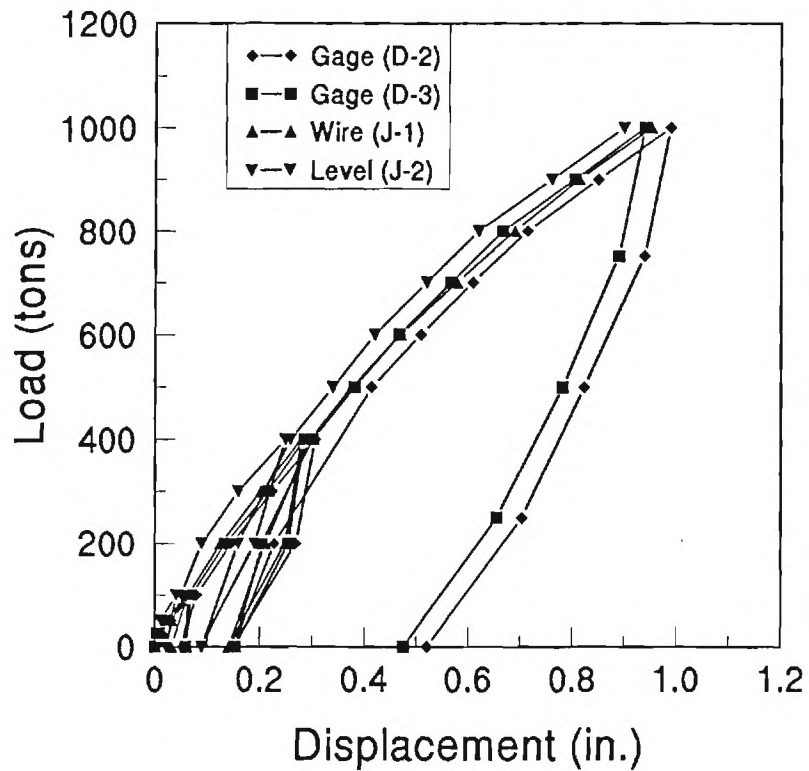


Figure 5-1. Axial Load-Displacement Response for End-Bearing Shaft C1.

and one scale attached to the jack read using a survey level. The maximum difference in settlements obtained by the four readings was typically less than 2.5 mm (0.1 in.).

The initial loading curves are nonlinear. Note also the two unload-reload loops performed at load levels of 0.9 and 3.6 MN (100 tons and 400 tons) during the test. A maximum settlement of 2.56 cm (1.010 in.) was reached at a load of 8.9 MN (1000 tons). Loading of the shaft was then halted, since the maximum capacity of the jack had been reached. The shaft was subsequently unloaded in increments, with a permanent residual settlement of 1.288 cm (0.507 in.) remaining after all of the load was removed.

### 5.1.2 Floating Shaft C2

Figure 5-2 shows the load-displacement response from the 16.9 m (55.5 ft.) long floating pile (Shaft C2). The shaft was loaded to a maximum load of 4.5 MN (500 tons),

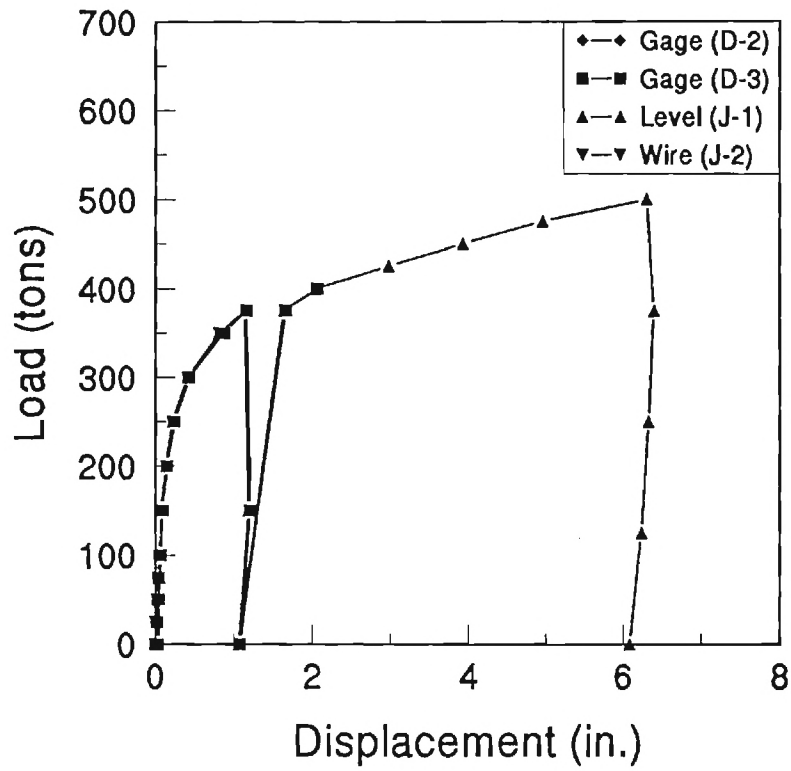


Figure 5-2. Full Range of Axial Load-Displacement Response for Floating Shaft C2.

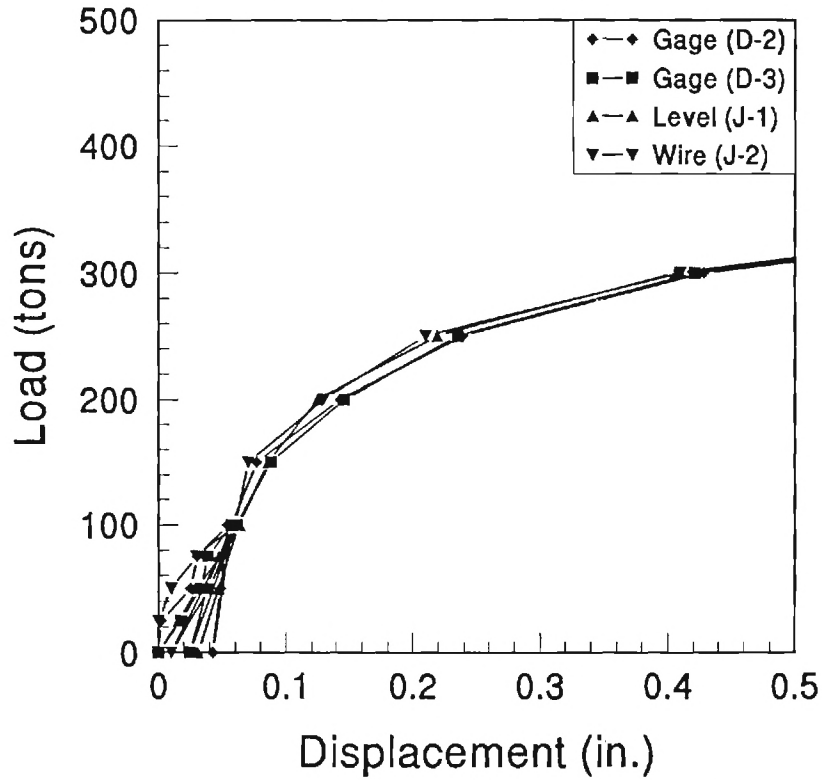


Figure 5-3. Low Range of Axial Load-Displacement Response for Floating Shaft C2.



where loading was halted, due to inability to maintain pressure by the hydraulic jack. A maximum butt settlement of 16.38 cm (6.45 in.) was recorded at this load.

Four measurements were also made of the load-displacement behavior of this shaft also, although it is difficult to distinguish each in Figure 5-2. Two unload-reload loops were performed during the load test at load levels of 0.9 and 3.3 MN (100 tons and 375 tons). An expanded load-displacement response has been presented in Figure 5-3 to show more detail of the early stages of the load test. This figure shows typical differences between individual measurements on the order of 2.5 mm (0.1 in.), as in shaft C1. After shaft C2 was unloaded, a residual settlement of 2.4 cm (6.1 in.) was recorded.

### 5.1.3 Deep Plate Load Test

Load-displacement readings from the deep plate load test (Test C3) are presented in tabular form in Appendix A. The large deflections recorded were difficult to measure accurately with the equipment and monitoring devices on site. The success of this test was severely hampered by the fact that the steel column and plate sat out for a week in the open cased hole because of unmatched treads on the dwidag bars and reaction frame. Consequently, the partially-weathered rock had deteriorated and softened appreciably due to exposure to air and water upon excavation.

### 5.1.4 Interpretation of Axial Capacity

The purpose of a load test is to determine the capacity or maximum load that can be sustained by the particular element in question. In the analysis of deep foundations, there are a variety of different criteria for defining axial capacity or failure load. Fellenius (1975, 1978, 1980) and Kulhawy and Hiraney (1988) review a number of these criteria with over 41 different methods having been proposed by building codes, researchers, and practitioners. In general, the methods are based either on a settlement limitation, graphical construction technique, or fit to a specific mathematical model. Table 5-1 lists a few of the common criteria.

Each of the methods in Table 5-1 rely on assumptions about the load-displacement behavior or the shape of the load-displacement curve. For example, the method of Chin (1970) fits the load test data to a hyperbola. Interpreted failure loads will therefore differ for each method. Fellenius (1978) suggests that several methods be used to evaluate the results of a load test, rather than selecting a single criterion. Within U.S. practice, perhaps the Davisson (1972) offset line method is the most widely used.

Table 5-1. Methods of Interpreting Axial Capacity For Shafts.

- 
1. Vander Veen (1953).
  2. Hansen (90%) (1963).
  3. Hansen (80%) (1963).
  4. De Beer (1967).
  5. Chin (1970).
  6. Fuller and Hoy (1970).
  7. Mazurkiewicz (1972).
  8. Davisson (1972).
  9. Butler and Hoy (1977).
- 

Each of the nine methods above was applied to the results of the ASCE/ADSC drilled shaft load tests. For shaft C1, most of the methods did not clearly define that a failure load had been reached. The Davisson method indicated that failure of C1 was imminent and would have occurred at a projected load of only about 9.3 MN (1050 tons). When these methods above were applied to the data from shaft C2, interpreted failure loads ranged from 2.2 to 5.1 MN (251 to 574 tons). Figure 5-4 shows a summary load-displacement curve generated for shaft C2 by averaging the four displacement readings. Interpreted failure loads from each of the methods are indicated on the figure. The average of the nine interpreted failure loads was 3.2 MN (360 tons), close to the point on the curve where the behavior apparently changes from primarily elastic to plastic behavior. The Davisson offset line, used by many state transportation departments, indicates an axial capacity of 2.7 MN (312 tons), just below the average failure load. The most conservative value was 2.2 MN (251 tons), arrived at using the graphical method by DeBeer. Using the Chin method, a failure load of 5.2 MN (574 tons) was interpreted.

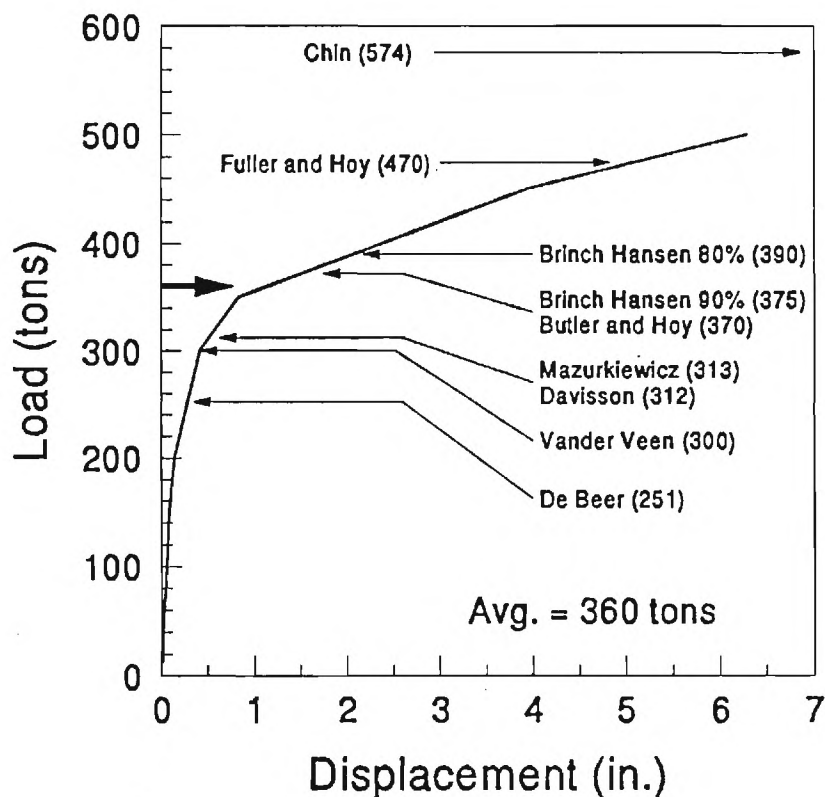


Figure 5-4. Different Interpreted Failure Capacities for Shaft C2.

Considering the average capacity interpretation at 3.2 MN (360 tons) and the apparent change in behavior occurring after 25 mm displacement (1 in), the ultimate capacity has henceforth been taken to be 3.1 MN (350 tons).

## 5.2 LOAD TRANSFER DISTRIBUTIONS

Load transfer distributions were obtained by measuring strains at several depth levels along the shaft length. The difference in magnitude between two axial load measurements from successive depths along the shaft indicates the amount of the shaft load carried by side resistance over that depth interval. Axial load measurements were made at each instrumented depth for selected load increments during each of the load tests.

The axial load was measured using the vibrating wire strain gauges which were welded to the reinforcing steel, and embedded in the concrete of each test shaft. Output

from the strain gauges consisted of period readings, representing the period of oscillation of the vibrating wire contained in the strain gauge. Each period reading was converted to a strain reading, representing the axial strain at that depth within the drilled shaft. Using this measured value of axial strain, the modulus of elasticity of the reinforcing steel and value of concrete modulus, the axial load at that gauge location depth was computed. The values from each gauge at the same depth were then averaged to determine the axial load for that depth. The gauges at the top of the shaft were related to the magnitudes of applied loads and used as reference values for the lower gauges. Differences between the individual gauges were usually small and only 3 of the 60 gauges failed to perform. Period readings and measurements are included in Appendix A.

### 5.2.1 Load Distribution Curves

The average transferred axial loads for shaft C1 are summarized in Figure 5-5. The difference in measurements at successive depths is indicative of the magnitude of the side resistance occurring within that depth range. Review of Figure 5-5 reveals that a majority of the load transfer for the end-bearing shaft C1 occurs along a section from depths between 16.8 to 21.4 m (55 to 70 ft). This corresponds to the zone where partially weathered rock was encountered at this shaft location. In contrast, Figure 5-6 shows the transferred load distribution for floating shaft C2. A relatively constant load transfer with depth is evident for shaft C2 which was constructed entirely within the soil profile, explaining the more constant distribution.

### 5.2.2 Shaft and Base Components

The vibrating wire measurements can also be used to determine the percentages of the total load carried by side and tip resistance, throughout the load test. The tip load was measured by the instrumentation at the bottom of the shaft, and can be subtracted from the total load to determine the portion carried by side resistance. Corresponding shaft displacements can be taken from the load-displacement results discussed previously, and the variation of the side and tip resistance with settlement can be plotted as function of butt

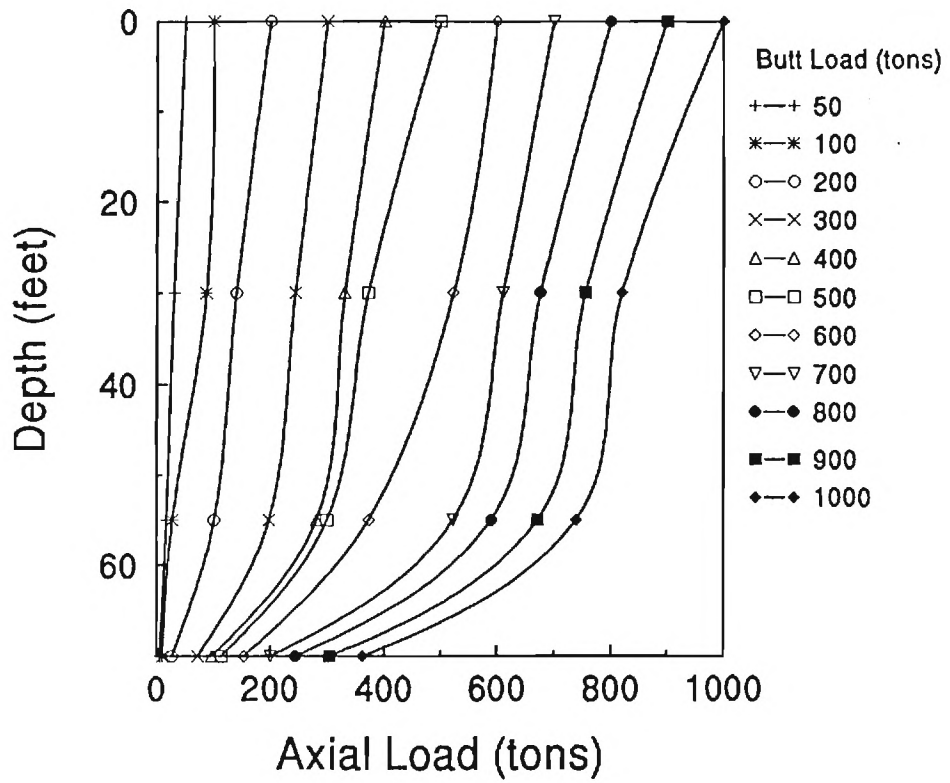


Figure 5-5. Axial Load Transfer Distribution for End-Bearing Shaft C1.

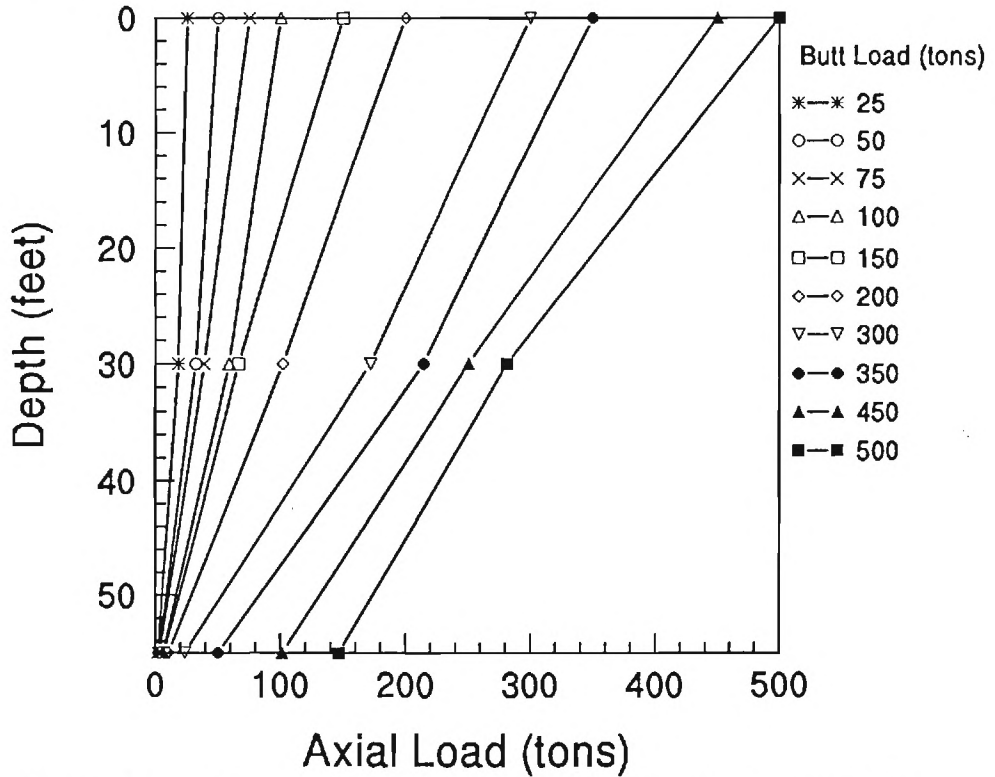


Figure 5-6. Axial Load Transfer Distribution for Floating Shaft C2.

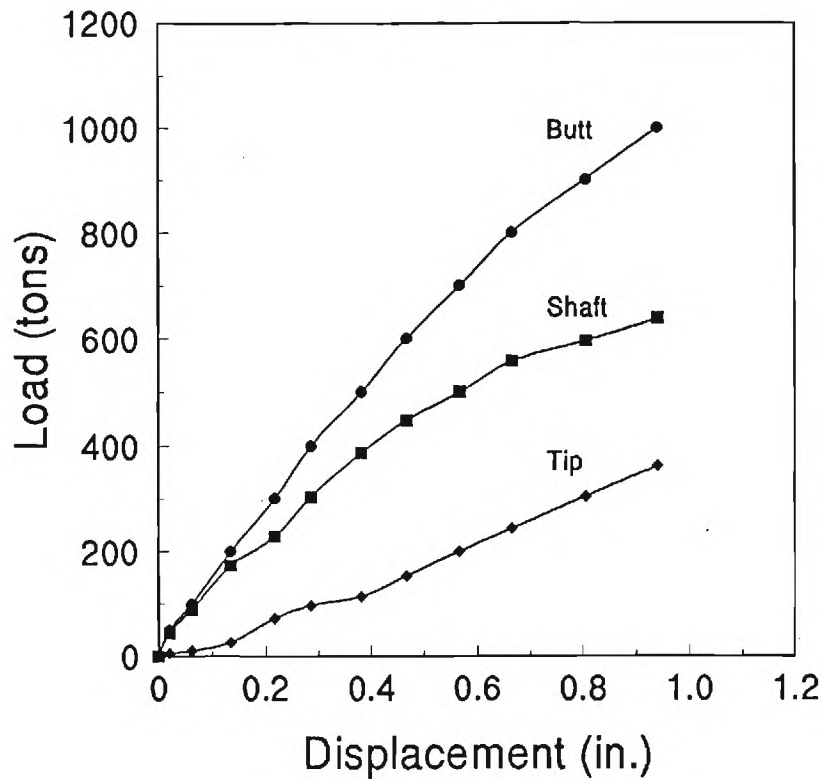


Figure 5-7. Components of Side and Base Capacity for End-Bearing Shaft C1.

deflection. The separate load components from end-bearing shaft C1 are shown in Figure 5-7, suggesting the test was not fully loaded to ultimate capacity. The shaft component curve shows indication that the side resistance component was nearly fully mobilized. The tip load shows no such indication of nearing a maximum value, however. At a butt deflection of 25 mm (1 in), the total load of 8.9 MN (1000 tons) was carried by 5.7 MN (650 tons) along the shaft and 3.2 MN (350 tons) in end-bearing.

In contrast, the results from floating shaft C2 are rather dramatic in comparison (see Figure 5-8). The shaft load component clearly reaches a plateau in the later stages of loading with no post peak softening observed. The tip resistance component curve continues to increase. At a reference butt displacement of 25 mm (1 in), the total axial load of 3.1 MN (350 tons) was carried by 2.7 MN (300 tons) in shaft capacity and 0.4 MN (50 tons) in end-bearing. For the final applied load of 4.4 MN (500 tons) corresponding to 165 mm (6.5 in) of deflection, the components of shaft and end-bearing were 3.1 MN (350 tons) and

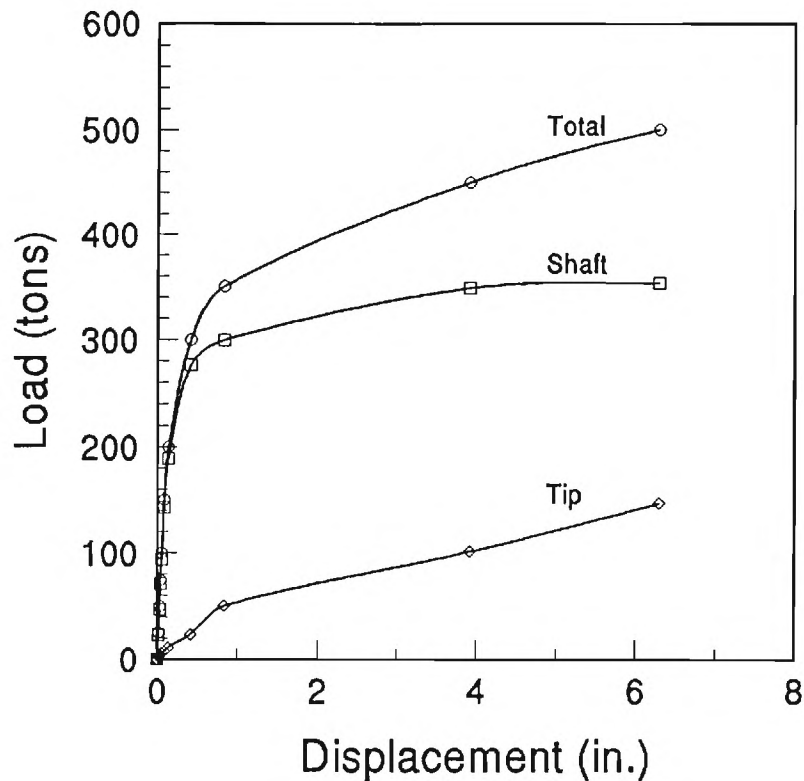


Figure 5-8. Components of Side and Base Capacity for Floating Shaft C2.

1.3 MN (150 tons), respectively. It is clear from Figures 5-7 and 5-8 that the majority of the shaft load was carried by side resistance. In shaft C1, 64 percent of the total load was carried by side resistance at the final load increment. In Shaft C2, approximately 85 percent of the total load was carried by side resistance at the Davisson limit, and at extreme displacements, about 70 percent of the axial load taken in side resistance.

The relative percentages of axial load carried by side resistance are higher at load levels which would be considered to be within the service load range. Typically, at service loads, corresponding to design load levels with factors of safety  $FS = 2$ , side resistance components typically carry 80 to 95 percent of the design loads in axial compression.

### 5.2.3 Tell-Tale Measurements

Instrumentation used in the load tests also included tell-tales mounted to measure displacement of the pile tip. Figures 5-9 and 5-10 show applied load vs. tip displacement

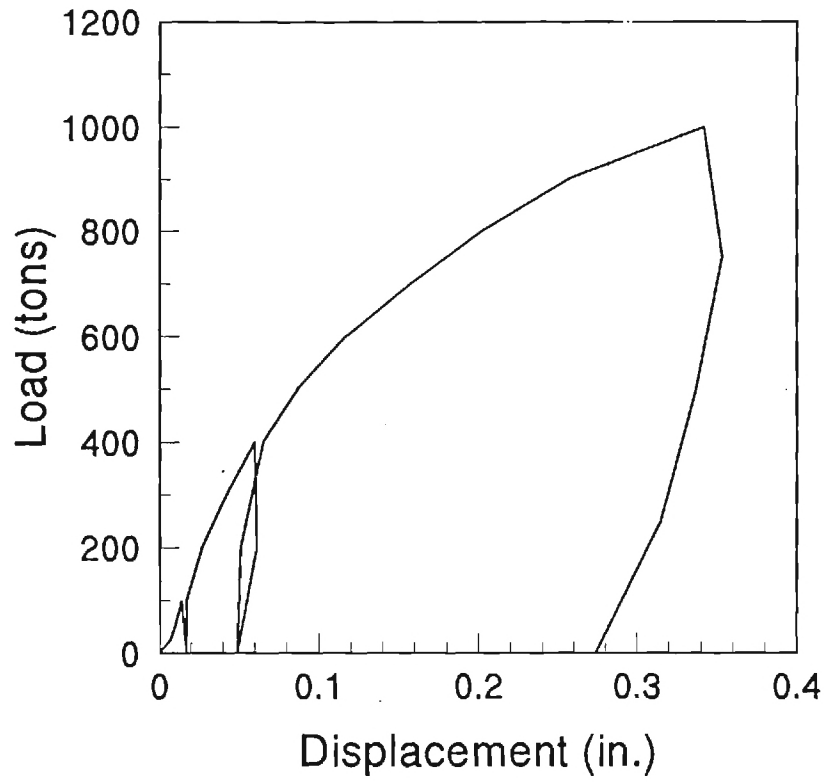


Figure 5-9. Applied Axial Load vs. Telltale Tip Displacement for Shaft C1.

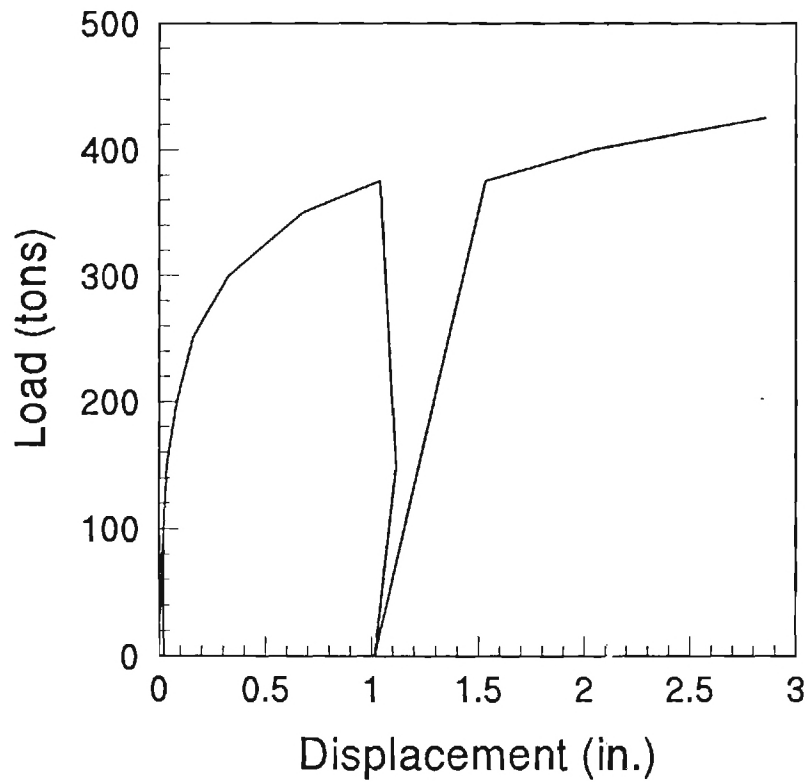


Figure 5-10. Applied Axial Load vs. Telltale Tip Displacement for Shaft C2.



curves from the tell-tales installed in shafts C1 and C2, respectively. Tell-tales are useful in evaluating the amount of pile compression that occurs between butt and base. Methods of estimating the load transfer components from tell-tale measurements are described by Fellenius (1978) and Leonards and Lovell (1979). For such an analysis, the relative side friction distributions contributed by overburden soil ( $f_{s1}$ ) and partially-weathered rock ( $f_{s2}$ ) must be assumed. If the unit side friction distributions are assumed to be uniform within each layer and in the ratio  $0.4 < (f_{s1}/f_{s2}) < 1.0$ , then the tell-tale data indicate 9 to 21 percent of the applied load is transferred to the tip. This interpretation seems consistent with the strain gauge data.

#### 5.2.4 Unit Side and Base Resistance

Using the load transfer distributions, unit side and base resistance components can be computed for shaft C2. Since shaft C1 could not be loaded to failure, ultimate values could not be determined, but maximum recorded unit side resistances can be obtained. Inspection of Figure 5-8 indicates that in the load test data of C2, after the load level reaches a value of 2.7 MN (300 tons), relatively little additional load is carried by side resistance, although increased loads are supported by the shaft. For shaft C2, an average side resistance of 66 kPa (0.7 tsf) was calculated over the total shaft area. In shaft C1, at the maximum total load of 8.9 MN (1000 tons), load transfer curves indicate that 2.9 MN (328 tons) was supported by side resistance in the residual soil and 2.6 MN (288 tons) was taken by the partially weathered rock. These values translate to average unit side resistances of 73 kPa (0.8 psf) for residual silty sand and 234 kPa (2.4 psf) for the partially weathered rock.

Full development of end-bearing resistance was apparently not achieved in either load test. At the maximum applied load of 8.9 MN (1000 tons) for testing of shaft C1, the end-bearing stress on partially-weathered rock was at least 7 MPa (71 tsf). For shaft C2, the measured end-bearing resistance in residual soil was 1 MPa (10 tsf) was recorded at movements of  $\delta = 25$  mm (1 in), corresponding to the interpreted failure. Subsequently, the end-bearing component increased upon additional loading to a final stress value of 3 MPa (30 tsf) at  $\delta = 165$  mm (6.5 in).

### 5.3 SUMMARY

Axial load compression tests were performed on two drilled shafts situated in the Piedmont. The load-displacement response of the end-bearing shaft (C1) showed no apparent ultimate capacity up to the final applied load of 8.9 MN (1000 tons) and corresponding butt displacement of 25 mm (1 in). The Davisson offset line method indicated a projected ultimate capacity of about 9.3 MN (1050 tons). A review of nine methods of interpreting failure from load tests results gave ultimate capacity estimates for the floating shaft (C2) ranging from 2.2 to 5.1 MN (251 to 574 tons), with an average of 3.2 MN (360 tons). This corresponded favorably with the Davisson offset line criterion. An ultimate capacity of 3.1 MN (350 tons) was adopted henceforth for analysis.

In the end-bearing shaft (C1), approximately 64 percent of the maximum applied load was shed in side friction and 36 percent of the applied load was transferred to the base. At the interpreted failure load of shaft C2, 85 percent of the load was supported by side resistance and only 15 percent transmitted to the tip. At a factor of safety of  $FS = 2$ , 92 percent of the total load was supported by side friction. Ultimate values of the unit side resistance ranged from  $f_s = 65$  kPa to 75 kPa (0.7 tsf to 0.8 tsf) in the residual soil. A maximum unit side resistance of  $f_s = 235$  kPa (2.4 tsf) was obtained in the partially weathered rock in shaft C1, although full mobilization of resistance may not have been achieved.

End-bearing resistances were apparently not fully-mobilized in either of the two shaft load tests. For the quick load test procedures, the floating shaft C2 gave an apparent undrained end-bearing resistance of  $q_{ult} = 1$  MPa (10 tsf) at failure loads corresponding to 25 mm (1 in) displacement. However, at much higher displacements, unit end-bearing values up to 3 MPa (3 tsf) were achieved. For the end-bearing shaft C1, applied unit stresses of 7 MPa (70 tsf) were attained in base resistance.

## CHAPTER 6

### 6.0 ULTIMATE CAPACITY IN AXIAL COMPRESSION

In a rational framework, the calculation of ultimate axial capacity of deep foundations relies heavily on a proper assessment of the strength properties and state of stress of the soil medium. For a total stress analyses, the evaluations of undrained shear strength ( $s_u$ ) and empirical  $\alpha$  factor are of interest, whilst effective stress analyses requires the determination of the effective friction angle ( $\phi'$ ) and lateral stress coefficient ( $K_o$ ). Alternatively, axial capacities can be calculated directly from test results using empirical methodologies that are based on back-figured load test data. These approaches are discussed in the section in concert with evaluations of axial capacities established by the two load tests reported herein.

### 6.1 SOIL PROPERTY CHARACTERIZATION

A major difficulty occurs in the interpretation of engineering properties from in-situ and laboratory test results of the Piedmont materials since they behave strictly neither as clay nor sand. Classical interpretation procedures routinely address a total stress approach for undrained behavior (i.e., clay) or an effective stress analysis with a purely drained and frictional response (i.e., sand). The very silty fine sands (SM) and fine sandy silts (ML) of the Piedmont exhibit certain aspects that are characteristic of both cohesive and cohesionless soils, and therefore, are somewhat confusing to describe using conventional geotechnical procedures.

Locally, in the Atlanta area, the soils are termed "Georgia Red Clay", even though laboratory index tests more often indicate the percent fines range from 30 to 70 percent and most of the fines are silt-size. Specifically, at the Georgia Tech site, the residual soils and partially-weathered rock material classify as silty sand, according to the Unified Soil Classification System. The consequence is that, in addition to the vagaries associated with soil classification, the determination and relevance of routine soil properties (i.e.,  $s_u$ ,  $K_o$ ,  $\phi'$ ,  $\sigma_p'$ , E) are also unclear. Discussion of these parameters is provided in the following paragraphs.

### 6.1.1 Soil Strength

The effects of partial drainage, rate effects, and partial saturation hinders the interpretation of strength test results on Piedmont soils. These uncertainties led Sowers and Richardson (1983) to evaluate both total and effective stress parameters from extensive triaxial tests on Piedmont silts for the Atlanta subway system. In partially-weathered rock material of the Piedmont, Gardner (1987) utilizes a classical  $s_u$  interpretation in an analysis of bearing capacity of drilled shaft foundations in this material. In contrast, data reduction of dilatometer results in the Atlanta Piedmont often interprets a drained effective  $\phi'$  in the Piedmont soils using the DILLY5 software.

The results of the in-situ and laboratory tests were used to calculate both drained and undrained parameters for analysis using conventional interpretative methods. Figure 6-1 shows the derived profiles of undrained shear strength ( $s_u$ ) from different tests. The value of  $s_u$  has been made dimensionless by normalization to atmospheric pressure ( $p_a$ ), so that units are not required. Note that  $p_a = 1 \text{ bar} \approx 1 \text{ tsf} \approx \text{kg/cm}^2 \approx 100 \text{ kPa}$ . For the

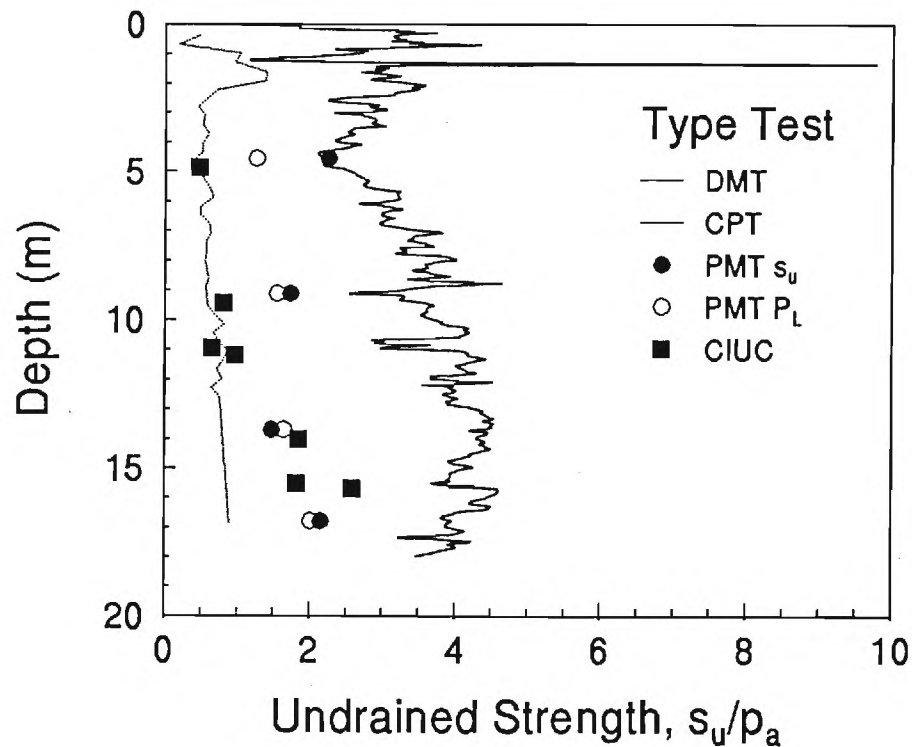


Figure 6-1. Interpreted Profiles of Undrained Shear Strength in Piedmont Residuum.

laboratory CIUC triaxial shear tests performed on saturated specimens of Piedmont residuum, the value of  $s_u$  has been interpreted as the maximum shear stress,  $q_{\max} = \frac{1}{2}(\sigma_1 - \sigma_3)$ , from stress-strain curves and/or q-p' plots. This interpretation appears consistent with values of  $s_u$  from two methods obtained with the PMTs in the residual soil: (1)  $s_u =$  slope of applied pressure vs.  $\log(\Delta V/V)$  as recommended by Wroth (1984); and (2)  $s_u = (p_L - p_{ho})/N_c$  where the bearing factor = 5.5 (Baguelin, et al. 1978). The CPT data has been used to determine a profile of undrained strength using the conventional expression (Robertson and Campanella, 1983):  $s_u = (q_c - \sigma_{vo})/15$ . Finally, Figure 6-1 shows an estimate of  $s_u$  from the DMT data via the empirical relationship given by Marchetti (1980):  $s_u/\sigma_{vo}' = 0.22(K_D/2)^{1.25}$ , although the measured  $I_D$  values are above the range for which the expression is claimed to be valid. Considering all four tests (TX, CPT, DMT, and PMT), the interpreted profile of  $s_u$  does not appear to be unique and consistent in the Piedmont soils at the ADSC/ASCE site.

The strength was also evaluated in terms of drained effective stress parameters ( $c'$  and  $\phi'$ ) from conventional Mohr-Coulomb interpretations. In this case, the CIUC triaxial tests determined the following average values:  $c' = 0$  and  $\phi' = 36.1^\circ$ . Figure 6-2 shows the profile of individual values of  $\phi'$  with depth from the specific triaxial specimens. These values appear consistent with the DMT evaluations of  $\phi'$  which are obtained using the DILLY5 program. Figure 6-2 also shows an evaluation using CPT data and the relationship given by Robertson and Campanella (1983) for clean sands:  $\phi' = \arctan[0.1 + 0.38 \log(q_c/\sigma_{vo}')] ]$ . In each case, reasonable agreement among the various tests is apparent.

The strength of Piedmont residuum appears dependent on strain rate effects. Total stress analyses give conflicting interpretations of  $s_u$  because different stress paths and rates of testing are followed by the various tests. Effective stress interpretations by several in-situ and lab tests apparently provide relatively consistent profiles of  $\phi'$ .

### 6.1.2 Effective Horizontal Stress

The in-situ effective horizontal stress ( $\sigma_{ho}'$ ) corresponds to a geostatic state of stress. Reference values are difficult to obtain, except via self-boring pressuremeter tests (SBPMT) or total stress cells (TSC). At the Georgia Tech site, pre-bored Menard-type PMTs were performed and permitted an interpretation of the total horizontal stress  $p_{ho} = \sigma_{ho}$  from the

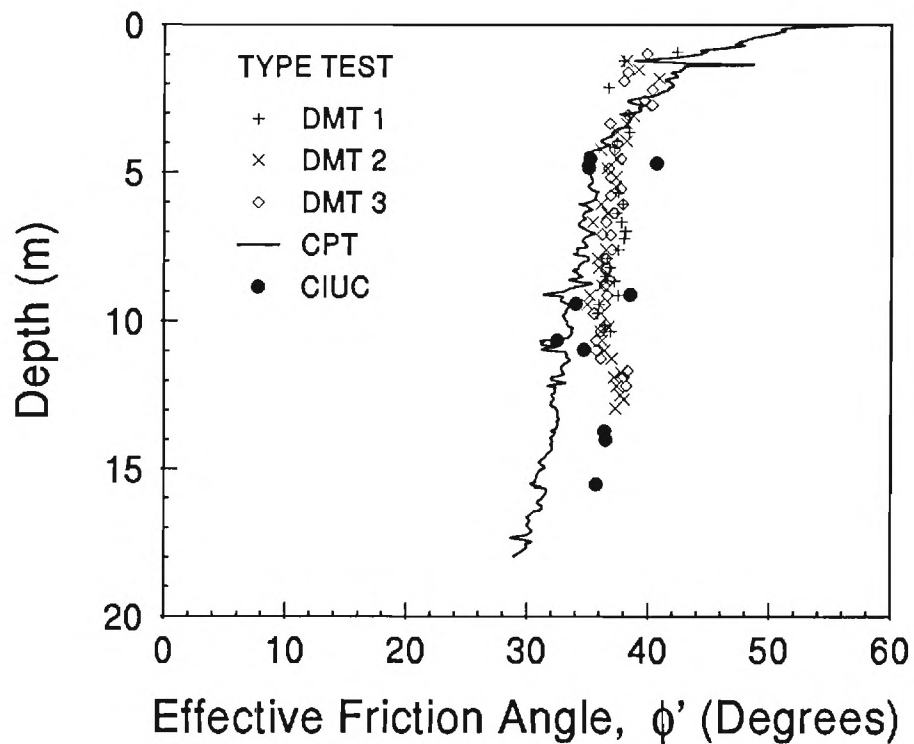


Figure 6-2. Interpreted Profiles of  $\phi'$  in Piedmont Residuum.

inspection of lift-off pressures during probe inflation, as indicated in Figure 6-3. While these are somewhat subjective, the values shown represent the average of two independent assessments by the authors of this report.

The empirical evaluations of  $\sigma_{ho}' = K_o \sigma_{vo}'$  from DMTs (Marchetti, 1980) is shown to be in general agreement with the PMT results. A recent CPT method proposed by Masood and Mitchell (1988) suggests that  $K_o = \text{fctn}(f_s/\sigma_{vo}')$ , and therefore, Figure 6-3 has superimposed the profile of  $f_s$  from the cone soundings as an approximate measure of  $\sigma_{ho}'$ . Additional research using SBPMT and TSC would be a welcome asset in further defining in-situ  $K_o$  values in the Piedmont.

### 6.1.3 Preconsolidation Stress

In the Piedmont, specimens extruded from thin-walled Shelby tube samples often exhibit an "Alzheimers" effect, whereby the very silty and sandy soil forgets that it has an

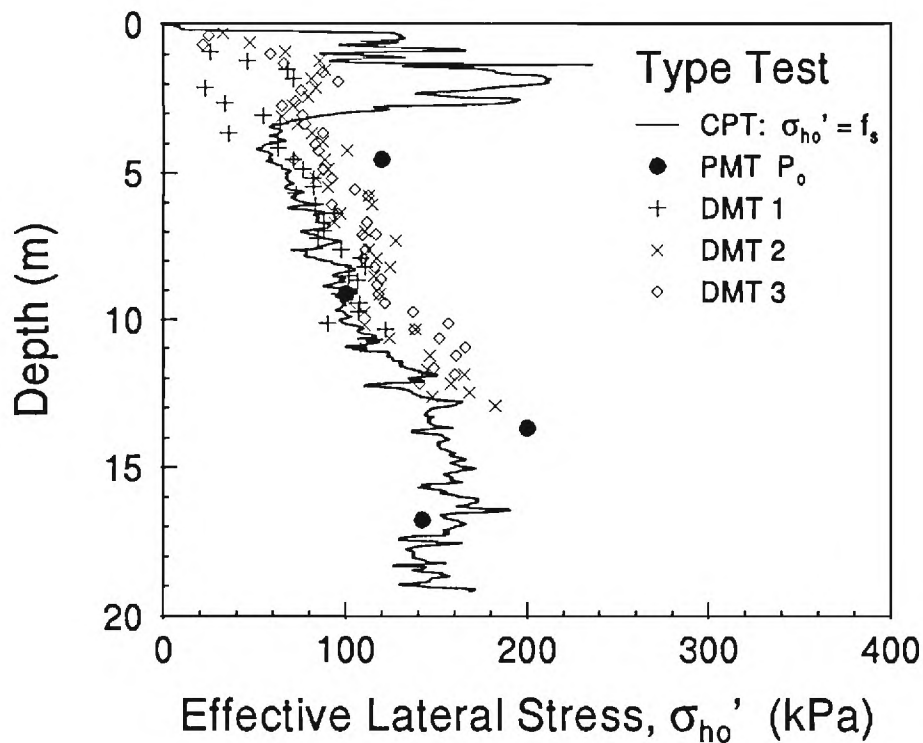


Figure 6-3. Interpreted Profiles of  $\sigma'_{ho}$  in Piedmont Residuum.

apparent quasi-preconsolidation stress ( $\sigma'_p$ ). This occurs when the geostatic stress state ( $\sigma'_{vo}$  and  $\sigma'_{ho}$ ) is completely removed in the laboratory prior to specimen insertion into an oedometer ring. Severe sample disturbance and moderately-high mica contents may cause specimen swelling, with the result that oedometer test results often overpredict foundation settlements. Consequently, calculations of settlements in the Piedmont often rely upon empirical correlations between in-situ tests and backcalculated moduli from field performance data (Barksdale, et al., 1982, 1986; Martin, 1977, 1987; Willmer et al. 1982, Mayne and Frost, 1988).

Clayey residual soils from Indonesia and New Zealand show a clearly-defined apparent  $\sigma'_p$  in oedometer tests (Wesley, 1990). An analysis of Wesley's data on these residual soils show that companion series of undrained triaxial shear tests may be used in an inverted SHANSEP manner for independently assessing an in-situ value of apparent OCR. The procedure is outlined in Mayne (1988) and for CIUC tests is simply:

$$\text{OCR} = [(s_v/\sigma_{v_o}')/(0.75\sin\phi')]^{1.33} \quad [6-1]$$

A review of the geotechnical characteristics of residual soils by Townsend (1985) also notes the occurrence of an apparent  $\sigma_p'$  and attributes this quasi-preconsolidation to cementation, agglomeration, and/or possibly soil suction. Desiccation and capillarity may also be mechanisms of overconsolidation in the Piedmont.

The clear delineation of a yield stress in the Piedmont residual soils is not well-established. A variety of different test procedures was attempted during this program to minimize specimen disturbance effects, however, no special sampling techniques (Laval sampler, Sherbrooke sampler, ring sampler) were utilized in retrieving samples from the field. Also, a number of different graphical techniques were tried in order to better define yield, as discussed in Section 3.3.3. In these cases, a reconstruction technique (Holtz and Kovacs, 1981) and work energy method (Becker, et al. 1987) appeared somewhat consistent and useful in evaluating  $\sigma_p'$  from the oedometer curves.

The derived profile of  $\sigma_p'$  is presented in Figure 6-4, indicating nominal overconsolidation ratios (OCR) in the range  $1.2 \leq \text{OCR} \leq 2.5$  within the residual soil zone.

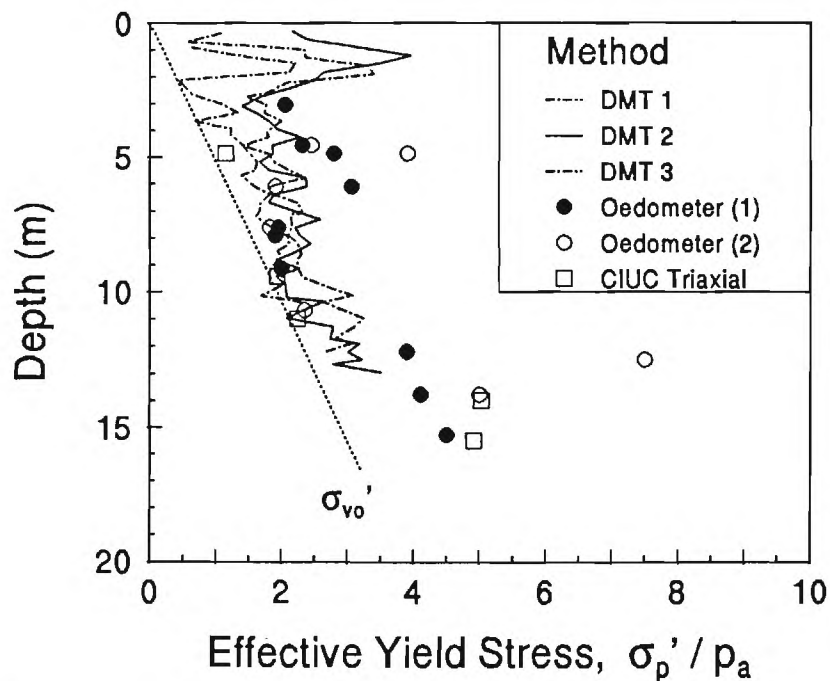


Figure 6-4. Interpreted Profile of  $\sigma_p'$  in Piedmont Residuum.



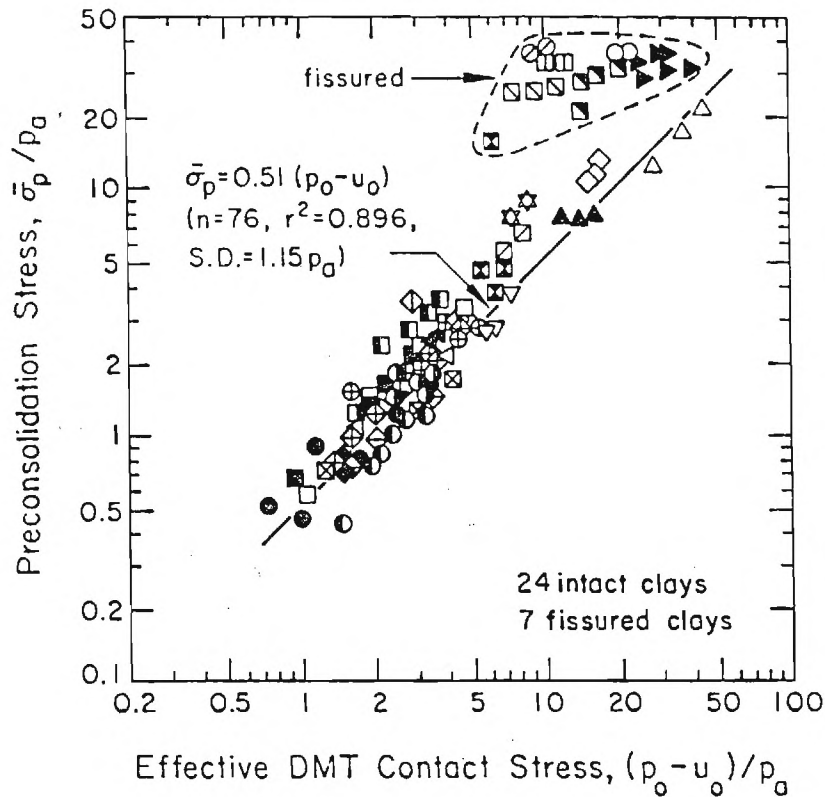


Figure 6-5. Statistical Relationship Between  $\sigma_p'$  and DMT Contact Stresses in Clays.  
(from Kulhawy and Mayne, 1990)

The interpreted OCRs from the triaxial tests are shown to be in general agreement. In-situ dilatometer tests also are useful in providing estimates of  $\sigma_p'$ . Figure 6-5 illustrates the statistical relationship between  $\sigma_p'$  and net contact pressure  $(p_o - u_o)$  from DMTs in 31 different clays worldwide (Kulhawy and Mayne, 1990):

$$\sigma_p' = 0.51(p_o - u_o) \quad [6-2]$$

A recent review of well-documented clean sands with known stress history profiles indicates that this relationship may also be appropriate for different soil types. The derived profiles of  $\sigma_p'$  from the three DMT soundings do indeed seem compatible with the oedometer and triaxial results shown in Figure 6-4. These values also are consistent with the semi-empirical

relationship between  $K_0$  and OCR that was derived from laboratory data on 171 clays, silts, and sands (Mayne and Kulhawy, 1982).

The derived profiles of  $\sigma_p'$  at this site are similar in trend to those reported for various in-situ tests on Brazilian clayey soils (Décourt, 1992) and clayey sedimentary deposits (Kulhawy and Mayne, 1990). Figure 6-6 shows a summary graph of the recommended correlation between effective yield stress ( $\sigma_p'$ ) and corrected SPT resistance,  $N_{60}$ . A variety of different soil types are noted including: intact and fissured sedimentary-type clays and silts from worldwide sources, Brazilian clay soils, U.S. Piedmont residual soils, and clean sedimentary sand from the Po River in Italy. Similar relationships are observed between  $\sigma_p'$  and other in-situ tests (cone, piezocone, dilatometer, and pressuremeter), may be found in Kulhawy and Mayne (1990).

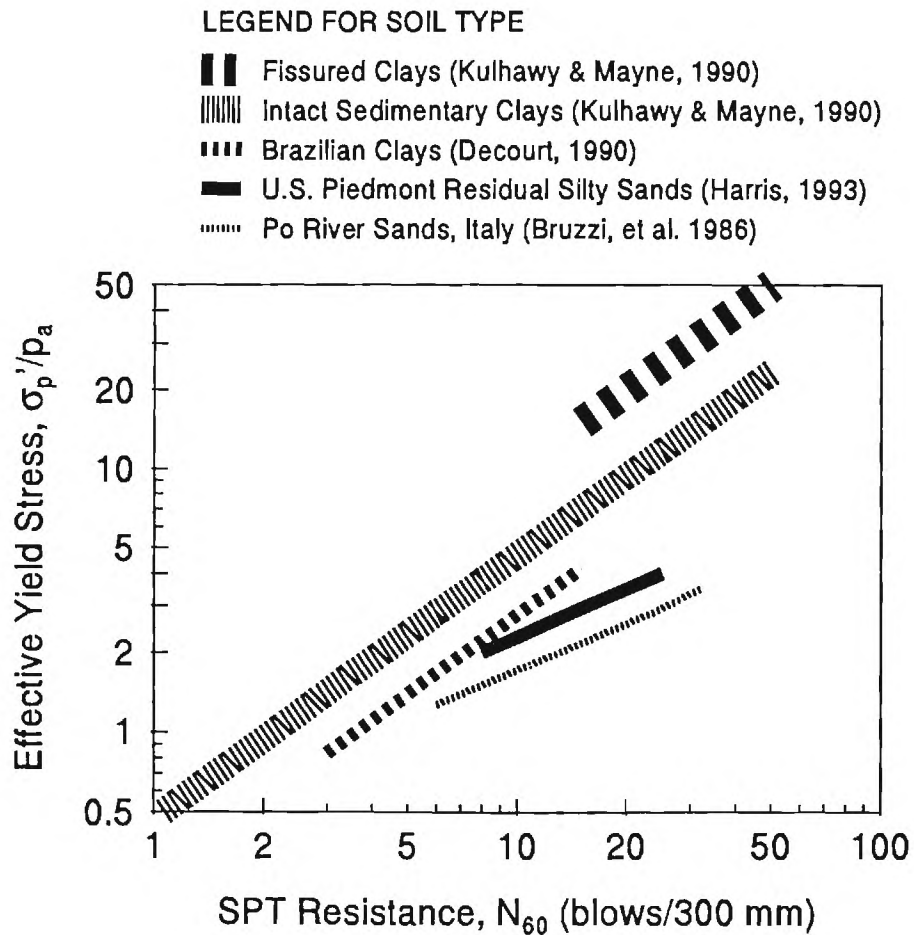


Figure 6-6. Relationships Between  $\sigma_p'$  and  $N_{60}$  for Different Soil Types.

## 6.2 ROUTINE CALCULATIONS OF ULTIMATE CAPACITY

The use of empirical methodologies for estimating the axial capacity of shaft C-2 is summarized in Table 6-1. In these common and published approaches, components of side and end-bearing are calculated using field data directly. Input data are from either SPT, CPT, or PMT. The LPC design method using PMT data are shown to provide the best match with the interpreted failure load on test shaft C2.

Table 6-1. Calculations of Ultimate Axial Capacity for Shaft C-2 From In-Situ Test Data

Method	Input	$Q_{\text{shaft}}$	+	$Q_{\text{base}}$	=	$Q_{\text{total}}$
Meyerhof (1976)	SPT	70 <sup>t</sup>		147 <sup>t</sup>		217 <sup>t</sup>
Reese & Allen (1977)	SPT	216 <sup>t</sup>		25 <sup>t</sup>		241 <sup>t</sup>
Decourt (1982)	SPT	337 <sup>t</sup>		245 <sup>t</sup>		582 <sup>t</sup>
Busamante & Ganeselli (1982)	CPT	191 <sup>t</sup>		135 <sup>t</sup>		326 <sup>t</sup>
Menard (1963)	PMT	302 <sup>t</sup>		135 <sup>t</sup>		437 <sup>t</sup>
LPC (1985)	PMT	324 <sup>t</sup>		56 <sup>t</sup>		380 <sup>t</sup>
Measured in Static Load Test:		300 <sup>t</sup>		50 <sup>t</sup>		350 <sup>t</sup>

## 6.3 ANALYSIS OF DRILLED SHAFT CAPACITY IN THE PIEDMONT

Of the in-situ penetration tests, only the SPT is capable of making the difficult transition from residual soil to partially-weathered rock in the Piedmont. In addition, although DMT and PMT are utilized in some geographic portions of the Piedmont, generally

only the SPT is routinely carried out by the majority of geotechnical consultants and foundation contractors. For practical use, therefore, the following methodology has been developed from a derived relationship between the in-situ yield stress ( $\sigma_p'$ ) and energy-corrected SPT resistance ( $N_{60}$ ). Based on the results obtained herein from three separate drill crews, all working with safety hammers and cathead systems, the importance of calibrated SPT entru measurements must be reiterated since the N-values themselves are meaningless without corrections to  $N_{60}$ .

### 6.3.1 Proposed Methodology

The proposed methodology utilizes an effective stress approach for calculating side resistance in the silty sands and sandy silts of the Piedmont, and a total stress analysis for the component of end-bearing resistance. The logic for such may be explained in part on the rate effects, particularly since the two load tests reported herein were conducted using the quick load test procedure. Side resistance determinations using effective stress methods ( $f_s = \beta\sigma_{vo}'$ ) have been successfully applied to both cohesionless and cohesive soils. One hypothesis is that the shaft interface acts as a path of drainage during loading. In fact, for undrained loading of piles in clay, available experimental measurements of pore water pressures along the shaft show essentially no development of excess  $\Delta u$  (Konrad and Roy, 1987; Coop and Wroth, 1989). In contrast, for piles in soft and stiff clays,  $\Delta u$  measurements beneath the foundation base show strong development of positive pore water pressures during axial compression loading, since this is a high compression zone.

Additional support for these arguments is given by two piezocone soundings recently advanced in Piedmont soils near Atlanta Hartsfield Airport. Two types of piezocone were used, with one having a porous element positioned on the cone face (Type 1) and the other having the element located on the shaft, just above the cone tip (Type 2). The results indicate the development of positive  $\Delta u$  beneath the cone tip (up to 40%  $q_c$ ) and negative  $\Delta u$  or "zero-ish" values on the shaft portion of the cone. Therefore, for purposes of analysis herein, drained loading is assumed along the shaft, while undrained loading is appropriate directly beneath the base.

For energy-corrected SPT resistances, the adopted relationship for estimating the yield stress profile is given by:

$$\sigma_p' = 0.2N_{60}p_a \quad [6-3]$$

The preconsolidation stresses are used to calculate the relevant profiles of  $OCR = \sigma_p'/\sigma_{vo}'$  and associated values of  $K_o$  assuming:

$$K_o = (1 - \sin\phi')OCR^{\sin\phi'} \quad [6-4]$$

where the estimate of  $\phi'$  is obtained from the relationship for sands given by Schmertmann (1975). For computer analyses, this relation is approximately given by the expression (Kulhawy and Mayne, 1990):

$$\phi' = \arctan\{[N_{60}/(12.2 + 20.3\sigma_{vo}'/p_a)]^{0.34}\} \quad [6-5]$$

where  $p_a = 1 \text{ atmosphere} = 1 \text{ bar} \approx 1 \text{ tsf} \approx 1 \text{ kg/cm}^2 \approx 100 \text{ kPa}$  is introduced to make the equation dimensionless. The interface between the soil and concrete is assumed to be perfectly rough, such that the interface friction may be taken as  $\delta = \phi'$ . In addition, it is assumed that (1) proper construction techniques are employed so that minimal disturbance of the supporting soil medium occurs, (2) concrete is placed soon after excavation, and (3) that the ambient geostatic stress state is fully recovered prior to foundation utilization. If so, the effective (drained) side resistance is calculated as:

$$f_s = K \tan\delta \sigma_{vo}' \approx K_o \tan\phi' \sigma_{vo}' \quad [6-6]$$

Below the foundation base, the undrained shear strength is determined using the normalized strength ratio corresponding to simple shear loading (Jamiołkowski, et al., 1985):

$$(s_u/\sigma_{vo}')_{DSS} = 0.23 OCR^{0.8} \quad [6-7]$$

Therefore, we calculate the end-bearing as resistance from:

$$q_{ult} = N_c s_u = N_c (s_u/\sigma_{vo}')\sigma_{vo}' \quad [6-8]$$

where the bearing factor  $N_c = 9.33$  is appropriate for deep circular foundation elements.

### 6.3.2 Application to Load Test Results

Using the aforementioned methodology, the calculated axial capacities for test shafts C1 and C2 have been made based on the average profile of SPT- $N_{60}$  resistances shown in Figure 3-6. An average depth to groundwater is taken as 16.8 m (55 ft). The calculations of total, side, and base components of axial capacity are listed in Table 6-2. For comparison, the measured capacities correspond to the values discussed previously in Section 5, and roughly correspond to the Davisson offset line method of interpretation. Note that the end-bearing shaft C1 was not fully mobilized to failure due to limited capacity of the load frame and hydraulic jack. Considering the uncertainty associated with SPT values, the agreement between measured and predicted capacities is quite reasonable.

Table 6-2. Axial Capacity Prediction for Test Shafts (tons)

Shaft Type	Test No.	Shaft Capacity		End-Bearing		Total Capacity	
		Calc.	Measured	Calc.	Measured	Calc.	Measured
End-Bearing	C1	784	650	365	350	1149	1000
Floating	C2	317	300	63	50	379	350

Note: 1 ton = 8.9 kN

## 6.4 SUMMARY

The calculated capacities of drilled shaft foundations under axial compression loading in the Piedmont residuum can be accomplished using an empirical methodology that relates  $\sigma_p'$  with in-situ test data. Side resistance is calculated using an effective stress procedure whereby  $f_s \approx K_o \tan \phi'$ . Base resistance is determined by assuming undrained behavior below the foundation tip and a total stress analysis is utilized. Therefore, the suggested approach is a hybrid  $\alpha$ - $\beta$  method. The total capacity is calculated as the sum of side and base components. Due to the prevalence of SPT as a tool in the Piedmont, the methodology is discussed in terms of corrected  $N_{60}$  data.

## CHAPTER 7

### 7.0 LOAD-DISPLACEMENT BEHAVIOR FOR AXIAL COMPRESSION

The prediction of load-displacement response of drilled shafts subjected to axial compression loading in the Piedmont is also of interest. The relative proportions of load carried by the shaft and base at working loads are also desired. Consequently, elastic continuum theory is utilized to describe the load-transfer distribution and load-displacement response at the top of the foundation. The procedures have been developed using boundary element formulations (Poulos and Davis, 1980; Poulos, 1989) and approximate closed-form solutions by Randolph and Wroth (1978, 1979) and Randolph (1989). The generalized method characterizes the soil with two elastic constants: soil modulus ( $E_s$ ) and Poisson's ratio ( $\nu_s$ ). The soil modulus may be taken either uniform with depth (constant  $E_s$ ) or a Gibson-profile (linearly increasing  $E_s$  with depth), as illustrated in Figure 7-1.

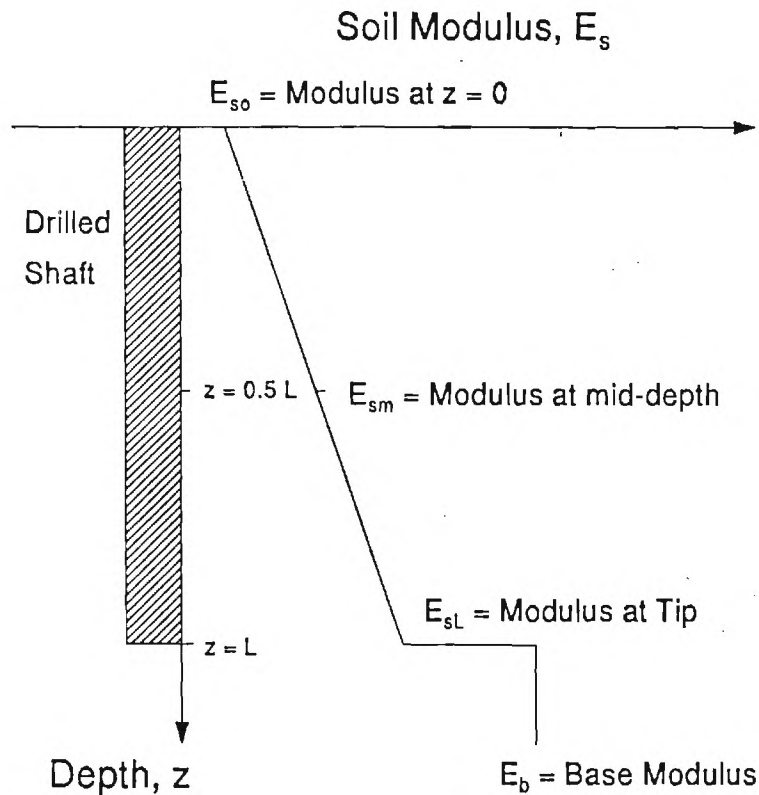


Figure 7-1. Definition of Soil Moduli for Drilled Shaft Problem.



## 7.1 AXIAL DISPLACEMENT PREDICTIONS

The elastic theory solution for axial displacement ( $w$ ) or vertical settlement of a pile foundation is expressed by:

$$w_t = P_t I_p / (E_{sL} d) \quad [7-1]$$

where  $P_t$  = applied axial load at the top of the shaft,  $E_{sL}$  = soil modulus at the foundation base,  $d$  = foundation diameter, and  $I_p$  = influence factor. The values of  $I_p$  are given in approximate closed-form (Randolph and Wroth, 1978, 1979; Poulos, 1989):

$$I_p = 4(1+\nu) \frac{\left\{ 1 + \frac{1}{\pi\lambda} \frac{8}{(1-\nu_s)} \frac{\eta \tanh(\mu L)}{\xi} \frac{L}{d} \right\}}{\left\{ \frac{4}{(1-\nu_s)} \frac{\eta}{\xi} + \frac{4\pi\rho \tanh(\mu L)}{\zeta} \frac{L}{d} \right\}} \quad [7-2]$$

where  $\eta = d_b/d =$  eta factor ( $\eta = 1$  for straight shafts with  $d_b =$  diameter of base).

$\xi = E_{sL}/E_b =$  xi factor ( $\xi = 1$  for floating pile).

$\rho = E_{sm}/E_{sL} =$  rho ( $\rho = 1$  for uniform soil;  $\rho = 0.5$  for simple Gibson soil).

$\lambda = 2(1+\nu_s)E_p/E_{sL} =$  lambda factor.

$\zeta = \ln\{[0.25 + (2.5\rho(1-\nu_s) - 0.25)\xi] (2L/d)\} =$  zeta factor.

$\mu L = 2(2/\zeta\lambda)^{0.5} (L/d) =$  mu factor.

$E_p =$  pile modulus (concrete plus reinforcing steel).

$E_{sL} =$  soil modulus at foundation base (pile tip).

$E_{sm} =$  soil modulus at mid-depth of shaft.

$E_b =$  soil modulus below foundation base.

$\nu_s =$  Poisson's ratio of soil.

$d =$  shaft diameter.

$L =$  shaft length.

The solution is general and can accommodate soil models with constant  $E_s$  or linearly-varying  $E_s$  with depth. For the Piedmont, a Gibson-soil model appears appropriate, based on the trends of measured moduli profiles by both the SASW geophysics survey and the DMT soundings. A possible range of  $0 \leq \rho \leq 1$  was investigated for shafts C1 and C2, and subsequently, a rho factor  $\rho = 0.5$  was adopted as best characteristic of Piedmont residuum.

## 7.2 LOAD TRANSFER

Elastic continuum theory can also evaluate the distribution of load transfer with depth. The ratio of the displacements at the top of the foundation (butt settlement,  $w_t$ ) to the foundation base (tip settlement,  $w_b$ ) is given simply by:

$$w_t/w_b = \cosh(\mu L) \quad [7-3]$$

The displacement at the foundation base ( $w_b$ ) may also be expressed in terms of the magnitude of load at the base ( $P_b$ ):

$$w_b = P_b(1-\nu_s)(1+\nu_s)\eta/(E_b d) \quad [7-4]$$

Combining Equations [7-1], [7-3] and [7-4], the percentage of load transmitted to the tip or foundation base for a compressible pile in a generally vertically inhomogeneous soil medium can be evaluated from:

$$P_b/P_t = I_\rho / \{ \xi \eta \cosh(\mu L) (1-\nu_s)(1+\nu_s) \} \quad [7-5]$$

where  $I_\rho$  is obtained from [7-2]. Equation [7-5] applies for  $\xi = E_{s1}/E_b \leq 20$  and gives values comparable to chart solutions given in Poulos and Davis (1980). However, the latter apply only to uniform profiles of  $E_{su}$ .

The methodology permits a prediction of the total load-displacement response at the butt, as well as for the separate components of shaft and end-bearing, following the outlines

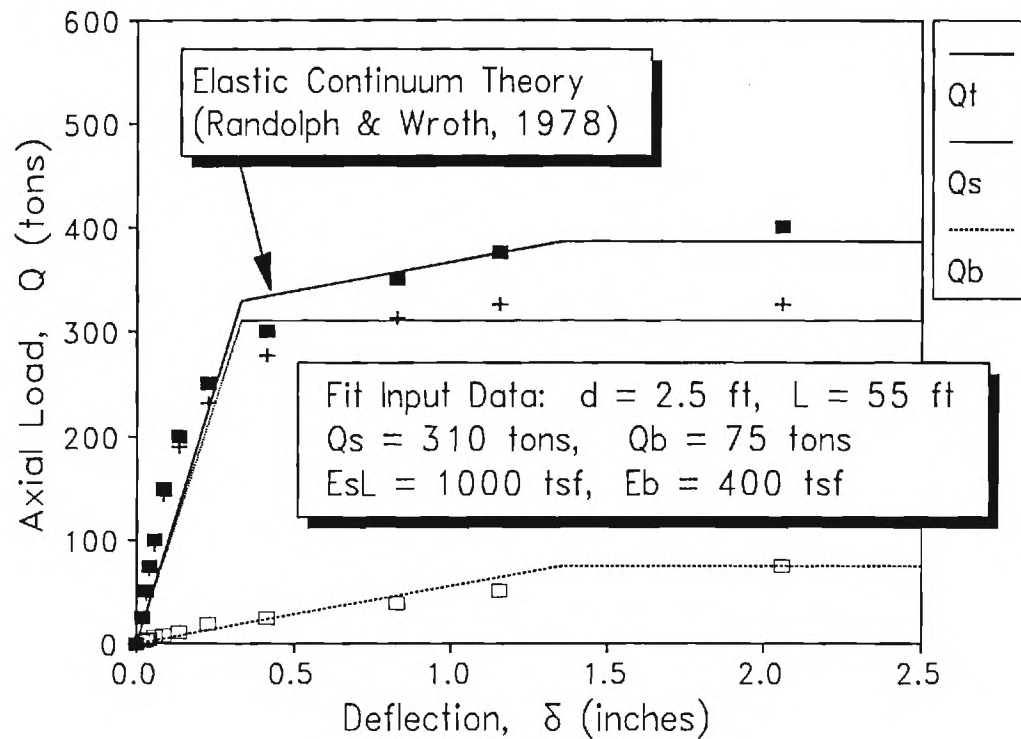


Figure 7-2. Fitted Prediction to Response of Shaft C2 Using Continuum Theory.

given by Poulos and Davis (1980) and Gardner (1987). In this case, elastic settlements are assumed to apply until full side resistance capacity is reached. Further increases in total capacity are attributed to additional mobilization of end-bearing resistance until the total capacity is achieved.

### 7.3 APPLICATION TO LOAD TESTS

The aforementioned methodology has been applied to the ASCE/ADSC drilled shaft load test results. The elastic continuum model was fitted by trial and error analysis to obtain a reasonable fit between the total response, as well as the side and base components. For the results shown above, a backfigured value of side capacity  $Q_s = 2.7$  MN (310 tons) and base capacity  $Q_b = 0.66$  MN (75 tons) is adopted. A Gibson modulus profile has been adopted with the corresponding tip modulus  $E_{sL} = 96$  MPa (1000 tsf) and base modulus  $E_b$ ,

adopted with the corresponding tip modulus  $E_{sL} = 96 \text{ MPa}$  (1000 tsf) and base modulus  $E_b = 38 \text{ MPa}$  (400 tsf). It is interesting to note that a softer base modulus is required than along the shaft at the level of the shaft tip. Note that the continuum approach is not able to model the nonlinear load-displacement relationships.

The practical use of the approach relies on energy-corrected SPT data. Since the SPT-N values extend the full depths of both the end-bearing shaft C1 and floating shaft C2, it is possible to predict the behavior of both load tests. The soil modulus at working stress levels is estimated using a correlation between dilatometer modulus and  $N_{60}$ , which has been verified with backfigured moduli from the performance of a number of full-scale foundations situated in Piedmont residuum (Mayne and Frost, 1987):

$$E_s = 22 p_a N^{0.22} \quad [7-6]$$

The empirical relationship between  $E_s$ , corresponding to working stress levels, and  $N_{60}$  is presented in Figure 7-3.

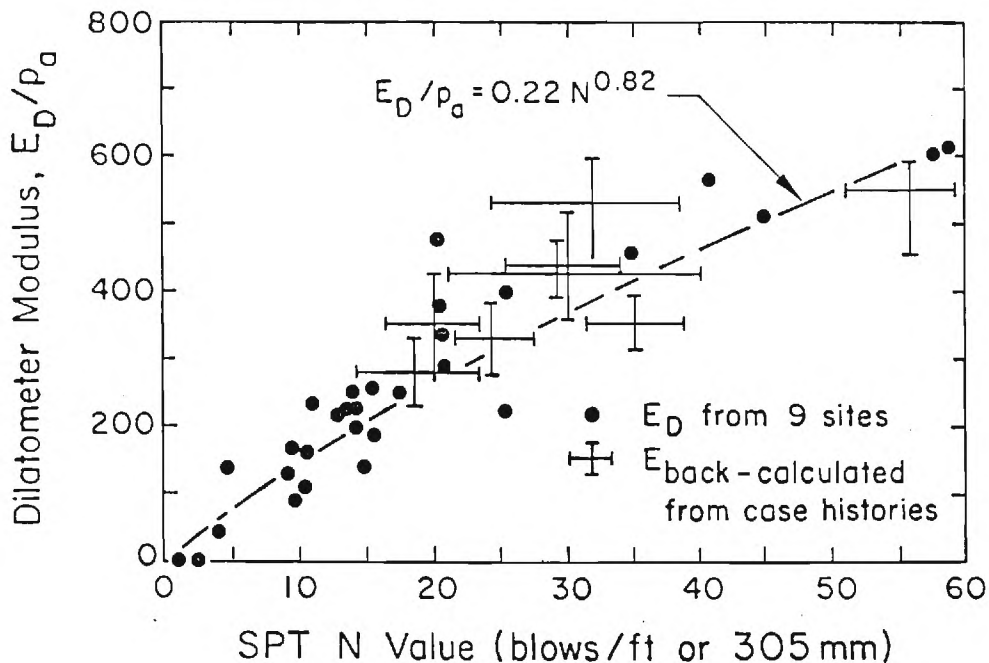


Figure 7-3. Correlation Between Soil Modulus and SPT- $N_{60}$  in Piedmont. (after Kulhawy and Mayne, 1990; Data from Mayne and Frost, 1988).

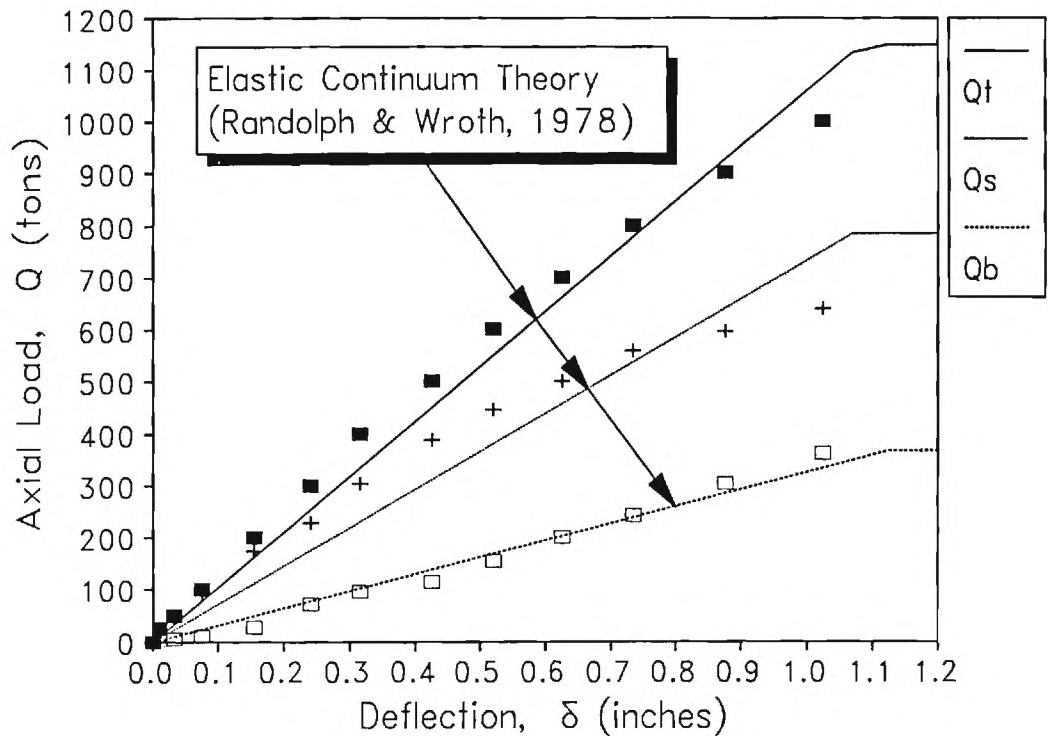


Figure 7-4. Measured and Predicted Response of Shaft C1 Using  $N_{60}$  Data.

The in-situ SPT resistances were measured in residual soils and the transitional material termed partially-weathered rock (PWR). The averaged  $N_{60}$  values gave the predicted capacities noted in Section 6.3. An estimate of the soil modulus using the aforementioned correlation gave  $E_{sL} = 43$  MPa (450 tsf) for residuum at the tip of shaft C2 and assuming a Gibson-type soil ( $\rho = 0.5$ ). Similarly, an extrapolated value  $E_b = 230$  MPa (2400 tsf) was obtained for the PWR material underlying shaft C1. Thus, the application of the SPT correlations results in estimates of load-displacement response for both shaft C1 and shaft C2 in terms of total, shaft, and base components. The predictions are given in Figures 7-4 and 7-5, respectively. Considering the lack of sophistication associated with SPT measurements, reasonable comparisons are noted between predicted and measured response for both load tests. For the C1 prediction, note that the applied end-bearing at a

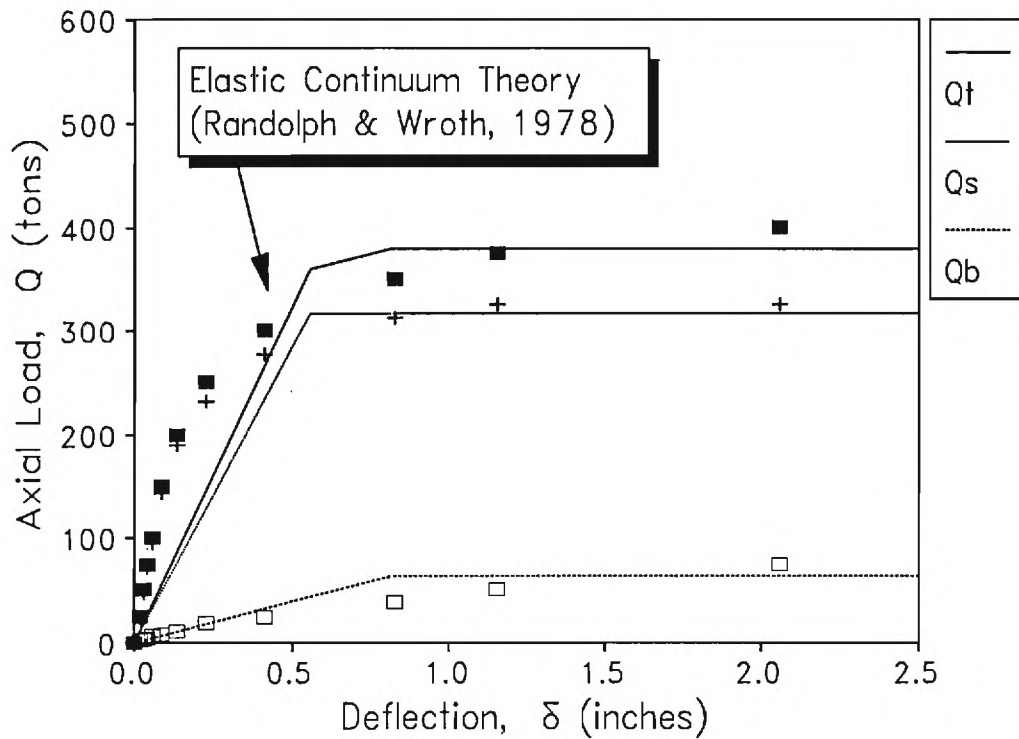


Figure 7-5. Measured and Predicted Response of Shaft C2 Using  $N_{60}$  Data.

butt deflection of  $\delta = 12$  mm (0.5 in) corresponds to the allowable bearing pressures recommended by Peck, Hanson, and Thornburn (1974) for jointed rock with an RQD = 25 percent.

The methodology has also been used to predict the behavior of a recent load test on a drilled shaft performed by the Georgia DOT in Coweta County, Georgia (O'Neill, 1992). This shaft foundation for a bridge abutment has a diameter of 0.91 m (36 inches) and length of 19.2 m (63 feet). Importantly, however, the groundwater is relatively shallow at this site and lies at a depth of  $z_w = 3$  m (10 feet), in contrast to the deep water table at the Georgia Tech site ( $z_w = 16.8$  m = 55 feet). Predicted and measured load-displacement results are presented in Figure 7-6 for the instrumented Coweta shaft.

Finally, the results of a load test in Piedmont residuum at the Fairfax Hospital Complex in Fairfax County, Virginia have been reviewed. The drilled shaft has a 0.91

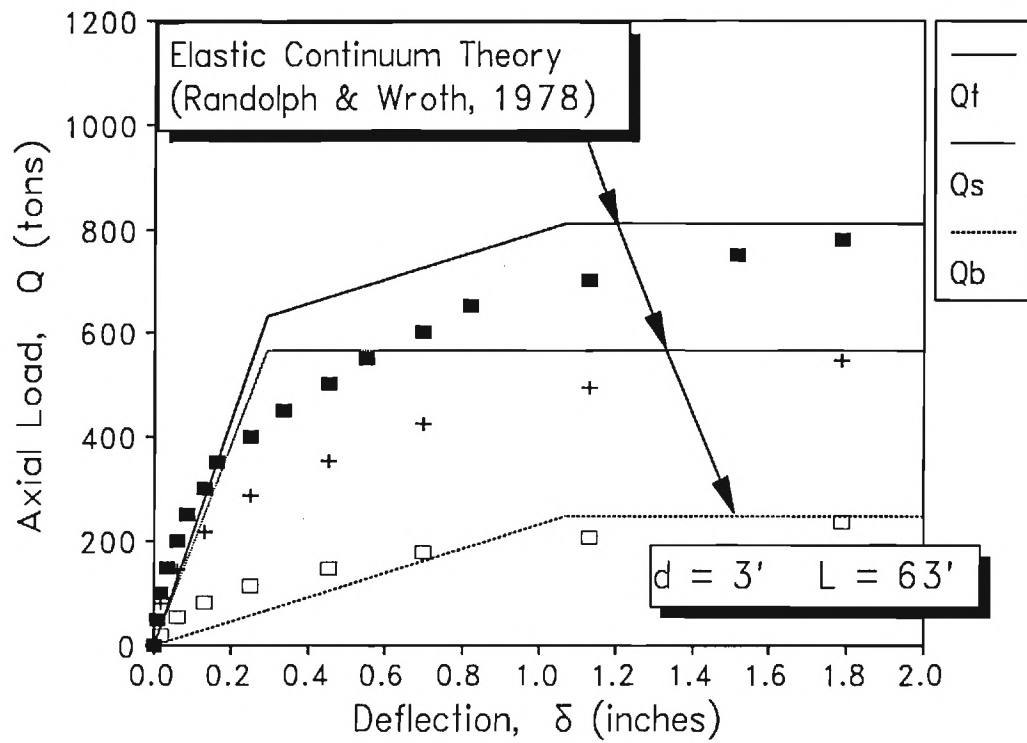


Figure 7-6. Measured and Predicted Response of Coweta Shaft, Georgia.

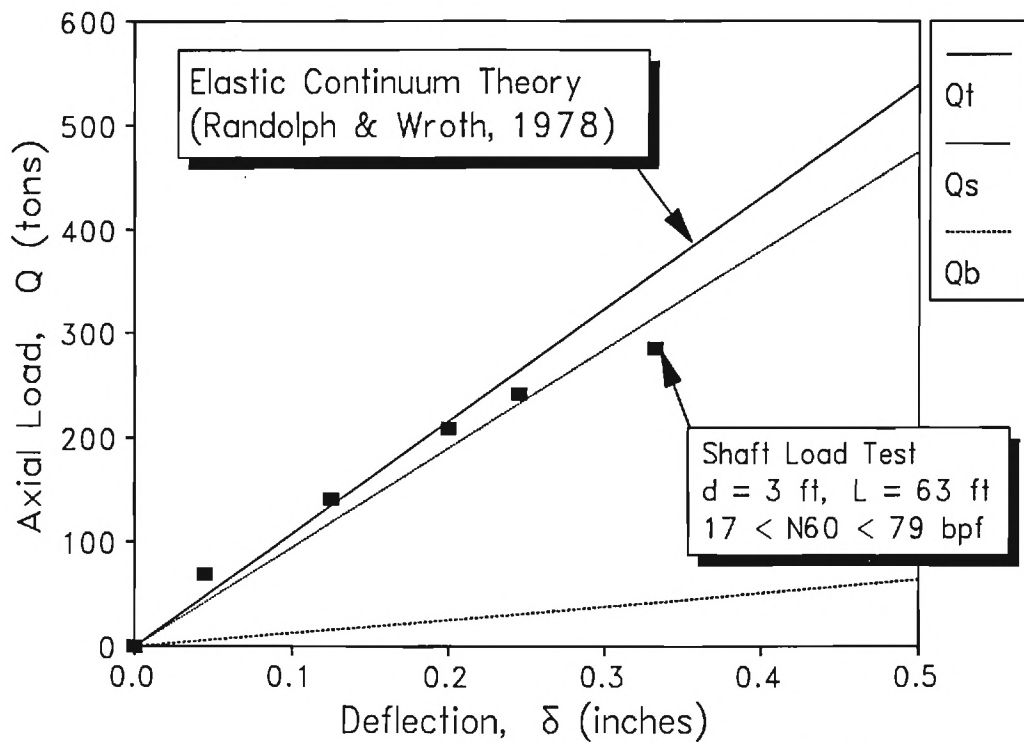


Figure 7-7. Measured and Predicted Response of Fairfax Hospital Shaft, Virginia.

meter diameter (36 inches) and 19.8 meter length (65 feet). Groundwater lies approximately 10 m (30 feet) below grade. SPT resistances increase with depth from about 15 bpf near the surface to over 100 bpf at 20 meters (66 ft). Mean profiles of SPT are presented by Mayne and Frost (1988). Figure 7-7 shows the comparison of measured and predicted behavior.

#### 7.4 SUMMARY

The load-displacement behavior of drilled shafts can be modelled using elastic continuum methods (Poulos and Davis, 1980; Randolph and Wroth, 1979). While load test data are clearly nonlinear, this approximate approach appears suitable for routine practical use. The method is convenient and easy to use, and permits a separate consideration of the side and base components in analysis.



## CHAPTER 8

### 8.0 CONCLUSIONS AND RECOMMENDATIONS

#### 8.1 SUMMARY OF RESULTS

A simplified analysis of the performance of drilled shaft foundations under axial compression loading in the Piedmont has been presented. The work was centered around the response of two instrumented drilled shafts tested at the Georgia Tech campus. Efforts were supplemented by a number of in-situ and laboratory tests. Discussions of the difficulties in site characterization of Piedmont soils were presented and a framework for interpretation of soil properties was established. These results were utilized in calculations of ultimate capacities using a combined  $\alpha$ - $\beta$  approach and an elastic continuum model for representing the load-displacement-transfer response.

Drilled shafts designed to bear in the Piedmont should be analysed for axial compression capacities in terms of a side resistance component and end-bearing resistance. Instrumented load test data from this program indicate that side resistance typically accounts for 80 to 95 percent of the support. This is consistent with previous research on load transfer behavior of piles and shafts (Reese, 1978; Poulos, 1989; Kulhawy, 1991)

#### 8.2 DIRECTIONS FOR FUTURE RESEARCH

The tasks of understanding residual soil materials is unfinished and will undoubtedly require many more research programs. One recent topic of interest in drilled shaft research are the uses of nondestructive testing for integrity evaluation and prediction of stiffness and capacity. A companion study to this report obtained wave propagation data on the two test shafts from this project and evaluated three of NDT techniques for this purpose (Rix, Jacobs, and Reichart, 1993).

At the completion of this study, several topics that might be addressed in the near future have been cited for better characterization of the Piedmont residuum. These items

include the following suggestions and recommendations to the local geotechnical engineers of Atlanta, Georgia:

1. Calibrate SPT  $N_{60}$  Enthu Energy for All Drill Rigs (ASTM D-4633).
2. Establishment of Permanent Geotechnical Test Sites for Experimentation.
3. Series of Self-Boring Pressuremeter Tests (SPBMT) for Evaluation of  $K_0$ .
4. Special Sampling Procedures to Minimize Alzheimer's Effect.  
(Laval Piston Sampler, Sherbrooke Sampler, Split Ring Sampler, Freezing).
5. Piezocone Penetration Tests (PCPT) to Measure Pore Water Pressures.
6. Measurement of Degree of Saturation and Suction Matrix Potential.
7. Develop Model for Partially-Saturated Soils and Role of Capillarity.
8. Testing Program to Evaluate Shafts Under Lateral and Moment Loading.

The implementation of these tasks represents an undertaking for a better knowledge of the performance of foundations and structures in residual soils and saprolitic materials. With an improved understanding, modern designs can offer more economical, productive, and safer systems for the public.

## 9.0 REFERENCES

American Society for Testing and Materials (1992), "Standard Test Method for Stress Wave Energy Measurement for Dynamic Penetrometer Testing Systems (D-4633)", *Annual Book of Standards*, Vol. 4.08, ASTM, Philadelphia, pp. 943-947.

American Society for Testing and Materials (1992), "Standard Method for Penetration Test and Split Barrel Sampling of Soils (D-1586)", *Annual Book of Standards*, Vol.4.08, ASTM, Philadelphia, PA, pp. 221-225.

American Society for Testing and Materials (1992), "Standard Test Method for One Dimensional Consolidation Properties of Soils (D-2435)", *Annual Book of Standards*, Vol 4.08, ASTM, Philadelphia, pp. 314-324.

American Society for Testing and Materials (1992), "Test Method for Pressuremeter Testing in Soils (D-4719)", *Annual Book of Standards*, Vol. 4.08, ASTM, Philadelphia, pp. 881-888.

American Society for Testing and Materials (1992), "Standard Practice for Diamond Core Drilling for Site Investigation (D-2113)", *Annual Book of Standards*, Vol. 4.08, ASTM, Philadelphia, pp. 227-280.

American Society for Testing and Materials (1992), "Standard Test Method for Liquid Limit, Plastic Limit, and Plasticity Index of Soils (D-4318)", *Annual Book of Standards*, Vol. 4.08, ASTM, Philadelphia, pp. 675-685.

American Society for Testing and Materials (1992), "Standard Test Method for Consolidated-Undrained Triaxial Compression Test on Cohesive Soils (D-4667)", *Annual Book of Standards*, Vol. 4.08, ASTM, Philadelphia, pp. 675-685.

American Society for Testing and Materials (1992), "Standard Test Method for Particle Size Analysis (D-422)", *Annual Book of Standards*, Vol. 4.08, ASTM, Philadelphia, pp. 94-100.

American Concrete Institute (1983), Committee 318, "Building Code Requirements for Reinforced Concrete", *Manual of Concrete Practice*, American Concrete Institute, Detroit.

Baguelin, F., Jezequel, J.F., and Shields, D.H. (1978), *The Pressuremeter and Foundation Engineering*, Trans Tech Publications, Clausthal, France, 1978, 617 p.

Barksdale, R.D., Bachus, R.C., and Calnan, M.B. (1982), "Settlements of a Tower on Residual Soil", *Engineering and Construction in Tropical and Residual Soils*, ASCE Specialty Conference, Honolulu, pp. 647-664.

Barksdale, R.D., Ferry, C.T., and Lawrence, J.D. (1986), "Residual Soil Settlement from Pressuremeter Moduli", *Use of In-Situ Tests in Geotechnical Engineering*, ASCE GSP 6, Blacksburg, pp. 447-461.

- Becker, D.E., Crooks, J.H.A., Been, K., and Jeffries, M.G. (1987), "Work as a Criterion for Determining In-Situ and Yield Stresses in Clays", *Canadian Geotechnical Journal*, Vol. 24, No. 4, pp. 549-564.
- Bruzzi, D., Ghionna, V., Jamiolkowski, M., Lancellotta, R., and Manfredini, G. (1986), "Self-Boring Pressuremeter in Po River Sand", *The Pressuremeter and Its Marine Applications*, ASTM STP 950, (2nd Intl. Symposium on Pressuremeters), pp. 57-74.
- Bustamante, M. and Gianceselli, L. (1982), "Pile Bearing Capacity Prediction by Means of Static Penetrometer CPT", *Proceedings of the Second European Symposium on Penetration Testing*, Vol. 2, Amsterdam, Balkema, Rotterdam, pp. 493-506.
- Butler H.D. and Hoy, H.E. (1977), "Users Manual for the Texas Quick Load Method for Foundation Load Testing", Federal Highway Administration, Office of Development, Washington, D.C., 59 p.
- Butterfield, R. (1979), "A Natural Compression Law for Soils", *Geotechnique*, Vol. 29, No. 4, Dec., pp. 468-480.
- Casagrande, A. (1936), "The Determination of the Preconsolidation Load and Its Practical Significance", *Proceedings*, 1st International Conference on Soil Mechanics and Foundation Engineering, Vol. III, Cambridge, MA, 1936, p. 60.
- Chin, F.K. (1970), "Estimate of the Ultimate Load of Piles Not Carried to Failure", *Proceedings*, 2<sup>nd</sup> Southeast Asian Conference on Soil Engineering, pp. 81-90.
- Coop, M.R. and Wroth, C.P. (1989), "Field Studies of An Instrumented Model Pile in Clay", *Geotechnique*, Vol. 39, No. 4, December, pp. 679-696.
- Crawford, C. (1985), "State of the Art: Evaluation and Interpretation of Consolidation Tests", *Consolidation of Soils: Testing and Evaluation*, ASTM STP 892, Philadelphia, pp. 71-106.
- Davisson, M.T. (1972), "High Capacity Piles", *Proceedings*, Lecture Series on Innovations in Foundation Construction, American Society of Civil Engineers, Illinois Section, pp. 1-52.
- DeBeer, E.E. (1967), "Proefondervindelijke bijdrage tot de studie van het grensdraagvermogen van zand onder fundenugen op staal", *Tijdschrift Der Openbare Werken van België*, pp. 6-67 and 1-68.
- Décourt, L. (1992), "The Standard Penetration Test: State of the Art Report", *Proceedings*, 12<sup>th</sup> International Conference on Soil Mechanics and Foundation Engineering, Rio de Janeiro, Session 2, Volume 4 (Norwegian Geotechnical Institute Report No. 179, Oslo, pp. 1-12).
- Esrig, M.E. and Kirby, R.C. (1979), "Advances in General Effective Stress Method for the Prediction of Axial Capacity for Driven Piles in Clay", *Proceedings*, 11<sup>th</sup> Offshore Technology Conference, Vol. 1, Houston, TX, pp. 437-448.

Fellenius, B.H. (1975), "Test Loading of Piles and New Proof Testing Procedure", *Journal of the Geotechnical Engineering Division*, ASCE, Vol. 101, No. GT9, September, pp. 855-869.

Fellenius, B.H. (1978), "Interpretation and Analysis of Pile Load Tests", *Deep Foundations*, Proceedings, 9<sup>th</sup> Ohio River Valley Soils Seminar, Fort Mitchell, KY, pp. 1-32.

Fellenius, B.H. (1980), "The Analysis of Results from Routine Pile Load Tests", *Ground Engineering*, Vol. 13, No. 6, September, pp. 19-31.

Fuller R.M. and Hoy, H.E. (1970), "Pile Load Tests including Quick Load Test Method, Conventional Methods and Interpretations", *Highway Research Board*, Vol. 333, Washington, D.C. pp 78-86.

Gardner, W.S. (1987), "Design of Drilled Piers in the Atlantic Piedmont", *Foundations and Excavations in Decomposed Rock of the Piedmont Province*, GSP 9, Ed. Ron Smith, ASCE, New York, 1-15.

Greer, D.M., and Gardner, W.S. (1986), *Construction of Drilled Pier Foundations*, John Wiley and Sons, Inc., New York, 246 p.

Hansen, W. (1986), "Static and Dynamic Elastic Modulus of Concrete as Affected by Mix Composition and Compressive Strength", *Concrete at Early Ages* (SP 95), Ed. J. F. Young, American Concrete Institute, Detroit, pp. 115-137.

Hansen, J.B. (1963), Discussion, "Hyperbolic Stress-Strain Response of Cohesive Soils", *Journal of the Soil Mechanics and Foundations Division*, ASCE, Vol. 89, No. SM4, pp 241-242.

Harris, D. (1993), "Axial Behavior of Drilled Shaft Foundations in the Piedmont Residuum", *MS Thesis*, Georgia Institute of Technology, School of Civil Engineering, Atlanta, GA.

Holtz, R.D. and Kovacs, W.D. (1981), *An Introduction to Geotechnical Engineering*, Prentice Hall, Englewood Cliffs, New Jersey, 731 p.

Jamiolkowski, M., Ladd, C.C., Germaine, J.T., and Lancellotta, R. (1985), "New Developments in Field and Laboratory Testing of Soils", *Proceedings*, 11<sup>th</sup> International Conference on Soil Mechanics and Foundation Engineering, Vol. 1, San Francisco, pp. 57-154.

Jamiolkowski, M., Lancellotta, R., Tordella, L., and Battaglio, M. (1982), "Undrained Strength From CPT", *Proceedings*, Second European Symposium on Penetration Testing, Vol. 2, Amsterdam, Balkema Publishers, Rotterdam, pp. 599-606.

Jamiolkowski, M., and Marchetti, S. (1969), "Determination of Preconsolidation Load From a Controlled Gradient Consolidometer", *Proceedings*, 7<sup>th</sup> International Conference on Soil Mechanics and Foundation Engineering, Vol. 1, Mexico, pp. 523-524.

- Janbu, N. (1969), "The Resistance Concept Applied to the Deformation of Soils, *Proceedings 7<sup>th</sup> International Conference on Soil Mechanics and Foundation Engineering*, Vol. 1, Mexico, pp. 191-196.
- Konrad, J.M. and Roy, M. (1987), "Bearing Capacity of Friction Piles in Marine Clay", *Geotechnique*, Vol. 37, No. 2, June, pp. 163-175.
- Kovacs, W.D., Salomone, L.A., and Yokel, F.Y. (1983), "Comparison of Energy Measurement in the SPT using the Cathead and Rope Method", *Report NUREG/CR-3545*, Nuclear Regulatory Commission, Washington, D.C., 69 p.
- Kulhawy, F.H. (1991), "Drilled Shaft Foundations", *Foundation Engineering Handbook*, Second Edition, Ed., H.Y. Fang, Van Nostrand Reinhold, New York, 1991, pp. 537-552.
- Kulhawy, F.H. and Hirany, A. (1988), "Conduct and Interpretation of Load Tests on Drilled Shaft Foundations", *Report EL-5915*, Electric Power Research Institute, Palo Alto.
- Kulhawy, F.H. and Jackson, C.S. (1989), "Some Observations on Undrained Side Resistance of Drilled Shafts", *Foundation Engineering: Current Principles and Practices*, Vol. 2, GSP 22, Ed. F.H. Kulhawy, ASCE, New York, 1011-1025.
- Kulhawy, F.H. and Mayne, P.W. (1990), "Manual on Estimating Soil Properties for Foundation Design", *Report EL-6800*, Electric Power Research Institute, Palo Alto, 306 p.
- Kulhawy, F.H., Trautmann, C.H., Beech, J.F., O'Rourke, T.D., and McGuire, W. (1983), "Transmission Line Structure Foundations for Uplift-Compression Loading", *Report EL-2870*, Electric Power Research Institute, Palo Alto, CA, 412 p.
- Leonards, G.A., and Lovell, W.D. (1979), "Interpretation of Load Tests on High Capacity Driven Piles", *Behavior of Deep Foundations*, ASTM STP 670, Ed. R. Lundgren, ASTM, Philadelphia, PA, pp. 388-415.
- Marchetti, S. (1980), "In-Situ Tests by Flat Dilatometer", *Journal of Geotechnical Engineering*, Vol. 106, No. GT3, March, pp. 299-324.
- Martin, R.E. (1977), "Estimating Foundation Settlements in Residual Soils", *Journal of the Geotechnical Engineering Division*, (ASCE) Vol. 103, No. GT3, 197-212.
- Martin, R.E. (1987), "Settlement of Residual Soils", *Foundations and Excavations in Decomposed Rock of the Piedmont Province*, ASCE GSP 9, New York, pp. 15-25.
- Masood, T., Mitchell, J.K., Lunne, T., and Hauge, E.A. (1988), "Joint U.C. Berkeley and Norwegian Geotechnical Institute In-Situ Testing at Hamilton AFB and Bay Farm Island, CA", University of California, Dept. of Civil Engineering, Berkeley, CA.

Mayne, P.W. (1988), "Determining OCR in Clays From Laboratory Strength", *Journal of Geotechnical Engineering*, Vol. 114, No. 1, Jan., 76-92.

Mayne, P.W. and Frost, D.D. (1988), "Dilatometer Experience in Washington, D.C. and Vicinity", *Transportation Research Record 1169*, Washington, D.C., 16-23.

Mayne, P.W. and Kulhawy, F.H. (1982), " $K_o$ -OCR Relationships in Soil", *Journal of the Geotechnical Engineering Division*, Vol. 108, No. GT6, June, 851-872.

Mayne, P.W., Kulhawy, F.H., and Trautmann, C.H. (1992), "Experimental study of Undrained Lateral and Moment Behavior of Drilled Shafts During Static and Cyclic Loading", *Report TR-100221*, Electric Power Research Institute, Palo Alto, 318 p.

Mazurkiewicz B.K. (1972), "Test Loading of Piles According to Polish Regulations", *Report No. 35*, Royal Southwest Academy of Engineering Sciences, Committee on Pile Research, Stockholm, 20 p.

Meyerhof, G.G. (1976), "Bearing Capacity and Settlement of Pile Foundations", *Journal of the Geotechnical Division*, ASCE, Vol. 102, No. GT3, Mar., pp. 197-228.

Neville, A.M. (1981), *Properties of Concrete*, Longman Scientific and Technical, Essex, UK, 780 p.

O'Neill, M.W. (1992), "Preliminary Data on Coweta County Drilled Shaft Test for I-85 Expansion", *Internal Report* for FHWA Contract DTFH61-91-z-0041, University of Houston, Dept. of Civil and Environmental Engineering, Houston, TX, 10 p.

Peck, R.B., Hanson, W.E., and Thornburn, T.H. (1974), *Foundation Engineering, Second Edition*, John Wiley & Sons, New York, 514 p.

Poulos, H.G. (1989), "Pile Behavior: Theory and Application", 29<sup>th</sup> Rankine Lecture, *Geotechnique*, Vol. 39, No. 3, September, pp. 363-416.

Poulos, H.G. and Davis, E.H. (1980), *Pile Foundation Analysis and Design*, John Wiley and Sons, New York, 397 p. (now published by University of Sydney Press, Australia).

Randolph, M.F. (1989), *PIGLET: Analysis and Design of Pile Groups*, Internal Report, Dept. of Civil Engineering, University of Western Australia, Nedlands, 35 p.

Randolph, M.F. and Wroth, C.P. (1978), "Analysis of Deformation of Vertically Loaded Piles", *Journal of the Geotechnical Engineering Division*, ASCE, Vol. 104, No. GT12, Dec., pp. 1465-1488.

Randolph, M.F. and Wroth, C.P. (1979), "A Simple Approach to Pile Design and the Evaluation of Pile Tests", *Behavior of Deep Foundations*, STP 670, ASTM, Philadelphia, PA, pp. 484-499.

- Reese, L.C. (1978), "Design and Construction of Drilled Shafts", 12th Terzaghi Lecture, *Journal of the Geotechnical Engineering Division*, Vol. 104, No. GT1, January, pp. 91-116.
- Reese, L.C. and O'Neill, M.W. (1988), "Drilled Shafts -Construction Procedures and Design Methods, *Report FHWA-HI-88-042*, Federal Highway Administration, McLean, Virginia, Vols. I and II.
- Rix, G.J., Jacobs, L.J., and Reichert, C.D. (1993), "Evaluation of Nondestructive Test Methods for Length, Diameter, and Stiffness Measurements on Drilled Shafts", *Transportation Research Record*, Preprint, 72<sup>nd</sup> Annual TRB, Washington, D.C., 19 p.
- Robertson, P.K. and Campanella, R.G. (1983), "Interpretation of Cone Penetration Tests", *Canadian Geotechnical Journal*, Vol. 20, No. 4, November, pp. 718-745.
- Schmertmann, J.H. (1986), "Suggested Method for Performing the Flat Dilatometer Test", *Geotechnical Testing Journal*, ASTM, Vol. 9, No. 2, June, pp. 93-101.
- Schmertmann, J.H. (1953), "The Undisturbed Consolidation Behavior of Clay", *Transactions ASCE*, Paper No. 2775, Vol. 120, 1955, pp. 1201-1233. (Also in Award Winning Papers 1950-1959, ASCE, New York)
- Schmertmann, J.H. (1975), "Measurement of In-Situ Shear Strength", *Proceedings, In-Situ Measurement of Soil Properties*, Vol. 2, ASCE Specialty Conference, Raleigh, NC, pp. 57-138.
- Schwartz, S.A. (1987), "Drilled Piers in the Piedmont - Minimizing Contractor, Engineer, and Owner Conflicts", *Foundations and Excavations in Decomposed Rock of the Piedmont Province*, GSP 9, Ed. Ron Smith, ASCE, New York, 80-90.
- Seed, H.B. and Reese, L.C. (1957), "The Action of Soft Clay Along Friction Piles", *Transactions ASCE*, Vol. 122, pp. 731-754. (Also in Award Winning Papers 1950-1959, ASCE, New York, 1977, pp. 351-384).
- Skempton, A.W. (1986), "Standard Penetration Test Procedures and the Effects on Sands of Overburden Pressure, Relative Density, Particle Size, Aging, and Overconsolidation", *Geotechnique*, Vol. 36, No. 3, Sept., pp. 425-447.
- Sladen, J.A. (1992), "The Adhesion Factor: Applications and Limitations", *Canadian Geotechnical Journal*, Vol. 29, No. 2, April, pp. 322-326.
- Sowers, G.F. (1979), *Introductory Soil Mechanics and Foundations: Geotechnical Engineering*, Macmillan, New York, 621 p.
- Sowers, G.F. and Richardson, T.L. (1983), "Residual Soils of the Piedmont and Blue Ridge", *Transportation Research Record 919*, Washington, D.C., pp. 10-16.



Stokoe, K.H., Rix, G.J., and Nazarian, S. (1989), "In-Situ Seismic Testing with Surface Waves", *Proceedings*, 12<sup>th</sup> International Conference on Soil Mechanics and Foundation Engineering, Vol. 1, Rio de Janeiro, pp. 331-334.

Tomlinson, M.J. (1957), "The Adhesion of Piles Driven in Clay Soils", *Proceedings*, 4th International Conference on Soil Mechanics and Foundation Engineering, Vol. 2, London, pp. 66-77.

Tomlinson, M.J. (1986), *Foundation Design and Construction*, Fifth Edition, Longman Scientific and Technical, Essex, UK, 842 p.

Townsend, F.C. (1985), "Geotechnical Characteristics of Residual Soils", *Journal of Geotechnical Engineering*, Vol. 111, No. 1, January, pp. 77-94.

Van der Veen C. (1953), "The Bearing Capacity of a Pile", *Proceedings*, 3<sup>rd</sup> International Conference on Soil Mechanics and Foundation Engineering, Vol. 2, Zurich, pp. 84-90.

Vaughan, P.R. (1985), "Mechanical and Hydraulic Properties of In-Situ Residual Soils", *Proceedings*, First International Conference on Geomechanics in Lateritic & Saprolitic Soils, Brazil, pp. 1-33.

Vesic, A.S. (1972), "Expansion of Cavities in Infinite Soil Mass", *Journal of Soil Mechanics and Foundations Division*, ASCE, Vol. 98, No. SM3, pp. 265-290.

Watson, F.X. (1970), "An Investigation of the Development of Skin Friction of Drilled Piers in Decomposed Rock", *PhD Thesis*, School of Civil Engineering, Georgia Institute of Technology, Atlanta GA.

Wesley, L.D. (1990), "Influence of Structure and Composition on Residual Soils", *Journal of Geotechnical Engineering*, Vol. 116, No. 4, April, pp. 589-602.

Willmer, J.L., Futrell, G.E., and Langfelder, J. (1982), "Settlement Predictions in Piedmont Residual Soil", *Engineering and Construction in Tropical and Residual Soils*, ASCE Specialty Conference, Honolulu, pp. 629-646.

Wroth, C.P. (1984), "The Interpretation of In-Situ Soil Tests", Rankine Lecture, *Geotechnique*, Vol. 34, No. 4, December, pp. 449-489.

## APPENDIX A

### IN-SITU TESTS AND FIELD DATA

This appendix includes data from the in-situ testing program and results of field load testing of the drilled shaft foundations. In-situ testing results include individual soundings for cone penetration tests (CPT), standard penetration tests (SPT), pressuremeter tests (PMT), dilatometer tests (DMT), and spectral analysis of surface waves (SASW).

The measured load-displacement data recorded during the axial compression tests on two drilled shafts (C1 and C2) and the deep plate load test (C3) are included in tabular form in this appendix on pages 96, 97, and 98, respectively. The applied loads were determined from the pressure gauge on a calibrated jack. Individual dial gauge readings taken at the butt of the shaft, telltale, and on the reaction shaft are listed. Tabulated load transfer data from the interpreted strain gauge measurements from shafts C1 and C2 are given on page 161 in Appendix D.

The relative locations of the in-situ tests are shown on Figure 3-2 (page 18). Results from the two CPT soundings are given as profiles of cone tip resistance ( $q_c$ ) and sleeve friction ( $f_s$ ) with depth. These records are presented together on the graphs on page 99. The three DMT soundings were developed using data reduction procedures via the DILLY5 software provided by GPE, Inc. The DMT records are given on pages 100 to 102. Soil boring logs have been prepared using the gINT software program. These logs indicate the measured N-values from the SPT and are included on pages 103 through 123. Data from the geophysical surface wave survey (SASW) is presented in tabular form on page 124 and recorded readings of pressure and volume change for the five Menard-type pressuremeter tests (PMT) are listed on page 125.

Table Measured Displacement, Shaft C1

Load (tons)	Gauge D1		Gauge D2		Gauge D3		Gauge J1		Gauge J2		Gauge R1	
	$\delta 1$ (in.)	$\delta 2$ (in.)	$\delta 1$ (in.)	$\delta 2$ (in.)	$\delta 1$ (in.)	$\delta 2$ (in.)	$\delta 1$ (in.)	$\delta 2$ (in.)	$\delta 1$ (in.)	$\delta 2$ (in.)	$\delta 1$ (in.)	$\delta 2$ (in.)
0	0.0000	0.0000	0.0000	0.0000	0.0000	0.0000	0.0000	0.0000	0.00	0.00	0.00	0.00
25	0.0070	***	0.0110	0.0000	0.0030	***	0.0160	***	0.01	***	0.00	***
50	0.0100	***	0.0310	0.0340	0.0200	***	0.0310	***	0.01	***	0.00	***
100	0.0140	***	0.0700	0.0760	0.0620	***	0.0630	***	0.04	***	0.00	***
0	0.0170	***	0.0520	0.0490	0.0590	***	0.0310	***	0.02	0.01	0.00	***
100	0.0170	0.0180	0.0790	0.0790	0.0700	0.0700	0.0630	0.0630	0.05	0.05	0.00	0.00
200	0.0270	0.0290	0.1460	0.1550	0.1350	0.1420	0.1250	0.1330	0.09	0.09	0.00	0.00
300	0.0420	0.0470	0.2250	0.2400	0.2170	0.2230	0.2030	0.2030	0.16	***	0.00	0.00
400	0.0600	0.0640	0.3060	0.3170	0.2860	0.2930	0.2810	0.2810	0.25	***	-0.02	-0.020
200	0.0610	0.0590	0.2690	0.2680	0.2560	***	0.2500	***	0.19	0.19	0.00	0.00
0	0.0490	0.0470	0.1510	0.1470	0.1540	0.0470	0.1410	0.1410	0.09	0.08	0.00	0.00
200	0.0510	0.0520	0.2290	0.2280	0.2050	0.1050	0.2110	0.2190	0.16	0.16	0.00	0.00
400	0.0650	0.0690	0.3290	0.3410	0.3020	0.2110	0.2970	0.3130	0.26	0.26	-0.02	-0.020
500	0.0870	0.0930	0.4140	0.4260	0.3820	0.2880	0.3750	0.3910	0.34	0.34	-0.04	-0.04
600	0.1170	0.1240	0.5090	0.5200	0.4670	0.3720	0.4690	0.4850	0.42	0.42	-0.08	-0.08
700	0.1570	0.1670	0.6080	0.6260	0.5670	0.4800	0.5780	0.5940	0.52	0.52	-0.16	-0.16
800	0.2020	0.2160	0.7130	0.7340	0.6660	1.6000	0.6880	0.7030	0.62	0.62	-0.22	-0.22
900	0.2570	0.2850	0.8500	0.8760	0.8050	0.7220	0.8130	0.8440	0.76	0.76	-0.30	-0.32
1000	0.3420	0.3570	0.9900	1.0100	0.9400	0.8640	0.9530	0.9850	0.90	0.90	-0.40	-0.40
1000	***	0.3640	***	1.0240	***	0.8790	***	***	***	***	***	-0.42
750	0.3530	0.3510	0.9390	0.9320	***	0.7880	0.9220	0.9220	0.85	0.85	-0.36	-0.36
500	0.3370	0.3380	0.8230	0.8240	***	0.6810	0.8280	0.8280	0.74	0.74	-0.30	-0.28
250	0.3150	0.3110	0.7040	0.6950	***	0.5510	0.7030	0.7030	0.60	0.60	-0.26	***
0	0.2740	0.2620	0.5210	0.5070	***	0.3570	0.5310	0.5000	0.41	0.40	-0.14	***

\*\*\* Reading not taken

D1 - Dial gauge and tell-tale

D2, & D3 - Dial gauges fixed to butt of shaft

J1, J2, R1 - Marked scales fixed to jack and reaction shaft

Measured Load-Displacement Data for Test Shaft C1.

Table Measured Displacement, Shaft C2

Load (tons)	Gauge D1		Gauge D2		Gauge D3		Gauge J1		Gauge J2		Gauge R1	
	$\delta 1$ (in.)	$\delta 2$ (in.)	$\delta 1$ (in.)	$\delta 2$ (in.)	$\delta 1$ (in.)	$\delta 2$ (in.)	$\delta 1$ (in.)	$\delta 2$ (in.)	$\delta 1$ (in.)	$\delta 2$ (in.)	$\delta 1$ (in.)	$\delta 2$ (in.)
0	0.0000	0.0000	0.0000	0.0000	0.0000	0.0000	0.0000	0.0000	0.00	0.00	0.00	0.00
25	0.0000	0.0000	0.0024	0.0024	0.0180	0.0180	0.0160	0.0160	0.00	***	0.00	0.00
50	0.0140	0.0140	0.0253	0.0255	0.0330	0.0350	0.0310	0.0310	0.01	***	0.00	0.00
75	0.0150	***	0.0303		0.0390	0.0400	0.0470	0.0470	0.03	***	0.00	0.00
100	0.0230	0.0230	0.0543	0.0543	0.0570	0.0580	0.0630	0.0630	0.06	***	0.00	0.00
50	0.0230	0.0230	0.0485	0.0481	0.0380	0.0390	0.0470	0.0470	0.04	0.04	0.00	0.00
0	0.0230	0.0230	0.0425	0.0376	0.0250	0.0190	0.0310	0.0310	0.01	0.01	0.00	0.00
100	0.0210	0.0210	0.0575	0.0575	0.0610	0.0650	0.0630	0.0630	0.06	0.06	0.00	0.00
150	0.0370	0.0370	0.0769	0.0797	0.0880	0.0920	0.0860	0.0940	0.07	0.07	0.00	0.00
200	0.0840	0.0870	0.1430	0.1483	0.1460	0.1560	0.1250	0.1410	0.13	0.13	0.02	0.02
250	0.1590	0.2640	0.2385	0.2443	0.2350	0.2490	0.2190	0.2340	0.21	0.24	0.02	0.02
300	0.3270	0.4390	0.4285	0.4415	0.4210	0.4430	0.4060	0.4220	0.41	0.44	0.04	0.04
350	0.6740	0.7150	0.8295	0.8443	0.7740	0.8310	0.8030	0.7970	0.81	0.81	0.04	0.05
375	1.0390	1.2670			1.1660	1.2960	1.1410	1.2660	1.16	1.26	0.06	***
150	1.1140	1.2060			1.2090	1.2040	1.1880	1.1880	1.20	1.20	0.05	0.05
0	1.0140	1.1080			1.0760	1.0620	1.0630	1.0630	1.08	1.06	0.02	0.02
375	1.5320	1.6670			1.6660	1.7970	1.6410	1.7660	1.66	1.80	0.06	0.06
400	2.0420	2.2190			2.0640	2.2560	2.0470	2.2340	2.06	2.26	0.07	0.07
425	2.8570	2.9660					2.9690	3.0780			0.08	0.08
450							3.9220	4.0940			0.09	0.10
475							4.9530	5.0780			0.10	0.10
500							6.2970	6.4530			0.10	***
375							6.3910	***			0.10	***
250							6.3280	***			0.08	***
125							6.2340	***			0.07	***
0							6.0780	6.0000			0.04	***

\*\*\* Reading not taken

D1 - Dial gauge and tell-tale; D2, & D3 - Dial gauges fixed to butt of shaft; J1, J2, R1 - Marked scales fixed to jack and reaction shaft

Measured Load-Displacement Data for Test Shaft C2.

Table Measured Displacement, Shaft C3

	Gauge C3-1	Gauge C3-2	Gauge C3-3	Gauge J1-E	Gauge J1-L	Gauge R3
Load (tons)	$\delta 1$ (in.)	$\delta 1$ (in.)	$\delta 1$ (in.)	$\delta 1$ (in.)	$\delta 1$ (in.)	$\delta 1$ (in.)
0	0.0000	0.0000	0.0000	0.0000	0.0000	0.0000
75	0.6970	***	0.7000	0.7656	0.7500	0.0060
0	0.0240	***	0.0230	0.0469	0.0400	0.0060
100	***	***	***	2.1094	2.0600	0.0000
150	***	***	***	4.8281	3.8800	0.0000
0	***	***	***	0.5625	3.7500	***
100	***	***	***	0.4219	0.4500	***
150	***	***	***	1.0156	1.0200	***
175	***	***	***	5.2969	5.3000	***
0	***	***	***	0.7500	***	***

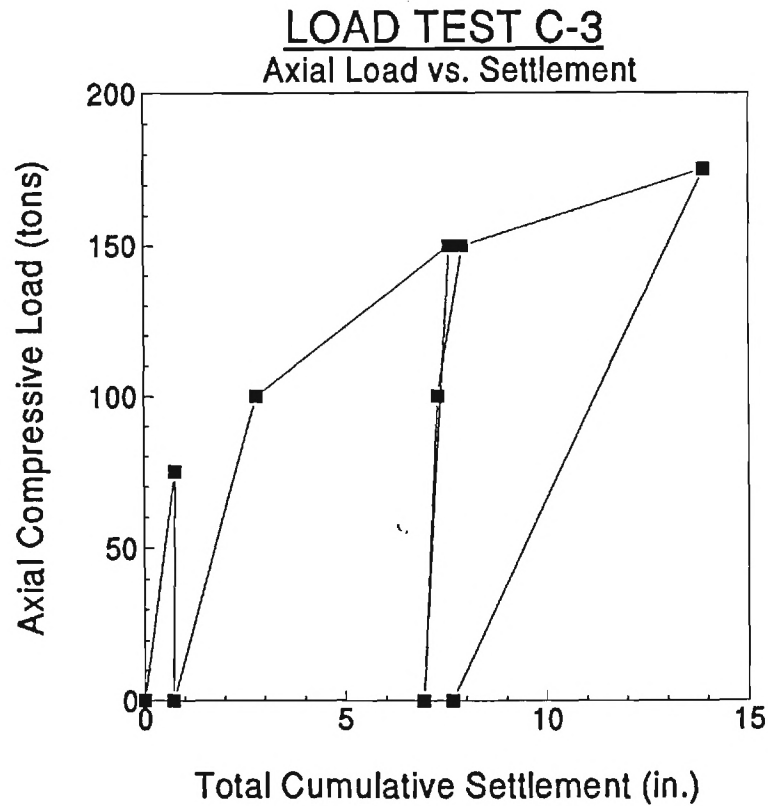
\*\*\* Reading not taken

C3-1 & C3-3 - Dial gauges and tell-tale

C3-2 - Gauge to top of beam

J1-E & J1-L - Marked scales fixed to jack

R3 - Marked scale fixed to reaction shaft

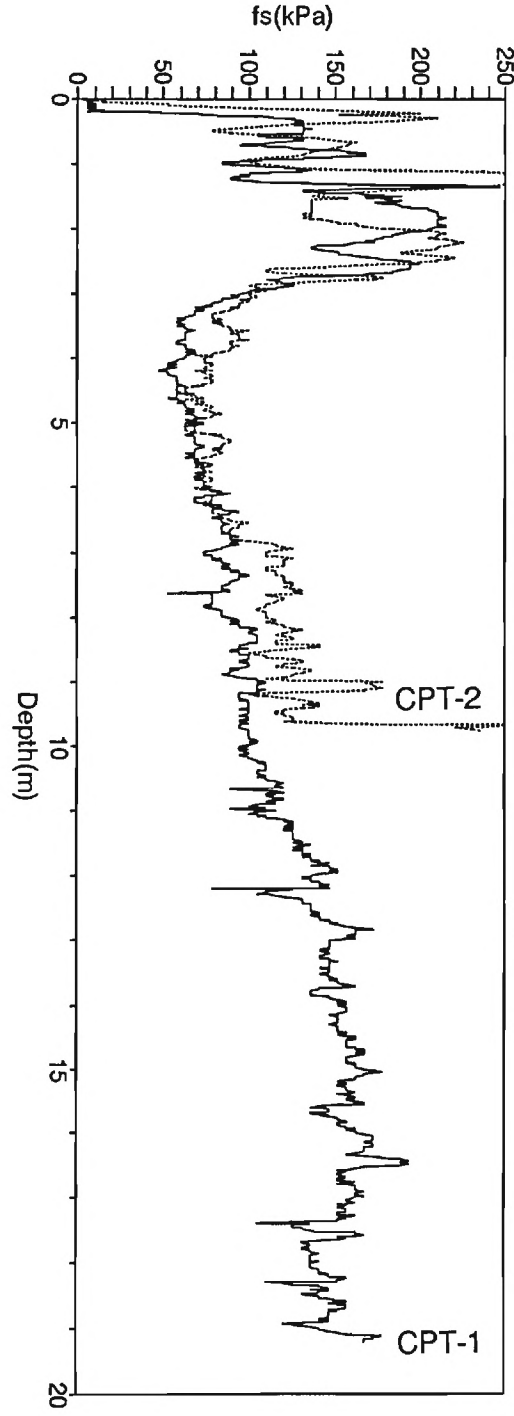
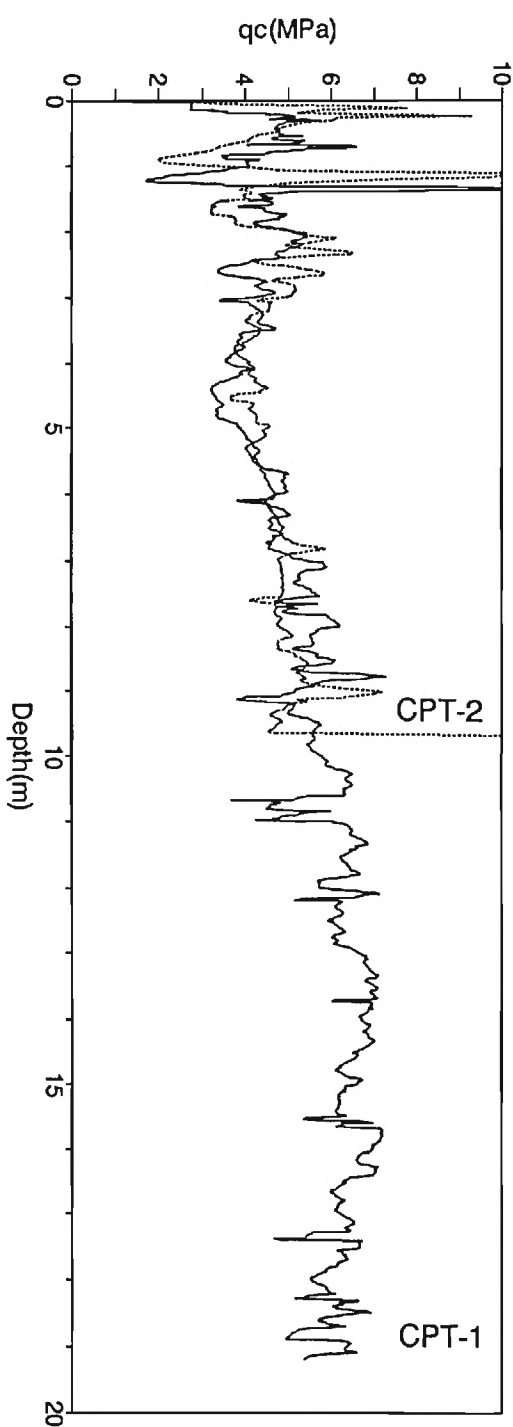


Measured Load-Displacement Data for Deep Plate Load Test C-3.

**Georgia Institute of Technology**  
**Cone/Piezocone Penetration Test**

Project: ASCE Drilled Shaft Load Test  
Client: \_\_\_\_\_  
Test Site: GT Campus, 16' NW of C-2  
Test Type/No.: CPT-1 & CPT-2  
Drill Rig: CME-55

Date: June 8, 1992  
GWL: -  
Pre-drilled: 0 ft  
Operator(s): Barry Chen  
Douq Brown



ATEC ASSOCIATES, INC.  
 FILE NAME: ASCE/ADSC DRILLED PIER RESEARCH PROJECT AT GEORGIA TECH  
 FILE NUMBER: GT-RES/VEST CAMPUS

RECORD OF DILATOMETER TEST NO. DMT-5  
 USING DATA REDUCTION PROCEDURES IN MARCHETTI (ASCE, J-GED, MARCH 80)  
 K0 IN SANDS DETERMINED USING SCHERTMANN METHOD (1983)  
 PHI ANGLE CALCULATION BASED ON DURGUNOGLU AND MITCHELL (ASCE, RALEIGH CONF, JUNE 75)  
 PHI ANGLE NORMALIZED TO 2.72 BARS USING BALIGH'S EXPRESSION (ASCE, J-GED, NOV 76)  
 MODIFIED MAYNE AND KULHAVY FORMULA USED FOR OCR IN SANDS (ASCE, J-GED, JUNE 82)

LOCATION: 1 foot north of TSB-5  
 PERFORMED - DATE: 28 MARCH 1992  
 BY: A. FRANK

CALIBRATION INFORMATION:  
 DELTA A = .20 BARS DELTA B = .92 BARS GAGE 0 = .00 BARS GWT DEPTH=16.80 M  
 ROD DIA.= 4.45 CM PR.RED.DIA.= 5.36 CM ROD VT.= 6.30 KG/M DELTA/PHI= .50 BLADE T=15.00 MM

1 BAR = 1.019 KG/CM2 = 1.044 TSF = 14.51 PSI ANALYSIS USES H2O UNIT WEIGHT = 1.000 T/M3

Z (M)	THRUST (KG)	A (BAR)	B (BAR)	ED (BAR)	ID	KD	UO (BAR)	GAMMA (T/M3)	SV (BAR)	PC (BAR)	OCR	K0	CU (BAR)	PHI (DEG)	M (BAR)	SOIL TYPE
.91	1400.	1.10	3.75	56.	1.31	7.11	.000	2.119	.172	.72	4.16	.73		42.4	120.8	SANDY SILT
1.22	1400.	2.65	8.40	169.	1.86	11.23	.000	1.900	.233	3.40	14.58	1.44		38.0	440.3	SILTY SAND
1.52	1400.	4.35	10.00	165.	1.10	15.03	.000	1.800	.288	6.69	23.26	2.35			476.3	SILT
1.83	1400.	4.15	9.50	154.	1.07	12.09	.000	1.800	.342	5.67	16.55	2.07			413.0	SILT
2.13	933.	.75	4.35	90.	3.15	2.10	.000	1.700	.394	.40	1.02	.41		36.7	103.3	SILTY SAND
2.65	778.	1.10	3.40	43.	1.00	2.60	.000	1.600	.478	.72	1.50	.69			49.6	SILT
3.05	1400.	2.10	5.50	83.	1.10	4.03	.000	1.700	.543	1.62	2.98	.99			132.7	SILT
3.35	1710.	2.55	6.50	103.	1.14	4.40	.000	1.700	.593	2.03	3.42	1.06			174.0	SILT
3.66	1710.	1.20	4.30	72.	1.60	2.02	.000	1.700	.645	.57	.88	.37		38.4	69.5	SANDY SILT
3.96	1866.	2.35	6.30	103.	1.23	3.47	.000	1.700	.695	1.47	2.11	.58		37.4	150.3	SANDY SILT
4.18	1866.	2.35	6.50	110.	1.33	3.28	.000	1.700	.731	1.45	1.98	.56		37.2	155.7	SANDY SILT
4.57	2022.	2.70	6.95	114.	1.20	3.44	.000	1.700	.796	1.86	2.34	.88			165.3	SILT
4.88	2022.	2.90	7.10	112.	1.10	3.47	.000	1.800	.850	2.00	2.36	.88			162.6	SILT
5.18	2022.	3.15	7.80	129.	1.17	3.52	.000	1.800	.903	2.18	2.41	.89			188.7	SILT
5.49	2022.	3.10	7.50	120.	1.10	3.28	.000	1.800	.957	2.07	2.16	.84			166.4	SILT
5.70	2333.	2.70	7.75	143.	1.53	2.72	.000	1.800	.995	1.54	1.54	.50		37.5	178.1	SANDY SILT
6.10	2644.	3.10	7.80	130.	1.20	2.93	.000	1.800	1.065	1.79	1.68	.52		37.9	168.3	SANDY SILT
6.40	2644.	3.60	9.40	171.	1.38	3.19	.000	1.800	1.118	2.21	1.98	.57		37.4	236.4	SANDY SILT
6.71	2799.	3.30	8.75	158.	1.38	2.80	.000	1.800	1.173	1.88	1.60	.51		37.8	198.8	SANDY SILT
7.01	2955.	3.30	9.10	171.	1.50	2.66	.000	1.800	1.226	1.81	1.47	.49		38.1	208.4	SANDY SILT
7.23	2955.	3.20	9.80	200.	1.84	2.47	.000	1.900	1.267	1.70	1.34	.47		38.0	235.4	SILTY SAND
7.62	2955.	3.70	10.30	200.	1.59	2.71	.000	1.800	1.338	2.13	1.59	.51		37.5	248.8	SANDY SILT
7.93	2799.	4.20	11.50	225.	1.59	2.94	.000	1.800	1.393	2.63	1.89	.57		36.6	298.0	SANDY SILT
8.23	2955.	4.25	11.30	216.	1.50	2.87	.000	1.800	1.445	2.62	1.81	.55		36.8	279.8	SANDY SILT
8.54	2799.	3.80	9.90	181.	1.39	2.50	.000	1.800	1.500	2.33	1.55	.52		36.5	208.8	SANDY SILT
8.69	3110.	4.05	11.30	223.	1.63	2.58	.000	1.800	1.527	2.37	1.55	.51		37.2	268.8	SANDY SILT
9.15	3266.	3.60	9.60	178.	1.44	2.21	.000	1.800	1.608	2.01	1.25	.46		37.5	184.2	SANDY SILT
9.45	2799.	4.05	10.90	209.	1.52	2.39	.000	1.800	1.661	2.55	1.53	.52		35.9	233.2	SANDY SILT
9.76	2799.	4.00	10.70	203.	1.49	2.29	.000	1.800	1.716	2.53	1.47	.52		35.8	218.2	SANDY SILT
10.15	2955.	3.45	11.30	245.	2.13	1.85	.000	1.900	1.787	2.01	1.13	.45		36.4	230.8	SILTY SAND
10.37	3421.	4.70	13.70	287.	1.84	2.47	.000	1.900	1.828	2.78	1.52	.51		36.9	338.1	SILTY SAND

END OF SOUNDING

Reduced Data From Dilatometer Sounding DMT-1.

ATEC ASSOCIATES, INC.  
 FILE NAME: ASCE/ADSC DRILLED PIER RESEARCH PROJECT AT GEORGIA TECH  
 FILE NUMBER: GT-RBS/WEST CAMPUS

RECORD OF DILATOMETER TEST NO. DMT-6  
 USING DATA REDUCTION PROCEDURES IN MARCHETTI (ASCE, J-GED, MARCH 80)  
 K0 IN SANDS DETERMINED USING SCHMERTMANN METHOD (1983)  
 PHI ANGLE CALCULATION BASED ON DURGUNOGLU AND MITCHELL (ASCE, RALEIGH CONF, JUNE 75)  
 PHI ANGLE NORMALIZED TO 2.72 BARS USING BALIGH'S EXPRESSION (ASCE, J-GED, NOV 76)  
 MODIFIED MAYNE AND KULHAVY FORMULA USED FOR OCR IN SANDS (ASCE, J-GED, JUNE 82)

LOCATION: 1.5 feet south of TSB-6  
 PERFORMED - DATE: 28 MARCH 1992  
 BY: A. FRANK

CALIBRATION INFORMATION:  
 DELTA A = .20 BARS DELTA B = .95 BARS GAGE 0 = .00 BARS GWT DEPTH=16.80 M  
 ROD DIA. = 4.45 CM FR. RED. DIA. = 5.36 CM ROD WT. = 6.30 KG/M DELTA/PHI = .50 BLADE T=15.00 MM  
 1 BAR = 1.019 KG/CM2 = 1.044 TSP = 14.51 PSI ANALYSIS USES H2O UNIT WEIGHT = 1.000 T/M3

Z (M)	THRUST (KG)	A (BAR)	B (BAR)	ED (BAR)	EO	KD	UO (BAR)	GAMMA (T/M3)	SV (BAR)	PC (BAR)	OCR	K0	CU (BAR)	PHI (DEG)	M (BAR)	SOIL TYPE
.30	2177.	4.35	12.00	237.	1.62	74.12	.000	2.119	.057						1041.2	SANDY SILT
.61	3110.	4.70	10.80	180.	1.12	39.90	.000	1.800	.117	12.43	****	4.07			687.2	SILT
.91	2644.	6.35	14.10	240.	1.11	36.20	.000	1.950	.172	15.74	91.63	3.87			894.1	SILT
1.22	3110.	8.05	19.50	375.	1.40	33.47	.000	1.950	.231	28.24	****	4.11	38.2		1367.4	SANDY SILT
1.52	3266.	7.15	18.00	353.	1.48	23.79	.000	1.950	.289	17.55	60.82	2.92	39.2		1173.6	SANDY SILT
1.83	3421.	5.30	13.40	253.	1.42	14.81	.000	1.950	.348	7.90	22.70	1.78	40.9		727.2	SANDY SILT
2.13	3110.	4.95	11.40	193.	1.14	12.12	.000	1.800	.403	6.70	16.62	2.07			517.9	SILT
2.44	2955.	4.15	9.80	164.	1.15	9.01	.000	1.800	.458	4.79	10.47	1.72			393.0	SILT
2.74	2488.	3.30	9.00	166.	1.46	6.41	.000	1.800	.511	2.54	4.97	.84	39.7		342.9	SANDY SILT
3.09	2122.	2.70	7.15	120.	1.27	4.78	.000	1.800	.573	1.82	3.17	.68	38.8	213.4		SANDY SILT
3.35	2155.	3.15	8.35	148.	1.35	5.09	.000	1.800	.619	2.29	3.69	.74	38.2	271.6		SANDY SILT
3.66	2122.	3.55	9.40	171.	1.40	5.22	.000	1.800	.673	2.73	4.05	.79	37.4	319.9		SANDY SILT
3.96	2488.	3.80	9.80	177.	1.36	5.17	.000	1.800	.726	2.79	3.85	.76	38.2	328.1		SANDY SILT
4.27	2117.	4.55	11.30	204.	1.32	5.72	.000	1.800	.781	3.96	5.07	.89	36.1	398.7		SANDY SILT
4.57	2333.	3.70	10.00	188.	1.48	4.37	.000	1.800	.834	2.58	3.09	.70	37.4	318.7		SANDY SILT
4.88	2177.	3.70	9.80	180.	1.42	4.11	.000	1.800	.889	2.62	2.95	.69	36.6	295.1		SANDY SILT
5.18	2333.	3.30	9.55	186.	1.65	3.45	.000	1.800	.942	2.06	2.19	.59	37.3	275.2		SANDY SILT
5.49	2488.	3.55	9.30	168.	1.37	3.53	.000	1.800	.997	2.26	2.27	.60	37.3	249.0		SANDY SILT
5.79	2488.	4.70	11.10	191.	1.19	4.42	.000	1.800	1.050	3.61	3.44	1.06		324.1		SILT
6.10	2488.	4.75	11.80	215.	1.33	4.22	.000	1.800	1.104	3.52	3.19	.72	36.1	355.9		SANDY SILT
6.40	2488.	3.75	9.60	171.	1.33	3.21	.000	1.800	1.157	2.42	2.09	.59	36.6	237.9		SANDY SILT
6.71	2177.	3.55	9.00	157.	1.28	2.92	.000	1.800	1.212	2.39	1.97	.59	35.4	202.3		SANDY SILT
7.01	2177.	4.35	10.20	171.	1.14	3.41	.000	1.800	1.265	2.91	2.30	.87		245.8		SILT
7.32	2644.	5.15	12.00	208.	1.18	3.84	.000	1.800	1.320	3.65	2.76	.96		322.9		SILT
7.62	2799.	4.45	12.40	248.	1.66	3.14	.000	1.800	1.373	2.85	2.08	.59	36.5	345.0		SANDY SILT
7.93	2644.	4.55	11.40	208.	1.34	3.13	.000	1.800	1.428	3.07	2.15	.61	35.8	283.4		SANDY SILT
8.23	2799.	4.85	11.60	204.	1.23	3.22	.000	1.800	1.481	3.30	2.23	.62	35.9	282.7		SANDY SILT
8.54	2955.	4.45	11.80	226.	1.50	2.83	.000	1.800	1.535	2.80	1.82	.56	36.5	288.9		SANDY SILT
8.84	2799.	3.85	11.20	226.	1.74	2.35	.000	1.800	1.588	2.34	1.47	.51	36.2	254.2		SANDY SILT
9.15	2644.	4.50	10.80	188.	1.22	2.70	.000	1.800	1.643	3.05	1.85	.58	35.2	227.4		SANDY SILT
9.45	2488.	3.85	10.90	215.	1.65	2.21	.000	1.800	1.696	2.52	1.49	.53	35.0	227.4		SANDY SILT
9.76	2955.	4.20	12.20	250.	1.77	2.32	.000	1.800	1.751	2.58	1.48	.51	36.1	277.8		SANDY SILT
10.21	3266.	4.25	13.20	284.	2.02	2.22	.000	1.900	1.833	2.48	1.35	.49	36.7	311.0		SILTY SAND
10.36	3266.	5.35	13.50	255.	1.41	2.79	.000	1.950	1.861	3.48	1.87	.57	36.1	321.5		SANDY SILT
10.67	3266.	4.75	13.20	266.	1.67	2.39	.000	1.800	1.918	2.94	1.53	.52	36.2	301.4		SANDY SILT
10.98	3266.	4.25	13.20	284.	2.02	2.06	.000	1.900	1.975	2.52	1.28	.48	36.4	291.3		SILTY SAND
11.28	3888.	5.70	15.50	315.	1.66	2.69	.000	1.950	2.031	3.46	1.70	.54	37.0	392.6		SANDY SILT
11.74	4354.	5.55	14.00	266.	1.42	2.54	.000	1.950	2.119	3.20	1.51	.51	37.8	311.0		SANDY SILT
11.90	4254.	6.45	15.70	295.	1.36	2.90	.000	1.950	2.150	4.03	1.88	.57	37.2	382.0		SANDY SILT
12.20	4354.	6.10	15.40	297.	1.45	2.67	.000	1.950	2.207	3.66	1.66	.53	37.4	362.2		SANDY SILT
12.50	4665.	6.60	17.50	355.	1.62	2.79	.000	1.950	2.265	3.92	1.73	.54	37.7	453.2		SANDY SILT
12.65	4665.	5.70	15.70	322.	1.70	2.38	.000	1.950	2.293	3.18	1.39	.49	38.0	364.9		SANDY SILT
12.96	4665.	7.15	17.60	339.	1.42	2.93	.000	1.950	2.353	4.46	1.89	.57	37.3	442.5		SANDY SILT

END OF SOUNDING

Reduced Data From Dilatometer Sounding DMT-2.



FILE NAME: ASCE/ADSC DRILLED PIER RESEARCH PROJECT AT GEORGIA TECH  
 FILE NUMBER: GT-RES/WEST CAMPUS

RECORD OF DILATOMETER TEST NO. DMT-8  
 USING DATA REDUCTION PROCEDURES IN MARCHETTI (ASCE, J-GED, MARCH 80)  
 K<sub>0</sub> IN SANDS DETERMINED USING SCHMERTMANN METHOD (1983)  
 PHI ANGLE CALCULATION BASED ON DURGUKOGLU AND MITCHELL (ASCE, RALEIGH CONF, JUNE 75)  
 PHI ANGLE NORMALIZED TO 2.72 BARS USING BALIGH'S EXPRESSION (ASCE, J-GED, NOV 76)  
 MODIFIED MAYNE AND KULHAVY FORMULA USED FOR OCR IN SANDS (ASCE, J-GED, JUNE 82)

LOCATION: 1.5 feet northwest of TSB-8  
 PERFORMED - DATE: 28 MARCH 1992  
 BY: A. FRANK

CALIBRATION INFORMATION:  
 DELTA A = .20 BARS DELTA B = .95 BARS GAGE 0 = .00 BARS GWT DEPTH=19.20 M  
 ROD DIA. = 4.45 CM FR. RED. DIA. = 5.36 CM ROD WT. = 6.30 KG/M DELTA/PHI = .50 BLADE T=15.00 MM

1 BAR = 1.019 KG/CM<sup>2</sup> = 1.044 TSP = 14.51 PSI ANALYSIS USES H<sub>2</sub>O UNIT WEIGHT = 1.000 T/M<sup>3</sup>

Z (M)	THRUST (KG)	A (BAR)	B (BAR)	ED (BAR)	ID	KD	UO (BAR)	GAMMA (T/M <sup>3</sup> )	SV (BAR)	PC (BAR)	OCR	K <sub>0</sub>	CU (BAR)	PHI (DEG)	M (BAR)	SOIL TYPE
*****	*****	*****	*****	*****	*****	*****	*****	*****	*****	*****	*****	*****	*****	*****	*****	*****
.38	622.	1.95	4.35	46.	.63	29.40	.000	2.119	.071	4.70	66.23	3.45	.450		160.4	CLAYEY SILT
.69	933.	.95	3.05	35.	.90	8.64	.000	1.600	.128	1.25	9.81	1.68			81.5	SILT
.99	2488.	4.70	12.20	231.	1.45	25.80	.000	1.800	.178	12.02	67.66	3.11		39.9	786.0	SANDY SILT
1.30	1866.	4.65	10.50	171.	1.07	19.86	.000	1.800	.232	8.35	35.91	2.77			539.3	SILT
1.60	2799.	6.65	15.70	288.	1.29	22.45	.000	1.950	.288	16.08	55.91	2.79		38.3	939.9	SANDY SILT
1.91	2799.	6.85	16.10	295.	1.28	19.16	.000	1.950	.347	14.53	41.87	2.41		38.0	919.4	SANDY SILT
2.21	2799.	4.10	10.30	184.	1.31	10.07	.000	1.800	.402	4.46	11.09	1.25		40.3	461.1	SANDY SILT
2.59	2488.	3.50	9.20	166.	1.38	7.40	.000	1.800	.469	3.03	6.45	.96		39.7	365.8	SANDY SILT
2.74	2488.	2.85	7.55	129.	1.30	5.79	.000	1.800	.496	1.96	3.96	.75		40.3	254.2	SANDY SILT
3.05	2177.	3.45	8.55	144.	1.20	6.27	.000	1.800	.550	2.88	5.23	.88		38.3	293.6	SANDY SILT
3.35	1866.	3.40	8.60	148.	1.25	5.63	.000	1.800	.603	2.83	4.69	.85		36.8	215.6	SANDY SILT
3.66	1710.	3.90	9.10	148.	1.09	5.92	.000	1.800	.658	3.58	5.44	1.31			292.1	SILT
4.05	2177.	3.50	8.90	155.	1.28	4.80	.000	1.800	.727	2.58	3.55	.74		37.4	275.5	SANDY SILT
4.27	2177.	3.55	9.30	168.	1.37	4.60	.000	1.800	.766	2.57	3.36	.72		37.2	292.0	SANDY SILT
4.57	2177.	2.75	7.70	138.	1.45	3.37	.000	1.800	.819	1.66	2.03	.57		37.7	200.1	SANDY SILT
4.88	2177.	3.55	9.20	164.	1.34	4.03	.000	1.800	.874	2.48	2.84	.67		36.7	264.5	SANDY SILT
5.18	2333.	3.75	10.10	189.	1.48	3.98	.000	1.800	.927	2.56	2.76	.67		36.9	304.8	SANDY SILT
5.58	2799.	4.35	10.90	197.	1.32	4.29	.000	1.800	.997	2.99	3.00	.64		37.7	329.1	SANDY SILT
5.79	2644.	4.70	11.40	202.	1.26	4.47	.000	1.800	1.034	3.46	3.35	.73		36.9	345.6	SANDY SILT
6.10	2799.	3.65	10.90	222.	1.81	3.25	.000	1.900	1.091	2.13	1.95	.56		37.9	319.2	SILTY SAND
6.40	2644.	3.70	9.90	184.	1.45	3.18	.000	1.800	1.145	2.29	2.00	.57		37.2	255.9	SANDY SILT
6.71	2644.	4.50	11.80	224.	1.47	3.66	.000	1.800	1.200	3.06	2.55	.65		36.5	342.1	SANDY SILT
7.10	2644.	4.65	11.70	215.	1.36	3.59	.000	1.800	1.269	3.21	2.53	.65		36.2	322.6	SANDY SILT
7.13	2799.	4.30	11.50	220.	1.51	3.29	.000	1.800	1.274	2.75	2.16	.60		36.9	314.8	SANDY SILT
7.62	2955.	4.35	11.90	233.	1.59	3.11	.000	1.800	1.361	2.70	1.98	.57		37.0	321.3	SANDY SILT
7.93	2799.	4.25	11.80	233.	1.63	2.92	.000	1.800	1.415	2.67	1.89	.57		36.5	307.8	SANDY SILT
8.23	2955.	4.50	11.80	224.	1.47	2.99	.000	1.800	1.468	2.85	1.94	.57		36.6	298.3	SANDY SILT
8.63	3110.	4.65	12.70	251.	1.61	2.93	.000	1.800	1.539	2.89	1.88	.56		36.8	332.2	SANDY SILT
8.84	2955.	4.50	11.80	224.	1.47	2.79	.000	1.800	1.576	2.85	1.81	.56		36.4	283.0	SANDY SILT
9.15	3110.	4.55	12.60	251.	1.64	2.70	.000	1.800	1.631	2.80	1.71	.54		36.6	313.6	SANDY SILT
9.45	3110.	4.65	12.10	230.	1.46	2.69	.000	1.800	1.684	2.92	1.73	.55		36.4	282.0	SANDY SILT
9.76	2955.	5.30	12.90	235.	1.31	2.97	.000	1.950	1.741	3.61	2.07	.61		35.5	308.6	SANDY SILT
10.15	3577.	6.25	15.70	302.	1.44	3.32	.000	1.950	1.816	4.18	2.30	.63		36.5	432.9	SANDY SILT
10.37	3266.	5.30	13.30	250.	1.39	2.78	.000	1.950	1.858	3.44	1.85	.57		36.1	312.7	SANDY SILT
10.67	3266.	5.90	14.20	261.	1.31	3.00	.000	1.950	1.915	4.01	2.10	.61		35.7	344.1	SANDY SILT
10.98	3421.	6.55	15.70	291.	1.32	3.22	.000	1.950	1.975	4.55	2.31	.64		35.7	405.4	SANDY SILT
11.28	3577.	6.30	15.70	301.	1.42	3.00	.000	1.950	2.032	4.20	2.07	.60		36.1	399.6	SANDY SILT
11.68	4665.	5.75	15.30	306.	1.59	2.62	.000	1.950	2.108	3.20	1.52	.50		38.3	371.9	SANDY SILT
11.89	4665.	6.25	16.10	317.	1.52	2.80	.000	1.950	2.149	3.64	1.69	.53		38.0	403.0	SANDY SILT
12.20	4665.	5.30	12.80	231.	1.29	2.35	.000	1.950	2.208	2.93	1.33	.47		38.2	-249.7	SANDY SILT




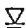
END OF SOUNDING

Reduced Data From Dilatometer Sounding DMT-3.

















**CORRELATION OF PENETRATION RESISTANCE  
WITH RELATIVE DENSITY AND CONSISTENCY**

NO. OF BLOWS, N	RELATIVE DENSITY	PARTICLE SIZE IDENTIFICATION
SANDS:	0-4	BOULDERS: 12 inches OR GREATER COBBLES: 3 inches to 12 inches GRAVEL: Coarse - 3/4 inches to 3 inches Fine - No. 4 to 3/4 inches SANDS: Coarse - No. 10 to No. 4 Medium - No. 40 to No. 10 Fine - No. 200 to NO. 40 SILTS & CLAYS: PASSING No. 200
	5-10	
	11-30	
	31-50	
	OVER 50	
	Very Loose	
	Loose	
	Medium Dense	
	Dense	
	Very Dense	
	CONSISTENCY	
	Very Soft	
	Soft	
SILTS	Firm	
&	Stiff	
CLAYS:	Very stiff	
16-30	Hard	
31-50	Very Hard	
OVER 50		

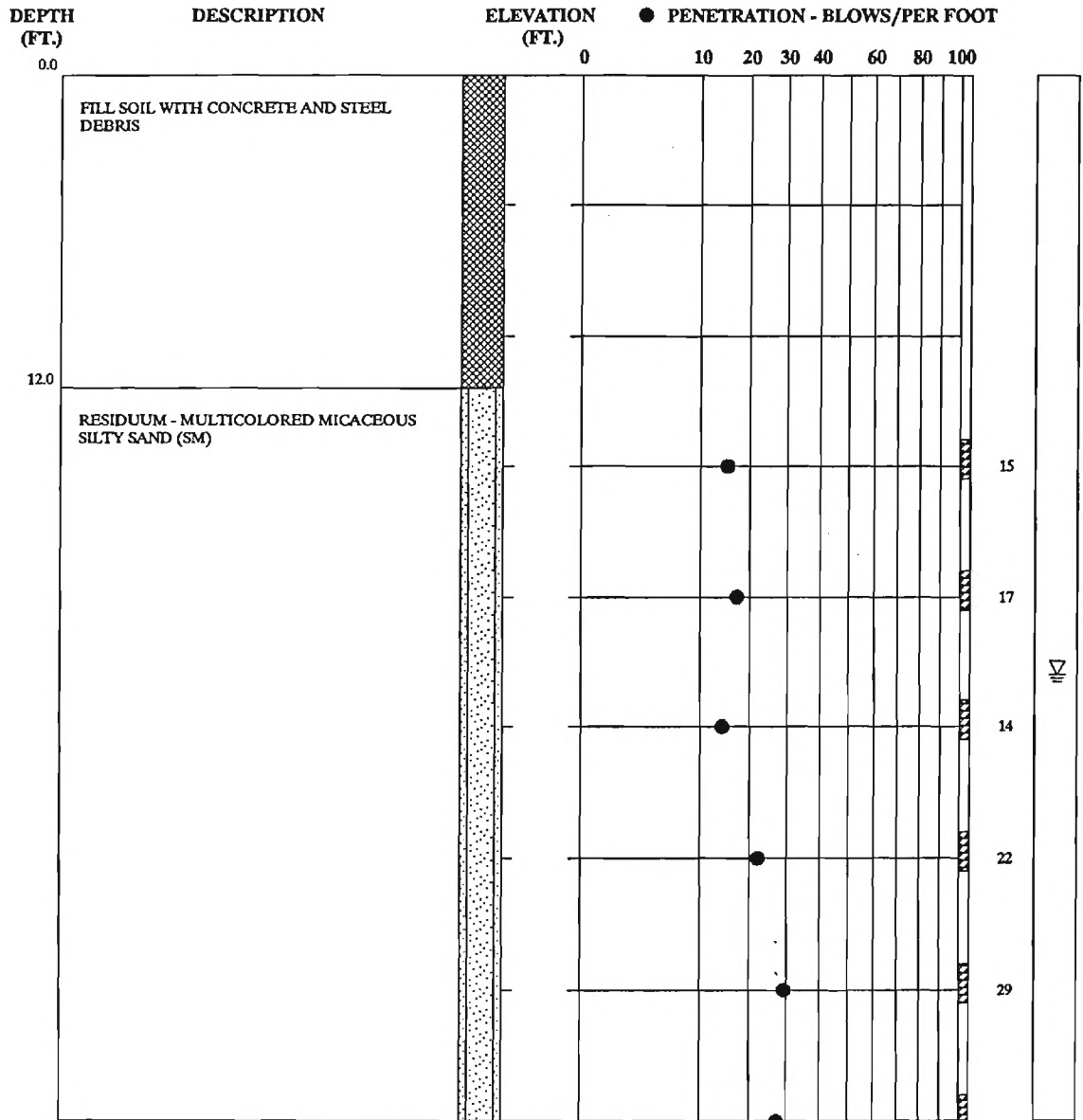
**KEY TO DRILLING SYMBOLS**

 Undisturbed Sample	 Water Table After 24 Hours
 Split Spoon Sample	 Water Table at Time of Drilling

**KEY TO SOIL CLASSIFICATIONS**

 SILTY CLAY	 ASPHALT
 SILT	 CONCRETE
 CLAYEY SILT	 GRAVEL
 SANDY SILT	 TOPSOIL
 SAND	 FILL
 SILTY SAND	 ALLUVIUM
 CLAYEY SAND	 PARTIALLY WEATHERED ROCK - A transitional material between soil and rock which retains the relic structure of the parent rock.
 SANDY CLAY	 ROCK

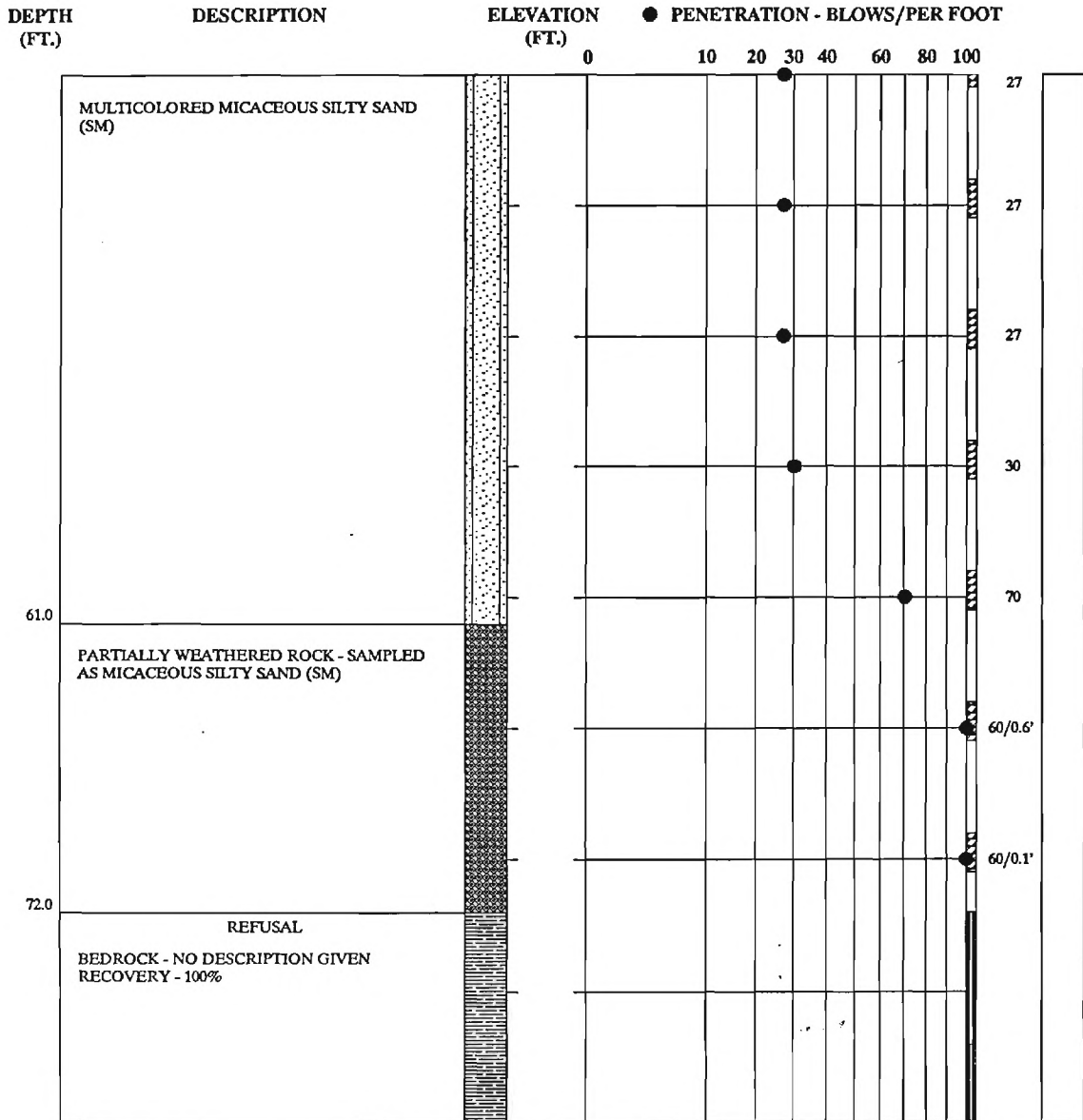
**Boring Logs and SPT-Data**



**REMARKS:**  
Boring performed by Georgia Department of Transportation

SEE KEY SHEET FOR EXPLANATION OF SYMBOLS AND ABBREVIATIONS USED ABOVE

SOIL TEST BORING RECORD	
BORING NUMBER	TSB-1
DATE DRILLED	April 13, 1992
PROJECT NUMBER	
PROJECT	ADSC/ASCE LOAD TEST
PAGE 1 OF 3	



**REMARKS:**  
Boring performed by Georgia Department of Transportation

SEE KEY SHEET FOR EXPLANATION OF SYMBOLS AND ABBREVIATIONS USED ABOVE

SOIL TEST BORING RECORD	
BORING NUMBER	TSB-1
DATE DRILLED	April 13, 1992
PROJECT NUMBER	
PROJECT	ADSC/ASCE LOAD TEST
PAGE 2 OF 3	

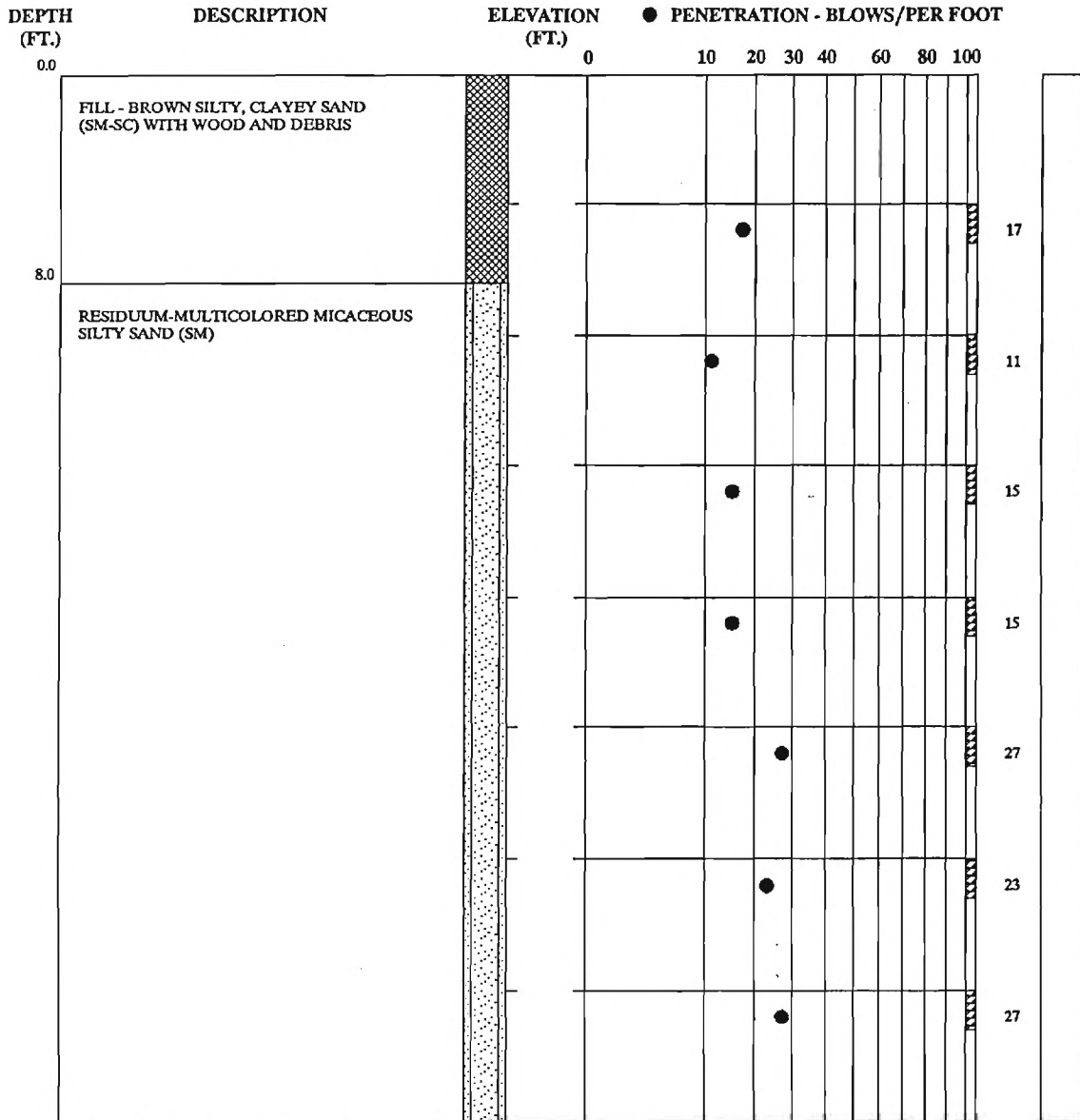
DEPTH (FT.)                      DESCRIPTION                      ELEVATION (FT.)                      ● PENETRATION - BLOWS/PER FOOT

DEPTH (FT.)	DESCRIPTION	ELEVATION (FT.)	● PENETRATION - BLOWS/PER FOOT																	
			0	10	20	30	40	60	80	100										
82.0	CORING TERMINATED																			

**REMARKS:**  
 Boring performed by Georgia Department of Transportation

SEE KEY SHEET FOR EXPLANATION OF SYMBOLS AND ABBREVIATIONS USED ABOVE

SOIL TEST BORING RECORD	
<b>BORING NUMBER</b>	TSB-1
<b>DATE DRILLED</b>	April 13, 1992
<b>PROJECT NUMBER</b>	
<b>PROJECT</b>	ADSC/ASCE LOAD TEST
<b>PAGE 3 OF 3</b>	

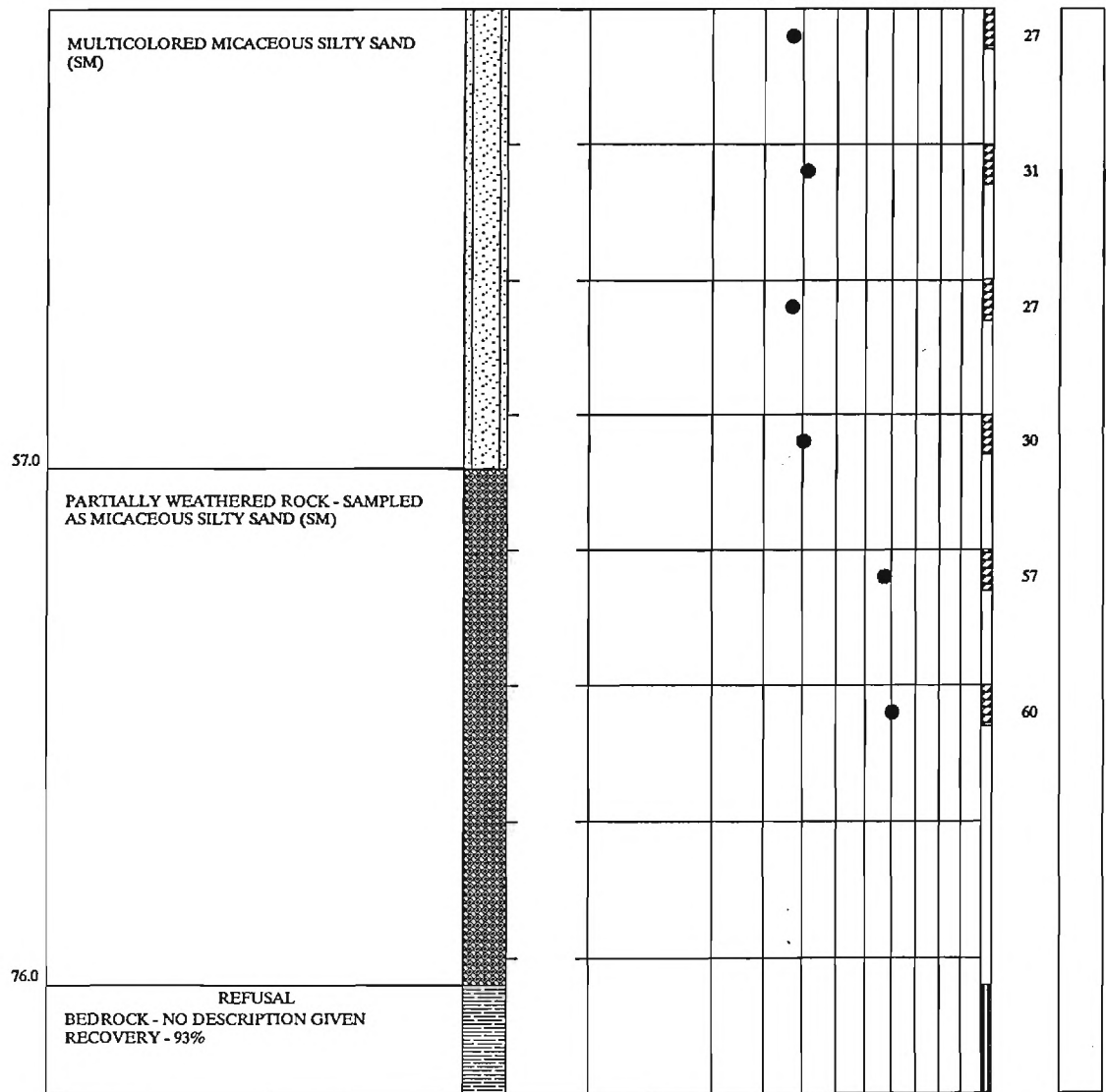


**REMARKS:**  
Boring performed by Georgia Department of Transportation

SEE KEY SHEET FOR EXPLANATION OF SYMBOLS AND ABBREVIATIONS USED ABOVE

SOIL TEST BORING RECORD	
BORING NUMBER	TSB-2
DATE DRILLED	April 13, 1992
PROJECT NUMBER	
PROJECT	ADSC/ASCE LOAD TEST
PAGE 1 OF 3	

DEPTH (FT.)                      DESCRIPTION                      ELEVATION (FT.)                      ● PENETRATION - BLOWS/PER FOOT



**REMARKS:**

Boring performed by Georgia Department of Transportation

SEE KEY SHEET FOR EXPLANATION OF SYMBOLS AND ABBREVIATIONS USED ABOVE

SOIL TEST BORING RECORD	
BORING NUMBER	TSB-2
DATE DRILLED	April 13, 1992
PROJECT NUMBER	
PROJECT	ADSC/ASCE LOAD TEST
PAGE 2 OF 3	

DEPTH (FT.)                      DESCRIPTION                      ELEVATION (FT.)                      ● PENETRATION - BLOWS/PER FOOT

DEPTH (FT.)	DESCRIPTION	ELEVATION (FT.)	● PENETRATION - BLOWS/PER FOOT																	
			0	10	20	30	40	60	80	100										
	BEDROCK - NO DESCRIPTION GIVEN																			
	RECOVERY - 63%																			
90.0	CORING TERMINATED																			

**REMARKS:**  
 Boring performed by Georgia Department of Transportation

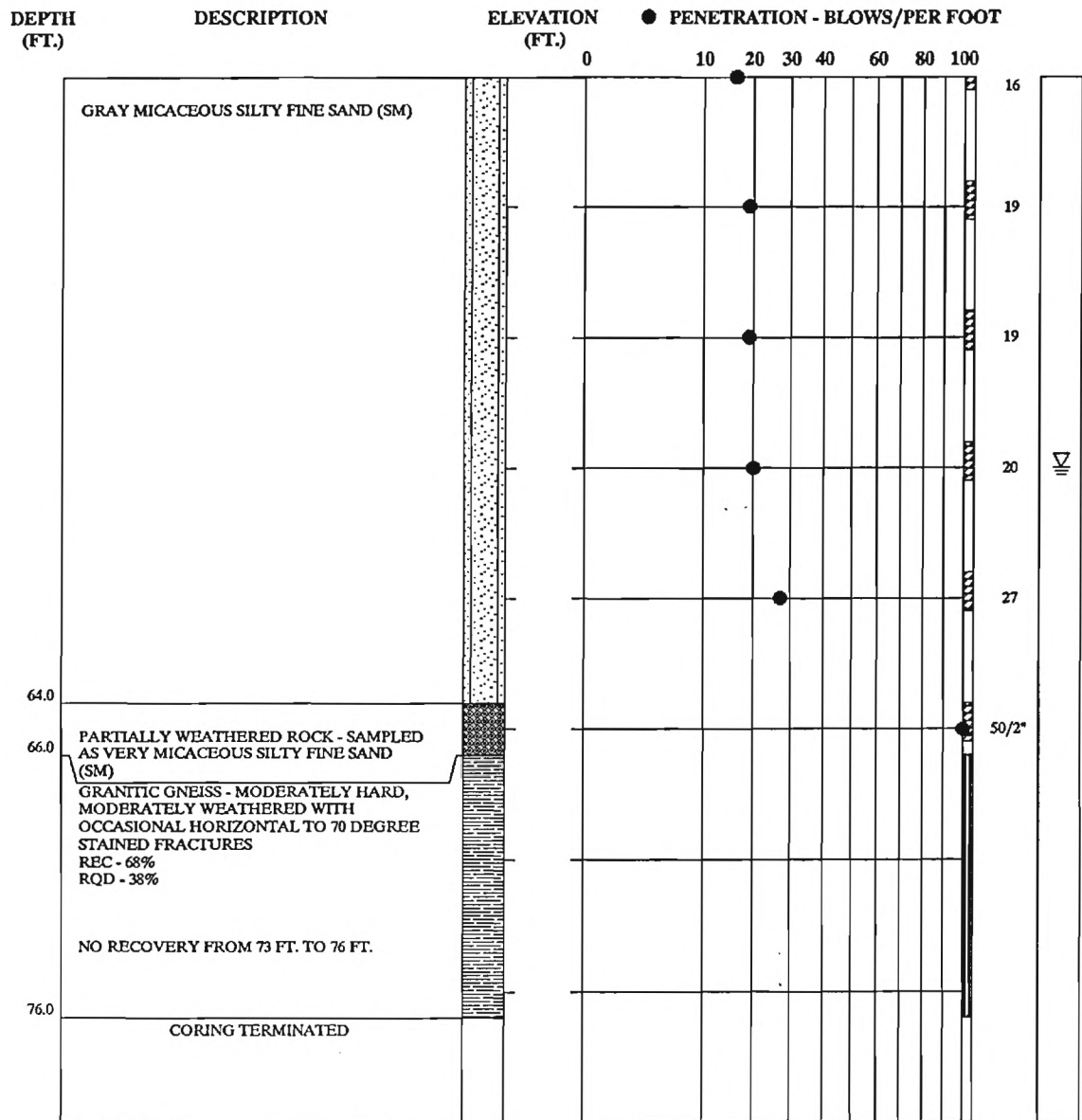
SEE KEY SHEET FOR EXPLANATION OF SYMBOLS AND ABBREVIATIONS USED ABOVE

SOIL TEST BORING RECORD	
BORING NUMBER	TSB-2
DATE DRILLED	April 13, 1992
PROJECT NUMBER	
PROJECT	ADSC/ASCE LOAD TEST
PAGE 3 OF 3	





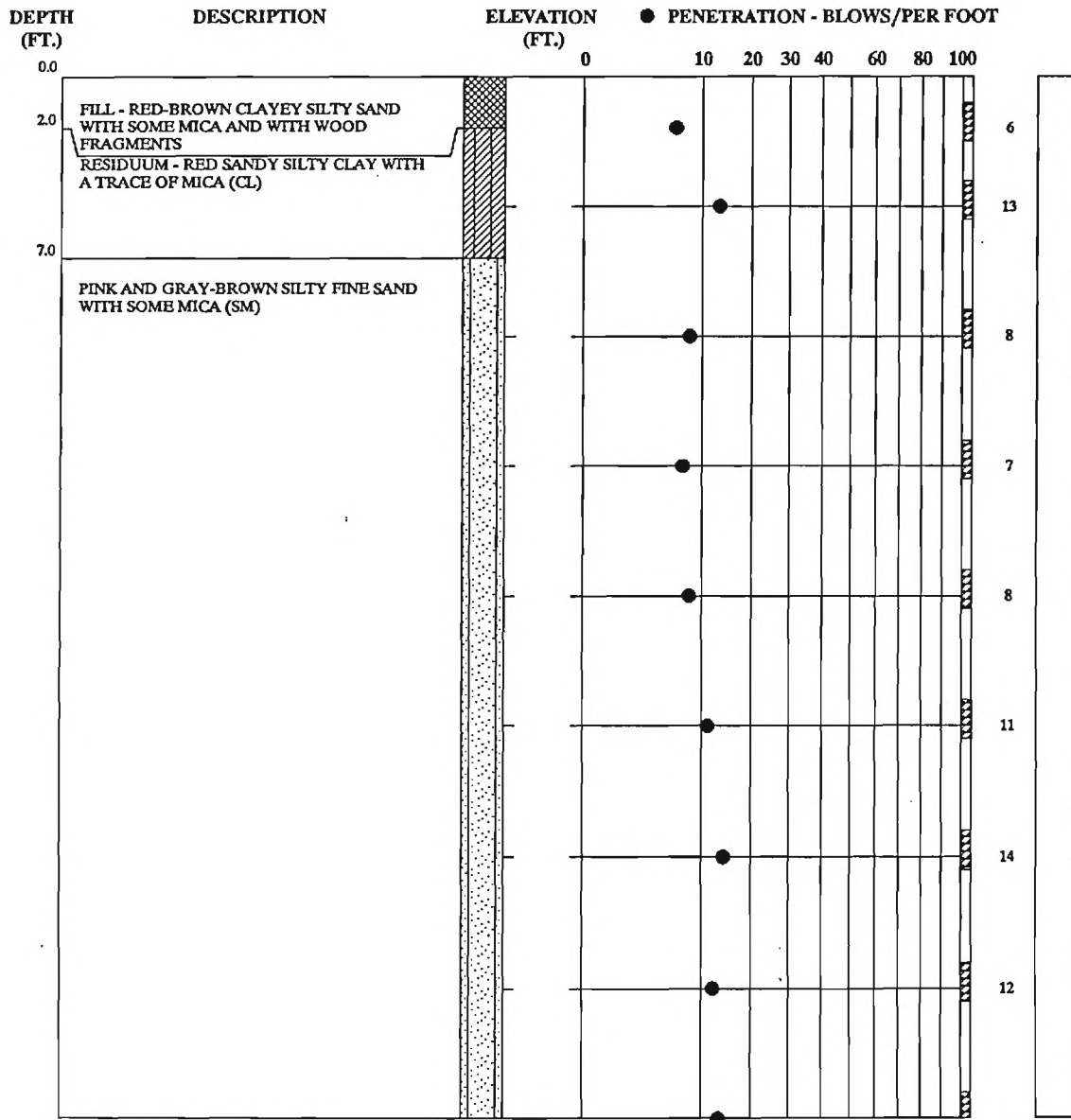




REMARKS:  
Boring performed by Atlanta Testing and Engineering

SEE KEY SHEET FOR EXPLANATION OF SYMBOLS AND ABBREVIATIONS USED ABOVE

SOIL TEST BORING RECORD	
BORING NUMBER	TSB-4
DATE DRILLED	April 2, 1992
PROJECT NUMBER	
PROJECT	ADSC/ASCE LOAD TEST
PAGE 2 OF 2	



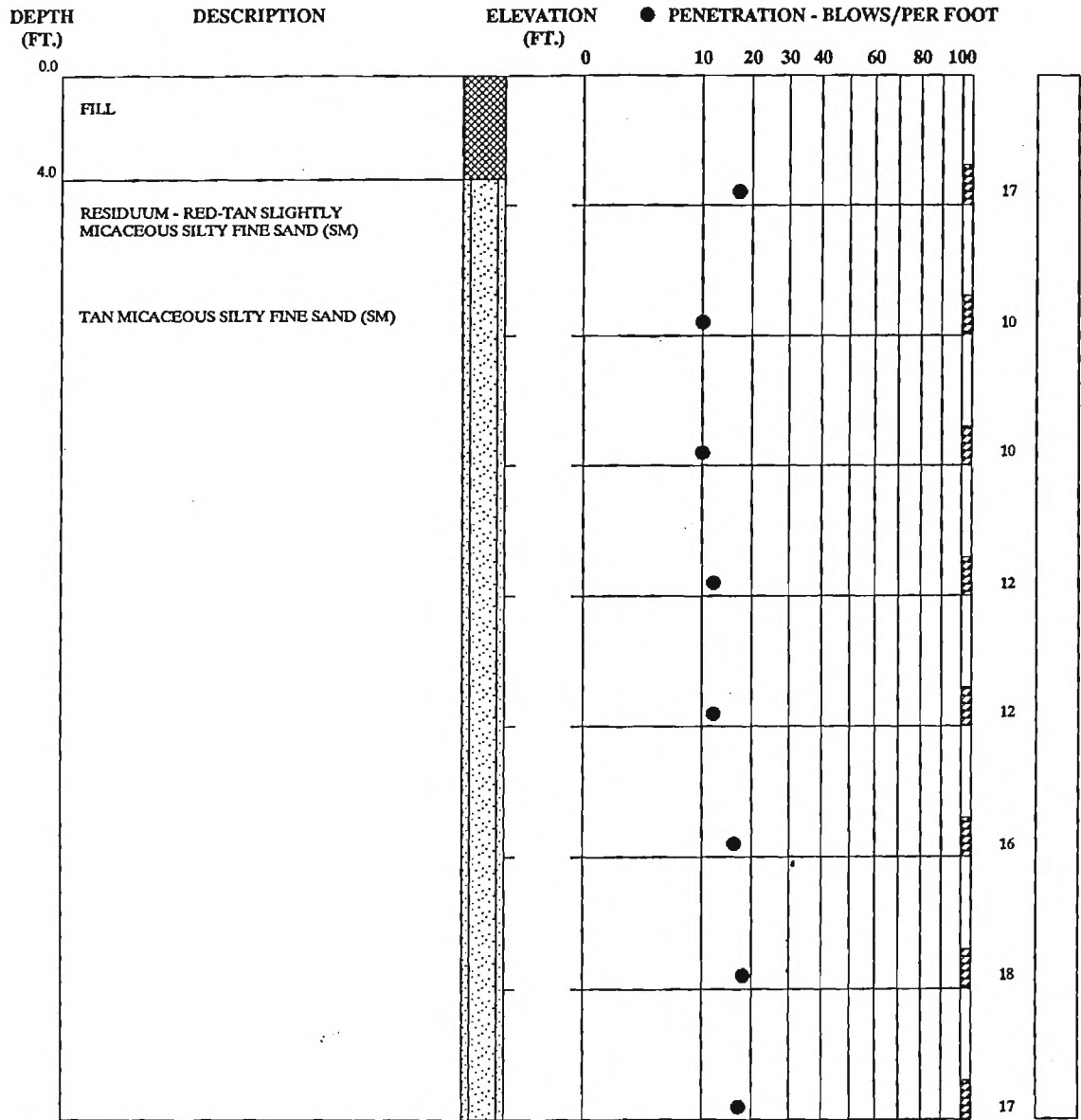
**REMARKS:**  
 Boring performed by Atlanta Testing and Engineering

SOIL TEST BORING RECORD	
BORING NUMBER	TSB-5
DATE DRILLED	April 9, 1992
PROJECT NUMBER	
PROJECT	ADSC/ASCE LOAD TEST
PAGE 1 OF 3	

SEE KEY SHEET FOR EXPLANATION OF SYMBOLS AND ABBREVIATIONS USED ABOVE







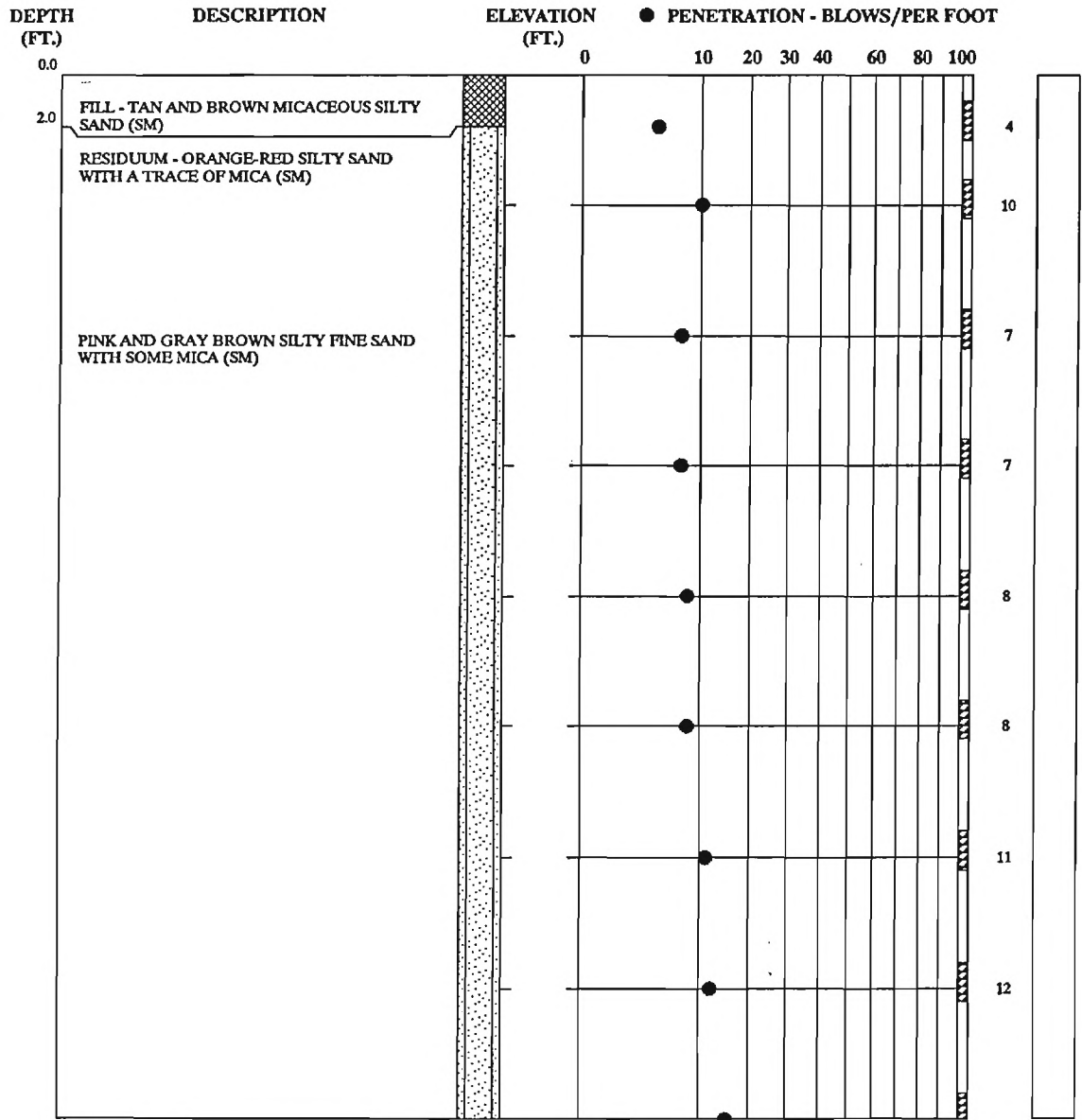
**REMARKS:**  
Boring performed by ATEC Associates, inc.

SEE KEY SHEET FOR EXPLANATION OF SYMBOLS AND ABBREVIATIONS USED ABOVE

SOIL TEST BORING RECORD	
BORING NUMBER	TSB-6
DATE DRILLED	March 21, 1992
PROJECT NUMBER	
PROJECT	ADSC/ASCE LOAD TEST
PAGE 1 OF 2	



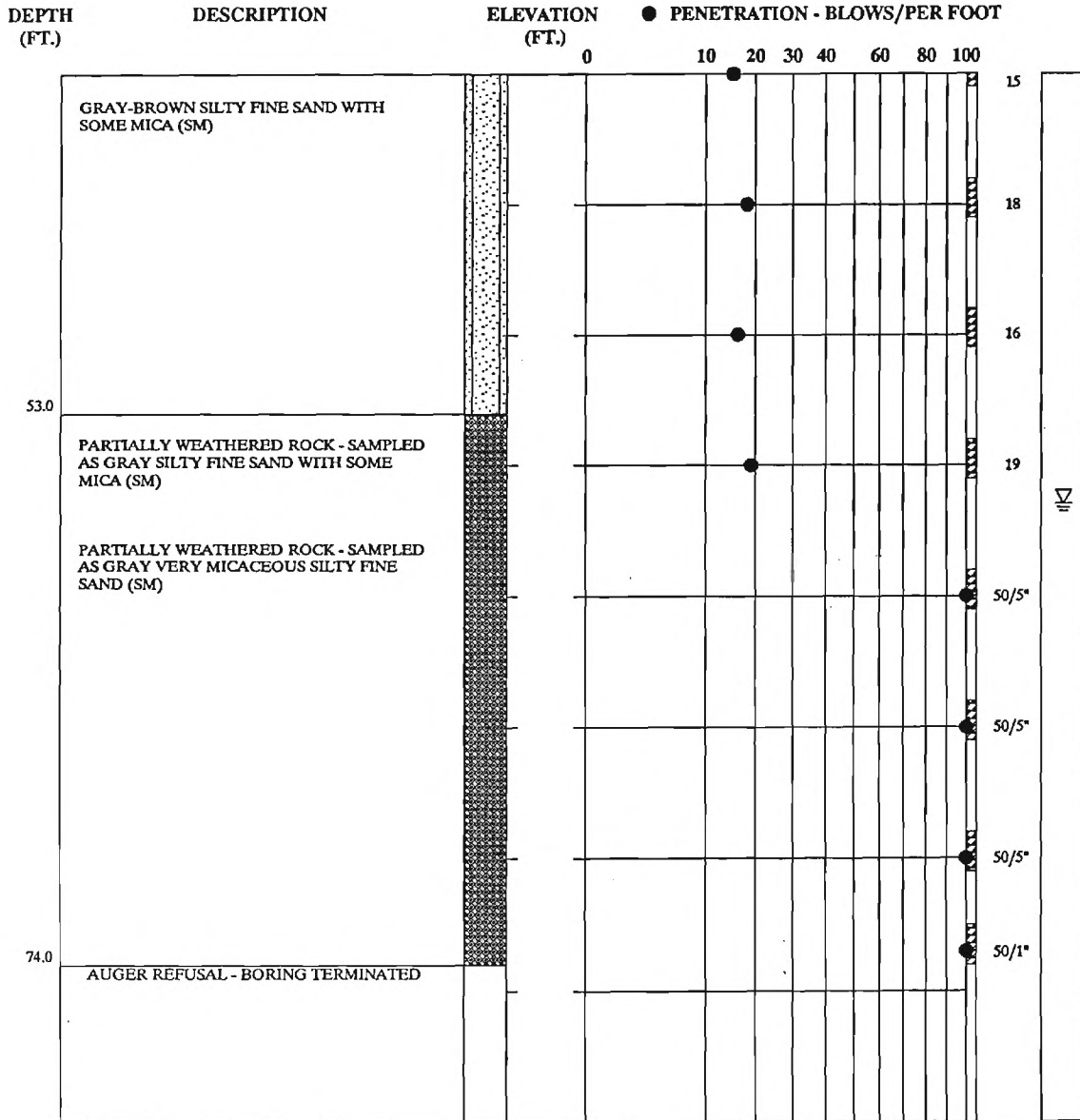




REMARKS:  
 Boring performed by Atlanta Testing and Engineering

SOIL TEST BORING RECORD	
BORING NUMBER	TSB-7
DATE DRILLED	April 7, 1992
PROJECT NUMBER	
PROJECT	ADSC/ASCE LOAD TEST
PAGE 1 OF 2	

SEE KEY SHEET FOR EXPLANATION OF SYMBOLS AND ABBREVIATIONS USED ABOVE



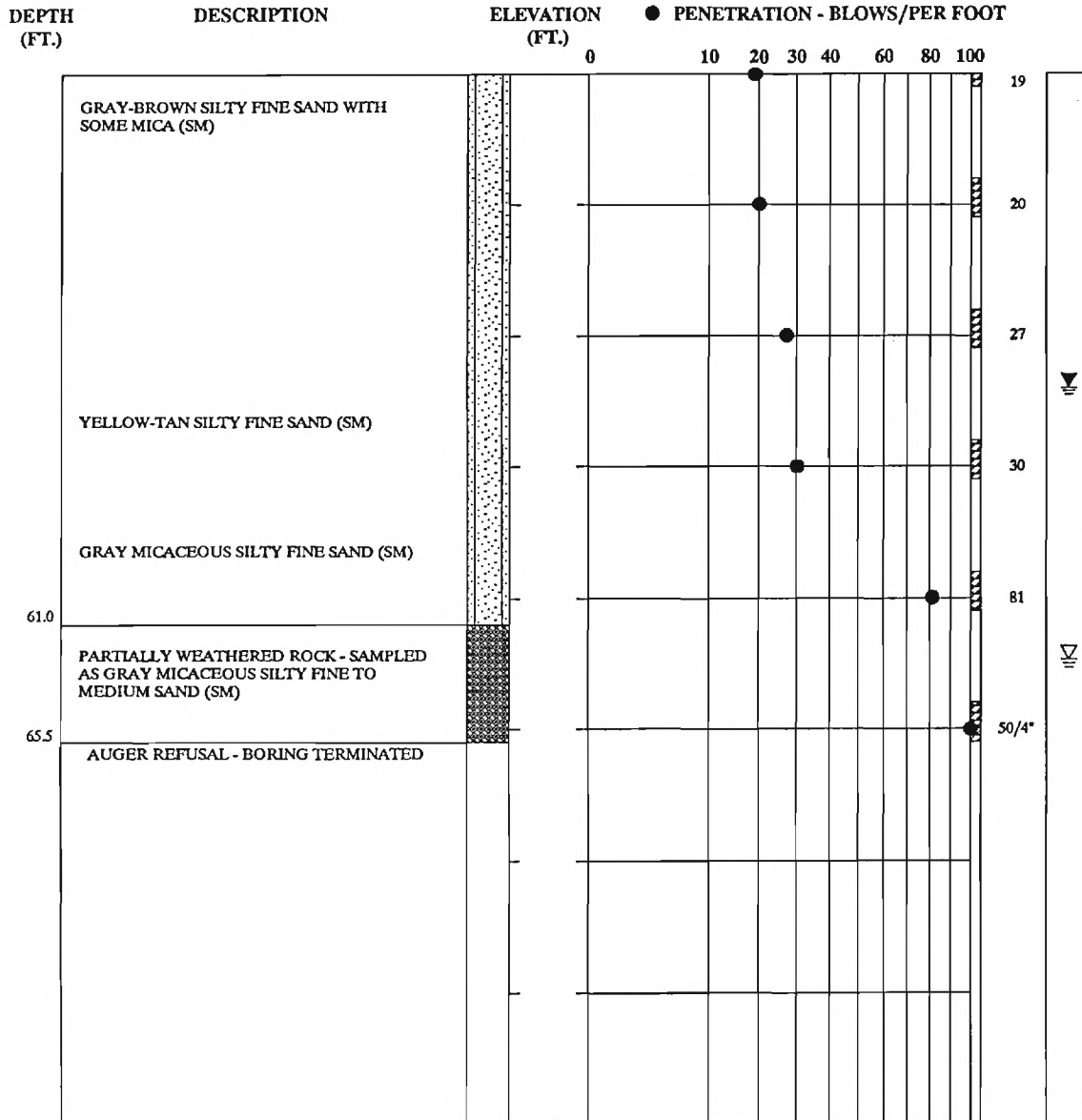
**REMARKS:**

Boring performed by Atlanta Testing and Engineering

SEE KEY SHEET FOR EXPLANATION OF SYMBOLS AND ABBREVIATIONS USED ABOVE

SOIL TEST BORING RECORD	
BORING NUMBER	TSB-7
DATE DRILLED	April 7, 1992
PROJECT NUMBER	
PROJECT	ADSC/ASCE LOAD TEST
PAGE 2 OF 2	





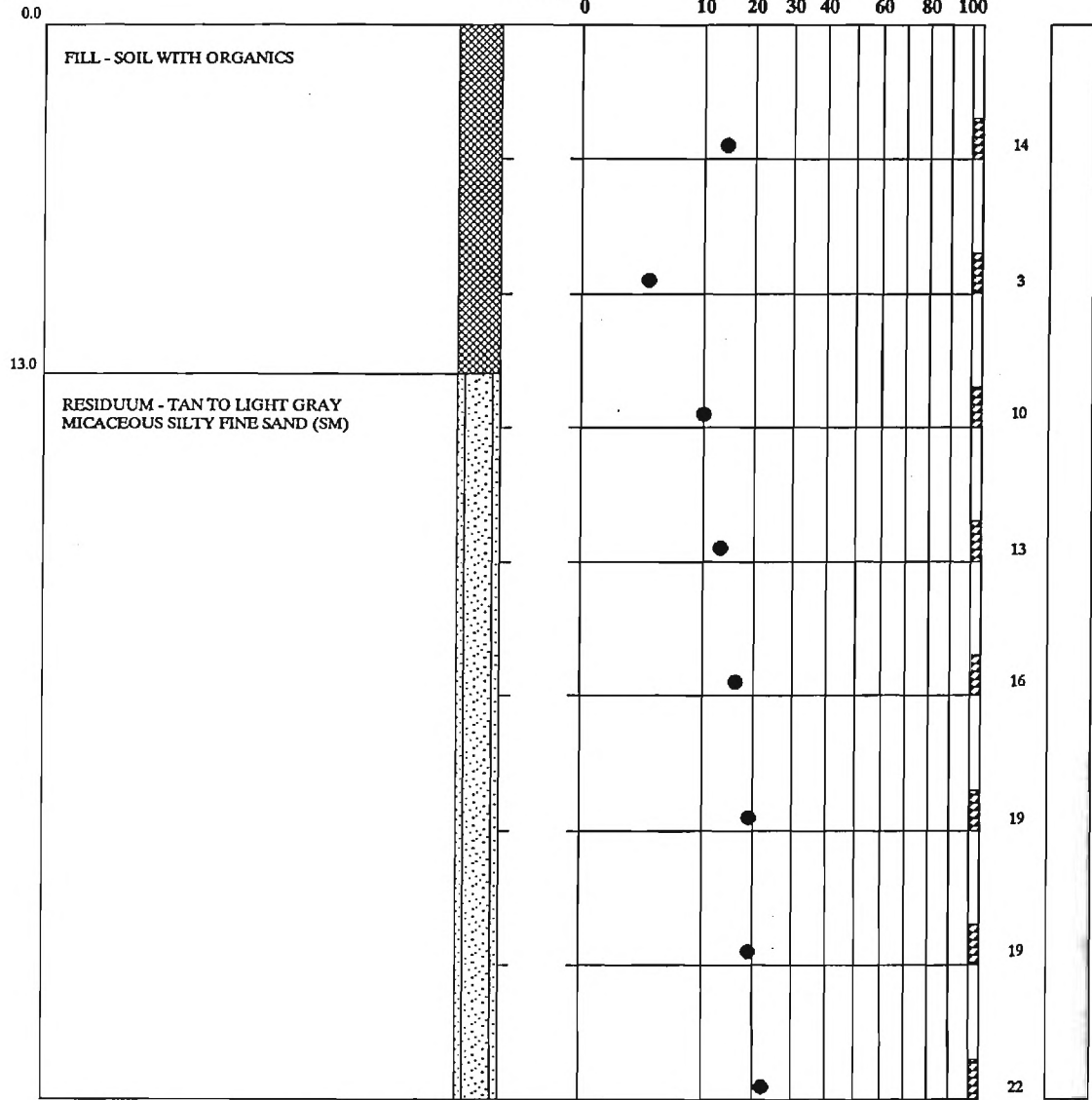
**REMARKS:**

Boring performed by Atlanta Testing and Engineering

SEE KEY SHEET FOR EXPLANATION OF SYMBOLS AND ABBREVIATIONS USED ABOVE

SOIL TEST BORING RECORD	
BORING NUMBER	TSB-8
DATE DRILLED	April 8, 1992
PROJECT NUMBER	
PROJECT	ADSC/ASCE LOAD TEST
PAGE 2 OF 2	

DEPTH (FT.)                      DESCRIPTION                      ELEVATION (FT.)                      ● PENETRATION - BLOWS/PER FOOT



REMARKS:  
Boring performed by ATEC Associates, inc.

SOIL TEST BORING RECORD	
BORING NUMBER	TSB-9
DATE DRILLED	March 26, 1992
PROJECT NUMBER	
PROJECT	ADSC/ASCE LOAD TEST
PAGE 1 OF 2	

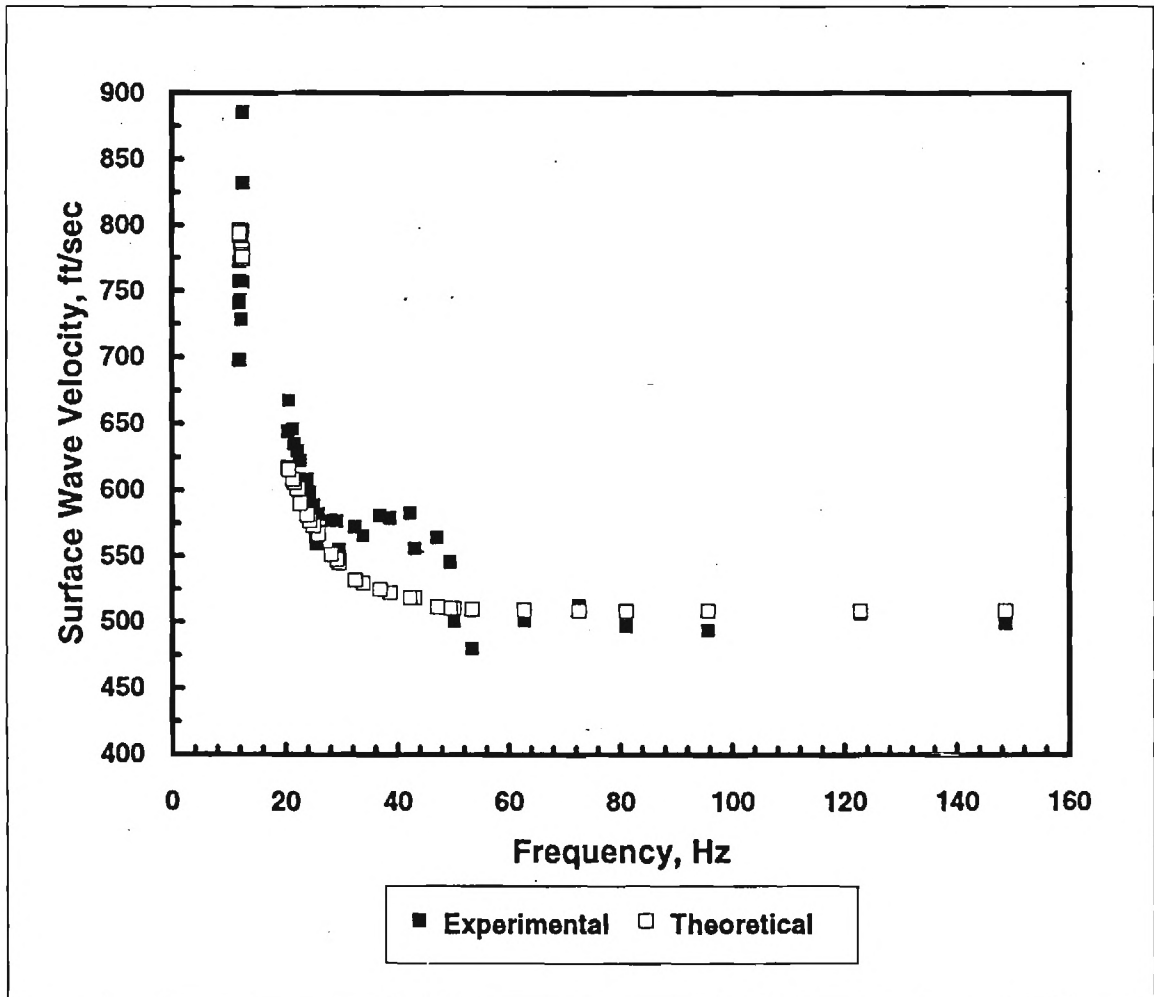
SEE KEY SHEET FOR EXPLANATION OF SYMBOLS AND ABBREVIATIONS USED ABOVE



ASCE-ADSC Load Test Site

Spectral Analysis of Surface Waves (SASW) Test Results

Layer No.	Thickness (ft)	Depth (ft)	Shear Wave Velocity (ft/sec)	Comp Wave Velocity (ft/sec)	Shear Modulus (psf)	Young's Modulus (psf)
1	10	10	551.24	1031.27	9.12E+05	2.37E+06
2	10	20	788.74	1475.59	1.87E+06	4.85E+06
3	10	30	932.94	1745.38	2.61E+06	6.79E+06
4	10	40	1058.26	1979.82	3.36E+06	8.74E+06
5	10	50	1168.5	2186.07	4.10E+06	1.07E+07
6	20	70	1268.73	2373.57	4.83E+06	1.26E+07
	Half space		1599.36	2992.13	7.67E+06	2.00E+07



Tabular Results of Geophysical SASW Survey.

ADSC/ASCE Load Test Site

Menard GaM Type Probe

Pressuremeter Testing

Boring TSB-11

Date performed : 4/28/92

Performed by Law Engineering

Test 1: Depth (feet) = 15						Test 4: Depth (feet) = 55					
Pressure (bars)	Volume (cc)	Volum. Strain	Cavity Strain	ln Vol Strain	log strain	Pressure (bars)	Volume (cc)	Volum. Strain	Cavity Strain	ln Vol Strain	log strain
0.21	50.0	0.06	0.03	-2.76	-1.20	0.50	3.0	0.00	0.0019	-5.57	-2.42
0.43	73.0	0.09	0.05	-2.38	-1.03	1.00	14.0	0.02	0.0090	-4.03	-1.75
0.88	115.0	0.15	0.08	-1.93	-0.84	1.50	26.0	0.03	0.0169	-3.41	-1.48
1.32	145.0	0.18	0.11	-1.70	-0.74	2.40	40.0	0.05	0.0263	-2.98	-1.30
1.74	192.0	0.24	0.15	-1.41	-0.61	3.40	60.0	0.08	0.0403	-2.58	-1.12
2.60	260.0	0.33	0.22	-1.11	-0.48	4.80	85.0	0.11	0.0586	-2.23	-0.97
3.54	309.0	0.39	0.28	-0.94	-0.41	5.80	103.0	0.13	0.0723	-2.04	-0.88
4.60	376.0	0.48	0.38	-0.74	-0.32	7.75	140.0	0.18	0.1024	-1.73	-0.75
5.05	461.0	0.58	0.55	-0.54	-0.23	9.70	205.0	0.26	0.1621	-1.35	-0.59
6.50	600.0	0.76	1.04	-0.28	-0.12	11.00	415.0	0.53	0.4514	-0.64	-0.28
						12.00	600.0	0.76	1.0391	-0.28	-0.12
Test 2: Depth (feet) = 30						Test 5: Depth (feet) = 65					
Pressure (bars)	Volume (cc)	Volum. Strain	Cavity Strain	ln Vol Strain	log strain	Pressure (bars)	Volume (cc)	Volum. Strain	Cavity Strain	ln Vol Strain	log strain
0.00	0.0	0.07	0.0356	-2.69	-1.17	0.00	5.0		0.0000		
0.50	4.0	0.07	0.0386	-2.62	-1.14	0.50	5.0	0.00	0.0000		-4.90
1.00	6.0	0.08	0.0401	-2.58	-1.12	1.00	6.0	0.00	0.0006	-6.68	-2.90
2.00	15.0	0.09	0.0470	-2.43	-1.06	2.00	12.0	0.01	0.0044	-4.73	-2.06
3.00	25.0	0.10	0.0549	-2.29	-0.99	3.00	20.0	0.02	0.0096	-3.97	-1.72
4.00	35.0	0.11	0.0629	-2.16	-0.94	4.00	27.0	0.03	0.0141	-3.59	-1.56
4.97	45.0	0.13	0.0711	-2.05	-0.89	6.00	42.0	0.05	0.0241	-3.07	-1.33
5.96	58.0	0.15	0.0821	-1.92	-0.84	7.90	56.0	0.06	0.0337	-2.75	-1.19
6.92	80.0	0.18	0.1014	-1.74	-0.76	9.85	73.0	0.09	0.0457	-2.46	-1.07
7.87	120.0	0.23	0.1394	-1.47	-0.64	11.80	84.0	0.10	0.0537	-2.31	-1.00
8.68	225.0	0.37	0.2615	-0.99	-0.43	13.80	95.0	0.11	0.0619	-2.18	-0.95
9.05	450.0	0.68	0.7559	-0.39	-0.17	15.80	106.0	0.13	0.0703	-2.06	-0.90
9.50	600.0	0.88	1.8674	-0.13	-0.06	17.80	120.0	0.14	0.0813	-1.93	-0.84
						19.80	135.0	0.16	0.0934	-1.81	-0.79
						22.10	160.0	0.19	0.1145	-1.63	-0.71
Test 3: Depth (feet) = 45											
Pressure (bars)	Volume (cc)	Volum. Strain	Cavity Strain	ln Vol Strain	log strain						
0.00	10.0		0.0000	Strain	strain						
0.25	15.0	0.01	0.0031	-5.08	-2.20						
0.50	16.0	0.01	0.0038	-4.89	-2.12						
1.00	26.0	0.02	0.0102	-3.91	-1.70						
2.00	45.0	0.04	0.0226	-3.13	-1.36						
2.92	80.0	0.09	9.0000	-2.44	-1.06						
3.90	97.0	0.11	0.0593	-2.22	-0.96						
4.88	112.0	0.13	0.0706	-2.06	-0.89						
5.85	127.0	0.15	0.0823	-1.92	-0.83						
7.78	165.0	0.19	0.1137	-1.64	-0.71						
9.65	260.0	0.31	0.2060	-1.16	-0.51						
10.80	555.0	0.68	0.7712	-0.38	-0.17						
11.25	600.0	0.74	0.9518	-0.30	-0.13						

Tabular Results of Menard Pressuremeter Tests.



## APPENDIX B

### LABORATORY TEST DATA

This appendix contains the results of the laboratory tests conducted on disturbed and undisturbed samples of the Piedmont residuum. Tests included: grain size distributions, index tests, one-dimensional consolidation, and isotropically-consolidated undrained triaxial compression tests. Detailed discussions of the tests have been given in Section 3 of this report. Index and grain sizes are reported in tabular form. Consolidation test results are presented in terms of void ratio vs.  $\log \sigma_v'$ . Deviator stress vs. axial strain curves are shown for the triaxial tests and a summary of the effective stress paths is also given.

Sample	1E-1S	1E-2S	1E-3S	1E-4S	1E-5S	1E-6S	1E-7S	1E-8S	1E-9S	1E-10S	1E-11S	1E-12S
Depth (ft)	15	20	25	30	35	40	45	50	55	60	65	69
N Value	15	17	14	22	29	27	27	27	30	70	60=6'	60=.1'
% Pass #4	100.0	100.0	100.0	100.0	100.0	100.0	100.0	100.0	100.0	100.0	99.6	100.0
% Pass #10	100.0	100.0	99.7	100.0	100.0	99.9	100.0	100.0	100.0	100.0	99.6	99.9
% Pass #40	88.0	82.6	87.1	85.0	86.6	87.1	85.4	88.0	85.2	83.4	83.5	92.1
% Pass #60	73.6	68.8	73.6	69.8	71.8	71.9	79.4	74.0	71.2	67.6	69.3	79.7
% Pass #200	30.2	31.2	33.1	31.6	30.8	30.0	31.8	33.8	33.4	31.6	32.7	35.0
%Clay	3.5	4.0	5.5	5.5	6.0	4.0	3.0	3.0	3.0	3.0	3.0	7.0

Sample	2-1S	2-2S	2-3S	2-4S	2-5S	2-6S	2-7S	2-8S	2-9S	2-10S	2-11S	2-12S	2-13S
Depth (ft)	5	10	15	20	25	30	35	40	45	50	55	60	65
N Value	17	11	15	15	27	23	27	27	31	27	30	57	60
% Pass #4	100.0	100.0	100.0	100.0		100.0	100.0	100.0	100.0	100.0	100.0	99.8	100.0
% Pass #10	100.0	100.0	99.8	100.0		99.5	100.0	100.0	100.0	100.0	100.0	98.5	99.8
% Pass #40	88.2	91.2	86.6	82.0		87.4	85.8	85.8	88.8	85.4	88.0	75.1	74.3
% Pass #60	77.8	68.2	72.1	66.4		73.4	71.8	71.8	74.0	69.6	71.2	58.5	58.5
% Pass #200	61.6	36.6	34.7	29.6		33.4	31.6	30.6	30.2	28.8	31.0	26.4	26.7
%Clay	37.5	8.0	4.0	4.5		4.0	4.0	3.0	3.0	2.0	4.0	2.0	2.0

Sample	3-1S	3-2S	3-3S	3-4S	3-5S	3-6S	3-7S	3-8S	3-9S	3-10S	3-11S	3-12S	3-13S	3-14S
Depth (ft)	1	4	9	14	19	24	28	34	39	44	49	54	59	63
N Value	4	15	10	9	10	12	17	17	21	22	23	73	52	50/4"
% Pass #4	100.0	100.0	100.0	100.0	100.0	100.0	100.0	100.0	100.0	100.0	100.0	99.9	100.0	100.0
% Pass #10	100.0	100.0	100.0	100.0	100.0	100.0	99.9	100.0	100.0	100.0	100.0	99.1	100.0	100.0
% Pass #40	73.4	85.2	88.0	83.4	75.6	86.4	85.5	86.0	91.2	80.0	80.8	76.9	92.4	96.4
% Pass #60	52.2	74.4	72.8	69.0	61.8	73.0	71.7	72.4	79.8	66.4	65.4	61.2	70.0	79.6
% Pass #200	26.0	54.6	36.0	31.2	30.0	38.2	31.8	31.2	35.6	35.8	26.0	24.2	27.0	31.2
%Clay	13.0	27.0	8.0	6.0	3.0	7.0	6.0	6.0	5.5	5.0	5.0	4.0	5.0	5.0

Sample	4-1S	4-2S	4-3S	4-4S	4-5S	4-6S	4-7S	4-8S	4-9S	4-10S	4-11S	4-12S	4-13S	4-14S
Depth (ft)	1	4	9	14	19	24	29	34	39	44	49	54	59	64
N Value	6	19	11	10	10	11	16	16	16	19	19	20	27	50/2"
% Pass #4	100.0	100.0	85.9	100.0	100.0	100.0	100.0	100.0	100.0	100.0	100.0	100.0	100.0	100.0
% Pass #10	99.6	99.4	85.0	100.0	100.0	100.0	100.0	100.0	98.8	100.0	100.0	99.7	99.2	100.0
% Pass #40	83.5	77.5	74.3	79.8	86.8	86.8	88.8	85.6	79.4	81.4	83.8	78.6	83.1	96.4
% Pass #60	70.1	62.0	62.7	64.6	70.0	70.4	75.2	70.8	65.0	54.4	67.0	62.6	68.6	81.8
% Pass #200	39.6	40.6	38.9	29.2	29.0	29.6	34.4	31.2	29.2	30.2	28.2	27.1	32.1	38.4
%Clay	15.9	16.0	12.0	6.0	5.0	6.0	5.0	6.0	5.9	5.0	5.5	4.0	4.0	12.0

Summary of Particle Size Distributions and Index Properties.

Sample	5-1S	5-2S	5-3S	5-4S	5-5S	5-6S	5-7S	5-8S	5-9S	5-10S	5-11S	5-12S	5-13S	5-14S	5-15S	5-16S	5-17S
Depth (ft)	1	4	9	14	19	24	29	34	39	44	49	54	59	63	68	73	78
N Value	6	13	8	7	8	11	14	12	13	13	20	19	50	50/4"	50/4"	50/2"	50/3"
% Pass #4	85.4	100.0	100.0	100.0	100.0	100.0	100.0	100.0	100.0	100.0	100.0	100.0	100.0	100.0	99.2	100.0	100.0
% Pass #10	84.8	100.0	100.0	100.0	100.0	100.0	100.0	100.0	100.0	99.8	99.8	100.0	100.0	100.0	95.7	100.0	91.9
% Pass #40	71.9	85.2	79.6	86.0	85.4	87.8	87.8	90.4	83.4	87.0	73.1	83.8	87.2	88.0	71.4	77.8	49.4
% Pass #60	60.5	76.0	66.4	70.2	68.8	72.2	73.6	76.6	70.6	74.3	53.3	66.2	70.4	59.2	54.0	61.8	37.9
% Pass #200	41.0	59.6	37.4	30.4	29.8	33.4	35.8	35.8	44.2	38.3	20.8	27.2	25.8	24.6	20.1	29.2	20.2
%Clay	18.0	38.0	9.0	6.0	6.0	6.0	6.0	6.0	6.0	6.0	4.0	3.0	4.0	6.0	5.0	7.5	8.0

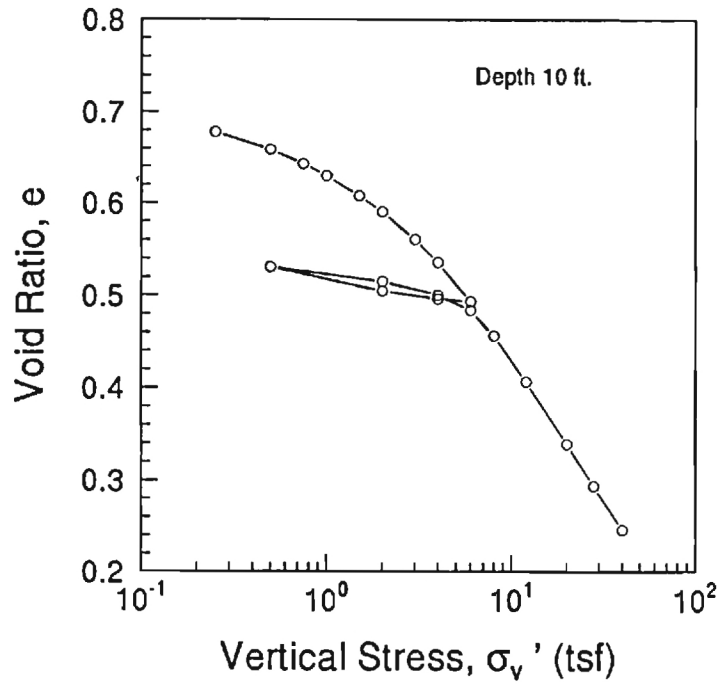
Sample	7-1S	7-2S	7-3S	7-4S	7-5S	7-6S	7-7S	7-8S	7-9S	7-10S	7-11S	7-12S	7-13S	7-14S	7-15S	7-16S
Depth (ft)	1	4	9	14	19	24	29	34	39	44	49	54	58	63	68	73
N Value	4	10	7	7	8	8	11	12	15	18	16	19	50/5"	50/5"	50/5"	50/1"
% Pass #4	100	100.0	100.0	100.0	100.0	100.0	100.0	99.5	100.0	100.0	100.0	100.0	100.0	100.0	100.0	100.0
% Pass #10	99.1	100.0	100.0	100.0	100.0	100.0	99.8	96.7	99.6	100.0	100.0	100.0	97.2	100.0	100.0	99.3
% Pass #40	87.2	87.0	79.8	88.0	84.8	81.6	84.8	83.2	83.5	87.6	78.2	74.8	79.9	96.8	94.6	75.3
% Pass #60	75.9	75.4	65.0	70.6	69.4	65.4	70.9	70.6	68.5	73.6	64.8	61.2	64.5	71.6	73.4	57.0
% Pass #200	43.6	47.2	29.4	28.4	28.8	27.4	36.1	33.2	32.3	34.2	37.0	32.2	31.9	26.2	27.8	22.6
%Clay	17.8	25.0	8.0	6.0	5.5	6.0	7.0	7.0	6.0	7.0	7.0	5.5	4.5	5.5	6.5	5.0

Sample	8-1S	8-2S	8-3S	8-4S	8-5S	8-6S	8-7S	8-8S	8-9S	8-10S	8-11S	8-12S	8-13S	8-14S
Depth (ft)	1	4	9	14	19	24	29	34	39	44	49	54	59	63
N Value	5	18	8	10	7	10	16	16	19	20	27	30	81	50/4"
% Pass #4	100.0	100.0	100.0	100.0	100.0	100.0	100.0	100.0	100.0	100.0	100.0	100.0	100.0	100.0
% Pass #10	98.9	100.0	100.0	100.0	100.0	100.0	100.0	100.0	99.8	100.0	100.0	99.8	100.0	100.0
% Pass #40	89.6	88.4	85.4	91.2	84.6	85.4	79.2	88.0	83.8	88.0	83.8	72.9	97.2	78.6
% Pass #60	78.1	80.4	68.2	79.2	68.8	70.4	63.0	74.4	67.5	72.0	67.8	58.1	85.6	62.0
% Pass #200	53.8	65.2	31.2	38.6	30.2	29.8	27.6	32.2	30.7	29.4	29.4	33.3	44.8	25.6
%Clay	22.0	50.0	7.5	11.0	6.0	6.0	6.0	7.0	7.0	6.0	5.5	7.5	6.0	5.0

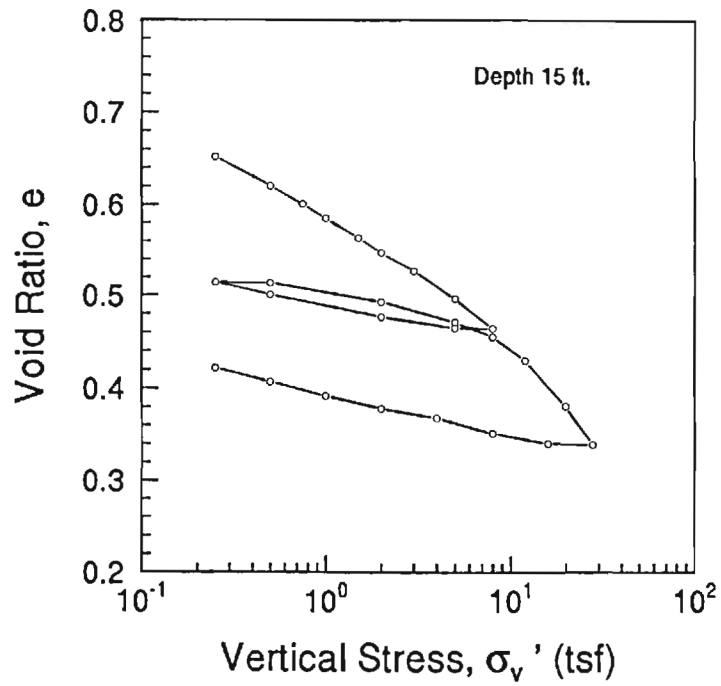
Sample	9-1S	9-2S	9-3S	9-4S	9-5S	9-6S	9-7S	9-8S	9-9S	9-10S	9-11S	9-12S	9-13S
Depth (ft)	5	10	15	20	25	30	35	40	45	50	55	60	65
N Value	14	3	10	13	16	19	19	22	28	26	28	33	50/6"
% Pass #4			100.0	100.0	100.0	100.0	100.0	100.0	100.0	100.0	100.0	100.0	100.0
% Pass #10			100.0	99.8	100.0	99.4	100.0	100.0	100.0	99.0	100.0	100.0	100.0
% Pass #40			88.6	87.2	87.4	82.3	87.8	88.2	86.2	79.0	83.0	81.6	87.8
% Pass #60			73.6	73.1	74.0	70.4	72.8	74.8	71.6	63.6	67.2	66.6	72.0
% Pass #200			31.0	34.3	36.6	36.3	34.8	37.4	37.4	29.1	28.8	32.6	30.2
%Clay			4.0	6.5	5.0	6.0	5.0	5.0	4.5	5.0	5.0	5.0	5.0

Summary of Particle Size Distributions and Index Properties.

### Sample 1, Specimen 1

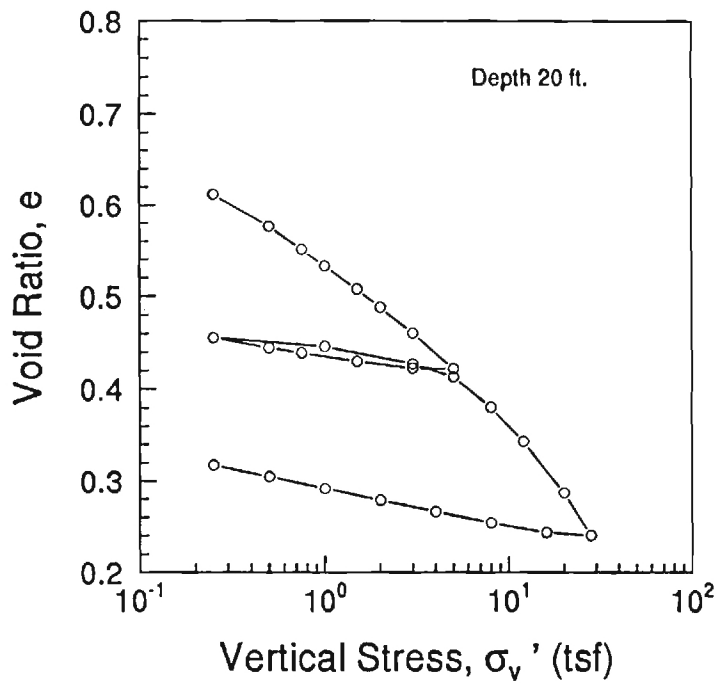


### Sample 2, Specimen 2

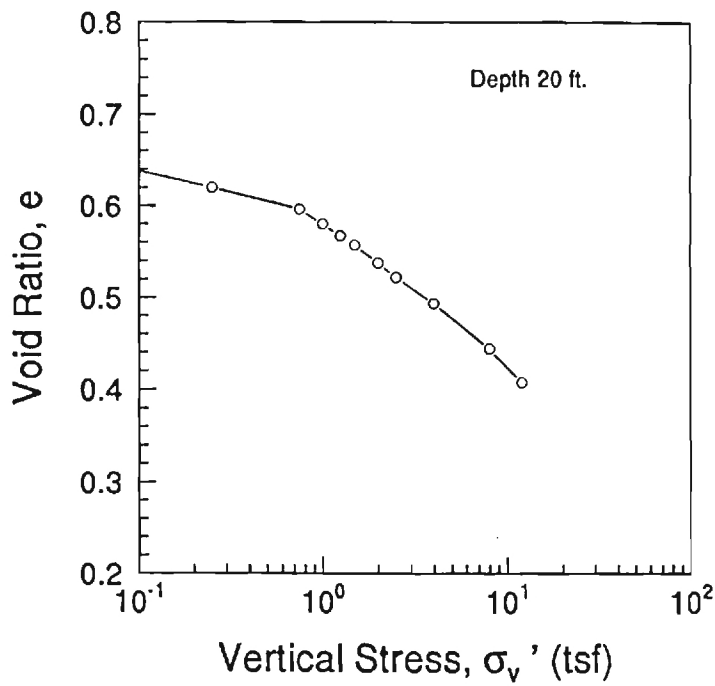


One-Dimensional Consolidation Test Results.

Sample 3, Specimen 1

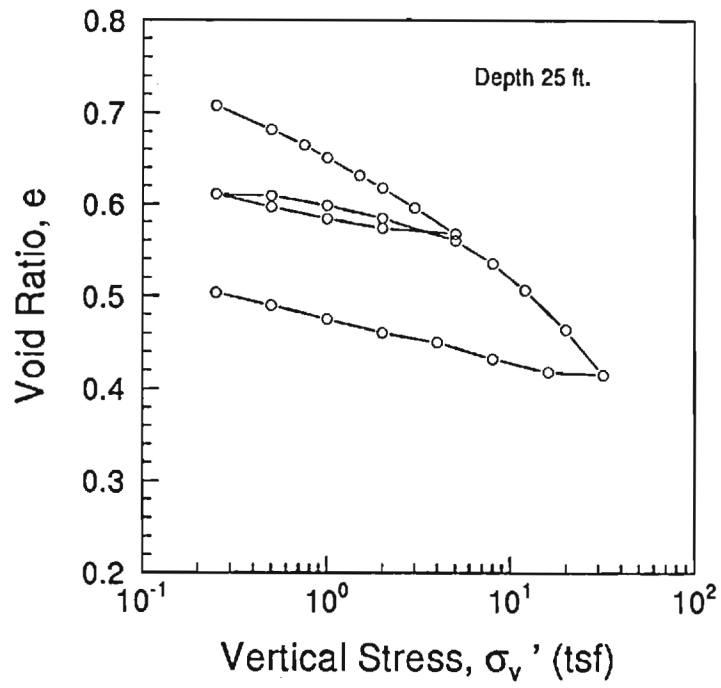


Sample 3, Specimen 2

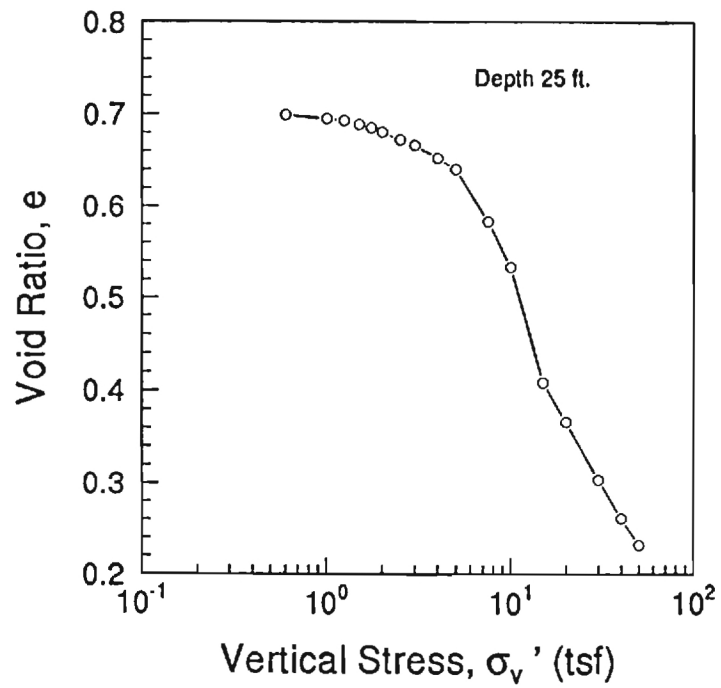


One-Dimensional Consolidation Test Results.

### Sample 4, Specimen 1

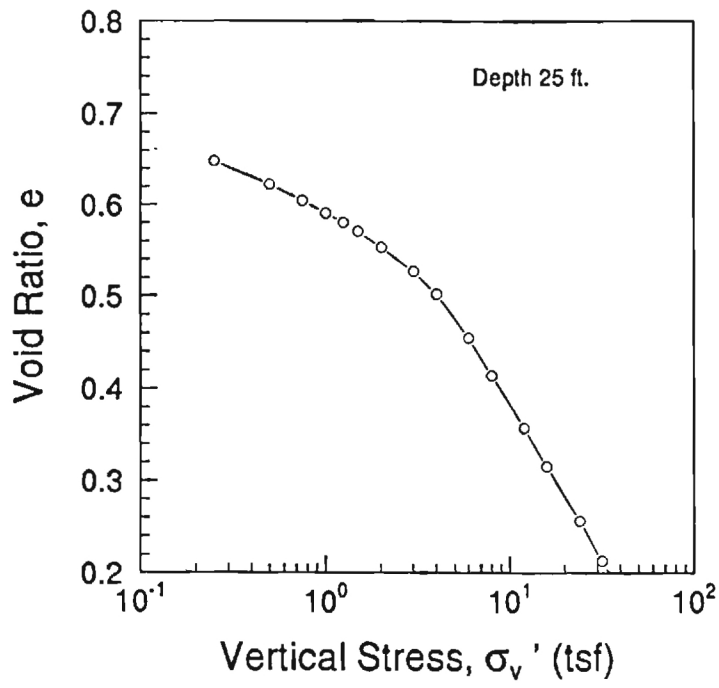


### Sample 4, Specimen 2

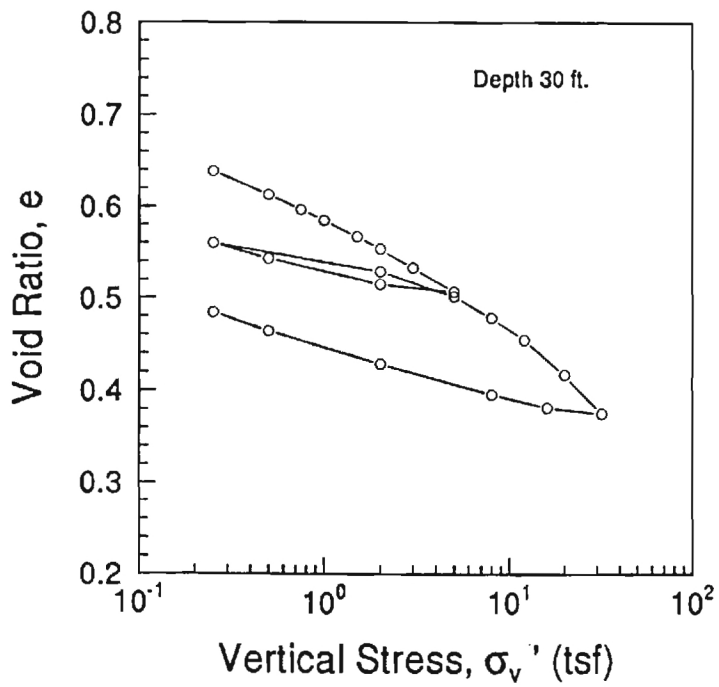


One-Dimensional Consolidation Test Results.

Sample 4, Specimen 3

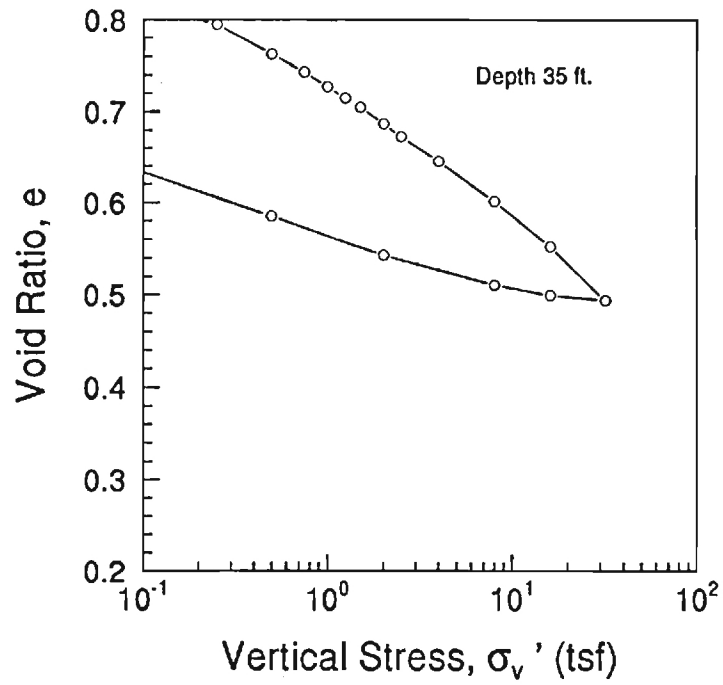


Sample 5, Specimen 1

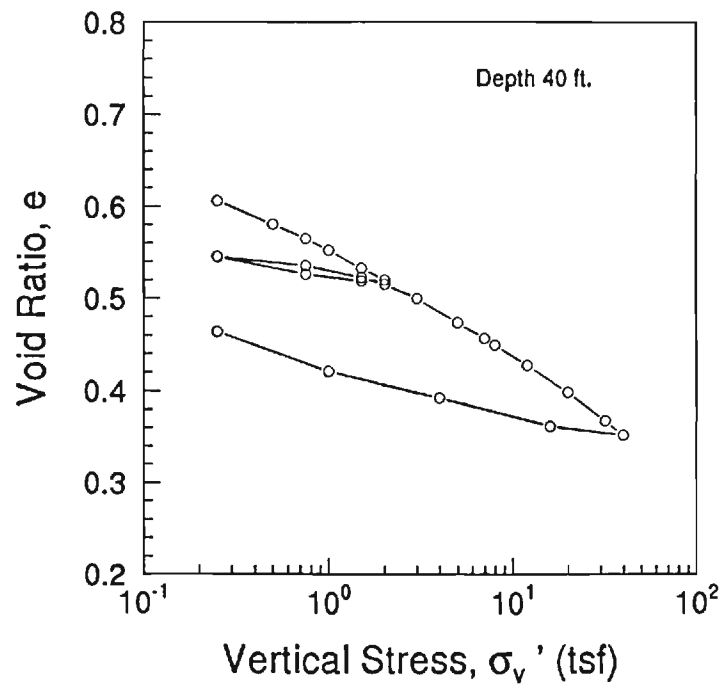


One-Dimensional Consolidation Test Results.

Sample 6, Specimen 1



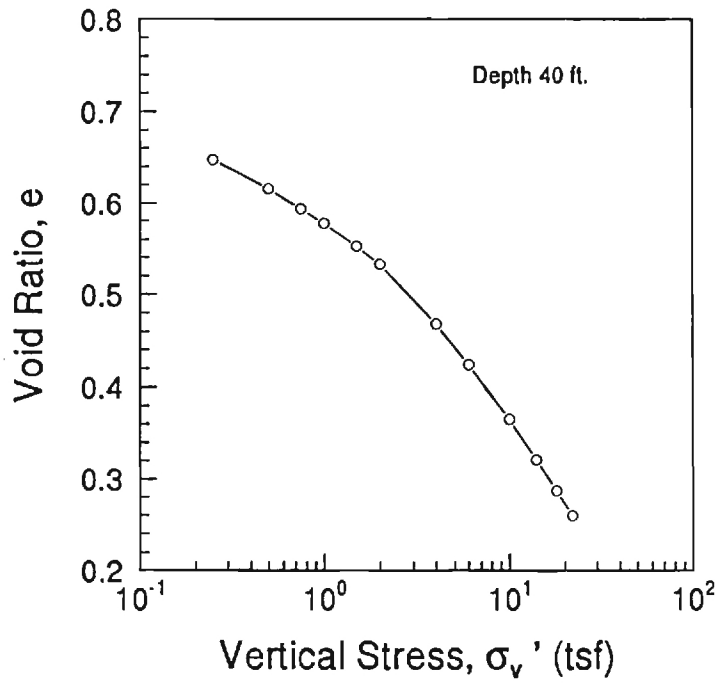
Sample 7, Specimen 1



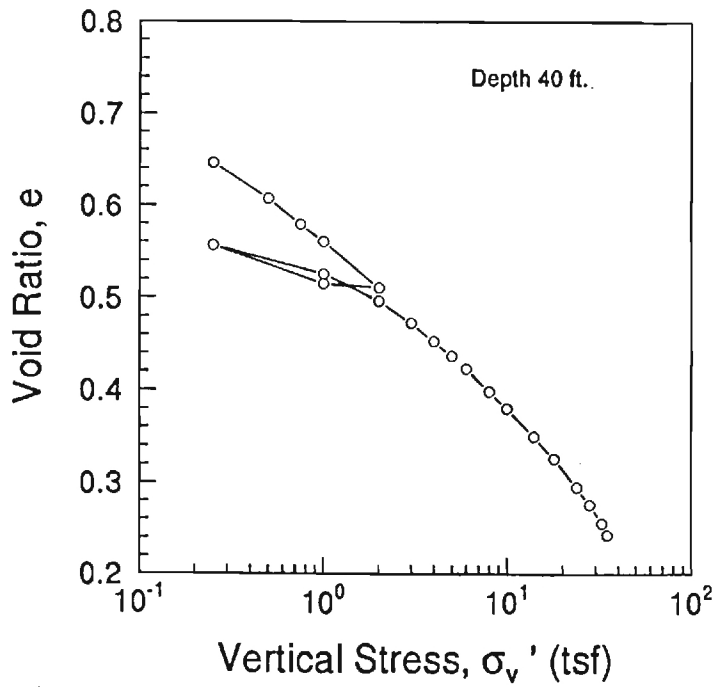
One-Dimensional Consolidation Test Results.



### Sample 7, Specimen 2

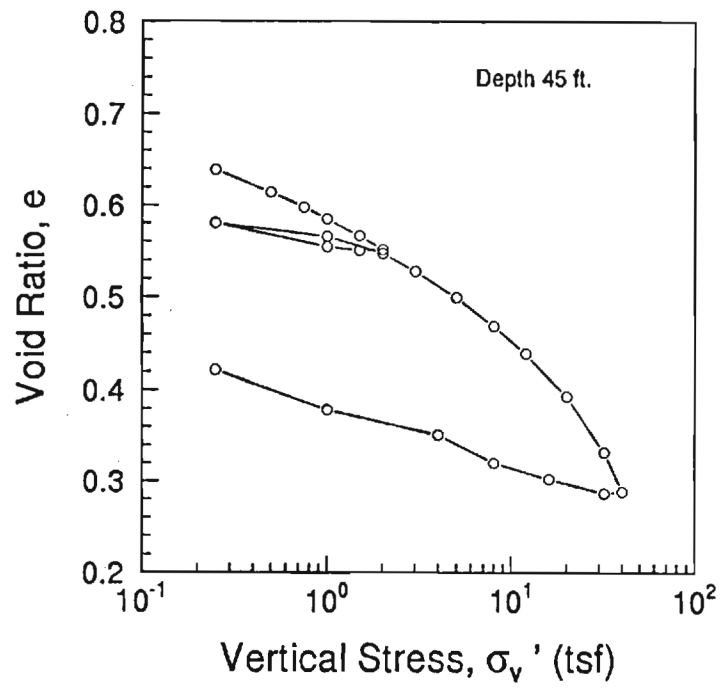


### Sample 7, Specimen 3

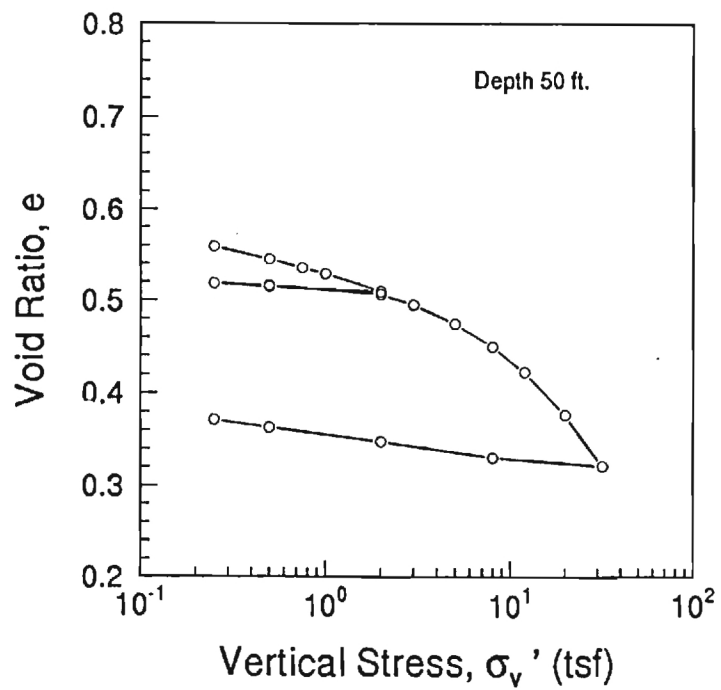


One-Dimensional Consolidation Test Results.

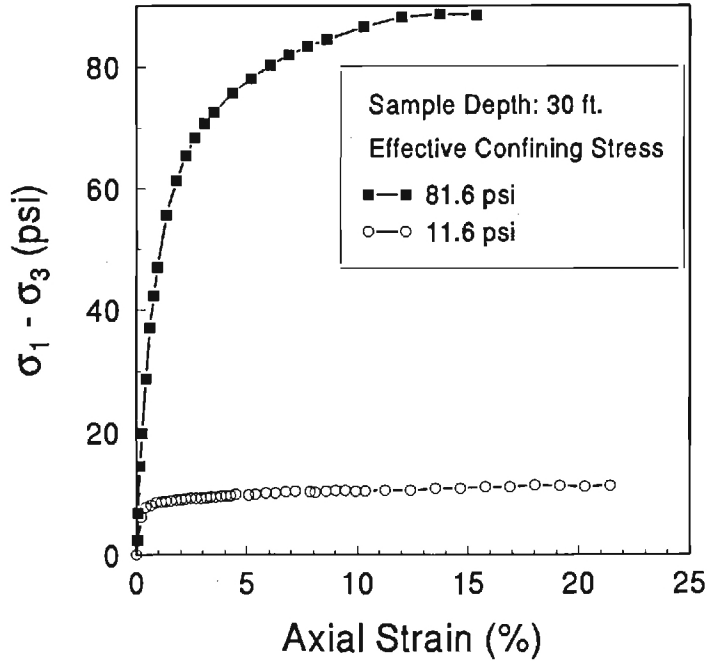
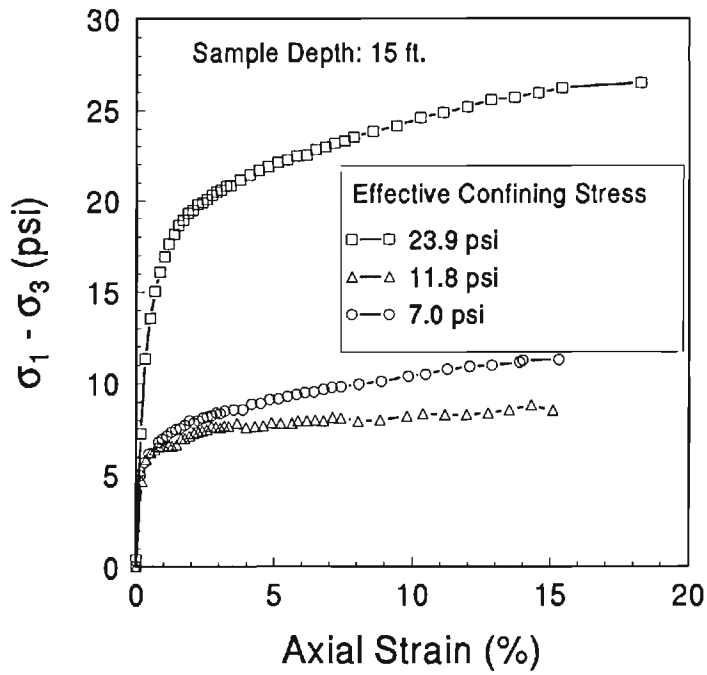
Sample 8, Specimen 1



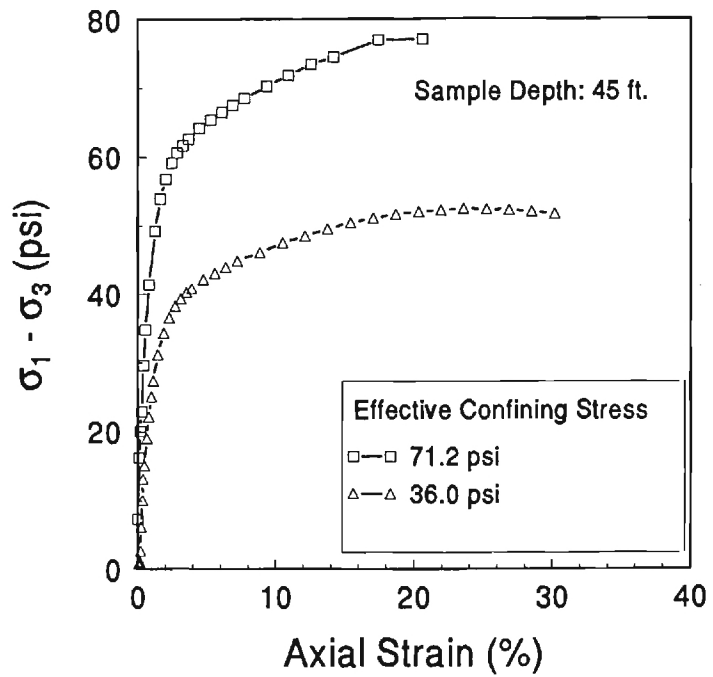
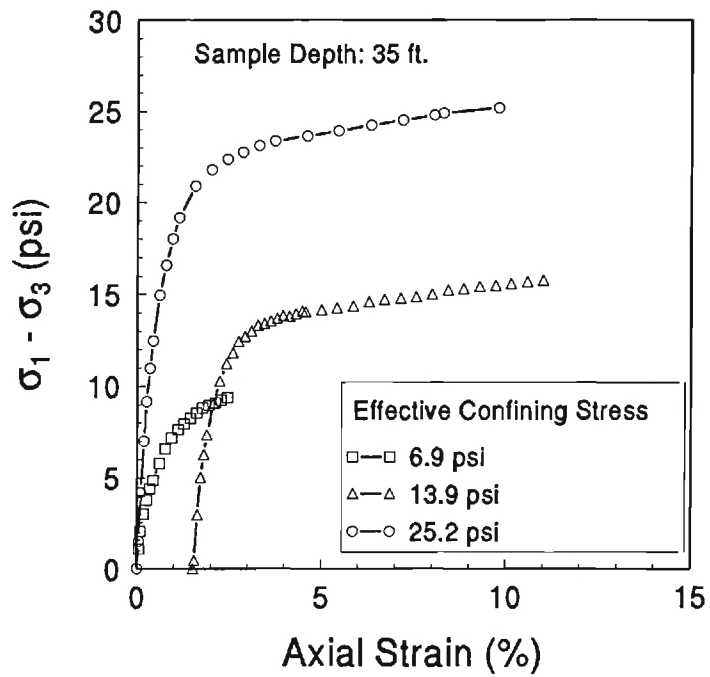
Sample 9, Specimen 1



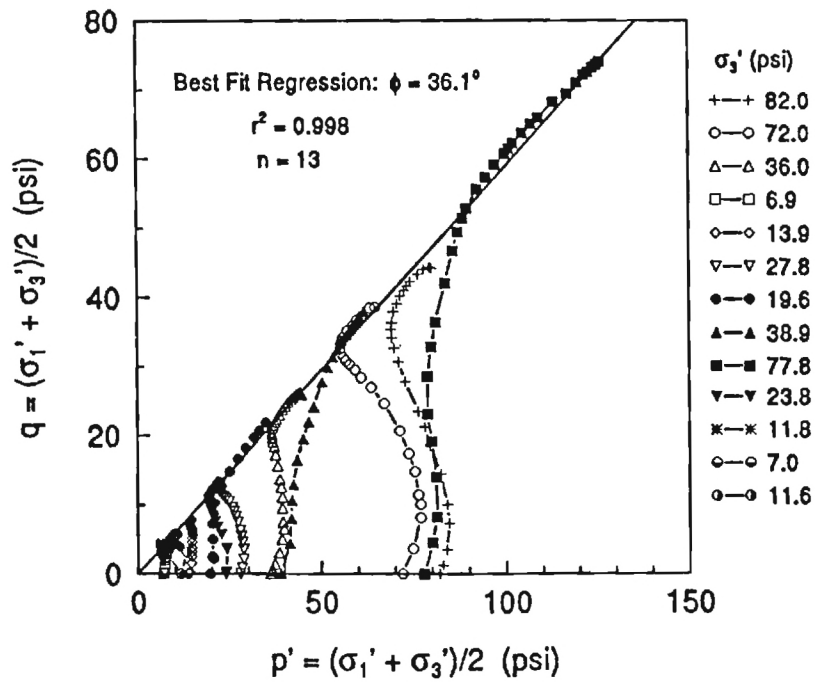
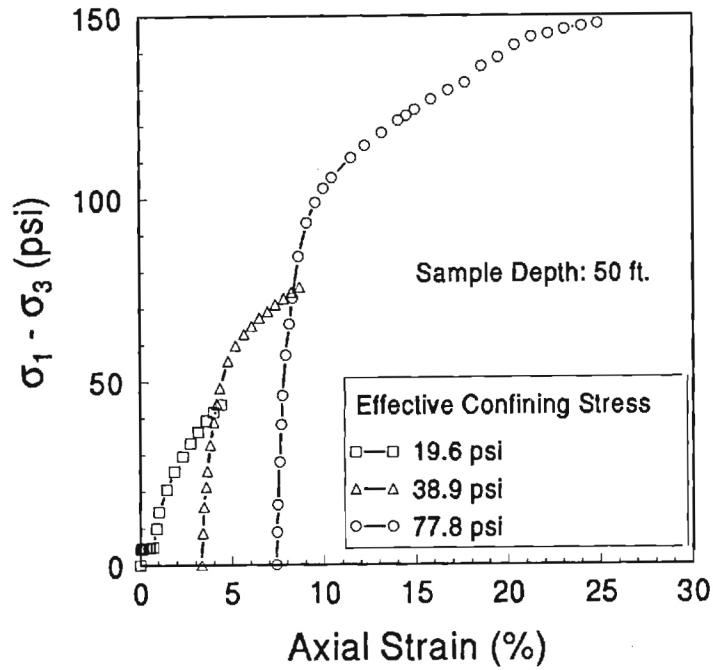
One-Dimensional Consolidation Test Results.



CIUC Triaxial Test Results.



CIUC Triaxial Test Results.



CIUC Triaxial Test Results.

## APPENDIX C

### LABORATORY TESTING OF CONCRETE

An accurate knowledge of the strength and stiffness of the concrete used in constructing the drilled shafts was needed for a proper evaluation of the load transfer results. Before beginning the load test, concrete had to cure to a sufficient strength to permit high-stress loading. Also, an analysis of vibrating wire strain gauge data required that the variation of the concrete modulus be known over a full range of stresses. Normally, the concrete modulus is estimated from measured compressive strengths. A more accurate knowledge of the concrete stiffness was required herein, however. The purpose of this section is to present the results of testing on the concrete used to construct the drilled shafts. Since the load tests were limited to axial compression loading, the scope of this evaluation has been restricted to determining the compressive strength of the concrete and nonlinear variation of the elastic modulus over a range of strain levels, particularly at early ages (3 to 14 days).

#### C.1. MIX DESIGN

The concrete used for this project was donated by the Thomas Concrete Company of Atlanta, Georgia. They developed the mix design primarily based on workability considerations, and the early strength requirements necessary for load testing soon after placement of the concrete. The mix design used Type III cement. The relative components by percentage weight were: water (7.9%), cement (16.8%), fly ash (4.5%), fine aggregate (22.8%), and coarse aggregate (47.8%). In addition to the materials, water reducing and air entraining admixtures were used, but actual amounts used were not reported in the mix design report.

#### C.2. STRENGTH AND STIFFNESS OF CONCRETE

The procedures for determining the compressive strength ( $f_c$ ) and modulus of elasticity

( $E_c$ ) of concrete are described in ASTM C39-86 and ASTM 469-87a, respectively, and generally consist of axial loading of 152 mm (6 in.) diameter by 305 mm (12 in.) tall cylinders to failure. Axial deformation readings must be made during compression to determine the modulus of elasticity. According to ASTM standards, the modulus should be reported as the secant modulus corresponding to 40 percent of ultimate strength. However, this definition is not appropriate for evaluating the vibrating wire strain gauge data, because the modulus varies over a wide range in strain levels.

The strength and stiffness of concrete are influenced by many factors, but due to the fast-track nature of this project, the age of the concrete is of primary concern. In standard practice, the strength of concrete is usually referenced to the 28-day strength ( $f'_c$ ) to provide a consistent basis for comparison. However, the 28-day strength is irrelevant to the load tests conducted herein due to the short time span between pouring the concrete and load testing the shafts. Other factors which can affect the strength and stiffness include the mix proportions, water/cement ratio, curing environment, specimen size, and the rate of loading (Neville, 1981).

#### C.2.1. Evaluation of Concrete

During the construction of the drilled shafts, concrete cylinders were cast from each concrete truck arriving at the site, and uniaxial compression tests were performed after a curing period (3 to 49 days). Nondestructive tests were used to investigate the integrity of the drilled shafts and included testing of one of the field cylinders (Rix et al., 1993). In addition, compressive strength tests were performed on additional laboratory-batched samples of concrete for measurement of the elastic modulus.

#### C.2.2. Compressive Strength of Field Cylinders

In the field, cylinders were made in plastic molds, 152 mm (6 in.) in diameter, and 305 mm (12 in.) in height. The cylinders were allowed to cure overnight at the load test site, and were then taken to a high humidity curing room for storage. Compressive tests were performed on six cylinders with ages ranging from 3 to 49 days. Cylinders

were capped using sulfur compound, and then tested using a hydraulic compression machine. Results of these compression tests are summarized in Table C-1. The strength of the concrete varied from 18.9 to 43.1 MN/m<sup>2</sup> (2742 to 6254 psi).

Table C-1. Compressive Strength Tests of Field Concrete

<u>Cylinder</u>	<u>Age (Days)</u>	<u>Compressive Strength (MN/m<sup>2</sup>)</u>
R-1-A	3	23.8
R-2-A	4	18.9
C-1	7	29.6
C-2	7	28.0
C-2-D	49	40.0
C-2-E	49	43.1

### C.2.3. Elastic Modulus of Concrete

Several means of estimating the modulus of elasticity of the concrete were investigated. These methods included empirical correlations with the compressive strength determined from the field cylinders and with the shear wave velocity data determined in the NDE testing. In addition, data from the wire strain gauges was used to calculate the modulus. Finally, a batch of the concrete was mixed in the laboratory and these cylinders were subjected to compressive strength and modulus determinations. In many construction projects, only the compressive strength of the concrete is determined. The modulus of elasticity is often estimated based on empirical correlations with the compressive strength. One such correlation is that recommended by the American Concrete Institute (1983) for normal weight concrete, as follows:



$$E_c = 14800 (f_c' p_a)^{0.5} \quad [C-1]$$

where  $p_a$  = atmospheric pressure = 1 bar = 14.7 psi  $\approx$  1 tsf  $\approx$  100 kPa. This correlation is based on the use of the 28-day strength of concrete made with Type 1 cement and references the modulus of elasticity at a specific stress level. Since each of the drilled shafts were tested only 9 days after pouring concrete, the relationship is not particularly applicable. The early strength and stiffness has been investigated by Hansen (1986) and Mayne, et al. (1992) who concluded that such correlations overestimated  $E_c$  at ages less than 28 days. Additionally, the concrete used for this project was composed of Type III cement.

#### C.2.4. Integrity Tests

Prior to load testing, a series of nondestructive integrity tests were performed on the drilled shafts. These tests have been summarized by Rix, et al. (1993), and included sonic echo tests. A concrete cylinder cast during construction of the shafts was evaluated in this manner to determine the compression wave velocity of the concrete. Correlations between the compression wave velocity and the modulus of elasticity have been reported, as noted in Table C-2.

Table C-2. Variation of  $E_c$  with Compression Wave Velocity.

<u>Compression Wave Velocity (m/sec)</u>	<u>Modulus of Elasticity <math>E_c</math> (GN/m<sup>2</sup>)</u>
Above 4,115	40.7
3292 - 4115	26.0 - 40.7
2743 - 3292	18.1 - 26.0
1920 - 2743	8.8 - 18.1
Below 1920	8.8

The stiffness of the field cylinder was measured by placing a piezoelectric

accelerometer at one end, and striking the other end with a hammer to directly measure the compression wave velocity. The test resulted in a measured compression wave velocity of 3700 m/s, and based on the correlations above, the estimated  $E_c$  is approximately 33.3 GN/m<sup>2</sup>. The stiffness indicated by such tests is applicable at low strain levels.

### C.3. STRAIN GAUGE DATA

The vibrating wire strain gauges were used to measure the strain of the steel, and thus are also a measurement of the strain in the concrete. Since the axial load at the top of the drilled shafts not reduced by side friction, it should be equivalent to the load applied by the jack. After subtracting the portion of the load carried by the reinforcing steel, the remaining axial load can be divided by the area of concrete, to calculate the compressive stress in the concrete. This stress can be used with the strain readings to determine the secant modulus of elasticity of the concrete.

The stress in the concrete and the modulus of elasticity were determined at each loading interval for both of the load tests. Since there were multiple gauges at the top

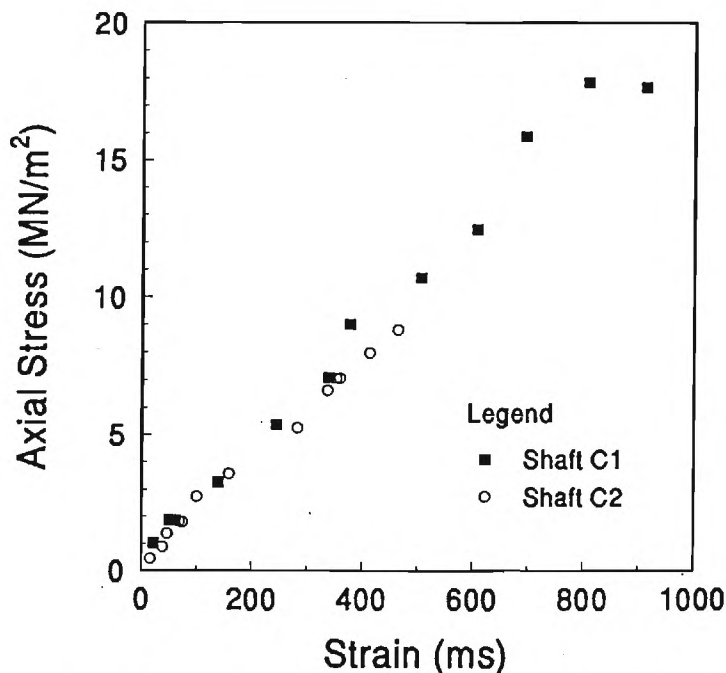


Figure C-1. Derived Stress-Strain Curves from Strain Gauge Data.

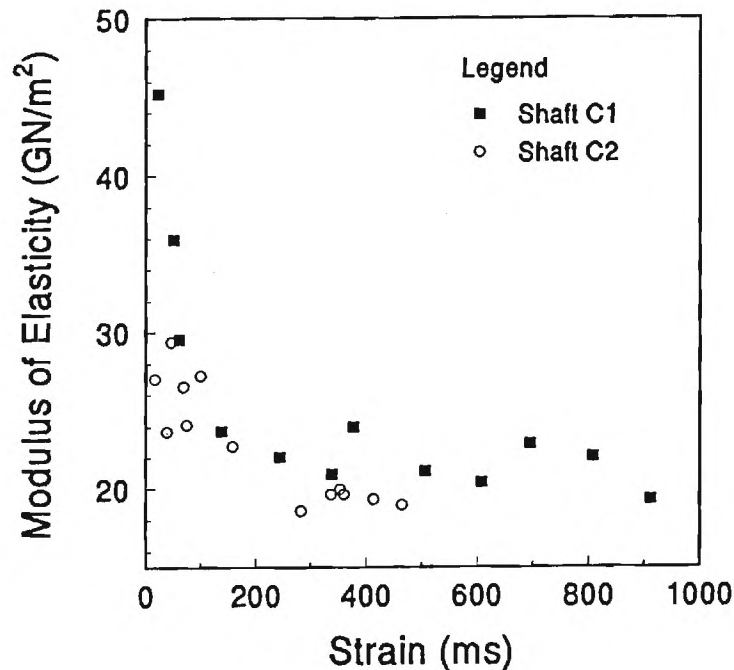


Figure C-2. Derived Modulus vs. Strain Curves from Strain Gauge Data.

of the shafts, several different values were determined for each load level. For shaft C1, four values of axial strain, axial stress, and elastic modulus were determined at each load increment. For shaft C2, only 3 values were determined due to an inoperative gauge.

The results of this evaluation were compiled in the form of axial stress (concrete) versus axial strain curves, as shown in Figure C-1. Alternatively, the results are shown as modulus of elasticity versus strain level in Figure C-2. In reduction of the data, some eccentric behavior was apparent in the calculated strain levels. That is, for a given load increment, the strain, and stress calculated from the multiple gauges varied. Therefore, for each load increment, the values of strain and stress were averaged, before computation of the modulus of elasticity, to provide a more clear representation. Data derived from both load tests (shaft C1 and C2) are shown together on both figures.

As shown by Figure C-2, the modulus varies throughout each load test, but becomes asymptotic at higher strain levels. In the low strain range, high values of the

modulus were calculated, particularly for shaft C1. The higher values are suspect, however, since at the low strain range, any inaccuracies in the strain measurement can have a much larger effect on the calculated modulus of elasticity.

The results of this evaluation indicate that use of a constant modulus of elasticity is not appropriate for reduction of the data from the deeper strain gauges. The hyperbola is the most commonly-used curve for modelling the nonlinear stress-strain behavior of materials:

$$\sigma = \epsilon / (1/E_i + \epsilon/f_c) \quad [C-2]$$

where  $\sigma$  = axial stress,  $\epsilon$  = axial strain,  $E_i$  = initial tangent modulus, and  $f_c$  = compressive strength. The compressive strength was determined from the test specimens made during construction. Table C-1 shows 7-day strengths of 28.0 to 29.6 MN/m<sup>2</sup>, and the higher value was chosen, considering the concrete had aged 9 days at the time of the test. The initial tangent modulus measured by integrity tests gave a value of 33.3 GN/m<sup>2</sup>. Figure C-3 shows a forward prediction of a hyperbolic stress-strain curve along with the strain gauge data again. The hyperbolic model fits the data well, except at

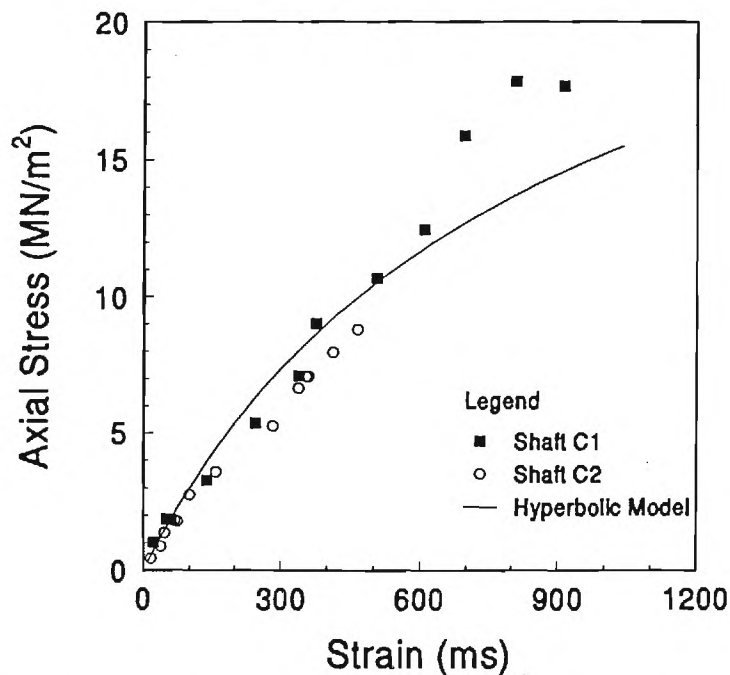


Figure C-3. Forward Prediction of Stress-Strain Using Hyperbolic Model.

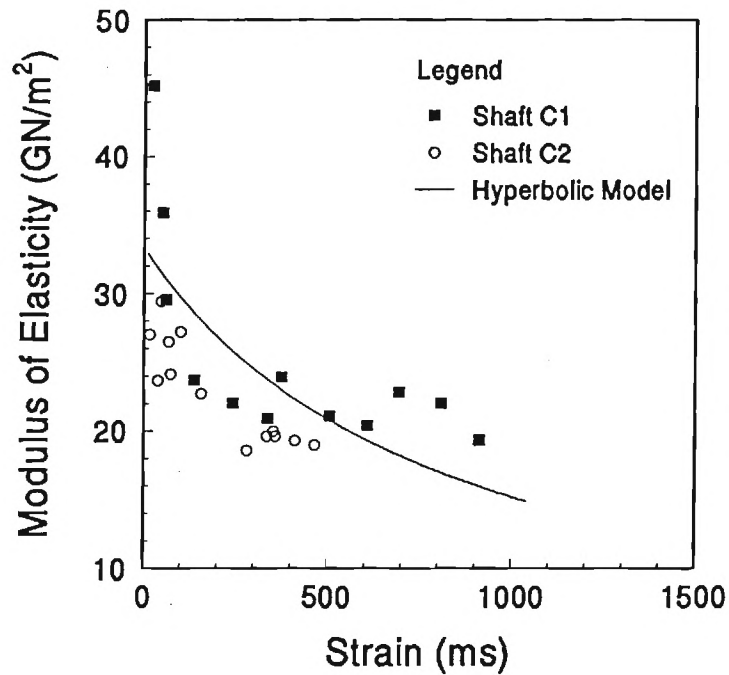


Figure C-4. Hyperbolic Prediction of Modulus Nonlinearity With Strain Level.

higher strain levels where the data points fall above the trend shown at low strain levels. An examination of the data points show an increase in the modulus of elasticity for the points, though the modulus should be decreasing. This may be a result of inaccurate load readings from the jack or other difficulties in measurements at high stress levels.

The hyperbolic model can also be used to represent the variation of the secant elastic modulus with strain, by dividing each side of Equation C-2 by strain to reach:

$$E_{sec} = 1/(1/E_i + \epsilon/f_c) \quad [C-3]$$

Using Equation [C-3], the curve shown in Figure C-4 was plotted, along with the data points shown from the vibrating wire gauges. Scatter is evident in this figure,

though the hyperbolic curve does fit the general trend. As noted before, an increase in the modulus of elasticity occurs at the higher strain readings.

#### C.4. LABORATORY CONCRETE PROPERTIES

A set of new cylinders were prepared in the laboratory specifically for determining the concrete modulus directly, using standard compression test procedures. Cylinders were cast using the same mix design and materials as used for the test shafts. Materials for the extra batch of concrete were donated by the Thomas Concrete company.

The concrete was batched using a rotating drum mixer. After mixing the concrete, nine 152 mm (6 in.) diameter by 305 mm (12 in.) tall cylinders were cast using plastic molds. The cylinders were covered with plastic and allowed to cure overnight, before being placed in a high humidity curing room. Specimens were tested after 3, 7, and 14 days of curing, using the same equipment as used in testing the original concrete cylinders. Three specimens were tested on each date. Mechanical compressometers were attached to each specimen to measure axial deflections during loading. Specimens were loaded to a point near failure and loading was temporarily halted to permit removal of the compressometers. Afterwards, loading was recommenced, and the specimens were loaded to failure.

Table C-3 lists the individual concrete cylinders made for the laboratory program and summarizes the compressive strengths and time of cure for each. Three specimens were tested at times of 3, 7, and 14 days. The individual axial stress-strain curves measured for these cylinders are shown in Figures C-5 through C-7.

### C.5. HYPERBOLIC MODEL

The hyperbola was used to predict stress-strain relationships for the test cylinders for comparison with the previous results. The initial tangent modulus for the laboratory concrete must be known. To determine this parameter, the equation can be rearrange:

$$\epsilon/\sigma = 1/E_i + \epsilon/f_c \quad [C-4]$$

The strain values from the compression tests were divided by the corresponding stress values, and the results plotted against the strain readings. Ideally, the results should

Table C-3. Compressive Strength of Laboratory Concrete Cylinders

<u>Cylinder</u>	<u>Age (days)</u>	<u>Compressive Strength (MN/m<sup>2</sup>)</u>
3-1	3	20.7
3-2	3	20.0
3-3	3	21.9
7-1	7	26.4
7-2	7	26.2
7-3	7	25.6
14-1	14	29.0
14-2	14	26.2
14-3	14	30.5

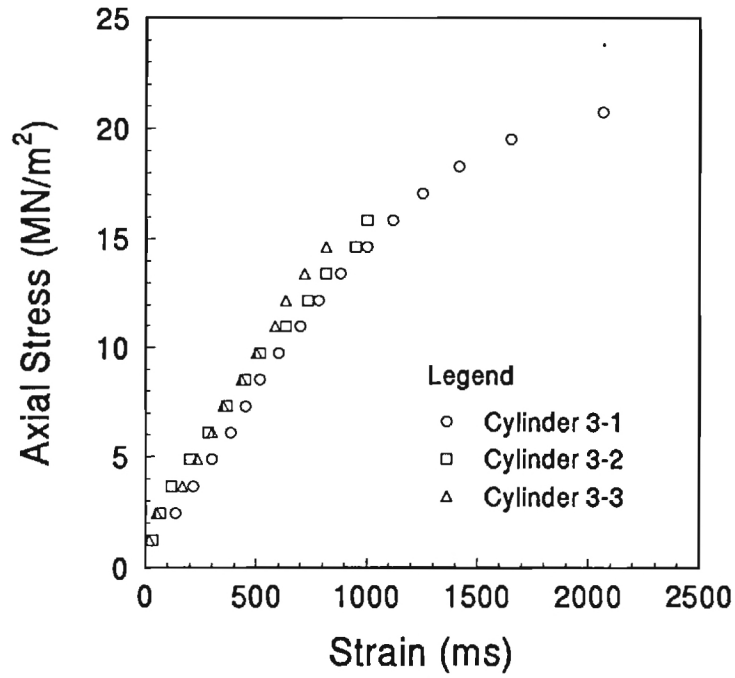


Figure C-5. Stress-Strain Curves for 3-Day Laboratory Concrete Cylinders.

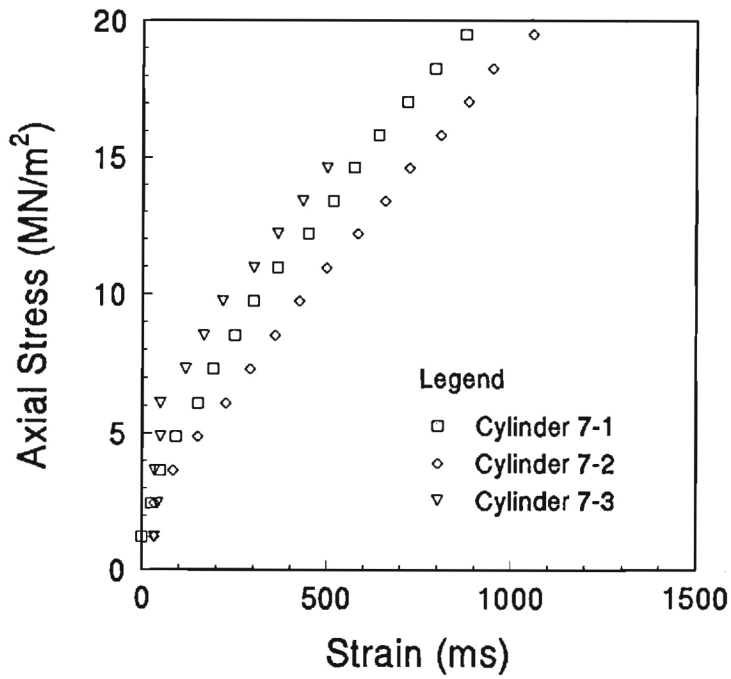


Figure C-6. Stress-Strain Curves for 7-Day Laboratory Concrete Cylinders.



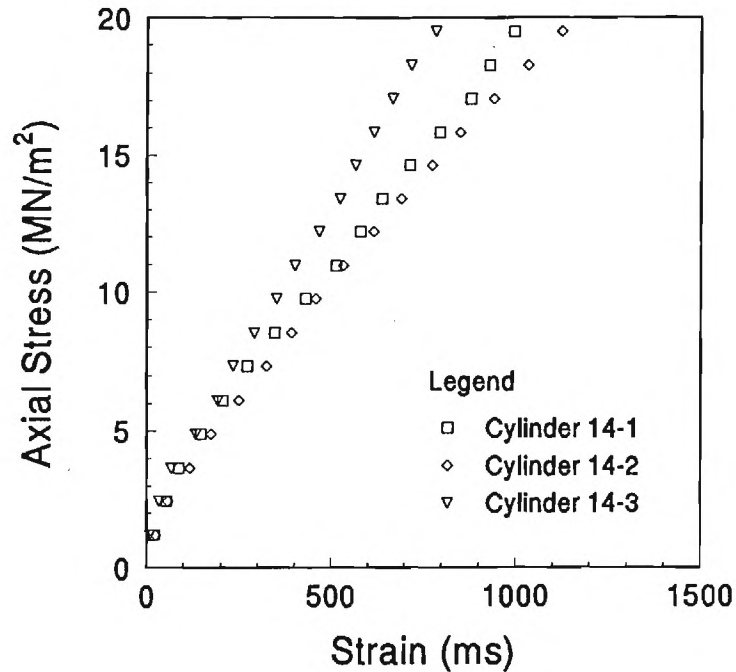


Figure C-7. Stress-Strain Curves for 14-Day Laboratory Concrete Cylinders.

form a straight line whose y-intercept is equal to the reciprocal of the initial tangent modulus, and whose slope is equal to reciprocal of the compressive strength. Using this method, initial tangent moduli of  $20.9 \text{ GN/m}^2$  (3.03 million psi),  $35.5 \text{ GN/m}^2$  (5.16 million psi), and  $25.5 \text{ GN/m}^2$  (3.71 million psi) were calculated for the 3 day, 7 day, and 14 day breaks, respectively. With these moduli, and the measured compressive strengths, model stress-strain curves were generated. These model curves are shown with the actual test data in Figures C8, C9, and C10.

Each of the models fits the data in the low stress ranges, however, in the high stress range, the model departs significantly from the actual behavior. The data from cylinders 7-2, and 7-3 indicate that the compressometer gauges may not have been securely fastened to the cylinders, and did not record deflections in the early portions of these tests. As a consequence, the stress-strain curves are shifted to the left of the curve

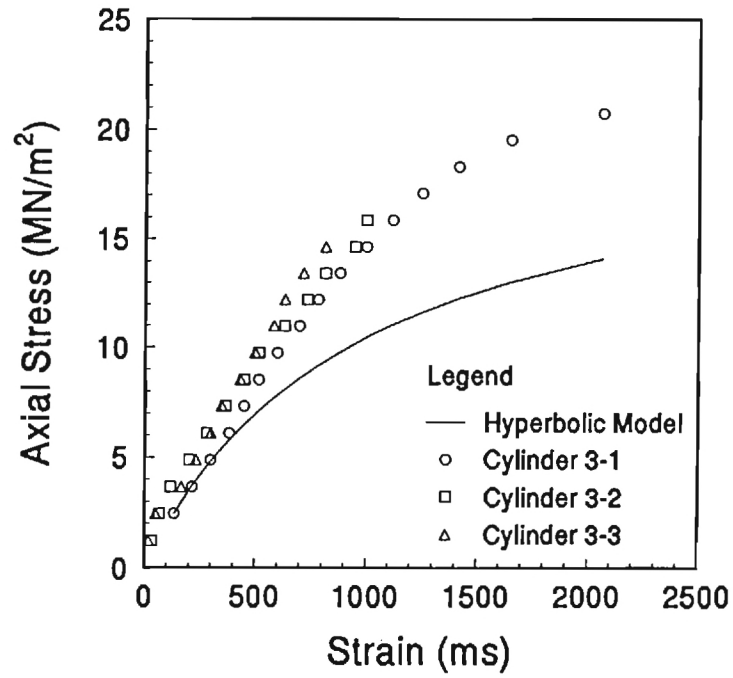


Figure C-8. Hyperbolic Prediction of 3-Day Concrete.

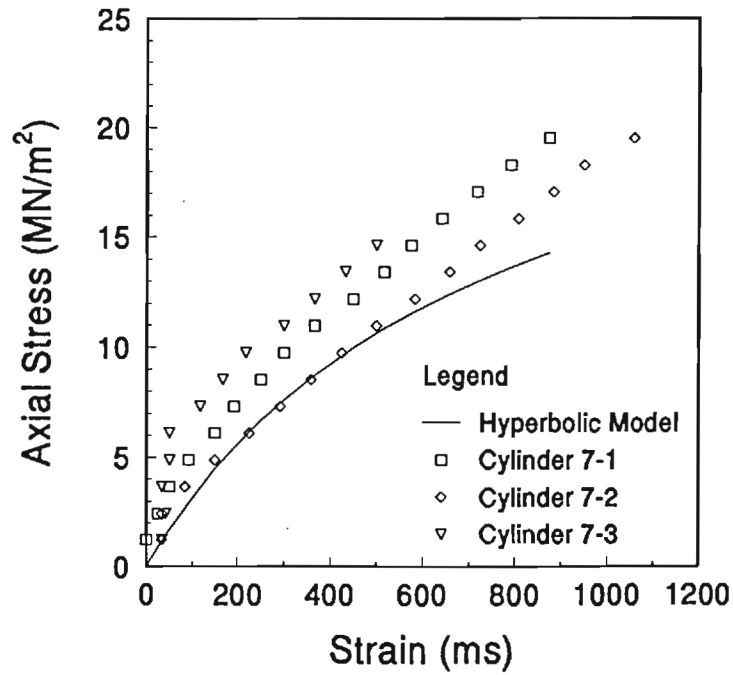


Figure C-9. Hyperbolic Prediction of 7-Day Concrete.

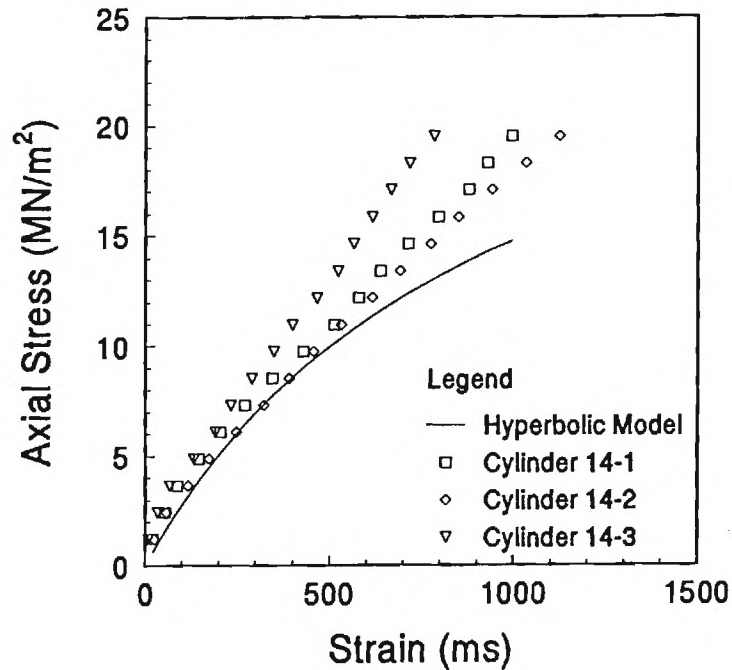


Figure C-10. Hyperbolic Prediction of 14-Day Concrete.

for cylinder 7-1. The models provide a good representation of the data within the strain ranges applicable to the vibrating wire gauges (0 to 1000 ms).

Elastic modulus versus axial strain data from the vibrating wire gauges and the hyperbolic models of the laboratory batched concrete are shown together in Figure C-11. From this figure, it can be seen that the moduli from the vibrating wire gauges are approximately equal to the moduli from the hyperbolic models of the 7-day and 14-day test cylinders. Some differences should be expected considering the differences in the placement of the concrete in the drilled shaft excavations as opposed to the casting of test cylinders, and due to the differences in the curing environment. The test cylinders cured in a high humidity environment with water available for hydration, but it is difficult to say how much water was available for the concrete in the drilled shaft excavations, most

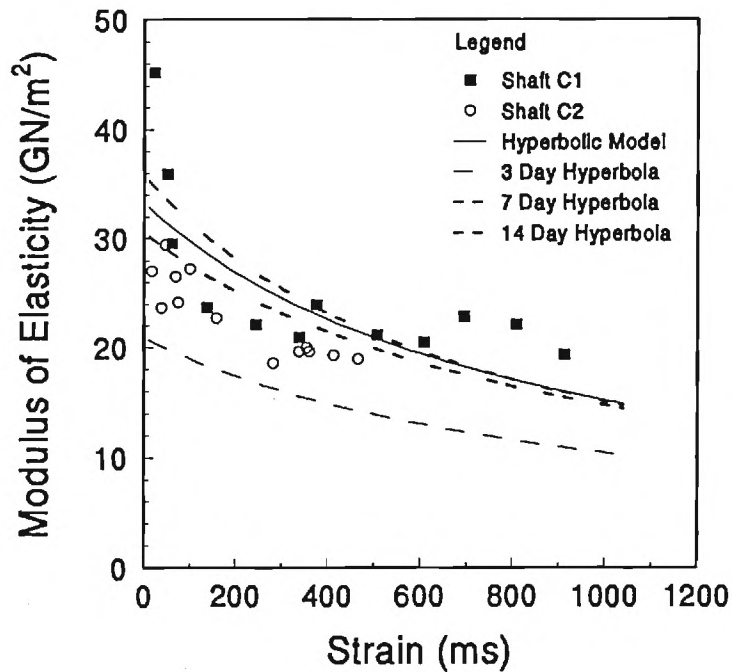


Figure C-11. Comparison of Hyperbolic Prediction and Measured Moduli Degradation.

of which was above the groundwater level. The residuals soils were likely partially-saturated due to capillarity effects. In addition, slight differences in the mix characteristics are to be expected.

#### C.6. SUMMARY

The strength and modulus of concrete were evaluated by laboratory tests, field data, and nondestructive techniques. The compressive strength of the shaft concrete was determined from compression tests on field cylinders taken during the pour. These tests were performed prior to the load test. Several means of estimating the modulus of elasticity were considered, including empirical correlations with the compressive strength, and dynamic measurements made during integrity testing of the drilled shafts. Strain measurements from the vibrating wire gauges at the top of the drilled shafts were also

used by utilizing the load readings from the hydraulic jack used to load the shafts. This method requires the assumption that the axial load at the level of the gauges was equivalent to the jack load. Moduli determined in this manner compared well with moduli determined from additional test cylinders cast from a batch of concrete prepared in the laboratory, using the same mix design. A hyperbolic relationship, with parameters defined based on the results of the integrity testing, was selected for use in reduction of the data from deeper gauges.

## APPENDIX D

### CALCULATIONS OF CAPACITY AND LOAD-DISPLACEMENT RESPONSE

The results of spreadsheet calculations of axial compression capacity and load-displacement response for the two drilled shaft foundations are given in this appendix. The capacities were calculated using the hybrid  $\alpha$ - $\beta$  methodology outlined in Chapter 6 of this report. In this approach, effective stress conditions are utilized to estimate side resistance factors and total stress analyses used for calculating end-bearing.

Load-displacement relationships for the shafts were estimated using the simplified elastic continuum theory approach discussed in Chapter 7. In addition, the continuum approach permitted backcalculated moduli from the measured load test data and the results for a Gibson-type soil profile with  $E_{s0} = 0$  increasing linearly to  $E_{sL}$  at the foundation base are included herein. The ratio of base modulus ( $E_b$ ) to tip modulus ( $E_{sL}$ ) was taken to be about 7. Additional analyses for other possible scenarios for uniform moduli profiles and with varying factors were investigated but not included in this appendix.

ADSC/ASCE SITE: Analysis of Drilled Piers with SPT-N60 Data

Shaft	d (ft)	L (ft)	av. f (tsf)	As (ft <sup>2</sup> )	Ave. Qs (tons)	Ab (ft <sup>2</sup> )	Cum. Qs (tons)	Sand qult (tsf)	Clay qult (tsf)	Sand Qb (tons)	Clay Qb (tons)	Sand Qtot (tons)	Ultimate Capacity	
													Clay Qtotal (tons)	Clay Qtotal (tons)
C1	2.5	70	1.17	550	690	4.91	694	3452	98	16945	491	17635	C1:	1181
C2	2.5	55	0.73	432	317	4.91	336	92	13	450	63	766	C2:	380

Correlation Factor for  $\sigma_p'$  = 0.2  
 Total Unit Weight (pcf) = 120  
 Depth of Groundwater (feet) = 55

Mean	81.7	2.21	16.34	6.69	40.90	1.03	1.85	69.73	5.52	364.38	782	2.24	20.93	715.3
SM	17.0	1.60	3.41	4.20	35.96	0.87	0.73	28.00	3.88	41.32	35	0.63	5.91	221.4
PWR	236.9	3.68	47.38	12.67	52.75	1.42	4.52	169.87	9.46	1139.71	2576	6.11	56.96	1900.7
Depth (ft)	ave. N (bpf)	(tsf) ovo'	(tsf) est. $\sigma_p$	OCR	$\phi'$	Ko	Incre fs	Cumul. Qs	Kp	Nq	Sand qult	Clay su	Clay qult	Modulus E (tsf)
1	5.0	0.06	1.00	16.67	35.6	2.15	0.09	0.72	3.78	36	1	0.13	1.17	82
4	15.5	0.24	3.10	12.92	44.1	1.80	0.42	9.88	5.57	116	17	0.41	3.81	208
9	8.8	0.54	1.76	3.26	35.7	0.83	0.32	12.65	3.81	37	12	0.31	2.85	131
14	10.6	0.84	2.12	2.52	35.3	0.72	0.43	16.83	3.74	35	17	0.39	3.62	152
19	11.3	1.14	2.26	1.98	34.2	0.64	0.50	19.56	3.56	30	21	0.43	4.05	161
24	13.8	1.44	2.76	1.92	34.5	0.63	0.62	24.37	3.62	31	27	0.53	4.97	189
29	17.4	1.74	3.48	2.00	35.4	0.63	0.78	30.52	3.75	35	37	0.67	6.22	229
34	19.0	2.04	3.80	1.86	35.1	0.61	0.87	34.22	3.71	34	41	0.74	6.89	246
39	20.1	2.34	4.02	1.72	34.6	0.59	0.95	37.26	3.63	32	45	0.79	7.41	258
44	22.7	2.64	4.54	1.72	34.9	0.58	1.07	42.17	3.67	33	52	0.90	8.36	285
49	23.6	2.94	4.72	1.61	34.4	0.57	1.14	44.94	3.60	31	55	0.94	8.81	294
54	36.6	3.24	7.32	2.26	37.7	0.64	1.60	62.89	4.15	47	92	1.37	12.77	421
59	74.5	3.42	14.90	4.36	44.1	0.85	2.81	110.20	5.58	118	241	2.44	22.78	754
63	139.0	3.53	27.80	7.87	49.9	1.14	4.78	150.09	7.51	313	663	4.05	37.77	1258
68	321.0	3.67	64.20	17.47	57.3	1.76	5.00	196.35	11.65	1566	3452	7.97	74.37	2499
73	450.0	3.82	90.00	23.57	60.0	2.07	5.00	196.35	13.90	3191	7310	10.52	98.19	3297
78	200.0	3.96	40.00	10.09	52.4	1.30	5.00	196.35	8.63	511	1216	5.54	51.71	1695

Elastic Settlement of Piles Under Axial Loading  
(Poulos, 1989; Randolph & Wroth, 1978, 1979)

Pile Diameter, d (feet)	2.5	(Es)L = Modulus at pile tip (tsf)
Pile Length, L (feet)	70	(Eb) = Modulus of Bearing Stratum (tsf)
Pile Modulus, Ep (tsf)	288000	(Es)mid = Mid-depth Modulus (tsf)
Poisson Ratio of Soil	0.3	(Eso) = Modulus at Ground Surface (tsf)
Xi = Ratio (Es)L/(Eb)	0.15	L/d Ratio 28 Slenderness
Eta = Base Effect	1.00	Pb/Pt Ratio 0.046 Uniform Only
Rho = Ratio (Es)mid/(Es)L	0.5	Zeta Term 2.958

Average Measured EsL/Eb 0.047  
Average Measured Pb/Pt 0.236

$$EsL = P(Ip)/\delta d$$

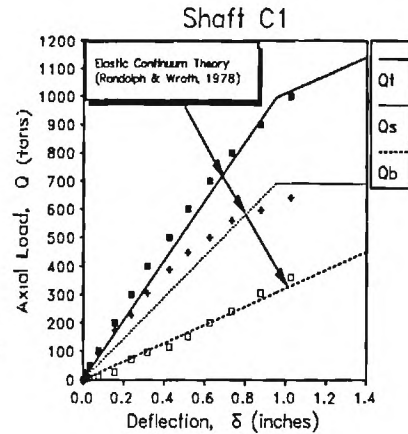
Axial Load q (tons)	Axial Defl. $\delta$ (inch)	Axial Defl. $\delta$ (ft)	Telltale Tip Defl. (in)	wt/wb Ratio	(Es)L Soil Modulus (tsf)	Assumed (Es)L (tsf)	cosh( $\mu$ L)	Lambda Ratio	Term $\mu$ L	Tanh( $\mu$ L) / $\mu$ L	Equation for Ip Numer. Denom.	
0	0.000	0.0000	0									
25	0.011	0.0009	0.007	1.57	1338	1321	6.919	567	1.9342	0.4958	8.29	67.59
50	0.034	0.0028	0.01	3.40	668	667	3.953	1123	1.3744	0.6400	7.21	76.17
100	0.076	0.0063	0.014	5.43	566	568	3.555	1318	1.2683	0.6728	7.00	78.12
200	0.155	0.0129	0.029	5.34	550	553	3.495	1354	1.2515	0.6782	6.97	78.44
300	0.240	0.0200	0.047	5.11	525	529	3.401	1416	1.2240	0.6869	6.91	78.96
400	0.317	0.0264	0.064	4.95	533	536	3.428	1397	1.2321	0.6844	6.93	78.80
500	0.426	0.0355	0.093	4.58	480	485	3.228	1544	1.1720	0.7038	6.81	79.96
600	0.520	0.0433	0.124	4.19	468	474	3.186	1580	1.1586	0.7082	6.78	80.23
700	0.626	0.0522	0.167	3.75	448	454	3.108	1649	1.1339	0.7164	6.73	80.71
800	0.734	0.0612	0.216	3.40	432	440	3.054	1702	1.1163	0.7223	6.70	81.06
900	0.876	0.0730	0.285	3.07	398	406	2.922	1844	1.0723	0.7370	6.61	81.94
1000	1.01	0.0842	0.357	2.83	378	388	2.853	1930	1.0483	0.7452	6.56	82.42

Axial Load q (tons)	Axial Defl. $\delta$ (inch)	Axial Defl. $\delta$ (ft)	Telltale Tip Defl. (in)	Meas. Tip Load Pb (t)	Meas. Pb/Pt	Backcalc Eb (tsf)	Tip EsL (tsf)	EsL/Eb	Influence Factor Ip	Stiffnes Kr = Ep/EsL
0	0.000	0.0000	0							
25	0.011	0.0009	0.007						0.1226	218
50	0.034	0.0028	0.01	5.17	0.103	5645.6	668.5	0.118	0.0947	432
100	0.076	0.0063	0.014	10.3	0.103	8034.0	566.1	0.070	0.0896	507
200	0.155	0.0129	0.029	26.8	0.134	10091.6	550.3	0.055	0.0888	521
300	0.240	0.0200	0.047	72.3	0.241	16798.2	525.4	0.031	0.0876	544
400	0.317	0.0264	0.064	96.7	0.242	16499.4	532.6	0.032	0.0879	537
500	0.426	0.0355	0.093	113.8	0.228	13362.3	479.8	0.036	0.0852	594
600	0.520	0.0433	0.124	153.5	0.256	13517.9	468.3	0.035	0.0846	608
700	0.626	0.0522	0.167	200.5	0.286	13110.5	447.8	0.034	0.0834	634
800	0.734	0.0612	0.216	243.7	0.305	12320.4	432.3	0.035	0.0826	655
900	0.876	0.0730	0.285	304.5	0.338	11667.2	397.9	0.034	0.0807	709
1000	1.01	0.0842	0.357	361.7	0.362	11063.8	378.4	0.034	0.0796	742
				0.236	12010	495	0.047			



Elastic Settlement of Piles Under Axial Loading  
(Poulos, 1989; Randolph & Wroth, 1978, 1979)

Pile Diameter, d (feet)	2.5	(Es)L = Modulus pile tip (tsf)	
Pile Length, L (feet)	70	(Eb) = Bearing Stratum (tsf)	
Pile Modulus, Ep (tsf)	288000	(Es)mid = Mid-depth Mod. (tsf)	
Poisson Ratio of Soil	0.3	(Eso) = Mod. at Surface (tsf)	
Soil Modulus, EsL (tsf)	450	L/d Ratio	28
Base Modulus, Eb (tsf)	2400	Ratio Pb/Pt	0.047
Rho = Ratio (Es)mid/(Es)L	0.5	Zeta Term	3.023
Shaft Capacity, Qs (tons)	690	Kr = Ep/EsL	640
Base Capacity, Qb (tons)	491	Ratio Ps/Pt	0.953
Total Capacity, Qt (tons)	1181		
		Load Transfer in Elastic Range	
Xi = Ratio (Es)L/(Eb)	0.188	Pb/Pt =	0.307
Eta = Base Effect	1	Ps/Pt =	0.693



Axial Load Q (tons)	Axial Defl. delta (inch)	Axial Defl. delta (ft)	Base Load Pb (tons)	Shaft Load Ps (tons)	Base delta (feet)	Shaft delta (feet)	Measured Loads from Test		
							Qt	Qbase	Qshaft
0	0	0	0	0					
996.0	0.952	0.07934	306.0	690.0	0.0464	0.032929			
1181.0	1.528	0.1273	491.0	690.0	0.0745	0.0329			
1181	20	20	491	690	20	20			
	0						0	0	0
	0.011						25	2.6	22.4
	0.034						50	5.17	44.83
	0.076						100	10.3	89.7
	0.155						200	27	173
	0.24						300	72	228
	0.317						400	97	303
	0.426						500	113	387
	0.52						600	154	446
	0.626						700	200	500
	0.734						800	243	557
	0.876						900	304	596
	1.024						1000	361	639

Axial Load Q (tons)	Axial Defl. delta (inch)	cosh(muL)	Lambda Ratio	Term muL	Tanh(muL) / muL	Numer.	Denom.	Influence Factor Ip
0	0							
996.0	0.952	1.691	1664	1.1165	0.7222	6.43	72.50	0.0886
1181.0	1.528	1.691	1664	1.1165	0.7222	6.43	72.50	0.0886

Elastic Settlement of Piles Under Axial Loading  
(Poulos, 1989; Randolph & Wroth, 1978, 1979)

Pile Diameter, d (feet)	2.5	(Es)L = Modulus at pile tip (tsf)	
Pile Length, L (feet)	55	(Eb) = Modulus of Bearing Stratum (tsf)	
Pile Modulus, Ep (tsf)	288000	(Es)mid = Mid-depth Modulus (tsf)	
Poisson Ratio of Soil	0.35	(Eso) = Modulus at Ground Surface (tsf)	
Xi = Ratio (Es)L/(Eb)	1	L/d Ratio	22 Slenderness Ratio
Eta = Base Effect	1	Ratio Pb/Pt	0.074 Uniform Es Only
Rho = Ratio (Es)mid/(Es)L	0.5	Zeta Term	3.577

Average Measured EsL/Eb 1.747  
Average Measured Pb/Pt 0.070

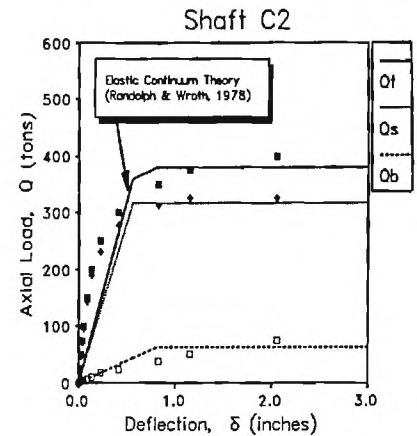
$$EsL = P(Ip)/\delta d$$

Axial Load Q (tons)	Axial Defl. $\delta$ (inch)	Axial Defl. $\delta$ (ft)	Telltale Tip Defl. (in.)	Ratio wt/wb	(Es)L Soil Modulus (tsf)	Assumed Modulus (Es)L (tsf)	cosh( $\mu L$ )	Lambda Ratio	Term $\mu L$	Tanh( $\mu L$ ) / $\mu L$	Numer.	Denom.
0	0.000	0.0000	0									
25	0.017	0.0014	0		1351	1351	2.097	576	1.3715	0.6409	5.92	30.93
50	0.032	0.0027	0.014	2.286	1477	1477	2.217	526	1.4340	0.6224	5.95	30.21
75	0.043	0.0036	0.015	2.867	1746	1746	2.482	445	1.5591	0.5870	6.01	28.84
100	0.060	0.0050	0.023	2.609	1628	1629	2.365	477	1.5060	0.6018	5.99	29.41
150	0.087	0.0073	0.037	2.351	1717	1722	2.458	452	1.5484	0.5900	6.01	28.96
200	0.136	0.0113	0.084	1.613	1357	1356	2.102	573	1.3740	0.6402	5.92	30.90
250	0.227	0.0189	0.159	1.428	899	899	1.694	865	1.1188	0.7215	5.79	34.04
300	0.414	0.0345	0.327	1.265	524	522	1.386	1490	0.8525	0.8122	5.65	37.54
350	0.829	0.0690	0.674	1.229	278	278	1.200	2797	0.6221	0.8883	5.55	40.48
375	1.154	0.0961	1.039	1.110	208	209	1.149	3721	0.5394	0.9131	5.51	41.44
400	2.056	0.1713	2.042		119	120	1.085	6480	0.4087	0.9478	5.47	42.79

Axial Load Q (tons)	Axial Defl. $\delta$ (inch)	Axial Defl. $\delta$ (ft)	Telltale Tip Defl. (in.)	Meas. Load at Tip Pb (t)	Meas. Pb/Pt	Backcalc Eb (tsf)	Tip EsL (tsf)	EsL/Eb	Influence Factor Ip	Stiffnes Kr = Ep/EsL
0	0	0	0	0						
25	0.017	0.0014	0	2.010	0.080		1350.9		0.1914	213
50	0.032	0.0027	0.014	2.930	0.059	881.5	1477.3	1.676	0.1970	195
75	0.043	0.0036	0.015	4.020	0.054	1128.8	1745.5	1.546	0.2085	165
100	0.060	0.0050	0.023	6.020	0.060	1102.4	1628.4	1.477	0.2036	177
150	0.087	0.0073	0.037	6.928	0.046	788.7	1717.1	2.177	0.2075	167
200	0.136	0.0113	0.084	10.900	0.055	546.6	1357.4	2.484	0.1916	212
300	0.414	0.0345	0.327	23.700	0.079	305.3	524.4	1.718	0.1701	320
400	2.056	0.1713	2.042	50.300	0.126	103.8	119.4	1.151	0.1506	552
									0.1370	1036
									0.1331	1378
									0.1278	2400
						0.068	693.9	1224.2	1.747	

Elastic Settlement of Piles Under Axial Loading  
(Poulos, 1989; Randolph & Wroth, 1978, 1979)

Pile Diameter, d (feet)	2.5	(Es)L = Mod. at pile tip (tsf)	
Pile Length, L (feet)	55	(Eb) = Mod. of Bearing Stratum	
Pile Modulus, Ep (tsf)	288000	(Es)mid = Mid-depth Mod.(tsf)	
Poisson Ratio of Soil	0.3	(Eso) = Modulus at Surface (tsf)	
Soil Modulus, EsL (tsf)	450	L/d Ratio	22
Base Modulus, Eb (tsf)	450	Ratio Pb/Pt	0.070 Uniform
Rho = Ratio (Es)mid/(Es)L	0.5	Ratio Ps/Pt	0.930 Uniform
Shaft Capacity, Qs (tons)	317	Zeta Term	3.651
Base Capacity, Qb (tons)	63	Kr = Ep/EsL	640
Total Capacity, Qt (tons)	380		
		Load Transfer in Elastic Range	
Xi = Ratio (Es)L/(Eb)	1	Ratio Pb/Pt =	0.120 General
Eta = Base Effect	1	Ratio Ps/Pt =	0.880



Axial Load Q (tons)	Axial Defl. δ (inch)	Axial Defl. δ (ft)	Base Load Pb (tons)	Shaft Load Ps (tons)	Base δ (feet)	Shaft δ (feet)	Measured Loads from Test		
							Qt	Qbase	Qshaft
0	0	0	0	0					
360.1	0.559	0.0466	43.1	317.0	0.0349	0.0117			
380.0	0.817	0.0681	63.0	317.0	0.0564	0.0117			
380	20	20	63	317	20	20			
	0						0	0	0
	0.017						25	2	23
	0.032						50	2.9	47.1
	0.043						75	4	71
	0.06						100	6	94
	0.087						150	6.9	143.1
	0.136						200	10.9	189.1
	0.227						250	18	232
	0.414						300	23.7	276.3
	0.829						350	38	312
	1.154						375	50	325
	2.056						400	75	325
	4						450	100	350
	6.3						500	150	350

Axial Load Q (tons)	Axial Defl. δ (inch)	cosh(μL)	Lambda Ratio	Term μL	Tanh(μL) / μL	Numer.	Denom.	Influence Factor Ip
0	0							
360.1	0.559	1.336	1664	0.7984	0.8306	5.41	37.16	0.1455
380.0	0.817	1.336	1664	0.7984	0.8306	5.41	37.16	0.1455

Tabulated Load-Transfer Data for End-Bearing Shaft C1

---

Deflection $\delta_s$ (in.)	Axial Loads From Strain Gauge Measurements (tons)			
	<u>z = 0 ft.</u>	<u>z = 30 ft.</u>	<u>z = 55 ft.</u>	<u>z = 70 ft.</u>
0.000	0	0	0	0
0.034	50	30.2	16.7	5.2
0.076	100	87.2	27.6	10.3
0.155	200	140.4	101.1	26.8
0.240	300	244.4	198.0	72.3
0.317	400	330.8	281.6	96.7
0.426	500	372.3	300.0	113.7
0.520	600	523.5	373.9	153.5
0.626	700	611.0	522.6	200.5
0.734	800	676.9	590.3	243.7
0.876	900	755.7	672.2	304.5
1.024	1000	819.9	739.6	361.7

---

Tabulated Load-Transfer Data for Floating Shaft C2.

---

Deflection $\delta_s$ (in.)	Axial Loads From Strain Gauge Measurements (tons)		
	<u>z = 0 ft.</u>	<u>z = 30 ft.</u>	<u>z = 55 ft.</u>
0.0	0	0	0
0.016	25	18.5	2.0
0.031	50	32.1	2.9
0.047	75	39.2	4.0
0.063	100	58.9	6.0
0.086	150	66.9	6.9
0.125	200	102.3	10.9
0.406	300	172.1	23.7
0.803	350	214.8	50.3
3.922	450	250.4	101.7
6.297	500	281.7	146.9

---

